

IMPROVED ANTLION SIZING OPTIMIZATION FOR VEHICLE-TO-GRID
CONSIDERING RULE-BASED ENERGY MANAGEMENT SCHEMES

ABDULGADER H ABDULGADER ALSHARIF

UNIVERSITI TEKNOLOGI MALAYSIA

UNIVERSITI TEKNOLOGI MALAYSIA**DECLARATION OF THESIS / UNDERGRADUATE PROJECT REPORT AND
COPYRIGHT**

Author's full name : Abdulgader H Abdulgader Alsharif

Date of Birth : 02/06/1987

Title : IMPROVED ANT-LION SIZING OPTIMIZATION FOR
VEHICLE-TO-GRID CONSIDERING RULE-BASED ENERGY
MANAGEMENT SCHEMES

Academic Session : 2022/2023-2

I declare that this thesis is classified as:

**CONFIDENTIAL**(Contains confidential information under the
Official Secret Act 1972)***RESTRICTED**(Contains restricted information as specified by
the organization where research was done)***OPEN ACCESS**I agree that my thesis to be published as online
open access (full text)

1. I acknowledged that Universiti Teknologi Malaysia reserves the right as follows:
2. The thesis is the property of Universiti Teknologi Malaysia
3. The Library of Universiti Teknologi Malaysia has the right to make copies for the purpose of research only.
4. The library has the right to make copies of the thesis for academic exchange.

Certified by:



SIGNATURE OF STUDENT


SIGNATURE OF SUPERVISOR

MATRIC NUMBER

NAME OF SUPERVISOR

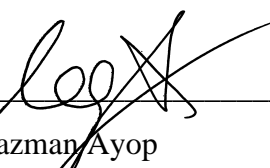
Date: 2 May 2023

Date: 2 May 2023

NOTES : If the thesis is CONFIDENTIAL or RESTRICTED, please attach with the letter from the organization with period and reasons for confidentiality or restriction

“I hereby declare that I have read this thesis and in my opinion this thesis is sufficient in term of scope and quality for the award of the degree of Doctor of Philosophy”

Signature : 
Name of Supervisor I : Assoc. Prof. Ir. Ts. Dr. Tan Chee Wei
Date : 2 MAY 2023

Signature : 
Name of Supervisor II : Dr. Razman Ayop
Date : 2 MAY 2023

BAHAGIAN A - Pengesahan Kerjasama*

Adalah disahkan bahawa projek penyelidikan tesis ini telah dilaksanakan melalui kerjasama antara _____ dengan _____

Disahkan oleh:

Tandatangan :

Tarikh :

Nama :

Jawatan :

(Cop rasmi)

* *Jika penyediaan tesis atau projek melibatkan kerjasama.*

BAHAGIAN B - Untuk Kegunaan Pejabat Sekolah Pengajian Siswazah

Tesis ini telah diperiksa dan diakui oleh:

Nama dan Alamat : **Prof. Ir. Dr. Hazlie bin Mokhlis**

Pemeriksa Luar : **Jabatan Kejuruteraan Elektrik,
Fakulti Kejuruteraan,
Universiti Malaya,
50603 Kuala Lumpur.**

Prof. Madya Ts. Dr. Shahrin bin Md Ayob

Nama dan Alamat : **Fakulti Kejuruteraan Elektrik,
81310 UTM Johor Bahru**

Pemeriksa Dalam II :

Nama Penyelia lain : **Dr. Razman bin Ayop**

(jika ada)

Disahkan oleh Timbalan Dekan di Fakulti Kejuruteraan Elektrik:

Tandatangan : ----- Tarikh : -----
Nama : **PROF. MADYA IR. DR. MUHAMMAD NADZIR
BIN MARSONO**

IMPROVED ANTLION SIZING OPTIMIZATION FOR VEHICLE-TO-GRID
CONSIDERING RULE-BASED ENERGY MANAGEMENT SCHEMES

ABDULGADER H ABDULGADER ALSHARIF

A thesis submitted in fulfilment of the
requirements for the award of the degree of
Doctor of Philosophy in Electrical Engineering

Faculty of Electrical Engineering
Universiti Teknologi Malaysia

APRIL 2023

DECLARATION

I declare that this thesis entitled "*Improved Antlion Sizing Optimization for Vehicle-to-Grid Considering Rule-Based Energy Management Schemes*" is the result of my own research except as cited in the references. The thesis has not been accepted for any degree and is not concurrently submitted in candidature of any other degree.

Signature : abdulgader alsharif...
Name : ABDULGADER H ABDULGADER ALSHARIF
Date : 2 MAY 2023

DEDICATION

To my parents, wife, children, brothers, sisters, and government for their support

ACKNOWLEDGEMENT

First of all, I would like to thank our almighty Allah (SWT) who has always been with me and blessed me to achieve the end of this work. Alhamdulillah.

Also, I would like to thank my supervisor Assoc. Prof. Ir. Ts. Dr. Tan Chee Wei for his generous support, recommendation, and guidance. Also, I would express my gratitude to my Co-supervisor Dr.Razman Ayop for his valuable and significant suggestions and guidance during the work of this research.

Also, my gratitude goes to Universiti Teknologi Malaysia (UTM) for providing a Library facility to acquire most of the database to achieve till the end of this work.

Then I would like to acknowledge the unlimited support from my parents and family, and special appreciation to my wife and children who shared all situations during the study and were very well understanding.

I would like to thank the Libyan government through the Ministry of Higher Education and Scientific for supporting this work in terms of providing the award in the form of scholarships. Special thanks go to the Centre for Solar Energy Research and Studies (CSERS) for providing annual climatology data and also acknowledgments to the General Electricity Company of Libya (GECOL) for providing load demand data for the area of study.

Eventually, my special thanks go to the colleagues who provided direct or indirect suggestions and quotes for the success of this work.

ABSTRACT

Renewable Energy Sources (RESs) integration with Electric Vehicles (EVs) and microgrids has become a popular system for providing an economic and green environment. In order to address power challenges, RESs such as solar and wind are exploited and integrated into a microgrid. EVs play a key role in reducing emissions and energy saving due to their free carbon nature, reducing fuel consumption, and can be used as storage or load. Tripoli-Libya (latitude 32.8872° N and longitude 13.1913° E) located in Northern Africa is one of the oils and natural gas producers that has been selected as the study area. However, the country is bedeviled with electric power problems. Microgrids are faced with planning issues, challenges associated with designing a proper model system, as well as stability which results in low power quality. The issue can be addressed by using metaheuristic algorithms combined with Energy Management Strategy (EMS). However, the conventional metaheuristic algorithms face premature convergence and acquire local optima quickly which needs to be improved. Thus, choosing suitable sizing metaheuristic algorithms is recommended to find the global optimum. Therefore, Improved Antlion Optimization (IALO) coupled with the Rule-Based Energy Management Strategy (RB-EMS) is proposed. An RB-EMS is used to control and monitor the flow of energy in the system using simple mathematical equations. Furthermore, in the literature review, rule-based is recommended due to the decision-making and providing the appropriate result. This study examines a grid-connected system aimed at addressing the current power challenges by integrating RESs into Electric Vehicle Charging Facility (EVCF) using Vehicle-to-Grid (V2G) technology. An objective function for the proposed grid-connected system mainly depends on measuring the per unit of generated electricity as Cost of Energy (COE), and reduction in Losses Power Supply Probability (LPSP) as means of stabilizing the system and maximizing the Renewable Energy Fraction (REF). Mathematical modeling for the Photovoltaic (PV), Wind Turbine (WT), EV, inverter, and Battery (BT) as the microgrid components for the case study (Tripoli-Libya) is adopted. The acquired result has been validated with other algorithms Antlion Optimization (ALO), Particle Swarm Optimization (PSO), and Cuckoo Search Algorithm (CSA). The obtained simulation result indicates that the proposed method IALO contributed lower COE (\$0.0936 /kWh), and high REF (99.40%) as compared to the counterpart algorithms. The IALO coupled with RB-EMS fills the gap in sizing and planning a cost-effective system to address the sizing limitations. The results affirm the low-cost nature of the proposed model of a grid-connected microgrid system using V2G technology. A further economic assessment is made using the Stochastic Monte Carlo Method (SMCM) used to estimate the load impact by integrating various numbers of EVs and the payback period. Sensitivity analysis was utilized to demonstrate the impact performance of the proposed components under various scenarios.

ABSTRAK

Integrasi Sumber Tenaga Boleh Diperbaharu (RES) dengan Kenderaan Elektrik (EV) dan mikrogrid telah menjadi sistem yang popular dalam menyediakan ekonomi dan persekitaran hijau. Untuk menangani cabaran tenaga, RES seperti solar dan angin dieksplotasi dan diintegrasikan ke dalam mikrogrid. EV memainkan peranan utama dalam mengurangkan pelepasan dan penjimatan tenaga kerana sifat bebas karbon, mengurangkan penggunaan bahan api, dan boleh digunakan sebagai tempat simpanan tenaga atau beban. Tripoli-Libya (latitud 32.8872°N dan longitud 13.1913°E) yang terletak di Afrika Utara merupakan salah satu pengeluar minyak dan gas asli yang telah dipilih sebagai kawasan kajian. Walau bagaimanapun, negara ini terganggu dengan krisis bekalan kuasa elektrik. Mikrogrid berhadapan dengan isu perancangan, cabaran yang berkaitan dengan mereka bentuk sistem model yang sesuai, serta kestabilan yang menyebabkan kualiti kuasa yang rendah. Isu ini boleh ditangani dengan menggunakan algoritma metaheuristik yang digabungkan dengan Strategi Pengurusan Tenaga (EMS). Walau bagaimanapun, algoritma metaheuristik konvensional mengalami masalah pramatang dan memperoleh optimum setempat dengan cepat yang perlu dipertingkatkan. Oleh sebab itu, memilih saiz algoritma metaheuristik yang sesuai adalah disyorkan untuk mencari tahap optimum global. Oleh itu, Pengoptimuman Antlion Dipertingkat (IALO) bersama dengan Strategi Pengurusan Tenaga Berasaskan Peraturan (RB-EMS) dicadangkan. RB-EMS digunakan untuk mengawal dan memantau aliran tenaga dalam sistem menggunakan persamaan matematik mudah. Tambahan pula, dalam kajian literatur, berdasarkan peraturan disyorkan kerana membuat keputusan dan memberikan hasil yang sesuai. Kajian ini mengkaji sistem tersambung grid yang bertujuan menangani cabaran kuasa semasa dengan mengintegrasikan RES ke dalam Fasiliti Pengecasan Kenderaan Elektrik (EVCF) menggunakan teknologi Kenderaan ke Grid (V2G). Fungsi objektif untuk sistem tersambung grid yang dicadangkan terutamanya bergantung pada pengukuran per unit elektrik yang dijana sebagai Kos Tenaga (COE), dan pengurangan Kebarangkalian Kehilangan Bekalan Kuasa (LPSP) sebagai cara menstabilkan sistem dan memaksimumkan Pecahan Tenaga Boleh Diperbaharu (REF). Pemodelan matematik untuk Fotovoltaik (PV), Turbin Angin (WT), EV, penyongsang dan Bateri (BT) sebagai komponen mikrogrid untuk kajian kes (Tripoli-Libya) digunakan. Hasil yang diperoleh telah disahkan dengan algoritma lain iaitu Pengoptimuman Antlion (ALO), Pengoptimuman Kelompok Zaraf (PSO), dan Algoritma Carian Cuckoo (CSA). Hasil simulasi yang diperoleh menunjukkan bahawa kaedah IALO yang dicadangkan menyumbang COE yang lebih rendah ($\$0.0936/\text{kWh}$), dan REF yang tinggi (0.9940%) berbanding dengan algoritma lawan. IALO yang diganding dengan RB-EES mengisi jurang dalam saiz dan merancang sistem yang kos efektif untuk menangani had saiz. Keputusan mengesahkan sifat kos rendah model cadangan bagi sistem mikrogrid tersambung grid menggunakan teknologi V2G. Penilaian ekonomi selanjutnya dibuat menggunakan Kaedah Stokastik Monte Carlo (SMCM) yang digunakan untuk menganggarkan kesan muatan dengan menyepadan pelbagai nombor EV dan tempoh bayaran balik. Analisis sensitiviti digunakan untuk menunjukkan prestasi impak komponen yang dicadangkan di bawah pelbagai senario.

TABLE OF CONTENTS

	TITLE	PAGE
DECLARATION		iii
DEDICATION		iv
ACKNOWLEDGEMENT		v
ABSTRACT		vi
ABSTRAK		vii
TABLE OF CONTENTS		viii
LIST OF TABLES		xii
LIST OF FIGURES		xiv
LIST OF ABBREVIATIONS		xviii
LIST OF SYMBOLS		xxi
LIST OF APPENDICES		xxiv
 CHAPTER 1 INTRODUCTION	 1	
1.1 Background of Research	1	
1.2 Problem Statement	4	
1.3 Research Objectives	6	
1.4 Scope of the Study	6	
1.5 Significance of the Study	8	
1.6 Research Methodology	8	
1.7 Organization of Thesis	10	
 CHAPTER 2 LITERATURE REVIEW	 13	
2.1 Introduction	13	
2.2 Microgrid Architecture	14	
2.3 Energy Management Strategy Algorithms	17	
2.3.1 Rule-Based Energy Management Strategy	18	
2.3.2 Optimization-Based Energy Management Strategy	19	

2.3.3	Learning-Based Energy Management Strategy	20
2.4	Microgrid Sizing Optimization Algorithms	21
2.4.1	Antlion Optimization	23
2.4.2	Particle Swarm Optimization	32
2.4.3	Cuckoo Search Algorithm	34
2.4.4	Objective functions	38
2.4.5	Constraints of the objective function	39
2.5	Vehicle-to-Grid Technology	39
2.5.1	Alternative Energy Resources	42
2.5.2	Vehicles-to-Everything Topologies	44
2.5.3	Energy Storage	45
2.5.4	Impacts of Electric Vehicles deployment	46
2.5.5	A critical review of the system components	49
2.6	The Research Gap	53
2.7	Chapter Summary	54

CHAPTER 3 VEHICLE-TO-GRID INTEGRATION FRAMEWORK 55

3.1	Introduction	55
3.2	The Case Study	57
3.3	The proposed microgrid	61
3.4	Operation modes of Rule-Based Energy Management Strategies	63
3.5	The Models of the proposed Microgrid Components	68
3.5.1	Photovoltaic Model	69
3.5.2	Wind Turbine Model	70
3.5.3	Battery Model	71
3.5.4	Converters Model	74
3.5.5	Electric Vehicle Charging Facility model	74
3.5.6	Utility Grid Model	74
3.6	Objective Functions Optimization of the proposed microgrids	77
3.6.1	Cost of Energy	77
3.6.2	Losses Power Supply Probability	79

3.6.3	Renewable Energy Fraction	79
3.6.4	Constraints in an optimization framework	80
3.7	The Test Function Application of the proposed algorithm	81
3.8	The Metaheuristic Optimization Algorithms	82
3.8.1	Antlion Optimization	83
3.8.2	The proposed Improved Antlion Optimization	84
3.9	The benchmark algorithms	90
3.9.1	Particle Swarm Optimization	90
3.9.2	Cuckoo Search Algorithm	92
3.10	Economic parameter analysis	95
3.10.1	The working principle of the Stochastic Monte Carlo Method	96
3.10.2	Operational analysis of the Stochastic Monte Carlo Method	96
3.10.3	Arrival and departure time prediction	99
3.10.4	Dynamic payback period analysis	101
3.11	Chapter Summary	101
CHAPTER 4	RESULTS AND DISCUSSIONS	103
4.1	Introduction	103
4.2	Input Parameters Data	104
4.2.1	Photovoltaic	104
4.2.2	Wind Turbine	107
4.2.3	Energy Storage Battery	110
4.3	Load profile	110
4.4	The Electric Vehicle Charging Facility	114
4.5	Comparative analysis of ALO, IALO, PSO, and CSA	117
4.6	Sizing Optimization result of the proposed microgrid	119
4.7	The Rule-Based Energy Management Strategy scheme for electricity generation	122
4.7.1	Seasonally analysis of electricity generation under different conditions	123

4.7.1.1	Winter electricity generation analysis	123
4.7.1.2	Spring electricity generation analysis	125
4.7.1.3	Summer electricity generation analysis	126
4.7.1.4	Autumn electricity generation analysis	128
4.7.2	Annual output power result	130
4.8	Economic analysis of the system	132
4.8.1	Economic breakdown of the components	133
4.8.2	Capital Costs and Net Present Cost	134
4.8.3	Objective function analysis	134
4.9	Impact of EVs integrating	136
4.9.1	Impacts of G2V integration	136
4.9.2	Impact of V2G integration	137
4.9.3	Impact of RESs2V integration	139
4.9.4	Impact of BT2V integration	140
4.10	The Sensitivity Analysis	141
4.10.1	Impact of Changes in Climatology Condition	142
4.10.2	Impact of deep cycle battery and EVs integration on the grid	143
4.11	Chapter Summary	144
CHAPTER 5	CONCLUSION AND RECOMMENDATIONS	147
5.1	Conclusion	147
5.2	Suggestions for Future Works	150
REFERENCES		152
LIST OF PUBLICATIONS		195

LIST OF TABLES

TABLE NO.	TITLE	PAGE
Table 2.1	Summary of the state-of-the-art of microgrid bus bars.	17
Table 2.2	Energy Management Strategy classification.	20
Table 2.3	Variations of antlion optimization.	31
Table 2.4	Advantages and disadvantages of antlion optimization.	32
Table 2.5	Advantages and disadvantages of particle swarm.	33
Table 2.6	Advantages and Disadvantages of cuckoo search algorithm	37
Table 2.7	Structures of charging Electric Vehicles.	42
Table 2.8	Energy Resources and their Applications.	44
Table 2.9	Mobility charging topologies of electric vehicles.	45
Table 2.10	Comparison between Li-ion & LiFePO ₄ batteries.	46
Table 2.11	Positive impact of EV on power grid.	47
Table 2.12	Negative impact of EV on power grid.	48
Table 2.13	The State-of-The-Art of RESs integration without EVs.	50
Table 2.14	State-of-the-art microgrid systems on-grid and off-grid in the literature with EVs.	51
Table 3.1	RB-EMS rules for a grid-connected system with V2G technology.	65
Table 3.2	Specification of EV (LiFePO ₄) battery.	73
Table 3.3	Summary of the hybrid system components.	76
Table 3.4	Unimodal and multimodal benchmark function.	82
Table 3.5	Steps of Antlion Optimization.	83
Table 3.6	Steps operation of the proposed IALO and its description.	88
Table 3.7	Steps of Particle Swarm Optimization Algorithm.	92
Table 3.8	Steps of Cuckoo Search Algorithm.	94
Table 3.9	The controlling parameters of the utilized optimization algorithms.	94

Table 3.10	The Entry constraints data of EV.	100
Table 4.1	House electric appliances loads with the usage hours per day.	113
Table 4.2	Statistic result of the test functions for the benchmark methods.	119
Table 4.3	Comparison of Results from Different Algorithms.	120
Table 4.4	Hourly Execution of 50 hours of Operation in Winter.	124
Table 4.5	Hourly Execution of 50 hours of Operation in Spring.	126
Table 4.6	Hour-by-hour execution of 50 hours of operation in summer.	127
Table 4.7	Hour-by-hour execution of 50 hours of operation in autumn	129
Table 4.8	The energy and cost breakdown of the system.	133

LIST OF FIGURES

FIGURE NO.	TITLE	PAGE
Figure 1.1	The typical energy management strategy for microgrids.	3
Figure 1.2	The proposed research methodology.	9
Figure 2.1	Pyramid automation layers for supervisory control.	14
Figure 2.2	Microgrid classifications.	15
Figure 2.3	Hybrid microgrid bus bars. (a) AC bus, (b) DC bus, and (c) DC/AC bus.	16
Figure 2.4	Sample of the rule-based algorithm.	19
Figure 2.5	Classification of widely used energy management strategies.	21
Figure 2.6	Classifications of microgrid sizing algorithms.	22
Figure 2.7	The process of the Antlion Algorithm (a) Hunting mechanism and (b) Life cycle.	24
Figure 2.8	The ant and antlion stochastic walk.	27
Figure 2.9	Flowchart of the antlion optimization algorithm.	30
Figure 2.10	Particle swarm optimization algorithm mechanism.	32
Figure 2.11	Flowchart of particle swarm optimization procedure.	34
Figure 2.12	Cuckoo search algorithm mechanism.	36
Figure 2.13	Cuckoo search algorithm procedure flowchart.	37
Figure 2.14	The bidirectional power flow diagram for Vehicle-to-Grid and Grid-to-Vehicle.	40
Figure 2.15	Residential and commercial charging diagram.	41
Figure 2.16	Impacts of Vehicle-to-Grid technology implementation.	47
Figure 3.1	A systematic approach for the research methodology and modeling the system and achieving the objectives.	56
Figure 3.2	The peak load growth in Libya from 2010 to 2021.	58
Figure 3.3	Direct normal irradiance for Libyan map .	59
Figure 3.4	Energy plan for the study area.	59

Figure 3.5	Non-renewable sources in Libya (a) Total energy consumption and (b) Crude oil exports to other countries.	60
Figure 3.6	Types and percentage of the fuel used in electricity generation.	60
Figure 3.7	Seasons of the year in Libya.	61
Figure 3.8	The architecture of the proposed Vehicle-to-Grid microgrid.	62
Figure 3.9	The RB-EMS implementation on the microgrid system (a) The RB-EMS flowchart of the system and (b) Discharging operation from BT.	66
Figure 3.10	The RB-EMS charging and discharging operation (a) Charging from BT and (b) Buying from the grid (G2V operation) and Selling to the grid (V2G operation).	67
Figure 3.11	Operation modes of the proposed system. (a) Renewable Energy Sources, (b) Deep Cycle Battery units, (c) Grid-to-Vehicle, and (d) Vehicle-to-Grid.	68
Figure 3.12	The ideal power curve of wind turbines and operation regions.	71
Figure 3.13	The essential concept of battery SoC and DoD.	73
Figure 3.14	Flowchart of Rule-Based Energy Management Strategy of ALO.	84
Figure 3.15	Flowchart of the proposed Improved ALO (IALO) Algorithm.	86
Figure 3.16	Flowchart of the proposed Rule-Based-Energy Management Strategy of IALO (RB-EMS-IALO).	89
Figure 3.17	Flowchart of the Rule-Based-Energy Management Strategy of Particle Swarm Optimization (RB-EMS-PSO).	91
Figure 3.18	Flowchart of the Rule-Based-Energy Management Strategy of Cuckoo Search Algorithm.	93
Figure 3.19	Flowchart of Stochastic Monte Carlo Method	96
Figure 3.20	Flowchart of Stochastic Monte Carlo Method operation.	98
Figure 3.21	Operational strategies flowchart of IF-Then conditions for SMCM.	99
Figure 4.1	Solar irradiance for Tripoli-Libya (a) Annual data and (b) Seasonal Contour plot.	105
Figure 4.2	Annual maximum and mean of solar irradiance.	105
Figure 4.3	Seasonal solar irradiance analysis for maximum and mean.	106

Figure 4.4	Ambient temperature data for Tripoli-Libya (a) Annual data and (b) Seasonal contour plot.	106
Figure 4.5	Annual maximum, minimum, and mean of ambient temperature (°C).	107
Figure 4.6	Generated Output Power from PV for Tripoli-Libya for one year.	107
Figure 4.7	Wind speed data for Tripoli-Libya. (a) Annual data (b) Seasonal Contour plot.	108
Figure 4.8	Seasonal maximum and mean wind speed (m/s).	108
Figure 4.9	Annual means and maximum wind speed (m/s).	109
Figure 4.10	Generated Output power from WT for Tripoli-Libya for one year.	109
Figure 4.11	Monthly annual output power from RESs.	110
Figure 4.12	Load profile (a) Counter plot (b) Daily, and (c) Seasonal load of the study area.	111
Figure 4.13	Seasonal maximum, and minimum power demand.	112
Figure 4.14	Annual peak, and minimum load demand.	112
Figure 4.15	Electric Vehicle Demand (a) Annual Vehicle Demand and (b) Daily Demand of EV.	114
Figure 4.16	Normal distribution of EV (a) SoC of arrival, (b) arrival time, and (c) departure time.	116
Figure 4.17	The benchmark result test function of the methods. (a) Sphere (F_1) (b) Schwefel2.22 (F_2), (c) Ackley (F_{10}), and (d) Penalized 2 (F_{13}).	118
Figure 4.18	Comparison convergence rates for IALO, ALO, PSO, and CSA.	121
Figure 4.19	Cost of Energy of the proposed system considering EMS.	121
Figure 4.20	The Annualized System Cost with RB-EMS of the utilized methods.	122
Figure 4.21	Daily output electricity generation in winter.	124
Figure 4.22	Daily output electricity generation in spring.	125
Figure 4.23	Daily output electricity generation in summer.	128
Figure 4.24	Daily output electricity generation in autumn.	129
Figure 4.25	Electricity generated (a) Annually charge/discharge, and load for one year, (b) A week Zoomed-in of (a).	130

Figure 4.26	The State of Charge of the battery (a) Annually and (b) Weekly for four seasons.	131
Figure 4.27	The V2G operation based on the State of Charge.	132
Figure 4.28	The break-even of the project over 25 years.	133
Figure 4.29	Breakdown of cash flow of the system components and cost categories.	134
Figure 4.30	Comparison of buying and selling energy.	135
Figure 4.31	The load impact of Grid-to-Vehicle for the scenarios for the first 24 hours (a) 10 EVs, (b) 30 EVs, (c) 60 EVs, and (d) no EVs.	137
Figure 4.32	The load impact of Vehicle-to-Grid for the first 24 hours (a) 10 EVs, (b) 30 EVs, (c) 60 EVs, and (d) no EVs hours.	138
Figure 4.33	Renewable Energy Sources impact for the first 24 hours (a) 10 EVs, (b) 30 EVs, (c) 60 EVs, and (d) no EVs.	140
Figure 4.34	Generated output power from the battery to EV for the first 24 hours (a) 10 EVs, (b) 30 EVs, (c) 60 EVs, and (d) no EVs.	141
Figure 4.35	Sensitivity Analysis: Comparison between <i>PPV</i> and <i>PWT</i> against COE.	143
Figure 4.36	Sensitivity Analysis: (a) Comparison of COE and REF of the microgrid system, (b) COE against EV increase, (c) COE against LPSP, and (d) SoC against the COE.	144

LIST OF ABBREVIATIONS

ABC	- Artificial Bee Colony
AD	- Autonomy days
ACO	- Ant Colony Optimization
AEV	- All-Electric Vehicle
AI	- Artificial Intelligent
ALO	- Antlion Optimizer
ASC	- Annualized System Cost
BAN	- Building Area Network
BT	- Battery
CO ₂	- Carbon Dioxide
COE	- Cost of Energy
CRF	- Cost Recovery Factor
CSA	- Cuckoo Search Algorithm
CSERS	- Center for Solar Energy Research and Studies
DCF	- Discounted Cash Flow
DP	- Dynamic Programming
DoD	- Depth-of-Discharge
ECMS	- Equivalent Consumption Minimization Strategy
EV	- Electric Vehicles
EVCS	- Electric Vehicle Charging Station
EVCF	- Electric Vehicle Charging Facility
EMS	- Energy Management Strategy
ESS	- Energy Storage Systems
FA	- Firefly Algorithm
FC	- Fuel Cell
G2V	- Grid-to-Vehicle
GHG	- Greenhouse Gas
GA	- Genetic Algorithm
GECOL	- General Energy Company of Libya
GOA	- Grasshopper Optimization Algorithm

GWA	-	Ground Water Authority
GWO	-	Gray Wolf Optimization
HAN	-	Home Area Network
HOMER	-	Hybrid Optimization Model for Electric Renewable
HRES	-	Hybrid Renewable Energy Source
HEV	-	Hybrid Electric Vehicle
IALO	-	Improved Antlion Optimization
ICEV	-	Internal Combustion Engine Vehicles
iHOGA	-	Integrated Hybrid optimization by Genetic Algorithm
IPT	.	Inductive Power Transfer
LAEC	-	Libya Atomic Energy Corporation
LF	-	Lévy Flight
Li-ion	-	Lithium-ion
LiFePO4	-	Lithium-iron Phosphate
LOA	-	Lion Optimization Algorithm
LPSP	-	Losses Power Supply Probability
LREA	-	Libyan Renewable Energy Authority
MPC	-	Model Predictive Control
MOPSO	-	Multi-Objective Particle Swarm Optimization
MOSaDE	-	Multi-objective self-adaptive differential evolution
MO	-	Multi-Objective
NAN	-	Neighbourhood Area Network
NECL	-	National Energy Council of Libya
NFL	-	No Free Lunch
NiCD	-	Nickel-Cadmium
NiMH	-	Nickel-Metal Hydride
NOC	-	National Oil Committee
O&M	-	Operation and Mantineans
OB	-	Optimization-Based
PHEV	-	Plug-in Hybrid Electric Vehicle
PV	-	Photovoltaic
PMP	-	Pontryagin's Minimum Principle
PSO	-	Particle Swarm Optimization

RB	-	Rule-Based
RE	-	Renewable Energy
REF	-	Renewable Energy Fraction
RESs	-	Renewable Energy Sources
REAOL	-	Renewable Energy Authority of Libya
RS	-	Renewable Sources
SA	-	Simulated Annealing
SDG7	-	Sustainable Development Goal Seven
SFO	-	Sun Flow Optimization
SG	-	Smart Grids
SO	-	Single-Objective
SoC	-	State-of-Charge
TNPC	-	The Total Net Present Cost
UN	-	United Nations
UPS	-	Untreatable Power Supply
V	-	Volt
V2B	-	Vehicle-to-Building
V2D	-	Vehicle-to-Device
V2G	-	Vehicle-to-Grid
V2H	-	Vehicle-to-Home
V2I	-	Vehicle-to-Infrastructure
V2L	-	Vehicle-to-Load
V2N	-	Vehicle-to-Network
V2P	-	Vehicle-to-Pedestrian
V2V	-	Vehicle-to-Vehicle
V2X	-	Vehicle-to-Everything
WPT	-	Wireless Power Transfer
WT	-	Wind Turbine

LIST OF SYMBOLS

Ah	-	Ampere hour
Antlion_j^t	-	Position of antlion
Ant_i^t	-	Position of ant
C_B	-	The battery capacity (Ah)
C_{grid}	-	The buying cost of power
C_{PV}	-	The cost of the solar panels
C_{SOL}^{INST}	-	The installation cost of the solar
C_{SOL}^{REP-C}	-	The replacement cost of the solar
$C_{SOL}^{O\&M}$	-	The annual maintenance cost of the solar
C_{WT}	-	The cost of the wind turbine
C_{WT}^{INST}	-	The installation cost of the wind turbine
C_{WT}^{REP-C}	-	The replacement cost of the wind turbine
C_{WT}^M	-	The annual maintenance cost of the wind turbine
C_{BATT}	-	The cost of the battery
C_{BT}^{INST}	-	The installation cost of the battery
C_{BT}^{REP-C}	-	The replacement cost of the battery
C_{BT}^M	-	The annual maintenance cost of the battery
C_{INV}	-	The cost of the inverter
C_{INV}^{INST}	-	The installation cost of the inverter
C_{INV}^{REP-C}	-	The replacement cost of the inverter
C_{INV}^M	-	The annual maintenance cost of the inverter
C_{bat}^{EV}	-	EV capacity
$P_{EV_{Dem}}$	-	EV power demand
$E_{grid(selling)}$	-	The selling energy
$E_{grid(purchased)}$	-	The purchasing energy
E_{served}	-	Primary load served
E_L	-	Load demand
EV_{demand}	-	Electric vehicle demand
E_{grid}	-	Energy from grid

G_t	- Solar irradiance
H	- Hub height
h_{ref}	- The reference height anemometer
i	- Annual interested rate
M_{Ant}	- The saving position of ants
M_{OA}	- The fitness function of ant
$M_{AntLion}$	- The saving position of antlion
M_{OAL}	- The fitness function of antlion
N_{PV}	- Number of solar panels
N_{WT}	- Number of wind turbines
N_{BATT}	- Number of batteries
$NP{C_x}$	- Net present cost
P_r	- Rated power
PV_{rated}	- Rated power for PV
P_{BT}	- Power delivered from the battery
P_l	- Power of load demand
P_p^{grid}	- The amount of purchased energy from the grid to EV
$P_S^{\text{grid}}(t)$	- The amount of energy sold from the EV to the grid
P_l^m	- The peak load demand
P_{inv}	- The inverter rating power
P_{PV}	- Output power from the photovoltaic
P_{WT}	- Output power from wind turbine
R_{grid}	- Revenue from selling energy to the grid
$rate_{feed-in}$	- Feed-in tariff rate
SOC_{BT}	- State-of-Charge of the battery bank
SOC_{EV}	- State-of-Charge of EV battery
T	- The difference between the arrival and departure times
T_{amb}	- Ambient temperature
T_{Arrive}^{EV}	- The arrival time of electric vehicles
$T_{C_{STC}}$	- Cell temperature
T_{Dep}^{EV}	- The departure time of electric vehicles
v_{ref}	- Wind speed

v	-	Rate turbine
v_r	-	Rated wind speed
v_{cut-in}	-	Cut-in wind speed
$v_{cut-out}$	-	Cut-out wind speed
σ	-	Self-discharge rate
η_b	-	Battery efficiency
η_{inv}	-	Inverter efficiency
α_{step}	-	Step size in lévy flight

LIST OF APPENDICES

APPENDIX	TITLE	PAGE
Appendix A MATLAB CODE		174
Appendix B PSEUDOCODE OF THE ALGORITHMS		182
Appendix C List of Classification of Terminologies		185
Appendix D MATLAB Software Environment		194

CHAPTER 1

INTRODUCTION

1.1 Background of Research

The grid-connected or on-grid system is a system considering Renewable Energy Sources (RESs) integrated with the utility grid to form a microgrid or hybridize system [1]. The significant difference between the microgrid and grid-connected system is, that a microgrid can be used as a support to an on-grid system to overcome conventional power limitations [2]. Besides, all available sources in the literature are in agreement that a cluster of loads can be termed a microgrid system [3]. Additionally, microgrid sources operate as a controllable scheme that provides heat, power, or both [4]. In terms of classification, a hybrid system can be categorized into two categories: grid-isolated and grid-connected [5]. Hence, a microgrid system is preferable because of its merits such as flexibility and efficiency [6]. Due to the increasing environmental concerns coupled with the increase in electricity demand among consumers, alternative energy sources are being utilized globally among scholars. Moreover, the hybrid system can address source and load problems in comparison with the traditional network [7].

Under the concept of Vehicle-to-Grid (V2G) as an accepted technology, the utility grid as an unlimited energy source is used to charge Electric Vehicles (EVs) [8]. The EV as a high-tech technology can absorb or distribute energy which is known as a charge or discharge operation [9]. This is because of the provided benefits such as simplicity, use as a mobile Uninterruptible Power Supply (UPS), and easily of plugging and play capability [10]. The V2G technology was pioneered by Amory Lovins in 1995 and carried out by William, EV is recognized as a possible and alternative solution to power and environmental problems [11]. The concept behind V2G is to enable to push of the power from the EV to the grid to balance the variations in energy production and consumption through a bidirectional converter [12].

Furthermore, when the load demand from the utility grid is high, the stored energy in the EV battery can be fed back to the utility grid (V2G) [13]. On the contrary, Grid-to-Vehicle (G2V) is when the grid load demand is low with the price, the unutilized energy from the utility grid can be sent back to the EV to avoid waste of energy [14]. Demand and supply must be balanced to support power transmission and keep the grid reliable [15]. Some of the acquired benefits of V2G technology can be better frequency control, stabilizing the grid operation in peak hours, lowering voltage fluctuation, and exchanging power among others [16].

In addition, ancillary services like peak shaving, load leveling, frequency and voltage regulation, and spinning reserve are counted as V2G benefits [17]. Nevertheless, RESs exploitation is classified under the ancillary services due to the green energy and supported power provided to the main grid [18]. Consequently, microgrid systems known as Smart Grids (SGs) are considered the future power solution. This is due to their intelligent used systems and components used capability such as integration with vehicles in Electric Vehicle Charging Station (EVCS) application and RESs [19]. There are four types of EVCS which are: grid-connected EVCS, EVCS with RESs, grid-connected EVCS with battery, and grid-connected with both RESs and battery [6]. This study considers residential grid-connected EVCS with RESs and Battery (BT) as the main concentration of microgrid systems under the domestic Electric Vehicle Charging Facility (EVCF) that refers to the home-based charger by utilizing home facilities to charge the EV. The last mentioned type has been chosen due to its merits such as reducing the electricity bill, better performance, and reducing the burden on the grid [20], [21]. Additionally, the use of RE requires less maintenance and prevents a spike in pricing [22].

The microgrid is comprised of the interconnection of numerous sources and systems that are connected such as Photovoltaic (PV), Wind Turbine (WT), and Fuel Cell (FC) [23]. The first two mentioned sources are considered to reduce the emission, reduce the impact on the grid, reduce the dependency on the grid, and satisfy the load demand [24]. Additionally, the integration of various energy sources can complement the drawbacks attributed to the use of an individual source. Energy Storage Systems

(ESSs) is a backup system or storage used in EVs to exchange the stored energy with the grid as V2G technology as demonstrated in Figure 1.1.

The straight black arrows in Figure 1.1 represent the power flow while the blue dots arrows refer to the communication and control lines. Residential AC load is realized with the help of converters and rectifiers to change the power form [16]. The presented grid-connected diagram consists of PV-WT-Inverter-BT integrated with EV. The aforementioned components are mathematically modeled to estimate the output power for each part to satisfy the load demand as will be presented in chapter 3 [21]. Due to the energy consumption of fossil fuels, new research windows are being explored by scholars to develop and implement a RESs integrated grid system to overcome power loss-related issues [25]. However, RESs are affected by weather conditions, while the integration operation can bring impact on the grid either positively or negatively [10]. In any case, if the two sources are optimally linked, the effect on the RESs can be partially fixed, resulting in a capable and cost-effective comprehensive system [26].

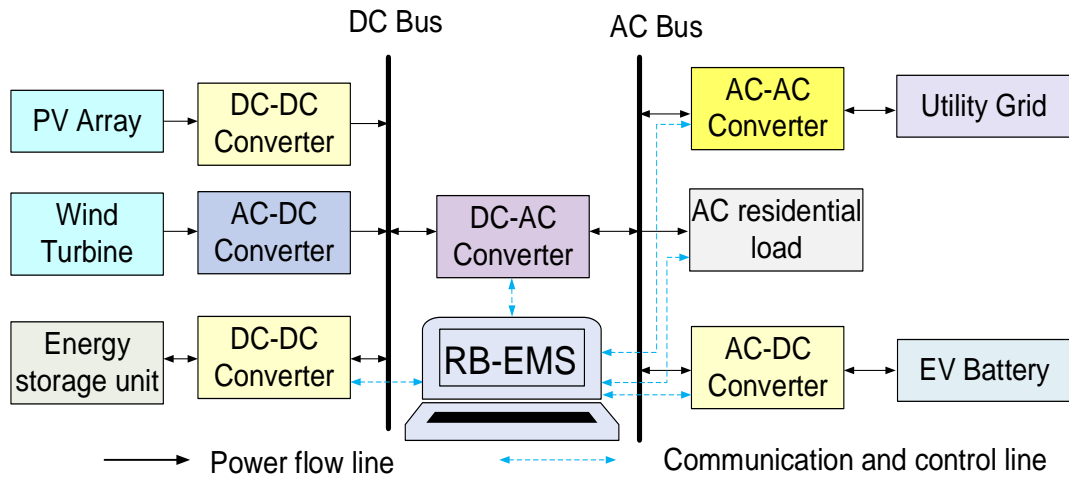


Figure 1.1 The typical energy management strategy for microgrids.

The effect of the implementation process can be regulated with supervisory control optimization methods known as Energy Management Strategy (EMS). The EMS is classified into three main categories: Rule-Based (RB), Optimization-Based (OB), and Learning-Based (LB) as reported in the literature [16], [27], [28]. In this regard, the feasibility of resources, cost, losses, and renewability is reliant on EMS.

One of the issues faced by the microgrid system is planning and designing a model system. Besides, there are several promising optimization algorithms were introduced to regulate power flow in the systems and used with the potential to ease the electricity generation operation [1].

The algorithms were created with the hybrid designed systems based on mathematical modeling equations that are factored in EMSs [29]. The EMS is used to conduct the combined system through the use of nature-inspired metaheuristic algorithms such as Ant Colony Optimization (ACO) [30] and Genetic Algorithm (GA). Additionally, Particle Swarm Optimization (PSO) [31], Cuckoo Search Algorithm (CSA) [32], and Antlion Optimization (ALO) [33] are also used. Nevertheless, the aforementioned optimization methods are not all suitable for solving power sizing problems and other issues as the No Free Lunch (NFL) theorem stated [34]. In addition, some of the studies considered in the literature utilize nature-inspired metaheuristic algorithms coupled with the EMS to control the flow energy among the other parameters [35]. The system of this study consists of RESs integrated into the national grid to charge and discharge EVs to form V2G technology. However, the integration system causes some challenges.

1.2 Problem Statement

With the availability of conventional sources (oil and natural gas) and the current low prices of these sources, conventional energy sources are widely used for electricity generation compared to RESs. Conventional sources and RES have the ability to be hybridized to run electric appliances and charge EVs. The integration of EVs in the hybridized system can address the power limitation issues, however, this increases the load due to having an uncertain number of EVs. Moreover, the use of alternative energy sources reduces the over-dependency on fossil fuels, reduces the peak load demand on the residential side, and overloading-related issues. However, integrating different RES would increase the system's cost and complexity. Metaheuristic sizing algorithms are facing challenge in achieving local optima, premature convergence, and running time speed. Additionally, controlling the power flow needs a suitable control algorithm like the EMS algorithm. However, EMS is

requiring technical information and some is requiring complex mathematical equations. Therefore, a proper adoption of EMS and sizing techniques in the hybrid power system becomes significantly important in identifying the most suitable capacity of the system components. Although there have been several techniques used to manage the existing power system, yet, some difficulties on the energy supply side due to improper management such as overloading remain a challenge. The aforementioned issue can be possibly addressed by scheduling a time for charging the EVs when the load of the utility grid is low (G2V) considering conventional or RESs. In general, Hybrid Renewable Energy Source (HRES) systems are reported to be efficient, economical, flexible, and cost-effective to overcome power management problems. The main advantages of HRES integration as a suitable system for stabilizing electric systems and improving power quality. Nevertheless, integrating HRESs into the utility grid faces challenges and issues related to the end-user side due to an increase in peak load demand which leads to the high cost of the system. The use of RESs in EV charging stations lowers the Cost of Energy (COE) and Losses of Power Supply Probability (LPSP) while maximizing the Renewable Energy Fraction (REF). Hence, reducing the cost and losses to gain an economic and reliable system while maximizing the renewability to reduce the dependency on the utility grid to obtain an economic system is needed. Additionally, economic and reliable performance are paired factors that restrict each other, which are also affected by the performance of the decision-maker.

The unplanned V2G process results in instability, inefficiency, and increase COE and unreliability that causes power barriers (overloading). Nevertheless, controlling and planning a proper design for the V2G system with RESs (RESs-EV) is a matter of technical and economic perspective. However, some of the worrying barriers of RESs for power system when used in the EV integration system for their intermittent nature and fluctuation in the power supply which leads to high penetration of EVs when using a huge number of EVs which causes power challenges in terms of loading and power quality. Thus, low power quality caused overload due to the uncertain number of charging vehicles in the charging area and an increase in COE. Similarly, difficulties faced in planning and designing such a system includes unstable weather condition and unknown load demand. Therefore, if RESs and EVs are integrated carefully, a balanced power grid resulting in lower energy costs, and less

reliance on conventional sources (fossil fuel) can be ensured. In addition, Carbone Dioxide (CO₂) emissions can be significantly reduced, which ultimately increases the system's reliability. Hence, adopting proper EMS and system sizing to guarantee the lowest investment cost for the system becomes necessary. Additionally by analysing the obtained economic result by the stochastic method in order to assess the impacts on the load from the EV.

1.3 Research Objectives

This research aims to propose a suitable EMS for the proposed microgrid consisting of PV-WT-BT connected to an electric vehicle charging facility. As a residential grid-connected system to achieve the following objectives:

1. To design a deterministic Rule-Based EMS to satisfy the load demand of a residential grid-connected system consisting of PV-WT-BT integrated with V2G technology.
2. To optimize the sizing of the proposed microgrid system using the Improved Antlion Optimization (IALO) to meet load demand at minimum COE, minimum LPSP, and maximum REF.
3. To compare and analyse the proposed components with ALO, PSO, and CSA in terms of COE, LPSP, and REF.

1.4 Scope of the Study

The main aims of the study are to size the system components by developing a metaheuristic algorithm for residential areas integrated into EVs to charge and discharge using PV-WT-BT. The subsequent scopes are considered:

- (a) This study is focusing on designing and proposing a sizing optimization metaheuristic method namely Improved Antlion Optimization (IALO) as a variant of ALO to optimize the microgrid with the utilized components. The attained result will be validated with ALO, PSO, and CSA.

- (b) Solar and wind energy sources are considered the main RESs in this study, due to their availability in the study location (Tripoli-Libya). While storage battery used as a backup integrated with an EV is used to supply an AC residential load (220 V and 50 Hz) when needed. The solar PV module used in the study is installed on the rooftop of the houses. While the WT is owned by the government and installed away from the residential area.
- (c) The objective functions of the study are to minimize the Cost of Energy (COE) and Losses of Power Supply Probability (LPSP) while maximizing the renewability which is called Renewable Energy Fraction (REF) to gain a cost-effective system.
- (d) The simulation concentrates on the domestic load using the implemented RESs (PV with 5 kW and 5 kW for WT) integrated with Lithium-iron Phosphate (LiFePO₄) 40 Ah EVs battery capacity and Li-ion deep cycle battery. Linked to the grid as a power source for charging and discharging that is based on the Libyan energy policy and Tripoli climatology data. The size of the charging station ranges between 10 to 60 EVs and can be extended to a flexible system or minimized and has been controlled by RB-EMS and the impact on the load for the arrival and departure EVs is estimated by Stochastic Monte Carlo Method.
- (e) The lifetime of the project is set as the PV age (25 years). Where components' (WT, BT, and inverter) age is 25, 10, and 15 years, respectively. The annual (1st January to 31st December 2019) hourly residential electricity demand data of 7.5 kW for Tripoli-Libya (latitude 32.8872° N and longitude 13.1913° E) was obtained from the General Electricity Company of Libya (GECOL). While climate data (wind speed, ambient temperature, and solar radiation) were collected from the Centre for Solar Energy Research and Studies (CSERS), accordingly.
- (f) The proposed system is simulated with MATLAB 2016b packaging code simulation and does not require any hardware implementation.

1.5 Significance of the Study

The contribution of this research is highlighted for the proposed microgrid hybrid system as stated below:

- a) Addressing the microgrid components sizing by the proposed metaheuristic algorithm called IALO for a residential grid-connected system consisting of PV-WT-BT integrated with EVCF to form V2G technology.
- b) Utilizing a supervisory control algorithm namely a Rule-Based Energy Management Strategy (RB-EMS) for controlling the flow of power in the system under four strategies. The strategies are supply system from RESs, supply system by BT, charging EVs using G2V, and discharging from EVs using V2G.
- c) Utilizing the Stochastic Monte Carlo Method (SMCM) to estimate the arrival and departure behavior of several EVs in the EVCF along with measuring the EV impact on the grid considering different sources. The sensitivity analysis is conducted to assess the COE of the main key affected sources.
- d) Assessing the COE in order to obtain the DPP based on the combination of DCF, and the statistic calculation of the payback period is performed for economic analysis.

1.6 Research Methodology

This section is a brief overview of the proposed methodology of the research and the techniques applied to obtain the research objectives. It is divided into several main tasks as shown in Figure 1.2 and further details on the methodology are presented in chapter 3.

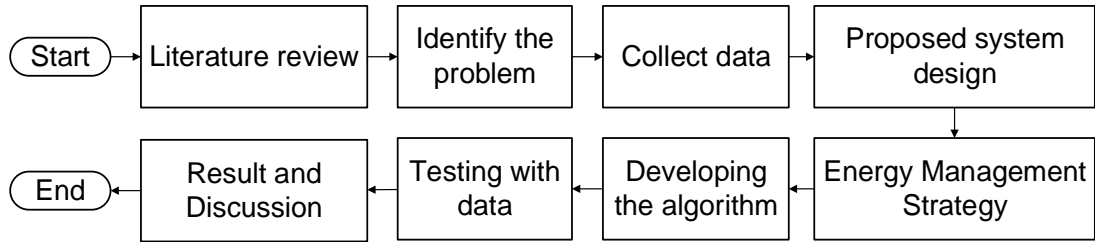


Figure 1.2 The proposed research methodology.

To establish a well understanding of the hybrid systems, a literature review becomes necessary. Literature on different metaheuristic algorithms, EMS algorithms, and RESs from various articles was carried out. The main aim of reviewing the articles is to have a good understanding of the hybrid systems with their components in addition to knowing their strengths and limitations. In this context, priority is given to quartile journals, high-impact factor journals, and indexed journals in Scopus.

As the study area (Tripoli-Libya) has four seasons, the climatology data and load demand for the area of study are required to be collected. To apply the mathematical equations to obtain the total generated power in each season with the help of solar irradiance (G), ambient temperature (T_{amb}), and wind speed (v) sourced from CSERS for one year (1st January to 31st December 2019) [7], [36]. Additionally, the load demand (P_l) for the area of study was obtained from GECOL [37].

Components such as PV-WT-BT integrated with EV are used to form the V2G technology as a grid-connected. The IALO is a sizing method used for the utilized components to provide a system with less cost and losses. In this research, a rule-based EMS algorithm is used to present the entire system operation mode and control the flow of power. Moreover, SMCM is exploiting to assess the impact behavior of arrivals and departure EVs to home. The utilized mathematical equations are widely used among scholars due to their simplicity and cover all the system components.

The results obtained from the IALO are benchmarked with ALO, PSO, and CSA algorithms as the most operating algorithms for a vast range of real-world problems. Additionally, in terms of EMS results, the obtained result from the RB-EMS-IALO is validated with RB-EMS-ALO, RB-EMS-PSO, and RB-EMS-CSA. The

RB-EMS-IALO performance has been investigated based on proposed objective functions (COE, LPSP, and REF) and provides a better result. In terms of economic analysis of the cost, the Discounted Cash Flow (DCF) is utilized with Net Present Cost (NPC) to obtain the Discounted Payback Period (DPP) of the system. Followed by sensitivity analysis results. Eventually, the results will be discussed, and the research is concluded.

1.7 Organization of Thesis

This thesis is organized into five chapters. Chapter 1 contains a general overview of the study, the problem statement, research objectives, the scope and significance of the study, and a brief explanation of the methodology.

Chapter 2 presents the literature review on different EMS considering different energy sources and a hybrid system. Classification of the EMS using metaheuristic sizing algorithms is also discussed. Furthermore, optimal sizing methods, their classifications, and applications-based nature-inspired metaheuristic algorithms are presented. Additionally, the classification of EVs is based on V2G technology with the impacts. A comprehensive review of research studies presenting the use of RES integration with the EVs forms the V2G technology with different objectives is discussed.

Chapter 3 presents the research methodology with the proposed hybrid microgrid system for the case study considering the mathematical simulation modal for each sector in the considered hybrid system. The analysis of climatology and load collected data for the considered location has been analyzed using MATLAB software. The utilized supervisory control scheme (RB) is figured out with the operational strategies.

Chapter 4 presents the simulation and analysis of the climate data and load demand profile. The Chapter also presents and compares the sizing result of the proposed method (IALO) with other results from ALO, PSO, and CSA. Similarly, the result obtained from the EMS algorithm of the proposed algorithm (RB-EMS-IALO)

is benchmarked with other algorithms (RB-EMS-ALO, RB-EMS-PSO, RB-EMS-CSA) and presented in this chapter. The compared results of the utilized test functions are also discussed. The comparison convergence curves for the proposed and benchmark methods are figured out and discussed in terms of cost. Consequently, the Dynamic Payback Period (DPP) analyzed using Discounted Cash Flow (DCF) analysis method is presented. Similarly, the Stochastic Monte Carlo Method implementation is used for estimating the behavior of EVs under various scenarios. The considered scenarios present the impact on the grid when having a minimum (10) units, medium (30) units, and maximum (60) units a number of EVs integrated into the grid. The obtained result of the aforementioned scenarios is also demonstrated and discussed along with the sensitivity analysis.

Chapter 5 concludes the thesis and lists the contribution of the proposed work is highlighted. Moreover, suggestions for future work areas are listed for scholars.

CHAPTER 2

LITERATURE REVIEW

2.1 Introduction

Renewable energy-based electrical systems can be obtained through a stand-alone, grid-connected, or hybrid system [20]. Stand-alone systems are widely used in rural and remote areas while grid-connected systems are suitable for urban areas due to high load demand [5]. Furthermore, the difference between the microgrid and the aforementioned systems is the capacity. However, due to the flexibility, the hybrid system can be used in both urban and rural areas [22]. Thus, the integration of many RESs comes along with economic development, employment opportunities, and knowledge acquisition of complex systems [38]. This chapter reviews and discusses the merits and demerits of RESs integration into the grid with an emphasis on Vehicle-to-Grid (V2G) technology [39]. Furthermore, high supervisory control algorithms for solving power flow problems of the microgrid system are also discussed [40]. Some of the metaheuristic algorithms for addressing optimization problems are discussed with objective functions followed by constraints. General terminologies related to V2G technology along with the impact types are discussed. Lastly, critical review analysis is followed by the gap of research that is comprehensively discussed.

Since EV has dual functionality which can act as a battery and load, it uses to shift the load from on-peak to off-peak and address the RES intermittency [15]. Many benefits can be acquired from the EVs integration such as improving RESs consumption, stabilizing the grid, decreasing grid losses, and enhancing economic efficiency [39]. Additionally, EVs increase profits from the perspective of investment, finance, reducing electricity bills, and tax payback by employing various RESs for charging and discharging [41]. All the complex microgrid hybrid systems have been supervisory controlled in order to guarantee proper operation for all integrated components and to maintain the supply of power [42]. The supervisory control layers

can be defined as the approaches for controlling the behavior of power in components [43]. Among the demonstrated layers in Figure 2.1, this study is limited to exploiting supervisory control in order to flow the power smoothly among the system components. The supervisory control algorithms classify into Rule-Based (RB), Optimization-Based (OB), and Learning-Based (LB) [28].

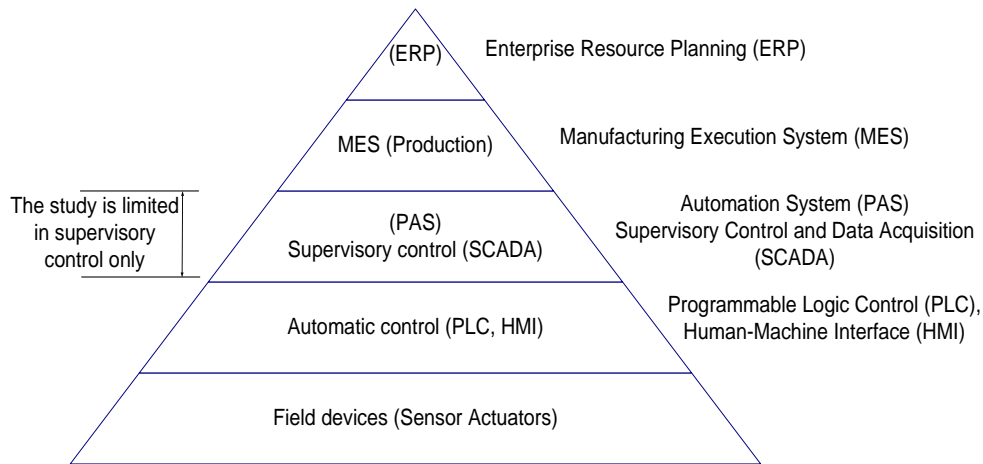


Figure 2.1 Pyramid automation layers for supervisory control [43], [44].

The first three presented levels, Enterprise Resource Planning (ERP), Manufacturing Execution System (MES), Process Automation System (PAS), and Supervisory Control and Data Acquisition (SCADA) are important levels for the manufacturing process. However, this study is limited by considering SCADA due to the consideration of the residential level and using software for optimization purposes. Besides, SCADA is responsible for monitoring the behavior of the flow of power in the system. While Programmable Logic Control (PLC), Human-Machine Interface (HMI), and Filed devices are not considered [44].

2.2 Microgrid Architecture

A microgrid can be defined as “*A group of interconnected loads and Distributed Energy Resources (DERs) within clearly defined electrical boundaries that acts as a single controllable entity with respect to the grid, which can connect and disconnect from the grid to enable it to operate in both grid-connected and island-*

connected mode" [3]. Further classifications of a microgrid are based on the operation modes, as an on-grid and an off-grid which is shown in Figure 2.2 [20]. The on-grid (grid-connected) system performs better than the off-grid (grid-isolated) that is reducing the cost and reliability [45], [46].

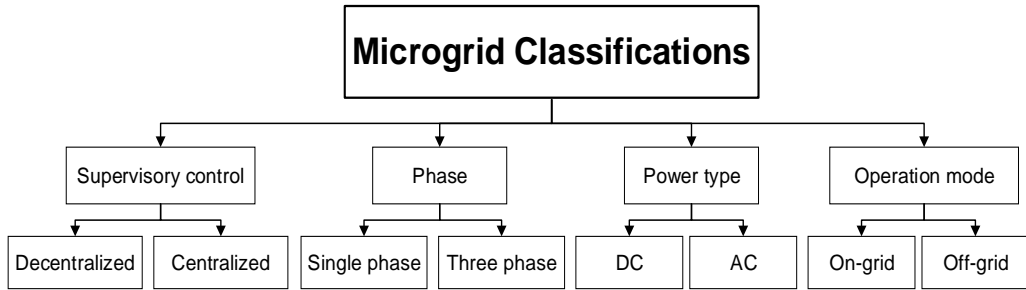


Figure 2.2 Microgrid classifications [3], [20].

In terms of supervisory control, the two types of supervisory control as classified in Figure 2.2 are decentralized and centralized [47]. The decentralized can be termed as distributed charging and the EV directly chooses its schedule for charging. However, it cannot guarantee achieving the global optimal solution. Besides, centralized refers to the master charging control and scheduled EV charging. The faced limitation of centralized charging is the optimization sizing when using a large amount of EVs. The aforementioned issue has been addressed by hierarchical-based control along with other control strategies such as online control and real-time charging [10]. The hierarchy represented the control method for communication and computational requirements [18].

Generally, a microgrid can be formed as a grid-connected and stand-alone system using different bus bars that are classified into three groups which are AC, DC, and DC/AC [48]. A bus bar refers to the junction between income and the outcome of electric components meeting together where the voltage is constant [3]. In addition, electric circuit diagrams of the various bus bar classification are shown in Figure 2.3. The features, benefits, and limitations of different microgrid bus bars are tabulated in Table 2.1. Due to the provided benefits of the grid-connected system, numerous researchers discussing them [3], [45], [46].

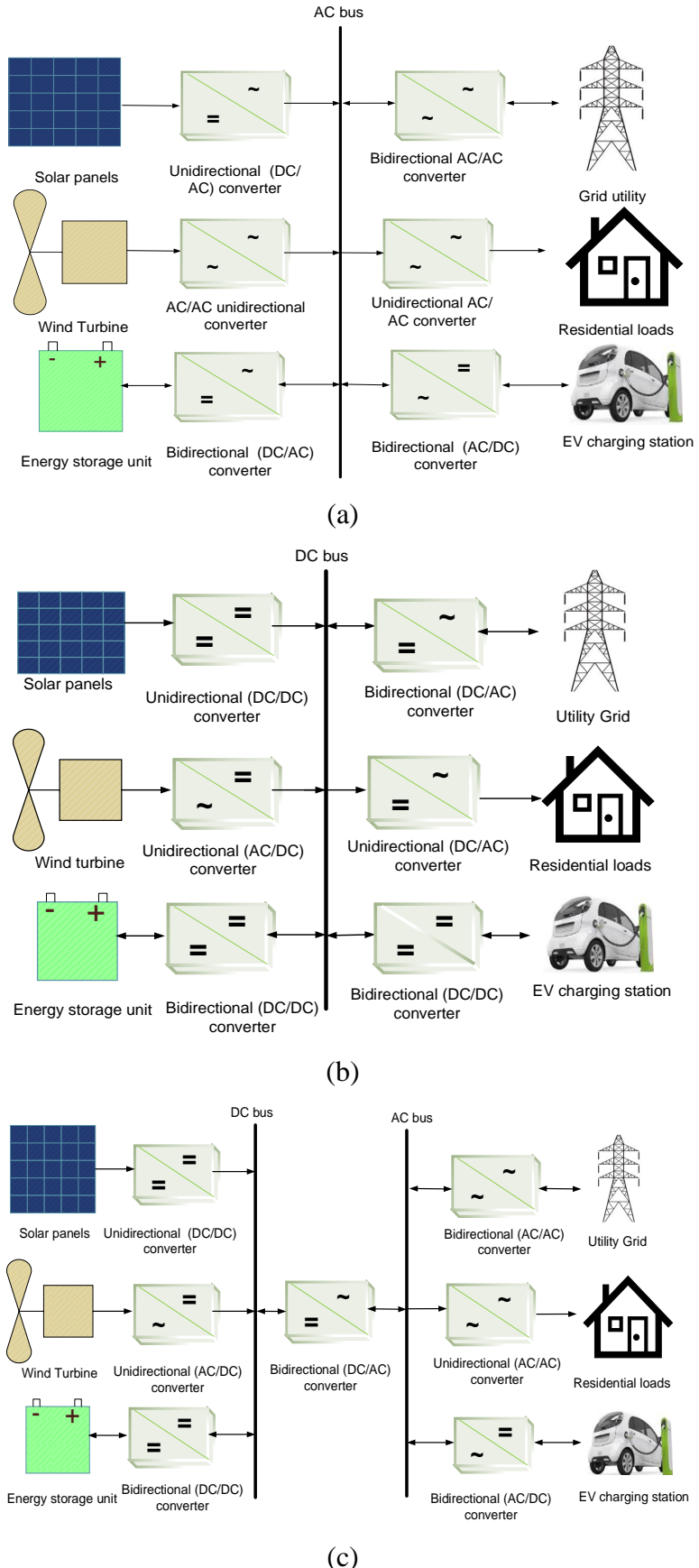


Figure 2.3 Hybrid microgrid bus bars. (a) AC bus, (b) DC bus, and (c) DC/AC bus [48], [49].

Table 2.1 Summary of the state-of-the-art of microgrid bus bars [48]–[50].

	AC microgrid bus	DC microgrid bus	DC/AC microgrid bus
Features	<ul style="list-style-type: none"> The ability to connect AC RESs directly to the AC bus or via AC/AC converter. Widely used in industries. 	<ul style="list-style-type: none"> Widely used in low-power applications. Reduce the losses. 	<ul style="list-style-type: none"> Most complex system. Preferably used due to its cost-effectiveness and flexibility of using AC and DC sources. Reduce power losses.
Merits	Low initial cost.	<ul style="list-style-type: none"> Low initial cost. Less maintenance. Operationally simple. Only one DC bus with converters to convert the power form. 	<ul style="list-style-type: none"> Provide maximum reliability and flexibility in the supply. Continuity of power supply.
Demerits	High maintenance cost.	<ul style="list-style-type: none"> The system will not supply the AC load in case of failures in the inverter. 	<ul style="list-style-type: none"> High maintenance cost Complexity in controlling.

The commonly used bus is the hybrid (DC/AC) instead of the DC bus due to the provided advantages such as lower conversion steps and improved efficiency [51]. However, it is a complex system due to the integration of various sources and power convergence.

2.3 Energy Management Strategy Algorithms

The EMS is a controlling algorithm used to reduce the cost and increase the lifetime of components [52]. Additionally, EMS classify into RB, OB, and LB as will be further explained in the next subsection. The main aim of using EMS is to balance the energy demand and production in the microgrid system by maximizing self-consumption using different metaheuristic algorithms [2]. Furthermore, EMS is coupled with optimization methods to ensure the continuity of load supply, minimize BT degradation, maximize the use of RESs, and decrease the cost of energy production [35].

However, choosing a proper metaheuristic algorithm in planning, sizing, and designing the microgrid systems is a difficult task due to the different behavior of algorithms and parameter details [47]. These may include some of the nature-inspired algorithms such as GOA, ALO, and PSO for their changing premature convergence and acquiring the local optima in the search space. The operation and management problems in the microgrid system is a complex problem that needs a suitable method to obtain an optimal solution such as EMS [53]. The output power from RESs is intermittent in nature thereby causing reliability issues, this challenge can be addressed by exploiting the energy storage system [2]. However, this approach requires a control strategy to coordinate and ensure an effective flow of power in the system smoothly [52].

2.3.1 Rule-Based Energy Management Strategy

The RB is a control-based algorithm that relies on human knowledge and can be implemented using different decisions as shown in Figure 2.4 [54]. This control technique can significantly optimize the accuracy of calculation and decrease the computation problem. Besides, acquiring a high-quality optimum solution when solving complex optimization problems [55]. The RB algorithm is defined as a condition of the *if-then* statement and can be classified into two groups which are deterministic RB and fuzzy-logic RB [56]. Furthermore, the classification of RB is tabulated in Table 2.2 and further explained in Figure 2.5, respectively [27]. The deterministic RB is used to control the flow of power in the microgrid system [20]. Similarly, the fuzzy logic RB is also *if-then* statement dependent, which is considered for EMS benchmarking in the literature due to its powerful and effective outcomes [35]. Simultaneously it can be integrated with other methods [28]. Likewise, it is used to control the charging and discharging process, but deterministic RB is performing better [18], [35]. Meanwhile, the fuzzy-logic method is providing an accurate result for a special predefined driving cycle but cannot guarantee optimal performance with other problems [57], [58].

In a microgrid, the EMS is an essential control for the optimal use of distributed energy in a secure, intelligent, and coordinated form [3]. Furthermore, the conducted

RB has been utilized in various studies to control the flow of power to charge the EV, BT, and appliances. In [57], the distributed power in a microgrid controlled by RB-EMS considers the PV/WT/BT [59]. Additionally, EV [27]. RB-EMS is used as an optimal power distribution to meet the design requirements for managing [60].

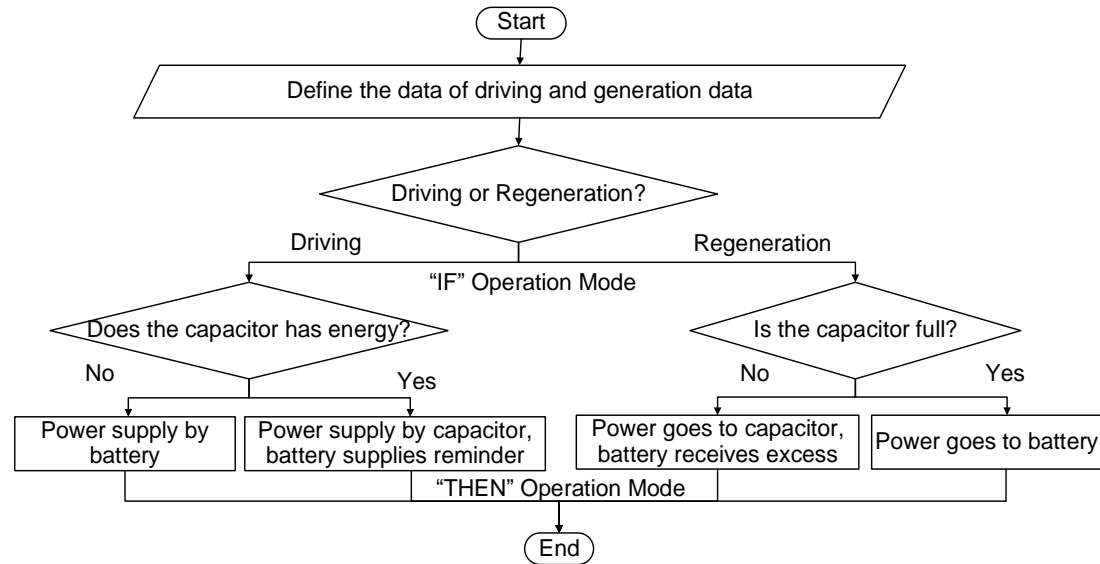


Figure 2.4 Sample of the rule-based algorithm [27], [28], [56].

2.3.2 Optimization-Based Energy Management Strategy

An OB is a control-based algorithm that is used to enhance the performance of the microgrid systems as used in many applications [61]. It is an easy computing algorithm that can be guided toward a variety of different optimization difficulties [61], however, it faces difficulties in addressing constraints [62]. The OB can be categorized into global optimization and real-time optimization as tabulated in Table 2.2 and shown in Figure 2.5. Furthermore, other methods such as Pontryagin's Minimum Principle (PMP) [20], Model Predictive Control (MPC) [41], and Equivalent Consumption Minimization Strategy (ECMS) [61] are reported to optimize different systems [28].

2.3.3 Learning-Based Energy Management Strategy

The LB is a control-based algorithm implemented for machine-learning purposes such as data mining schemes for real-time information to enhance system performance [58]. It is classified into reinforcement, supervised, unsupervised, and neural network as tabulated in Table 2.2 and shown in Figure 2.5. It differs between the RB and OB in making control decisions that no longer require the previous information [28].

Table 2.2 Energy Management Strategy classification [20], [56], [58], [63].

Strategies	Classifications	Advantages	Drawbacks
Rule-based	Deterministic Rule-Based Method	<ul style="list-style-type: none"> A complex mathematical equation is not required. Future data is not required. Faster decision-making. Low computational time. Small storage is required. Provide an exact solution. 	<ul style="list-style-type: none"> More technical knowledge is required to be implemented. It is not the best-predicting tool in terms of performance.
	Fuzzy Rule-Based Method		
Optimization-based	Real-Time Optimization	<ul style="list-style-type: none"> Effective for hard optimization problems. Less technical knowledge is required to implement it. It adopts a specific financial model regarding profitability and losses. Implemented for real-time application 	<ul style="list-style-type: none"> Mathematical equations are required. Complexity increases with an increased number of system variables (components) High computational time High storage is required.
	Global Optimization		
Learning-based	Reinforcement	<ul style="list-style-type: none"> Adaptive and learning capability Model-free control 	<ul style="list-style-type: none"> Time-consuming. It is difficult to use.
	Supervised and unsupervised		
	Neural network		

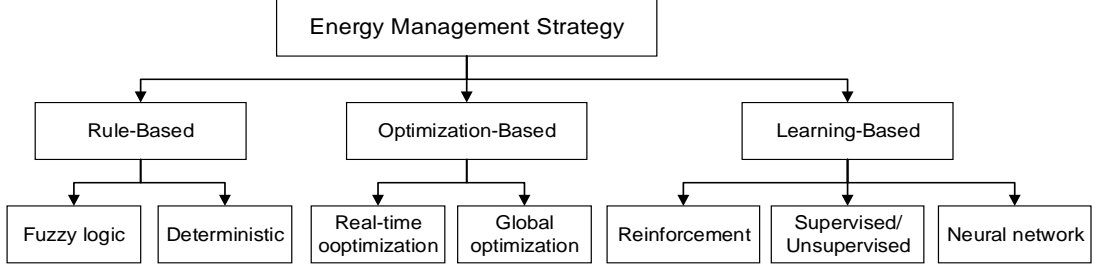


Figure 2.5 Classification of widely used energy management strategies [56], [61].

2.4 Microgrid Sizing Optimization Algorithms

Generally, optimization can be defined as the process to find the best solutions among the available alternate solutions for a particular problem [64]. Sizing and power flow control in RESs is a very difficult task due to the different characteristics of the system components and the objective function. Microgrid sizing optimization algorithms can be used to overcome the design variable limitations and they classify into stochastic and deterministic [65]. The “stochastic” is derived from Greek words that mean “target” or “aim” [54]. Furthermore, stochastic algorithms have a high probability as compared to the deterministic method and can be categorized into: heuristic and metaheuristic which are sub-division of Artificial Intelligence (AI) algorithms [54].

There is not much difference between heuristic and metaheuristic algorithms. The former refers to “to find” or “to discover or by trial error”. The latter refers to the further developments of the heuristic by adding the prefix “meta”, where meta means “beyond” or “higher” level as reported in the state-of-the-art [54]. In addition, the heuristic can be also defined as a technique designed to gain a balance between exploration and exploitation (Diversification and Intensification) or (Global and Local search). Thus, metaheuristic algorithms have the ability to effectively improve calculation accuracy and reduce the computation burden. In addition, obtain higher-quality results while solving complex optimization problems [66]. Moreover, there is no agreed definition in the literature for the two mentioned stochastic algorithms because they are exchangeable terms [21].

Optimal sizing of hybrid system components can be achieved by using either software tools or conventional nature-inspired metaheuristic algorithms [67]. The nature-inspired algorithms are used to achieve the optimum approach for optimization problems and classify into three groups which are trajectory, evolutionary, and swarm-based as shown in Figure 2.6 [68]. The software tools presented in the literature such as HOMER [69], RETScreen [70], iHOGA [47], MATLAB/Simulink [20], and TRNSYS are used for modeling and control systems [31], [56]. Software tools are widely used in the power systems industry because of their well-accepted accuracies [67]. However, some of the challenges faced by software tools are single-function minimization, black box coding, and the need for more computing time [67].

The metaheuristic algorithms address the shortcomings in hybrid systems while using software tools to achieve an optimal number of components [71]. Some of the metaheuristic methods will be presented in the following subsections which include Antlion Optimization (ALO) [33], Particle Swarm Optimization (PSO) [31], and Cuckoo Search Algorithm (CSA) [32]. The major issue associated with metaheuristic methods is the complex computation equations required to get a reasonably good solution [4]. It overcomes V2G issues such as alleviating power losses, reducing production costs, and others.

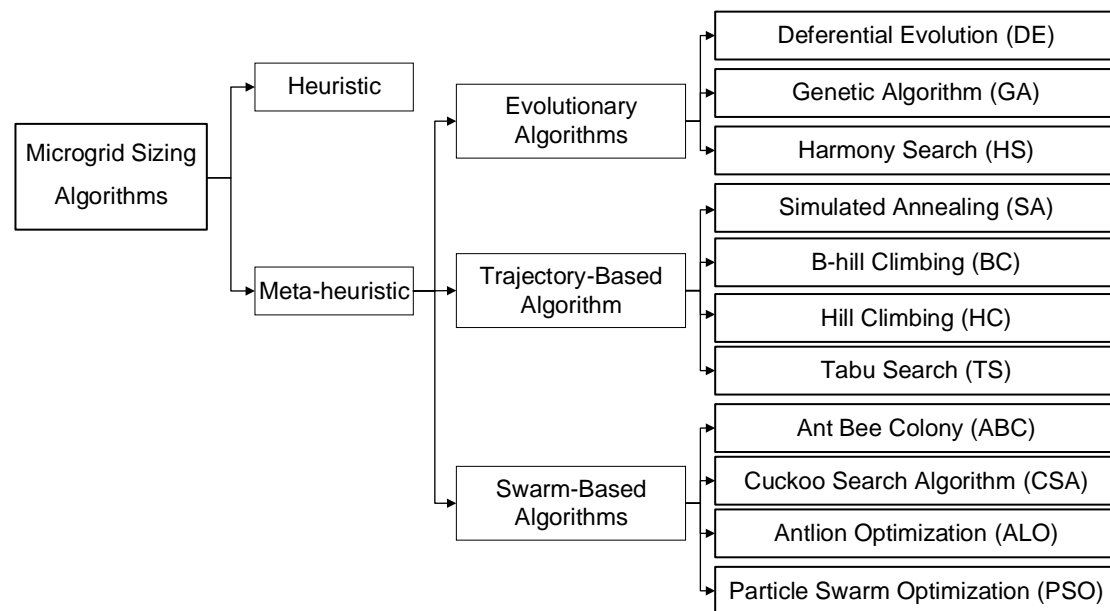


Figure 2.6 Classifications of microgrid sizing algorithms [61], [67], [68].

Evaluation-based, trajectory-based, and swarm-based are classified under sizing metaheuristic algorithms and counted for solving optimization problems. The first mentioned mimics the evolutionary principle of survival of the fittest (population), the second mention begins with a single provisional solution moving to the next neighbor which means staying in the same search space, and the last mentioned instance imitates a group of animals looking for food, respectively [68].

2.4.1 Antlion Optimization

The ALO is a metaheuristic algorithm introduced in 2015 by Seydali Mirjalili to address the constraint of continuous optimization problems [33]. In terms of applications, ALO got attention among scholars in many fields such as power system optimization problems for sizing the system components [72], networks, and benchmarking functions [67]. Additionally, smart grid systems, feature selection, and others [73]. It has been chosen due to the less number of parameters in comparison with the counterparts. However, it has some limitations such as premature convergence and acquiring a quick local solution and near-global optima [74]. Due to the aforesaid limitations, the ALO needs to be improved. ALO has attracted so much interest from scientific researchers due to making use of exploitation and exploration because it uses random walks. Random walking is responsible for causing premature convergence and stagnation as ALO challenges [75]. Additionally, a random process called a "random walk" involves taking a sequence of subsequent random steps [54]. The ALO algorithm mimics or emulates the hunting behavior of antlions (predators) searching for food like other insects (prey), the hunting steps of antlion are listed below [74].

- Random walk of ants
- Trapping in antlion traps
- Building traps
- Sliding ants toward antlion

- Catching the prey (ant) and rebuilding the traps
- Elitism (best solution).

The foregoing mechanism steps of the algorithm are shown in Figure 2.7 from (a-f) as illustrated in Figure 2.7 (a) and mathematically expressed from Eq. (2.1) - Eq. (2.13) and explained in Figure 2.9. Besides, the life cycle of the antlion is demonstrated in Figure 2.7 (b). The stage of hunting is the Larvae stage which has longer life while the adult stage is the shorter stage that is spent in reproduction. The size of the trap (cone shape) depends on the level of hunger or during the middle of the month (full moon) [33]. Since the ant is stochastically moving (random walk), it has been mathematically chosen by Eq. (2.1).

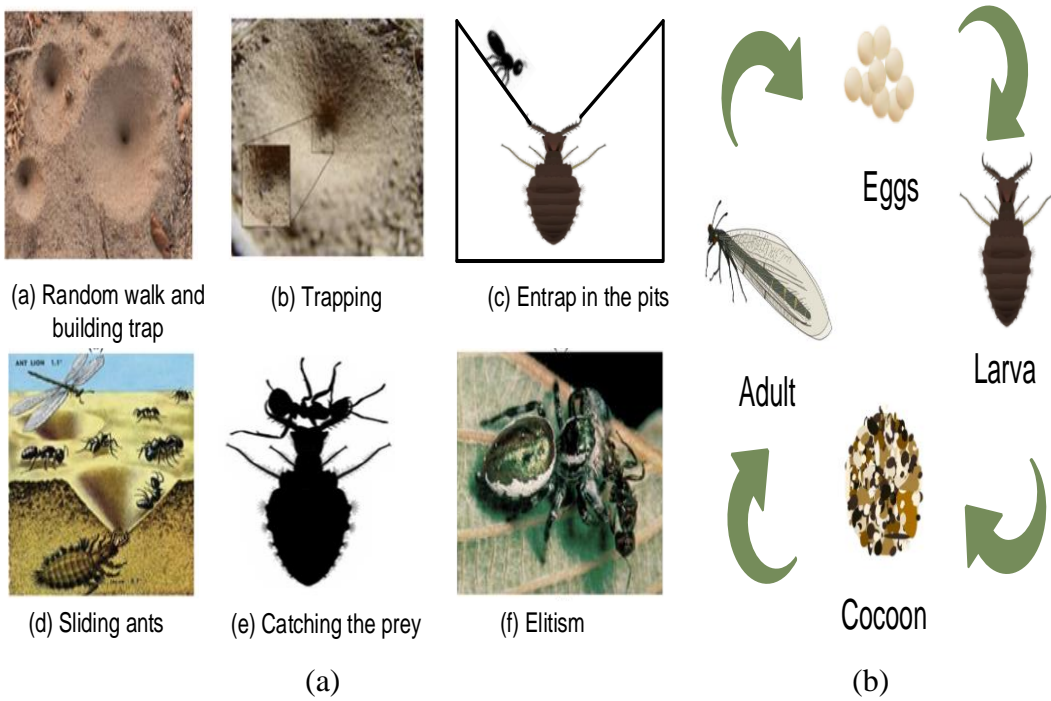


Figure 2.7 The process of the Antlion Algorithm (a) Hunting mechanism and (b) Life cycle [33].

$$X(t) = [0, \text{cumsum}(2r(t_1) - 1, \text{cumsum}(2r(t_2) - 1, \dots, \text{cumsum}(2r(t_n) - 1,] \quad (2.1)$$

where *cumsum* is the computed cumulative sum, *t* refers to the step of random walk (iterations), *n* is the maximum number of iterations, *r(t)* defined as the stochastic function and can be mathematically expressed in Eq. (2.2) [33].

$$r(t) = \begin{cases} 1 & \text{if } \text{rand} > 0.5 \\ 0 & \text{if } \text{rand} < 0.5 \end{cases} \quad (2.2)$$

where *rand* is the random number generated with uniform distribution in the interval of [0,1]. The random walk of the ants to attain the ant's position is presented in Eq. (2.3).

$$M_{Ant} = \begin{bmatrix} A_{1,1} A_{1,2} \dots A_{1,d} \\ A_{2,1} A_{2,2} \dots A_{2d} \\ \vdots & \vdots & \ddots & \vdots \\ \vdots & \vdots & \ddots & \vdots \\ \vdots & \vdots & \ddots & \vdots \\ A_{n,1} A_{n,2} \dots A_{n,d} \end{bmatrix} \quad (2.3)$$

where M_{Ant} is the saving position of ants, d is the number of variables, and $A_{i,j}$ refers to the dimension of i and j iterations. The behavior of ants in ALO is similar to the particles in PSO. The evaluation of each ant in the ALO can be prevented by utilizing the (fitness) objective's function (f) as shown in the matrix in Eq. (2.4) for storing the fitness values (M_{OA}) of all ants.

$$M_{OA} = \begin{bmatrix} f(|A_{1,1} A_{1,2} \dots A_{1,d}|) \\ f(|A_{2,1} A_{2,2} \dots A_{2d}|) \\ \vdots & \vdots & \ddots & \vdots \\ \vdots & \vdots & \ddots & \vdots \\ \vdots & \vdots & \ddots & \vdots \\ f(|A_{n,1} A_{n,2} \dots A_{n,d}|) \end{bmatrix} \quad (2.4)$$

In addition, to obtain the position of the antlion ($M_{AntLion}$) and store the objective function (fitness) of all antlions (M_{OAL}) that can be obtained through the following matrices Eq. (2.5) and Eq. (2.6), respectively. The $AL_{i,j}$ refers to the dimension of i and j iterations.

$$M_{AntLion} = \begin{bmatrix} AL_{1,1} & AL_{1,2} & \dots & AL_{1,d} \\ AL_{2,1} & AL_{2,2} & \dots & AL_{2d} \\ \vdots & \vdots & \ddots & \vdots \\ \vdots & \vdots & \ddots & \vdots \\ AL_{n,1} & AL_{n,2} & \dots & AL_{n,d} \end{bmatrix} \quad (2.5)$$

$$M_{OAL} = \begin{bmatrix} f(|AL_{1,1} AL_{1,2} \dots AL_{1,d}|) \\ f(|AL_{2,1} AL_{2,2} \dots AL_{2d}|) \\ \vdots \\ \vdots \\ f(|AL_{n,1} AL_{n,2} \dots AL_{n,d}|) \end{bmatrix} \quad (2.6)$$

The hunting mechanism presented in Figure 2.7 (a) is mathematically elaborated as follows as the operator of the antlion algorithm.

- Random walk of ants

The random walk as presented in Figure 2.8 is obtained based on Eq. (2.1) in order to update the position of each ant using Eq. (2.3). Eq. (2.3) is used to update the position of each ant while keeping the random walk (X_i^t) by using Eq. (2.7). Eq. (2.7) should be implemented in each iteration to guarantee the happening of random walks inside the design space or what is known as the search space.

$$X_i^t = \frac{(X_i^t - a_i) \times (d_i^t - C_i^t)}{(b_i - a_i)} + C_i^t \quad (2.7)$$

where a_i and d_i^t are the minimum $a_i = \min(X_i^t)$ and maximum $b_i = \max(X_i^t)$ normalization of random walking. While the C_i^t is the minimum and d_i^t is the maximum of i^{th} variable at t^{th} the iteration that can be calculated by Eq. (2.8) and Eq. (2.9), respectively [76].

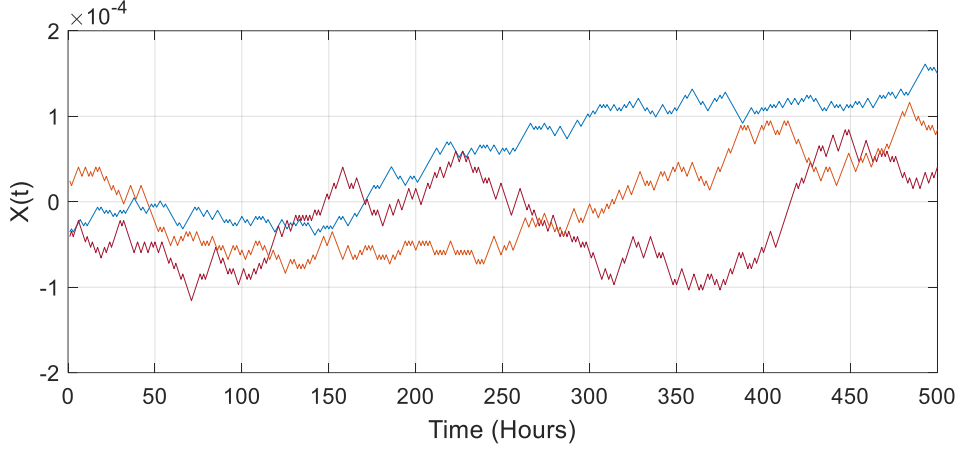


Figure 2.8 The ant and antlion stochastic walk.

- Trapping antlions pits

The random walks of ants are affected by antlions' traps. This effect can be mathematically expressed as presented in Eq. (2.8) and Eq. (2.9), respectively.

$$C_i^t = \text{Antlion}_j^t + C^t \quad (2.8)$$

$$d_i^t = \text{Antlion}_j^t + d^t \quad (2.9)$$

where C_i^t and d_i^t are the minimum and maximum of all variables at the iteration of ant of t^{th} , while the Antlion_j^t is the position of the selected j^{th} antlion at t^{th} iteration as presented in Eq. (2.5). While C^t and d^t are vectors in a spherical shape bounded chosen for ants and ant lion swarm randomly of all variables at t^{th} iteration.

- Building traps

Antlion has the ability to hunt and build traps. Additionally, antlion has a high possibility to catch ants due to the selected function exploited which is Roulette Wheel Selection (RWS). The RWS is a feature selection method that is responsible for achieving the local optima and the causes of stagnation.

- Sliding ants against toward antlion

Equations (2.10) and (2.11) run for the behavior of the escaping ants from the antlions' trap and sliding ants down (trapped) and updating the maximum and minimum variables randomly. The operation of sliding once the antlion detects an ant in the trap, antlions spray sand outward from the center of the hole.

$$C^t = \frac{C}{I} \quad (2.10)$$

$$d^t = \frac{d}{I} \quad (2.11)$$

where the C^t and d^t are the minimum and maximum of all variables at t^{th} iteration. While I is the sliding ratio that is equals $10^w \frac{t}{T}$ which is increasing during the optimization process. Besides, it uses to control the exploration and exploitation rate. The w refers to the constant of the defined current iteration and adjusting the accuracy level of exploitation which depends on t value. The t is the current iteration, and T is the maximum number of iterations.

- Catching prey and rebuilding the traps

As the stages of hunting by antlion, catching prey, and rebuilding the traps are the last steps after pulling the ant body inside the pits using its jaw for catching the prey and then rebuilding the pits. The aforementioned operation can be mathematically mimicked and updated the position for a new catching chance depending on the fitness value of the ant by Eq. (2.12).

$$Antlion_j^t = Ant_i^t, \quad if \quad f(Ant_i^t) > f(Antlion_j^t) \quad (2.12)$$

where $Antlion_j^t$ present the position of selected j^{th} at t^{th} iteration while the Ant_i^t shows the position of i^{th} of ants at t^{th} iteration and t present the previous iteration.

- Elitism

The term elitism refers to the best-obtained solution (best antlion) and can be obtained by Eq. (2.13) which shows the saved iteration from each step. It assumed for each ant walks randomly around the selected antlion considering the RWS and elite at the same time. The selection of the roulette wheel gives the fitness values of all the individuals and then each person is put on a wheel based on the percentage value of the total fitness sum [77].

$$\text{Ant}_i^t = \frac{R_A^t + R_E^t}{2} \quad (2.13)$$

where Ant_i^t indicate the position of i^{th} ant at t^{th} iteration, while R_A^t and R_E^t are the random walk around the antlion selected by RWS and the random walk around the elite, respectively. Figure 2.9 present the flowchart of the ALO algorithm.

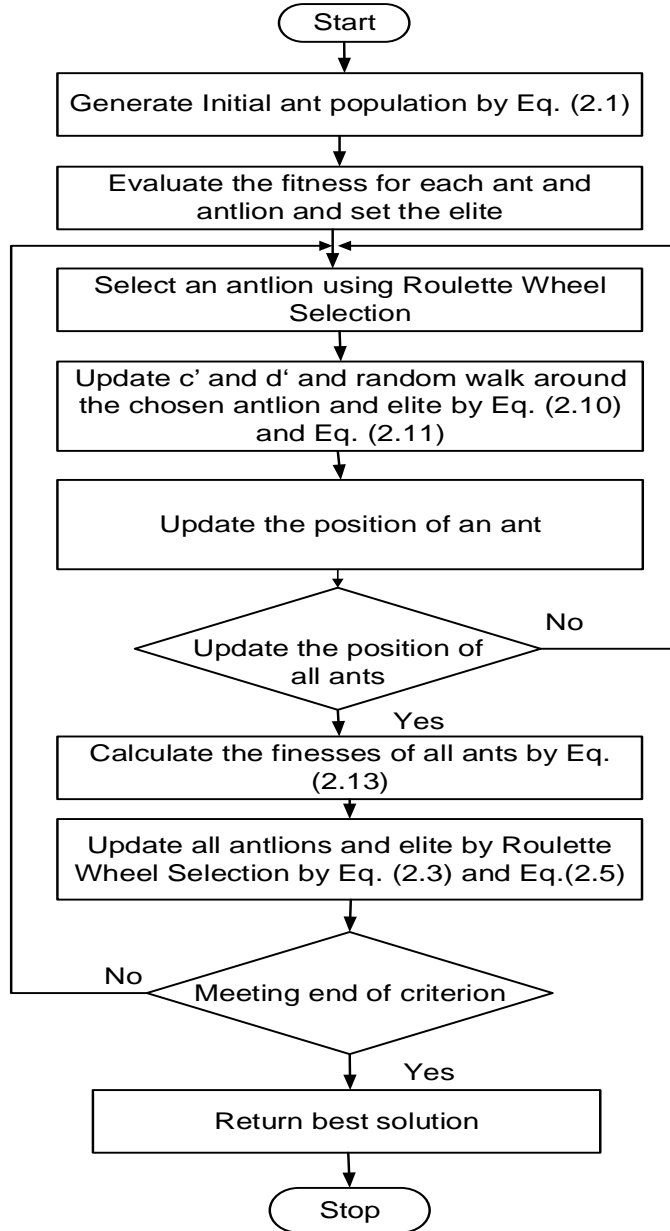


Figure 2.9 Flowchart of the antlion optimization algorithm [78].

The original ALO has been improved to size the number of configurations on the system to meet the proposed objectives and applied to address different problems in the literature [75]–[77], [79]–[88]. Some of ALO listed improvements are as follows: Enhanced Antlion Optimization Algorithm (EALO) [89], Modified Ant Lion Optimization Algorithm (MALO) [90], Tournament Selection Techniques Antlion Optimization algorithm (TSALO) [84], and other as tabulating in Table 2.3. While the Advantages and Disadvantages of ALO are tabulated in Table 2.4. Due to the tabulated drawbacks in Table 2.4 for ALO force to be enhanced.

Table 2.3 Variations of antlion optimization.

List of Improved ALO	Features	Ref.
IALO-ANN	Improvement has been done in the elitism operator of ALO hybridized with Artificial Neural Network	[83]
IALOT	<ul style="list-style-type: none"> Improved ALO using Tournament Selection instead of RWS as a feature selection as it provides a negative fitness value to reduce the running time. Implement (IALOT) to address Parallel Machine Scheduling (PMS) problem. 	[84]
TALO		[91]
IALO- VOA	Introducing new decreasing boundaries instead of step-by-step decreasing for shrinking of the boundary to decrease the Various Optimization Algorithm (VOA).	[85]
OB-ac-ALO	Opposition-Based acceleration coefficient (OB-ac) to reduce the order of time-invariant systems used in ALO	[86]
OB-C-ALO	Based on OB-Cauchy distribution-ALO in clustering the data.	[87]
LALO &OB ALO OB-LF-ALO	<ul style="list-style-type: none"> Using opposition-based Laplacian-ALO-Lévy flight random walk instead of uniform distribution random one It can examine large search spaces. 	[75] [88]
IALO-SCPSP	Replace RWS with spiral complex path searching patterns <ul style="list-style-type: none"> To breakthrough steps to enhance diverse exploration Through exploitation in each group 	[76]
IALO-NM	Hybridized with the Nelder-Mead algorithm to detect structural damage by improving the weighted trace lasso regulation	[79]
IALO-CMT	<ul style="list-style-type: none"> Using the absolute value of fitness value before applying the roulette wheel selection Additionally, integrating IALO into Chaotic Mapping Theory with initialization and random walk process 	[80]
P-ANN-IALO	Hybridized Parallel ALO with Artificial Neural Network in order to increase the power transfer capability between the source and load.	[81]
ALO-DM	<ul style="list-style-type: none"> ALO- Combining differential mutation techniques to enhance population diversity and obtain an effective solution. 	[92]
EALO	<ul style="list-style-type: none"> Enhanced ALO to improve the accuracy of thyroid diseases. They apply a stochastic function to generate a random number between [0,1] instead of a uniform distribution function. 	[89]

Table 2.4 Advantages and disadvantages of antlion optimization [74], [91].

Advantages	Disadvantages
<ul style="list-style-type: none"> • Easy adjustable. • Simply implemented. • Fast calculation speed. • High efficiency. • Good convergence. • Solving the economic dispatch issues for determining the generation. 	<ul style="list-style-type: none"> • The premature convergence is suffering. • Easily acquire the local optima or near-global value (stagnation). • Long-running time is caused by random walks.

2.4.2 Particle Swarm Optimization

The PSO as a very well-known algorithm was originally introduced by Kennedy and Eberhart in 1995 and has been applied in different scientific fields [93]. Figure 2.10 described the procedure mechanism of the PSO algorithm which start at the initial step (x_t^i), and then proceed to the new position (x_{t+1}^i) [94]. The PSO is a stochastic-based algorithm based on swarms that study the animal's social behavior where swarms are made up of a group of individuals known as particles. Each generation made an iteration of procedures of many particles. Every update in the algorithm is recorded for the global optimal best (p_t^g) and current velocity (v_t^i) by replacing the current position in order to satisfy the ending condition. The benefits and drawbacks of the PSO are tabulated in Table 2.5.

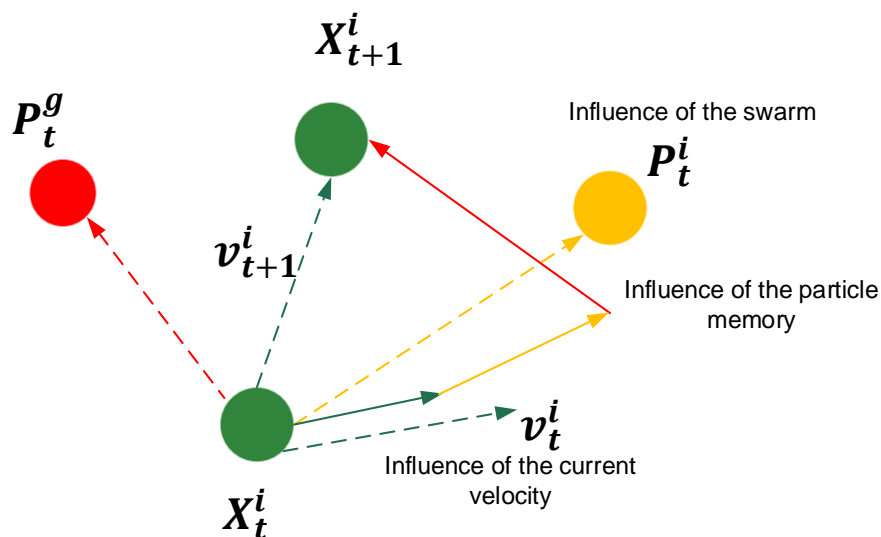


Figure 2.10 Particle swarm optimization algorithm mechanism.

PSO has been widely used due to its good quality solution provided for local search strategy. The PSO algorithm mechanism is mathematically presented in Eq. (2.14) and Eq. (2.15).

$$x_{t+1}^i = x_t^i + v_{t+1}^i \quad (2.14)$$

$$v_{t+1}^i = wv_t^i + c_1r_1\{P_{besti} - x_t^i\} + c_2r_2\{p_t^g - x_t^i\} \quad (2.15)$$

where x in Eq. (2.14) presents the particle position and v is the particle velocity in the iteration t . Eq. (2.15) presents the w which is the inertia weight damping ratio, c_1 and c_2 are learning coefficient or acceleration factors for P_{besti} and G_{best} equals 2, respectively. Moreover, r_1 and r_2 are random numbers between 0-1.

Table 2.5 Advantages and disadvantages of particle swarm [93]–[95].

Advantages	Disadvantages
<ul style="list-style-type: none"> • Easy and simple coding implementation. • Easy to find literature examples. • Robustness to control parameters. • Computational efficiency by generating high-quality solutions with shorter calculation time and stable convergence. • Have a few parameters to tune/adjust. • Less programming (math) complexity. • Fast convergence speed. • Free derivative algorithms can be used to solve any type of optimization problem. 	<ul style="list-style-type: none"> • Relatively lower performance for finding the global optimum compared to GA. • Not suitable for complex problems with a great number of parameters. • Can be difficult to define the initial design parameters. • Can converge prematurely and be trapped into a local minimum, especially with complex problems.

It is simulating the social behavior of the animals such as fish schooling and bird flocking as reported in the literature and further shows the flowchart in Figure 2.11 [31], [93]. The utilization of PSO is in a vast area of research such as network applications, size design, optimal shape, communication networks, and others as reported in the literature [94], [96].

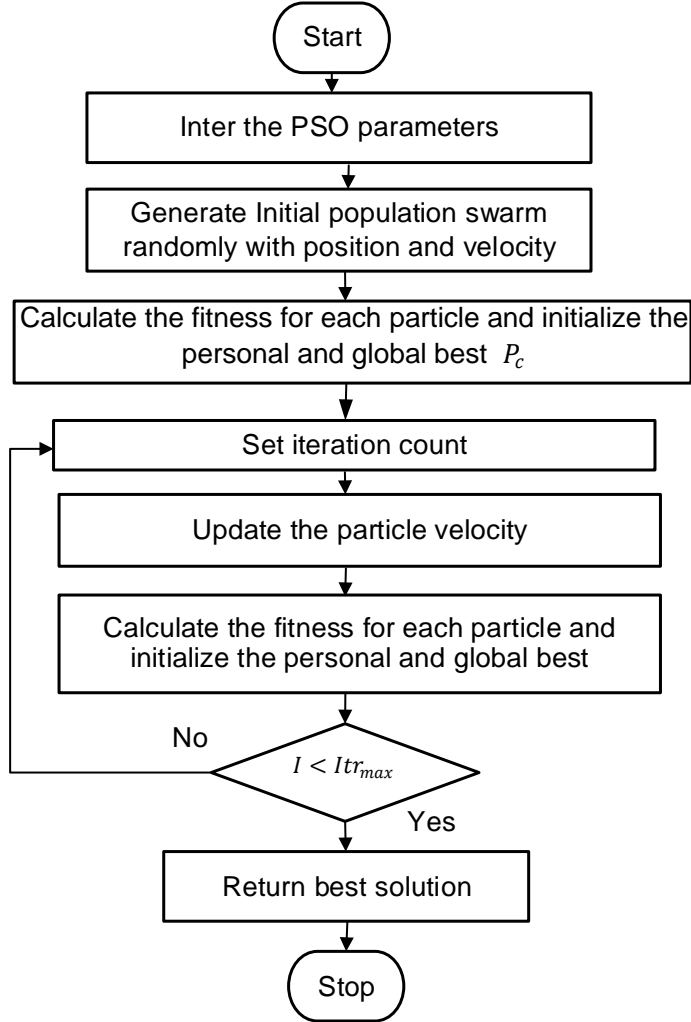


Figure 2.11 Flowchart of particle swarm optimization procedure.

2.4.3 Cuckoo Search Algorithm

The CSA is a recent nature-inspired metaheuristic algorithm developed by Xin-She Yang and Suach Deb in 2009 to solve structural optimization tasks and was improved in 2011 by Rajabioun [97]. The algorithm is inspired by fascinating the behavior of cuckoo birds that lay their eggs in the nest of other host birds [98]. It has a unique strategy of laying an egg in the nest while the cuckoo can lay an egg at a time. Moreover, it is a combination of some cuckoo species with lévy flights rather than the simple isotropic random walk as mathematically expressed in Eq. (2.16) - Eq. (2.18) [97].

$$x_i^{(t+1)} = x_i^{(t)} + \alpha_{step} \otimes \text{lévy}(\lambda) \quad (2.16)$$

where $x_i^{(t+1)}$ refers to generating a new generation, α_{step} is the step size and equals 1 that can be mathematically expressed as in Eq. (2.17), $x_i^{(t)}$ is the previous location, \otimes is entry-wise multiplication. Where the lévy value ranges between 1-3 as shown in Eq. (2.18).

$$\text{Levy} \sim u = g^{-\lambda} (1 < \lambda \leq 3) \quad (2.17)$$

$$\alpha = O\left(\frac{L}{10}\right) \quad (2.18)$$

The L refers to the lévy flight (lévy walk) method and 10 means the number of nests or different solutions. Additionally, the value of α should be greater than 0 in order to supervise the scale of L, u refers to the uniformly distributed value [1,3]. and O is a scale qual 1 used to balance the α to be greater than 0 [99]. Additionally, if the bird discovers the egg is not its own, it may throw it (worse solution) or leave the nest and build a new one (optimum solution).

Besides, some of the utilized applications of CSA were reported in the literature and used in various files [100]. CSA functioned to address engineering optimization problems, scheduling, supplier selection, data fusion in wireless sensor networks, and others as reported in the literature [101][102]. The presented birds in Figure 2.12 refer to the cuckoo bird and the blue color refers to the eggs with different seniors. The inspiration mechanism steps of laying eggs in the nests of host birds are obligate brood parasitism by searching for other ready nests considered as searching path (C1 and C2) in Figure 2.11 by stating their actions (L1 and L2) as shown in Figure 2.11.

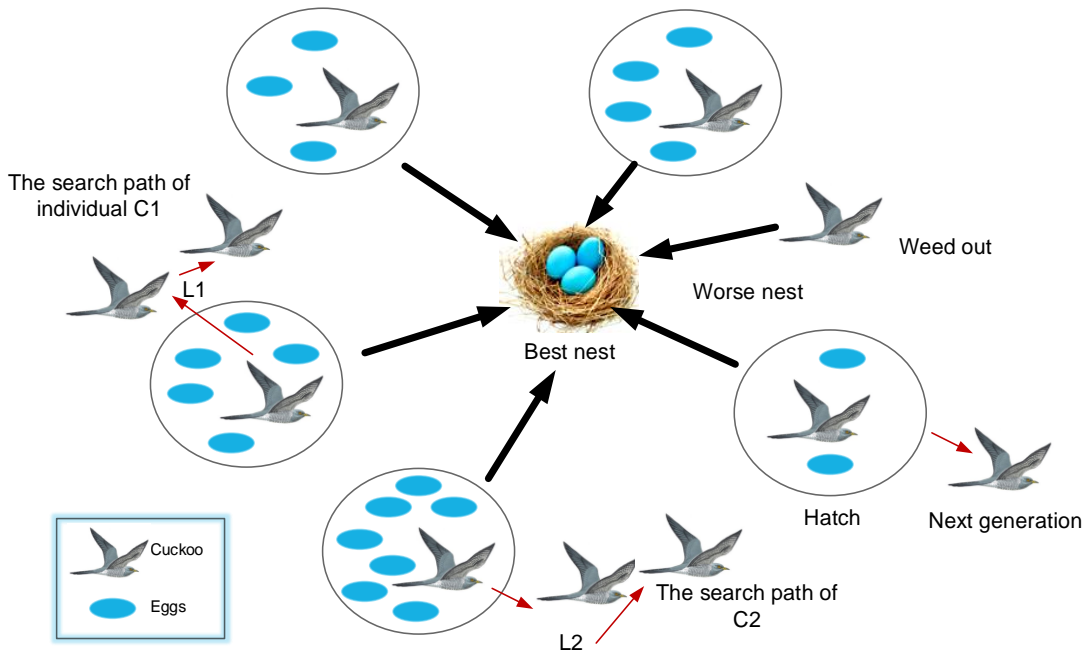


Figure 2.12 Cuckoo search algorithm mechanism [75], [88].

Some birds engage in direct conflict with intruding cuckoos at (worst nest) where some birds discover the eggs are not their own (when hatched as a new generation). After that, they either throw them away (weed out) or simply leave their nests and build another nest in another place. The flowchart of CSA is demonstrated in Figure 2.13 [68].

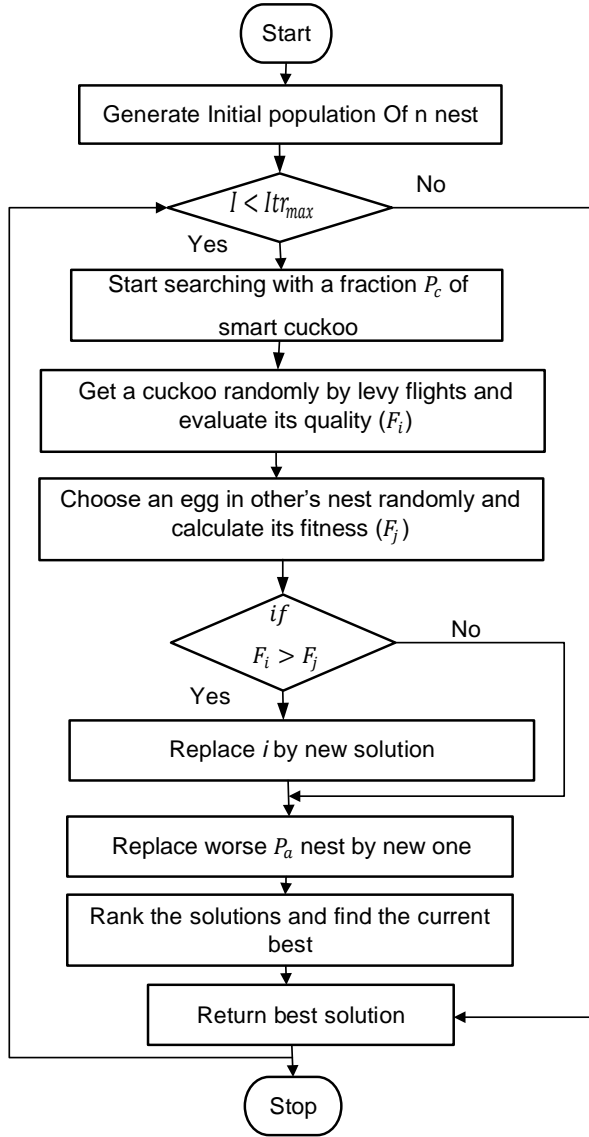


Figure 2.13 Cuckoo search algorithm procedure flowchart.

Due to the significance of utilizing the CSA algorithm in the literature by numerous scholars, a summary of the advantages and drawbacks of CSA has been tabulated in Table 2.6.

Table 2.6 Advantages and Disadvantages of cuckoo search algorithm [68], [103], [104]

Advantages	Disadvantages
<ul style="list-style-type: none"> • The simplicity of integrating with other methods. • It supports local and global search capabilities. 	<ul style="list-style-type: none"> • It is not able to solve discrete and multi-objective problems due to its convergence and slowness. • Has limitations in solving complex problems.

2.4.4 Objective functions

In any optimization method study, an objective function is needed to be defined as presented in the literature which considers the environmental, economic, and technical characteristics [105]. Besides, others utilized objective functions in a vast number of studies in the literature in order to gain a cost-effective system, reliable, renewable, and reduces pollution [106]. Different methods were utilized in the literature to evaluate the cost, reliability, and renewability as presented in [21].

The COE is one of the used objective functions in the literature that refers to the Cost of Energy (COE) and means the per capita of electricity [107]. It is the ratio of Total Net Present Cost (TNPC) and energy consumed by the system. It has various forms of evaluating the cost presented in the state-of-the-art such as Life Cycle Cost (LCC), Annualized Costs (ACS), Net Present Cost (NPC), Life Cycle Unit Cost (LCUC), and Levelized Cost Of Energy (LCOE) [108].

On the contrary, reliability is known as the ratio of the deficit in energy generation to the demand using different reliability measuring techniques such as Losses Power Supply Probability (LPSP) technology [8], [9], [108]–[110]. The value of LPSP ranges between 0 and 1, where the value of 1 refers to unsatisfied load while 0 is satisfied load [110]. The ability of the electric power system to continuously supply the load refers to the probability of power supply failure to meet the load demand. The other measuring forms of reliability are reported in the literature such as Loss of load Expected (LOLE), Loss of Energy Expected (LOEE), Loss Of Load Risk (LOLR), System Performance Level (SPL), Unmet Load (UL), Deficiency of Power Supply Probability (DPSP), Loss Of Load Probability (LOLP), and Loss of Load Hours (LOLH) [108], [110].

The renewability techniques are presented in the literature in order to estimate the output power generated from RESs or in other terms it is the quantity of energy produced from RESs [21], [111]. The utilized renewability techniques used in the literature are Renewable Energy Fraction (REF) which can be defined as the portion of the energy transferred to the load generated from RESs [44]. Besides, Loss of

Renewable Energy Generation (LREG), Renewable Energy Ratio (RER), and Penetration of Renewable Energy Generation (PREG) are some of the renewable exploited techniques utilized in the literature [110].

2.4.5 Constraints of the objective function

Constraints of the objective function can be explained as a rational verified relationship between design variables [112]. The constraint is exploited to provide the optimal solution for optimization studies that form inequality and equality (math equations) [33]. The grid-connected constraints are BT, SoC, areas of PV, and WT to overcome the constraints proper choice of metaheuristic algorithm was made. The set of constraints presented in the literature are REF and LPSP due to climatology changes and expectations of power failures [65]. The considered constraints have been reported in the literature for sizing the system components by using various optimization algorithms [113]–[115].

2.5 Vehicle-to-Grid Technology

The consideration of integrating RESs into the main grid and Electric Vehicle Charging Facility (EVCF) to charge (G2V) and discharge (V2G) EVs have been discussed in the literature [116]. Consequently, the general concept of V2G and G2V that was first introduced in [117] is shown in Figure 2.14. Furthermore, it is based on the concept of injecting electricity from an EV into the grid through a bidirectional converter and vice versa. The foregoing definition is the basic idea behind the V2G technology [12]. In spite of the economic and social benefits of EVs such as reducing the cost of energy during peak demand periods, source of revenue from the difference in price due to low and peak price periods, and zero pollution ability [118]. Recently, V2G is considered as one of the most well-known among Vehicle-to-Everything (V2X) technology [119]. At the same time, it faces several challenges including battery degradation and high maintenance rate, social barrier, high cost of investment [120], and connectivity standards [18]. The main of EVs components are a battery, charging port, DC/DC converter, drive system, power electronic controller, and charger [118].

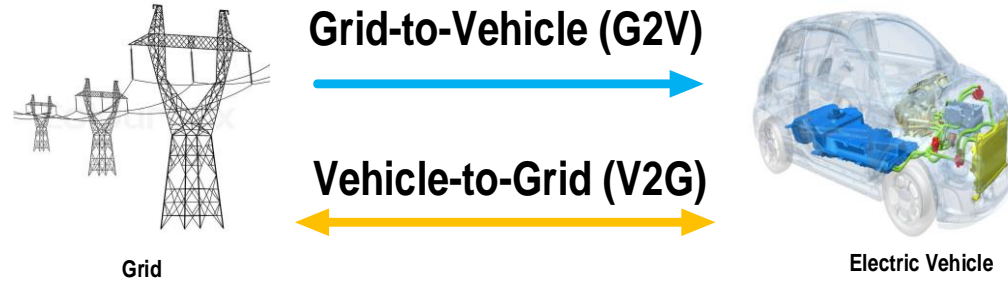


Figure 2.14 The bidirectional power flow diagram for Vehicle-to-Grid and Grid-to-Vehicle [117], [120].

Various nations adopting EVs include the US, Japan, Kenya, Algeria, Nigeria, Turkey, Ethiopia, Germany, Spain, Canada, India, Indonesia, and China [118]. In addition to the previous countries, Malaysia, Brazil, Denmark, Netherlands, Morocco, and the UK are also using EV charging technology [121]. The aforementioned countries are exploiting EVs, however, the EV broader market comes from Germany, the UK, China, and the US [10]. The fundamental advantage of an Electric Motor (EM) is that it converts electrical energy from a battery into mechanical energy, which is then used to push vehicles [122]. The EVs are preferable due to the provided advantage which includes eco-friendly vehicles and silent operation compared to Internal Combustion Engine Vehicles (ICEV) [8]. Besides, EVs are more stable and safer than RESs when considered as a source due to the provided limitation from RESs when integrating a large number of RESs due to the climatology changes to produce power [123]. On the other hand, it provides heavy stress on the grid when used as a load.

Different manufacturers around the globe present different types of powertrains (vehicles) to achieve zero-emission transportation or green electricity [1]. The most commonly used EVs for charging/discharging purposes are Plug-in Hybrid Electric Vehicles (PHEVs), Hybrid Electric Vehicles (HEVs), and Battery Electric Vehicles (BEVs) [11], [28]. Among the mentioned EVs, the PHEV has the potential for grid integration with larger storage systems when compared with HEV and lower oil dependency [1]. It is suitable for city driving and highways and can operate in charge-depleting mode and sustaining mode [124]. The charging station can be classified into two groups: residential and non-residential (commercial) stations as shown in Figure 2.15 [119].

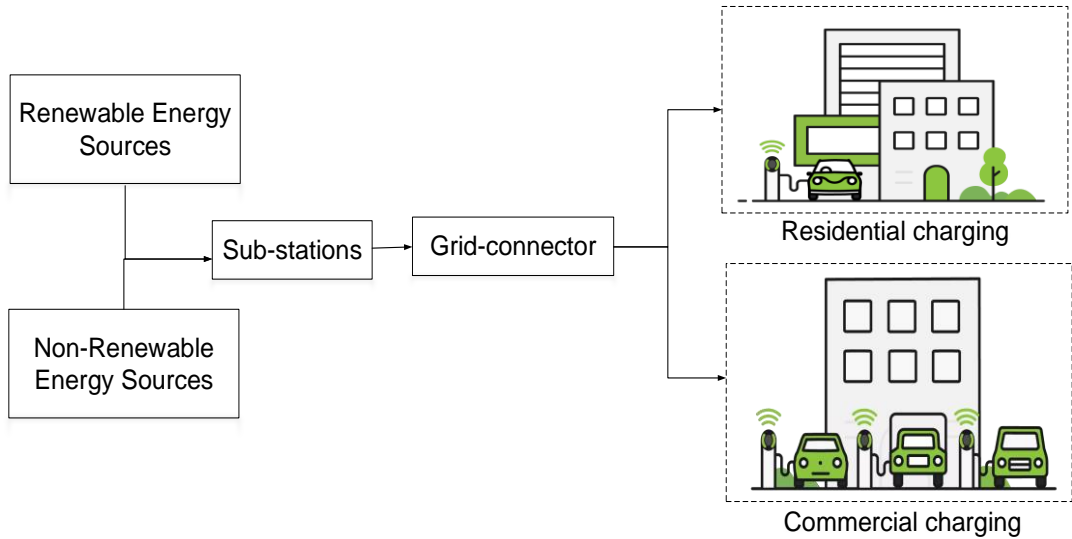


Figure 2.15 Residential and commercial charging diagram [10], [119].

In terms of power levels, there are three provided power levels for charging EVs namely: level one (AC), level two (AC), and level three (DC). The first mentioned power level's features are single-phase, on-board, charging long-hour, and using Society of Automotive Engineering (SAE) J 1772 as its connector standard [125]. Level one installation costs around 500-880 USD in the USA, and home and office charging, and cables are required [121]. The second level features are single/three-phase, less charging time than level one, cost around 150 USD for setting up, more preferable, private or public charging, using SAE J1772 or IEC 61851-1 as a connector standard [124]. Eventually, the third-level features are off-board and commercial. Japan has used these charging types and CHARGE de MOVE (CHAdeMO) is used as charging standards, a fast charger using DC, and costs around 3000-160000 USD for setting up [119]. Based on the location of EVCS, different power levels, charging circuits, and contacts are used to charge and discharge the EV as further elaboration and tabulated in Table 2.7.

Table 2.7 Structures of charging Electric Vehicles [10], [119], [122].

Structures	Classifications	Features
Power flow direction	Unidirectional	<ul style="list-style-type: none"> • Refers to charging process (G2V) mode. • A diode rectifier is used and a DC-DC converter charging control. • Less complexity. • Provide limited ancillary services compared to bidirectional.
	Bidirectional	<ul style="list-style-type: none"> • Refers to discharging process (V2G) or charging (G2V) mode. • Providing ancillary services (peak load shaving, voltage, and frequency regulation achieved with V2G bidirectional) to the grid.
Power Types	AC	<ul style="list-style-type: none"> • Intermittent Frequency. • Discrete signal.
	DC	<ul style="list-style-type: none"> • Continuous current • Charging directly without permission from utility suppliers • Faster charger.
Charging circuit communication	On-board	<ul style="list-style-type: none"> • It is located in the vehicle (EV) itself. • Can recharge the battery when electricity is available. • Lower cost compared to offboard.
	Off-board	<ul style="list-style-type: none"> • It is located outside the vehicle (charge station). • Expensive charging in terms of installation.
	Wireless	<ul style="list-style-type: none"> • Through electromagnetic waves. • Convenient charging.
Contacts	Contactless charging	<ul style="list-style-type: none"> • Using Inductive Power Transfer (IPT) or Wireless Power Transfer (WPT) technology. • Suitable for long-distance charging.
	Conductive charging	<ul style="list-style-type: none"> • Divided into slow charging (level 1 and 2) and fast (level 3 or DCFC) and using cables. • Suitable for short-distance charging.

2.5.1 Alternative Energy Resources

Electricity is the fastest-growing kind of energy depending on the available sources [50]. Energy is required to improve the standard of living of human beings in societies and develop the economy as an essential and crucial element of life [105].

RESs are presented as the state-of-the-art approach to enhancing the security of the power supply. They have been utilized to cover public facilities loads under different climate conditions [95]. Furthermore, the Hybrid Microgrid System (HMGS) formed using RESs can provide cost-effective, reliable, and optimal solutions for hybrid systems. Similarly, the impact on the environment from RESs is positive, due to the green energy produced and improved security of energy suppliers [58], [126]. Table 2.8 presents the application, benefits, and drawbacks of the applicable energy sources to charge the EVs [20], [47], [127]. The process of injecting the RESs with different outputs requires a converter to convert the power form and improve the quality of the power [108]. The main four converters used to shape the power form are DC/DC, AC/AC, DC/AC, and AC/DC converters to stabilize the grid to be in steady-state mode [128].

On the contrary, non-renewable energy sources are made by mankind as power plants such as oil and gas power stations [67]. Non-renewable energy sources are obtained from traditional sources such as fossil fuels (natural gas, coal, oil) and power plants. However, non-renewable energy sources cause harmful impacts on the economy and environment [59]. Nowadays, it has become necessary to utilize natural sources to gain development and a clean system to achieve Sustainable Development Goal Seven (SDG7) rather than using fossil fuels. The SDG7 objective is to connect the microgrid system with the changeable weather conditions in the environment [129].

Table 2.8 Energy Resources and their Applications.

Source Types	Sources	Applications		Pros	Cons		
Renewable [47], [115]	Wind	Water pumps, wind generators, and power generation, windmills.		<ul style="list-style-type: none"> • Use free resources like the sun and wind • O&M requirement s are low • No problem with pollution or waste of natural resources 	<ul style="list-style-type: none"> • Production is dependent on the natural cycle • The initial cost of these systems is higher than a comparably sized conventional generator. • Cannot handle the peak loads well without energy storage. • Unpredictable sources 		
	PV	<ul style="list-style-type: none"> • Water heaters, solar home systems, solar cookers, solar dryers, photovoltaic, and thermal power generation. 					
Non-renewable [10], [20], [130]	Fossil Fuels	Coal	Electricity generation, liquid fuel, steel production, and cement manufacture.	Widely available	<ul style="list-style-type: none"> • Generate Pollution. • Require Fuel to operate which attracts additional cost. 		
		Natural gas	Supply heat loads and heat-driven cooling equipment.				
		Oil	Takes hundreds of millions of years to change its form to various types of fuel, such as gasoline and diesel.				

2.5.2 Vehicles-to-Everything Topologies

Power can be flown in either direction from sources to load (G2V) or vice versa (V2G), which is advanced known as unidirectional or bidirectional [10]. Furthermore, bidirectional enables to use of V2X technology, when X refers to many technologies that can be used. Thus, V2X is a general term used to describe the usage of EV batteries when they are not being used. The various technologies of V2X are V2G, Vehicle-to-Home (V2H), and Vehicle-to-Vehicle (V2V) technology as reported in the literature and tabulated in Table 2.9 [28], [39], [105], [121], [123], [131].

The EV refers to a recharged battery that is charged from the RESs when there is excess power and discharged when there is a shortage of power [108]. The recharging ability of the secondary storage has caused a shift from the use of fuel-based transportation systems to electricity-based transportation. The foregoing process is going with the help of EVs using rechargeable BT to avoid power and environmental barriers [121].

Table 2.9 Mobility charging topologies of electric vehicles.

Topologies	Concept
Vehicle-to-Everything (V2X)	It is a general term where X is a variable representing Grid (G), Building (B), or Vehicle (V) [131], [132].
Vehicle-to-Device (V2D)	Energy is transferred from the EV to electric devices [10], [15].
Vehicle-to-Building (V2B)	<ul style="list-style-type: none"> • The energy is transferred from the EV to the building [15]. • It is similar to V2H but with a larger scale [123].
Vehicle-to-Vehicle (V2V)	This is the concept of transferring energy from EV to EV for the purpose of charging [10], [15].
Vehicle-to-Infrastructure (V2I)	This is a wireless communication system transferring from the EV to the antenna/tower/traffic light [10], [14], [15].
Vehicle-to-Network (V2N)	This can connect vehicles to the wireless communication system such as media streaming and traffic updating [121].
Vehicle-to-Grid (V2G)	This refers to a bidirectional energy transfer, which means from EV to the grid and vice versa in the bidirectional form [15], [41], [131], [133], [134].
Vehicle-to-Pedestrian (V2P)	This involves multiple vehicles working together to provide similar services for commercial purposes [10], [15].
Vehicle-to-Home (V2H)	This technology plays an important role in using energy from EVs to power domestic appliances [15], [105], [135].
Vehicle-to-Load (V2L)	It delivers electricity from EVs to feed a load such as a piece of hospital equipment and research centers in emergency cases [10], [15].

2.5.3 Energy Storage

This section presents the various types of energy storage devices presented in the literature [119], [136]. These batteries are Lithium-ion (Li-ion), Lithium-iron Phosphate (LiFePO₄), Nickel-Cadmium (Ni-Ca), Lead-Acid (LA), and Nickel-Metal Hydride (NiMH) [119]. The lithium battery as the most utilized battery was originally proposed by a British-American chemist called Michael Stanley Whittingham in the 1970s at Stanford University, afterward, it was improved by many scientists [136].

Lithium batteries are the most widely used EV storage system due to their high power density and lightweight profiles [137]. The considered battery for EV operations is LiFePO₄ due to its long-life cycles, ability to deliver high current, high energy density, very good thermal stability, and good cycle life [10], [119], [138], [139]. In addition, the batteries have good power ability, lighter in weight, and are smaller in size, while the Li-ion battery is considered a deep cycle battery with the same advantages [140], [141]. The comparison advantage, disadvantages, and applications for the EV and deep cycle batteries are formulated in Table 2.10.

Table 2.10 Comparison between Li-ion & LiFePO₄ batteries [10], [119], [139].

	Lithium-ion (Li-ion)	Lithium-iron Phosphate (LiFePO ₄)
Advantages	<ul style="list-style-type: none"> • High energy (10/200 Wh/kg) • Life cycle (500-1000) • Safety and Light • High efficiency • High charging acceptance • High-power density • Long-term storage (300 days) 	<ul style="list-style-type: none"> • High-energy-density (90/120 Wh/kg) • Long-life cycles (1000-10000) • Safety and Light • Cost-effective materials • Stability with high temperatures. • Voltage discharges are excellent when at higher temperatures. • Stable chemical and thermal chemistry • Recycling material is not needed
Drawbacks	<ul style="list-style-type: none"> • The higher energy density makes it more unstable, especially when dealing with higher operating temperature environments. 	<ul style="list-style-type: none"> • Low energy density.
Applications	<ul style="list-style-type: none"> • Electronic and mechanical devices. • Electric Vehicle 	<ul style="list-style-type: none"> • Electric motors for vehicles, medical devices, and military applications.

2.5.4 Impacts of Electric Vehicles deployment

The integration of RESs with EVCS to exchange power between the EV and utility grid causes a green impact as reported in [142]. The impacts of the integration on the EVs can be grouped as positive and negative impacts accordingly [125]. Moreover, the positive impact provides a bidirectional transfer of power between the EVs and the grid through a V2G technology, reduces the impact on ozone pollutants, and reduces the total emission [143]. The previous benefits have been obtained by two

factors which are shifting to EV instead of ICEV and decreasing the use of petroleum [17]. On the contrary, the negative impact can be grouped into three categories which are economic, environmental, and utility grid as illustrated in Figure 2.16 [144].

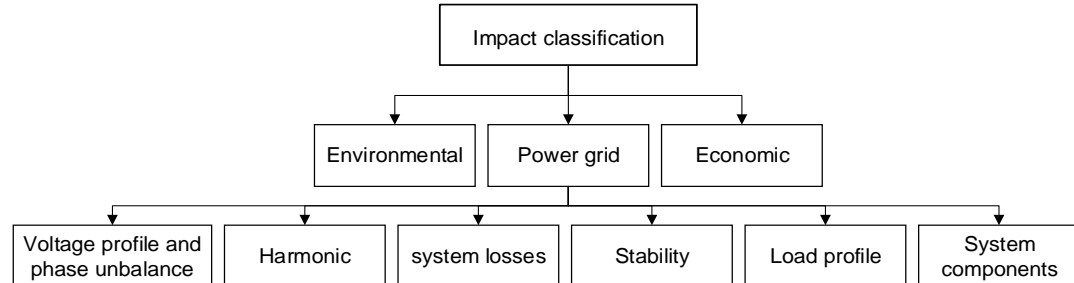


Figure 2.16 Impacts of Vehicle-to-Grid technology implementation [145], [146].

The economic impact is due to the increased consumption of fuel and generation leading to high running costs for the government and participants [145]. Thus, the environmental impact comes from charging EVs which leads to an increase in Carbon Dioxide (CO₂) emissions [8], [146]. Eventually, the impact on the power grid is due to an increase in load profile during peak hours, losses, and harmonics as in Denmark and Japan [20]. Further elaboration is presented in Table 2.11 and Table 2.12 for helpful and harmful impacts, respectively [145], [146].

Table 2.11 Positive impact of EV on power grid [145], [146].

Type of impacts	Remarks	Effects
Power quality improvement	It mitigates the effects of poor power quality resulting from voltage imbalance, harmonics injection, and a massive amount of real power consumption.	Affects the system's lifespan.
Voltage and frequency regulation	This addresses the effect of voltage and frequency fluctuations caused by voltage surges and deviations in grid frequency.	Affect the system's quality and lifespan.
Power management	<ul style="list-style-type: none"> • A good EMS should efficiently coordinate the flow of power from/to the system. • Increasing the element's lifespan, reducing the cost, and improving system performance. 	System degradation.
Renewable energy support	<ul style="list-style-type: none"> • RE integration into the grid increases the system flexibility, • Provides an environmentally friendly system and reduces the dependence on conventional sources. 	The uncertainty associated with RE sources.

Table 2.12 Negative impact of EV on power grid [10], [15], [147], [148].

Type of impacts	Remarks	Effects
Harmonic	<ul style="list-style-type: none"> EV is a DC device that generates harmonics. During power conversion harmonics are generated by electronic devices causing harmonic pollution. 	<ul style="list-style-type: none"> Poor power quality. EMI issues.
Stability	Nonlinear loads such as EVs draw a large amount of power within a short period, this creates instability in the power system.	<ul style="list-style-type: none"> Unstable power system Subject the overall power system to disturbance which takes a longer time to return to a steady state.
Increase in power loss	Large-scale EV integration into the grid consumes a large amount of real power leading to a loss in power.	Loss of power in the distribution system.
Imbalance in phase & voltage	<ul style="list-style-type: none"> EV chargers which are usually single-phase can cause voltage and current imbalance in large-scale EV integration if the chargers are used in the same phase. 	EVGI will generate a voltage drop and deviation at the interconnection point of EV chargers.
Load demand increase	Grid integration of EV serves as an additional load, this presents a problem for the utilities during peak load hours.	Uncertainties in the utilities during peak hours.
Component overloading	Overload is caused by the enormous vehicle demand and other electric components.	Additional load demands affect the system's lifespan.

In the nutshell, integrating a large number of EVs causes an impact on the aforementioned categories (positive and negative). A real example of the EV's positive impacts on the grid considered in Istanbul-Turkey by integrating PV and WT that helps to mitigate the dependency on the grid has been conducted in [143]. Besides, switching to EV reduces the CO₂ impact by 85% on the environment which improves air quality as the most significant impact in Denmark in comparison with ICEV [149]. While negative impact on the stability of the utility grid has been investigated in the UK by an 18% hike in the demand from the utility grid when increasing 10% of EV charging load [119].

2.5.5 A critical review of the system components

The critical review and analysis of the utilized components, objectives, methods, and scenarios of the system are discussed in this section. The components in the literature related to the microgrid system are used in stand-alone and grid-connected systems which do not consider EV as reported in Table 2.13 using nature-inspired algorithms. The listed approaches used mathematical modeling analysis with MATLAB and other software as advanced computer simulation tools to obtain the output of the mathematical equations and plot the result. Table 2.14 presents the summary of the literature on integrating EVs along with the PV and WT integrated systems under commercial and residential loads. Overall, the conducted studies formed the microgrids (standalone and grid-connected) integrated into EVs.

The microgrid is applicable in various areas such as residential, commercial, military, and industrial [150]. Regarding different EV charging areas, various studies presented commercial [151], university, shopping centers, and military charging loads. Other studies considered residential charging loads as they consume almost 32% of energy globally [152]. The difference between residential and commercial charging is in the time of charging, the charging power level, and the cost of charging the EV(ratting tariff) [153]. Additionally, residential charging has been chosen by using different optimization and controlling techniques due to its competitive cost compared to commercial charges [154]. Besides, residential charging is flexible charging and preferable because it does not require service fees, and considers lower feed-in tariff (lower charging cost) [155].

In terms of sizing optimization problems, there are two forms that can be used to solve sizing optimization of hybrid systems: Single-Objective (SO) and Multi-Objective (MO). The former is mostly considered in literature due to its benefits. One key advantage related to SO is finding the best solution for a specific problem. The latter is used complex mathematical equations and it's time-consuming [156]. The MO is a decision-maker which considers more than one objective function. Furthermore, heuristic and metaheuristic algorithms are used to address sizing problems [45].

Table 2.13 The State-of-The-Art of RESs integration without EVs.

Ref	System Configuration					Approach	Objectives	Scenario
	BT	WT	FC	PV	DG			
[100]	✓	✓	x	✓	x	• Economic • CSA-PSO-GA • MCS	• To solve the optimization problem by CSA and validate the acquired result by GA and PSO. • To size the main components of the system (PV, WT, and BT) and calculate the LOLE and EENS using MCS	Residential Off-grid
[157]	✓	x	x	✓	✓	• Mathematical model • PSO	• To reduce the total cost, losses of load probability, and CO ₂ of HMGS in Algeria and to reveal the importance of PV and Battery bank. • To Size the HRESs (PV, DG, BT) using PSO • To compare the optioned result from PSO with HOMER	Residential Off-grid
[21]	✓	✓	x	✓	x	• MOPSO	• To maximize the renewable energy fraction (REF) and minimize the cost of energy and LPSP under various weather conditions • To utilize mathematical modeling for the system to estimate the output of the system. • To classify the result of MOPSO to lowest COE, highest REF, and lowest GHG emission.	Residential On-grid
[43]	✓	✓	✓	x	x	• MCS • PSO	• EMS for a microgrid system consists of micro-turbine, FC, WT, rubbish-burning power plant, boiler, anaerobic reactor-reformer, BT, Inverter, and rectifiers using MCS for sizing components and validated by PSO.	Residential On-grid
[158]	✓	✓	x	✓	✓	• RB-EMS-Matlab simulation package • GOA	• To size the microgrid system by determining the optimal system configuration • To solve power problems by GOA Algorithm and compared with PSO and CS. • Decreases of 14% and 19.3 are achieved in the capital cost	Residential Off-grid
[159]	✓	✓	x	✓	x	• PSO and filter algorithm	• To propose a system to minimize the energy cost and fluctuation • To size the system components by PSO	Residential On-grid

Table 2.14 State-of-the-art microgrid systems on-grid and off-grid in the literature with EVs.

Ref	System Configuration					Approach	Objective	Scenario
	BT	WT	FC	PV	DG			
[41]	✓	✓	✓	✓	x	•MOPSO •MPC •Matlab/Simulink	•To descript the V2G system as a hybrid system using Grid-connected with RESs and EV integration into the grid. •To use MOPSO to solve the energy management optimization and determine and distribute the power for each time step •To use MPC to plan PEV charging energy to increase the use of RESs	Residential On-grid
[113]	✓	✓	x	✓	✓	•MOSaDE	•To meet load demand at low COE, LPSP, and maximum REF using Multi-Objective Self-Adaptive Differential Evolution (MOSaDE). •To attain an optimal economic system. •To strategies the power of EMS.	Residential Off-grid
[114]	✓	✓	x	✓	x	•ALO, PSO •HS, FA, and DE	• To optimize an off-grid system •Utilize ALO to find an optimal value to meet the load demand, and reduce COE, losses, and NPC in Iran.	Residential Off-grid
[160]	✓	x	x	✓	x	•Matlab/Simulink	• To manage energy flow for a grid-connected system integrated with RESs and battery (PV-BT) to meet the demand via DC bus.	Residential On-grid
[161]	✓	✓	x	✓	x	•HOMER	•Sizing system components (PV-WT-BT) using HOMER for charging EVs in Izmir-Turkey as a case study •Exploiting RESs to charge EVs for cost reduction and make investment	Residential On-grid
[9]	✓	✓	x	✓	x	•MOPSO •MCS	•To size the system components using MOPSO and investigate the LPSP and COE. • To measure the uncertain number of arrival and departure EVs	Residential On-grid
[115]	✓	✓	x	✓	x	•HGS	•To analyze and optimize a system consisting of PV-WT-BT-EV using the Hunger Games Search Algorithm (HGS)	Residential On-grid

Table 2.14 (cont.)

Ref	System Configuration					Approach	Objective	Scenario
	BT	WT	FC	PV	DG			
[127]	✓	✓	x	✓	x	•ABC •PSO	•To reduce the power exchange with the grid from EVs to attain fewer losses and minimum power cost in India •Formulating the mathematical modeling for the PV-WT-BT incorporated with the EVs	Residential On-grid
[162]	✓	x	x	✓	✓	•HOMER pro	•Integrating solar and biogas with the main grid in Gaza to generate sustainable electrification. •Simulating result for the residential area to obtain 2.30\$ NPC and \$0.438/kWh COE.	Residential On-grid
[57]	✓	x	x	✓	x	•FIS	•EMS for microgrid including EV using Fuzzy Inference System (FIS) with battery	Residential On-grid
[134]	x	✓	x	✓	x	•MPPT controller	•Considering novel grid-connected wind and solar to power EV charging stations for large-scale through MPPT. •Implementing V2G technology through a DC bus	Residential On-grid
[8]	✓	✓	✓	✓	✓	•MOPSO •NGA-II •MCS	•Optimizing a hybrid system consisting of (PV-WT-BT-FC-EL-HT-DG) in 5 various scenarios based on MOPSO and Non-Dominant Sorting Genetic Algorithm (NGA-II) with EV. •To obtain a system with minimum LPSP, LCC, CO ₂ emission. •Uncertain of RES and Load modeled by Taguchi and MCS to model EVs.	Residential On-grid
[163]	✓	✓	x	✓	x	•HOMER	• To examine the technical and economical feasibilities of hybrid RESs (PV and WT) and BT to charge EVs for environmental improvements in five areas in China. • Sensitivity Analysis was utilized for load, EV, and BT to investigate the reliability and economics of the EVCS.	Commercial On-grid

To sum up, the main motivation for considering residential charging loads is due to the provided benefits of V2G technology by preventing blackouts and reducing the need for additional power generation infrastructure which overcomes home load limitations. Furthermore, the integration of EVs in the grid-connected system has a positive effect that forming V2G technology as EVs can be used as a dual function (storage and load) and earn a profit when discharging from the EV to the grid along with reducing the electricity bill [23].

2.6 The Research Gap

Utilizing the articles in the literature in order to fill the research gap of designing and planning the microgrid hybrid grid-connected system integrated with the EVs [8], [27]. The Rule-Based Energy Management Strategy (RB-EMS) as a supervisory control method complemented by IALO as a developed nature-inspired algorithm to control the power and size components [28], [33]. While the RB-EMS limitation is requiring more technical knowledge in order to meet the optimal result. The RB-EMS is a human-based knowledge which means depends on the designer for implementing on the system components, previous studies considered the RB-EMS for controlling the power flow in microgrid systems. This study is implementing the RB-EMS as an adoptive for changing conditions for the V2G technology system considering residential load to meet the demand under a set of rules. The combination is necessary for addressing some challenges of ALO as one of the metaheuristic algorithms that is faced with premature convergence, running time speed, and easily acquiring the local optima value. The optimization method is utilized to meet the objective functions (COE, LPSP, REF) and enhance the system performance.

Similarly, a Lévy Flight (LF) can be used to address the aforementioned ALO limitation by replacing the Roulette Wheel Selection (RWS) as a feature selection method. However, overloading is a V2G integration challenge that is caused by integrating different energy sources and the uncertain number of vehicles [120], [148]. Therefore, the foregoing challenge can be further investigated. The aforementioned issue can be possibly addressed by scheduling the charging process for daytime or nighttime [15]. The impacts on the load when integrating uncertain numbers of EVs into the grid can be estimated by the stochastic methods, for instance, Stochastic Monte Carlo Method (SMCM) is one of the methods that can be used [8], [9], [69].

2.7 Chapter Summary

This chapter presented a review of the literature on different microgrid systems consisting of different microgrid components. Different EMS presented in the literature are also reported with their advantages and drawbacks. In terms of energy resources, various of RESs and conventional energy resources are discussed and compared for supplying power systems followed by energy storage. The hybrid system consisting of an integration of various RESs into the grid based on V2G technology is as well deliberated. This work considers RB-EMS based on RESs (PV and WT) charging EVs in terms of V2G to reduce the burden on the grid, overloading issues, and meet the objective functions [8], [148], [164]. The IALO is proposed to size the system components and address the mentioned issues and control the power with the help of RB-EMS. The benefits and limitations of the various EVs are enumerated. Similarly, challenges associated with charging EVs are highlighted followed by the V2G challenges are also discussed. An overloading and high peak load occurs when not using a proper management system while charging the EV [27], [148].

Finally, nature-inspired metaheuristic optimization algorithms such as ALO, PSO, and CSA are fully described and considered as counterparts because of their simplicity and ability to provide the optimal solution. Furthermore, some of the presented algorithms are multi-functional in various fields. Due to the premature convergence suffering in ALO and easily acquiring the local optima value, IALO is proposed. The IALO is coupled with a rule-based strategy for an accurate result in terms of reducing cost, power losses (reliability), and maximizing renewability. The IALO is proposed for obtaining an optimal number of configurations (sizing) used in the system to meet the load demand with the proposed objectives and address the limitation of benchmarking methods. The IALO as a metaheuristic algorithm coupled with RB-EMS can close the research gap in planning and designing such a proper system considering RESs with V2G technology integration. The SMCM is used to estimate the impacts on the load when integrating uncertain numbers of EVs into the grid along with the sensitivity analysis [9]. The various approaches used to address the problems of optimization by the different algorithms are reported.

CHAPTER 3

VEHICLE-TO-GRID INTEGRATION FRAMEWORK

3.1 Introduction

In the previous chapter, the state-of-the-art of microgrid integration systems with various energy sources has been presented. Choosing reliable sources for producing electricity is the base needed for any community to improve living standards and cost-effectiveness to evaluate microgrid systems. The Energy Management Strategies (EMS) as a supervisory control method has been presented along with its classification, advantages, and disadvantages. A number of papers on EMS have been investigated in the literature, and Rule-Based EMS is shown to be the most effective method in decision-making. Various nature-inspired optimization algorithms in terms of artificial intelligent methods with the objective function followed by constraints were highlighted. The technology of Vehicle-to-Grid (V2G) fundamental terminology has been defined with the applicable integrated Renewable Energy Sources (RESs), and the topologies and the impacts were discussed. Consequently, the research gap of the study has been closed in the chapter summary after a critical review of the literature. The proposed system for this study uses a grid-connected system considering a residential load area integrated with RESs and batteries to charge and discharge the EVs is discussed in this chapter.

This chapter presents the systematic methodology for achieving the objective functions of this study along with the proposed algorithm namely Improved Antlion Optimization (IALO) as shown in Figure 3.1. The chapter also presents an explanation of the case study with the proposed system along with mathematical models for system components. Similarly, RB-EMS accompanied by its constrain has been presented to meet the study's objective functions. The proposed IALO algorithm is compared with Antlion Optimization (ALO), Particle Swarm Optimization (PSO), and Cuckoo Search Algorithm (CSA) are presented. Moreover, estimating and analyzing the uncertain

number of arrival and departure EVs as well as the behavior impact of Electric Vehicles (EVs) on the grid using the Stochastic Monte Carlo Method (SMCM) is illustrated. The systematic approach of presenting the research methodology of the study in order to achieve the objective functions and the result is illustrated in Figure 3.1. Starting with step one of data collection (weather, EV, and load demand) to obtain the anticipated result (data figure will be presented in chapter 4). Followed by step two of choosing the utilized system components (WT, PV, Inverter, and BT) for the proposed model integrated with EV to form the V2G system. Subsequently, the proposed high supervisory control algorithm (RB-EMS) is applied for acquiring optimum results. Then, the proposed sizing method (IALO) complemented the RB-EMS for the microgrid to achieve an economic system and then validated it with other utilized methods. Finally, the results obtained from IALO will be analyzed to gain the estimated impact on the grid when integrating an uncertain number of EVs under different scenarios using SMCM. The proposed scenarios (V2G, G2V, RESs2V, BT2V) considered a different number of EVs which are classified as minimum, medium, and maximum EVs (10, 30, and 60), respectively.

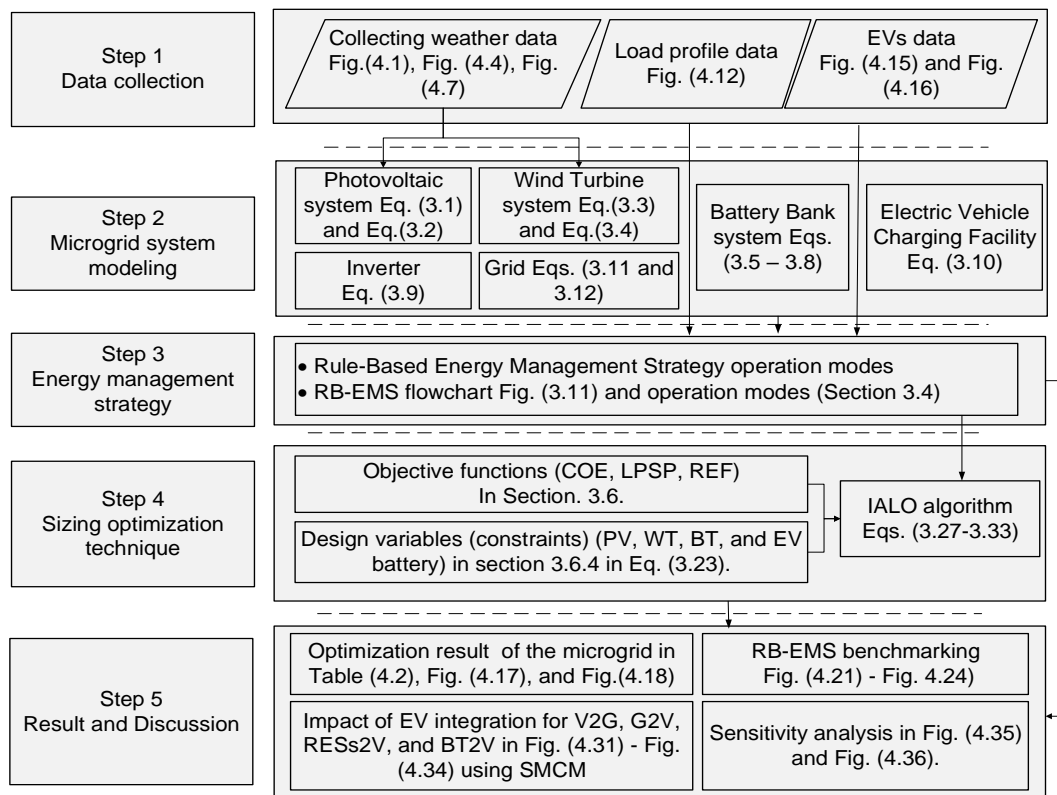


Figure 3.1 A systematic approach for the research methodology and modeling the system and achieving the objectives.

In the first instance, the microgrid test case system is designed using an RB algorithm as integration architecture which is listed below. Subsequently, implementing the proposed optimization method (IALO) for sizing the microgrid components, was then compared with ALO, PSO, and CSA. The process of using RB-EMS and metaheuristic algorithms is a reasonable integration to meet the objective functions [56].

- Evaluation of climatology data (Solar irradiance (W/m^2), Wind Speed (m/s), Ambient temperature ($^{\circ}C$), and check the load profile for the grid.
- Structural components of the system.
- Mathematically model the system components.
- Design and simulate the Energy Management strategy of the system.
- Sizing the components system by IALO then compared with ALO, PSO, and CSA.

3.2 The Case Study

Libya is located in the center of North African countries and has high horizontal solar irradiance which reaches up to 7.1 and 8.1 kWh/m²/day in the coastal and southern regions, respectively [165]. The population is around 6 million people spreading on land out over 1750,000 km² [166]. The considered location in this study is located in the north-west region of Libya (Tripoli) with coordinates: 32.8872° N latitude and 13.1913° E longitude [7]. Tripoli's area, inhabitants, and sea-level evaluation are 1507 km², 3 million, and 21 m, respectively [167]. The climatic conditions of Libya are influenced by the Mediterranean Sea to the north and the Sahara to the south under four seasons [7]. The average duration of sunlight in Libya is more than 3000 h/year according to a provided report from the Libyan Renewable Energy Authority (LREA) [165]. Besides, wind speed has a high average in the

country as reported in [166] is 7.5 m/s in Derna, 6.6 m/s in Misrata, and 6.5 m/s in Tripoli, respectively [7]. In addition, the direct normal irradiance for the studied area is shown in Figure 3.3.

The main sources of energy in Libya are fossil fuel-based (oil and natural gas) [7]. However, due to the rapidly increasing population in the country, electricity requirements have increased as demonstrated in Figure 3.2. The increase in population causes an increase in electricity demand and environmental problems in the country. Due to the foregoing reason, scholars are trying to utilize the alternative resources that are available in the country such as wind and PV to combat the energy crisis. General Electricity Company of Libya (GECOL) is the only company distributing electricity (administrated) in the country [168]. According to a provided study by the world bank, almost 99.8 % of the citizens had access to electricity as it is the driver of any economy [169]. Libya like other countries in the world suffered from rapid demand growth, environmental issues, and high energy consumption. Moreover, the issues and usage including energy production, distribution, and consumption are considered [170].

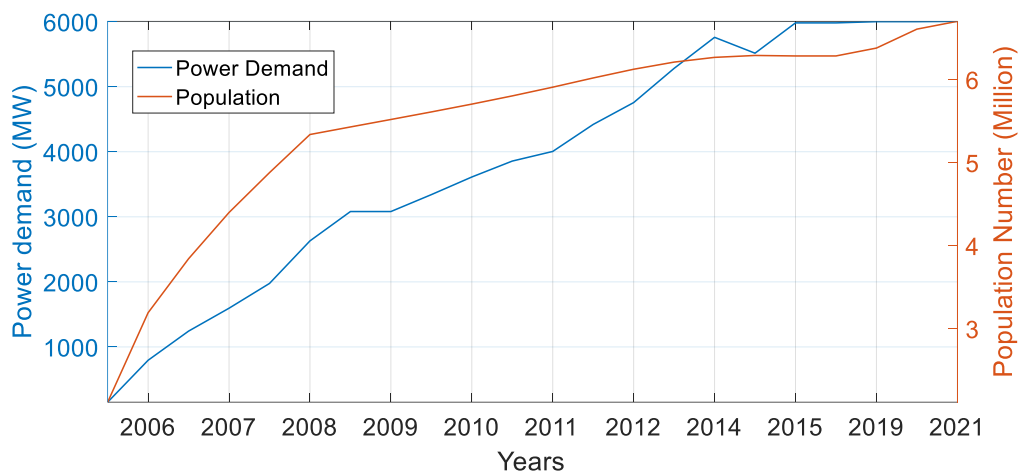


Figure 3.2 The peak load growth in Libya from 2010 to 2021 [7], [167].

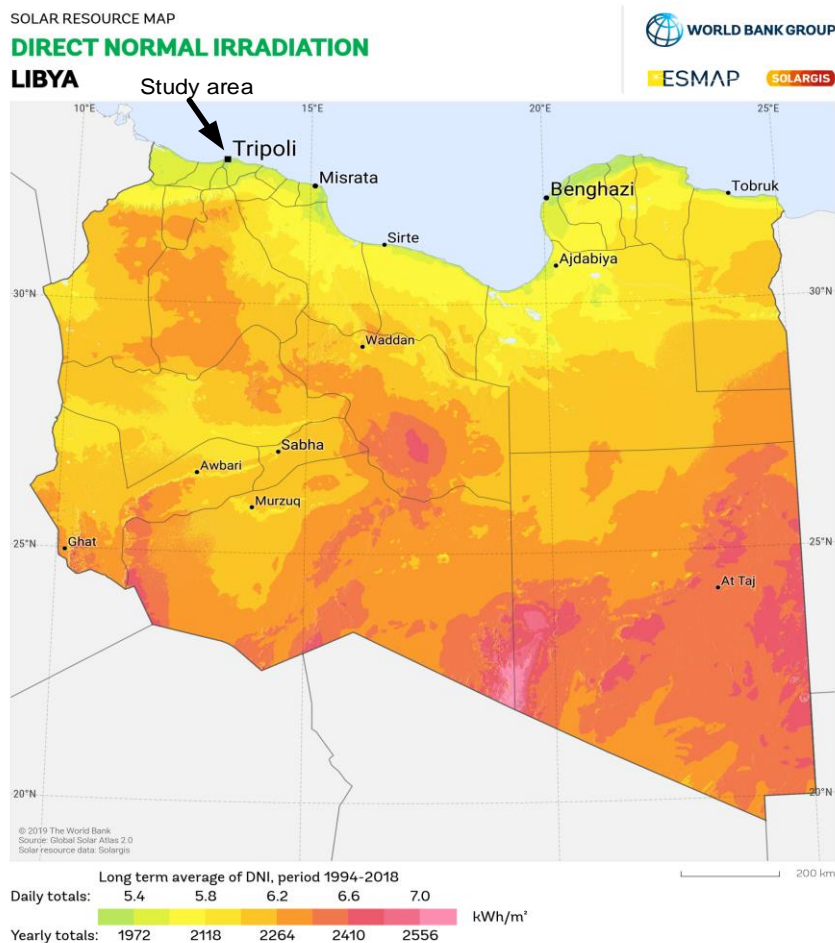


Figure 3.3 Direct normal irradiance for Libyan map [171].

The reason for considering the energy policy in this study is to present how the government or organizations plan and address the growth in energy [7]. The status planning of energy generation in Libya is shown in Figure 3.4 [167]. The energy policy of the country is utilizing crude oil and natural gas as the main essence of the economy as demonstrated in Figure 3.5 (a) with the exported oil and gas to different countries shown in Figure 3.5 (b), respectively [167].



Figure 3.4 Energy plan for the study area [167].

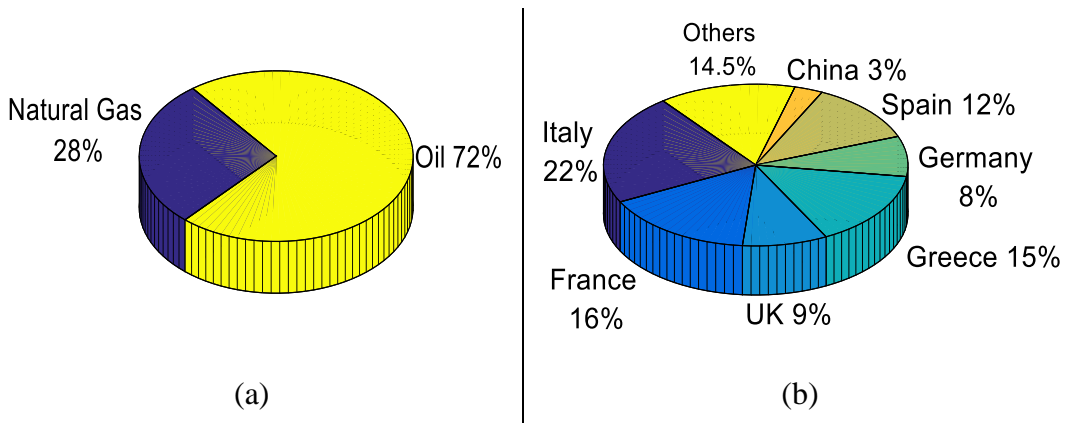


Figure 3.5 Non-renewable sources in Libya (a) Total energy consumption and (b) Crude oil exports to other countries [167].

The country is rich in natural sources such as gold, oil, and the sun. Libya ranked as the fourth country in Africa as an oil producer as the main source of economic [167]. However, due to the increasing environmental issues globally and climate changes, the United Nations (UN) are treating the aforementioned issues by utilizing the available RESs to reduce Carbon Dioxide (CO₂) and Greenhouse Gas (GHG) emissions by 80 % by 2050 [166]. In terms of fuel, the power stations in the country depend on light and heavy oil, and natural gas as percentages are presented in Figure 3.6 [167].

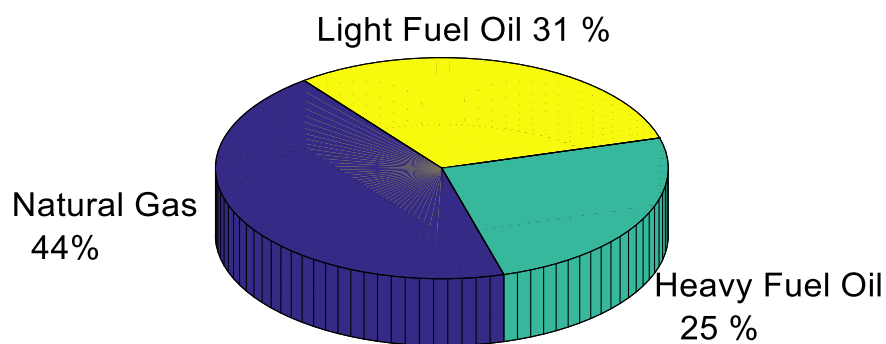


Figure 3.6 Types and percentage of the fuel used in electricity generation [167].

The country is signed several agreements over many years as a member of various organizations to achieve Sustainable Development Goal Seven (SDG7). Libya is a member of the Organization of Petroleum Exporting Countries (OPEC), the agreement was signed in the 1992 Rio declaration (Brazil). In addition, in 1997 Kyoto

Protocol (Japan), and in 2009 Copenhagen (Denmark), respectively [166]. A Libyan organization and planning strategies working in energy and water sectors are National Energy Council of Libya (NECL) and it belongs which are GECOL, Renewable Energy Authority of Libya (REAOL), Libya Atomic Energy Corporation (LAEC), National Oil Committee (NOC), and Ground Water Authority (GWA) [165].

The establishment of the solar system in Libya started in 1976 while the wind system in 2004 [172]. The latter examined the potential of wind speed which was around 6-7.5 m/s at a height of 40 meters. The utilization of PV in lighting and rural electrification in 2003 and water pumping in 1984 [165]. Some solar companies started promoting and installing alternative resources in residential and commercial areas due to the interruption in electricity using PV [166]. Depending on the climate changes for the mentioned location, the four seasons of the year are presented in Figure 3.7 [167].

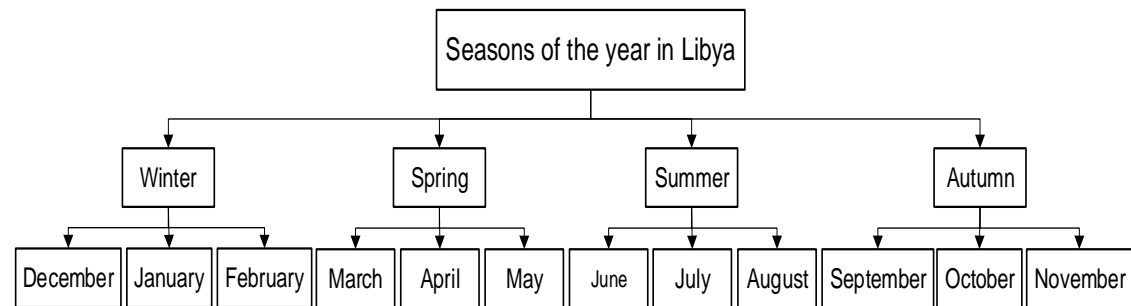


Figure 3.7 Seasons of the year in Libya.

3.3 The proposed microgrid

Many studies focus on the design, optimization, and scheduling operation of microgrids [3]. The illustrated system in Figure 3.8 is considered a hybrid DC/AC system with RESs (PV and WT), BT, and residential AC load as the EVCF to form a V2G to charge and discharge a number of EVs. Energy issues and air pollution are two reasons for choosing green sources [116]. The use of RESs to charge EVs in form of RESs2V technology is a challenge because of the few articles that introduced this technique and the intermittency in the weather [18]. The proposed system utilizes two RESs (PV and WT) to generate green energy which has accessibility to the grid.

The management of the battery for charge/discharge of the EV and the system is made through the DC-DC bidirectional converter [20]. Additionally, the generated power from PV used the aforementioned converter for regulating the DC output. Whereas the generated output power from WT passes through the AC-DC converter. During the charging stage, the DC/DC converter functions as a buck converter, and when discharging, it functions as a boost converter [120]. On the other hand, the exploited converter for charging/discharging from the EV is a bidirectional AC-DC that connects with the grid to stabilize the voltage and frequency for a steady-state situation [121].

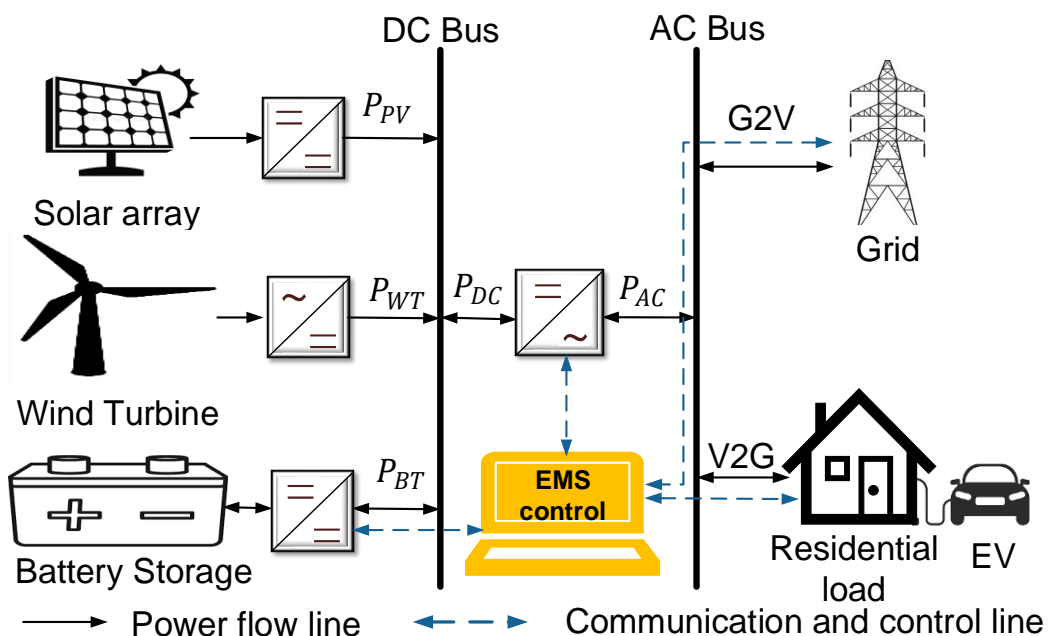


Figure 3.8 The architecture of the proposed Vehicle-to-Grid microgrid.

The working operation steps to meet the proposed objectives in different modes of the microgrid as an EMS using RB-EMS as presented in Figure 3.9. The presented flowchart in Figure 3.9 (a) and (b) is a graphical representation of an RB-EMS algorithm, to simulate the RB-EMS algorithm for the proposed system as listed in Table 3.1. Furthermore, RB-EMS was planned to make a decision since it depends on human knowledge when to sell/buy/store from the utilized sources. Furthermore, no prior data is necessary, and there are no difficult mathematical calculations in RB-EMS.

3.4 Operation modes of Rule-Based Energy Management Strategies

The main mechanism of RB-EMS depends on the (*if and then*) statement in the form of operation modes of the system presented in Figure 3.9 and Figure 3.10 for one year of hourly collected data. The first rule refers to Mode 1 considering powering the system from the RESs in case of grid absence as the priority source to meet the renewability function. The second rule is Mode 2 which uses the BT in the case of the absence of the utility grid and RESs are not satisfied. The third one is Mode 3 which depends on the grid to supply the MG system to charge the EV and other appliances which is known as G2V technology. The last rule is Mode 4 which implements the operation of discharging the stored energy from the EV battery (V2G) in case of the absence of the utility grid and not enough supply from RESs and BT. The one-year hourly essential data for the study area as an ambient temperature (T_{amb}), solar irradiance (G), State-of-Charge (SoC), load demand (P_l), EV demand (EV_{dem}), and wind speed (v). Besides, the load profile collected data to produce the output power from PV (P_{PV}) and output power from WT (P_{WT}) are required.

The EMS presented in Figure 3.9 and Figure 3.10 shows the four proposed scenarios that started with the general management diagram of the system presented in Figure 3.9 (a) where the priority is given to RESs to power the system. Where Figure 3.9 (b) represents the discharge operation considering the deep cycle battery (BT) with 20% and 100% as SoC_{min}^{BT} and SoC_{max}^{BT} in the case of not enough energy can be taken from RESs. Figure 3.10 (a) is denoted for charging situations when the absence of RESs or the utility grid supplies the system. Eventually, the operation of utilizing the grid to charge the vehicle (G2V) and utilizing the stored energy in the EV battery to power the home appliances is known as V2G technology is considered in Figure 3.10 (b). The boundaries of SoC_{EV} is considered as $SoC_{EVmin}(0.2\%)$ and $SoC_{EVmax}(0.95\%)$, respectively [8].

The presented RB-EMS diagrams in Figure 3.9 (a-b) and Figure 3.10 (a-b) are considering various input data such as P_{PV} , P_{WT} , SOC of BT (E_{BT}), output stored energy of BT in charging mode BT (E_{ch}), and stored energy from BT in discharging mode (E_{dich}). Besides, the maximum output energy of BT (E_{BTmax}), minimum

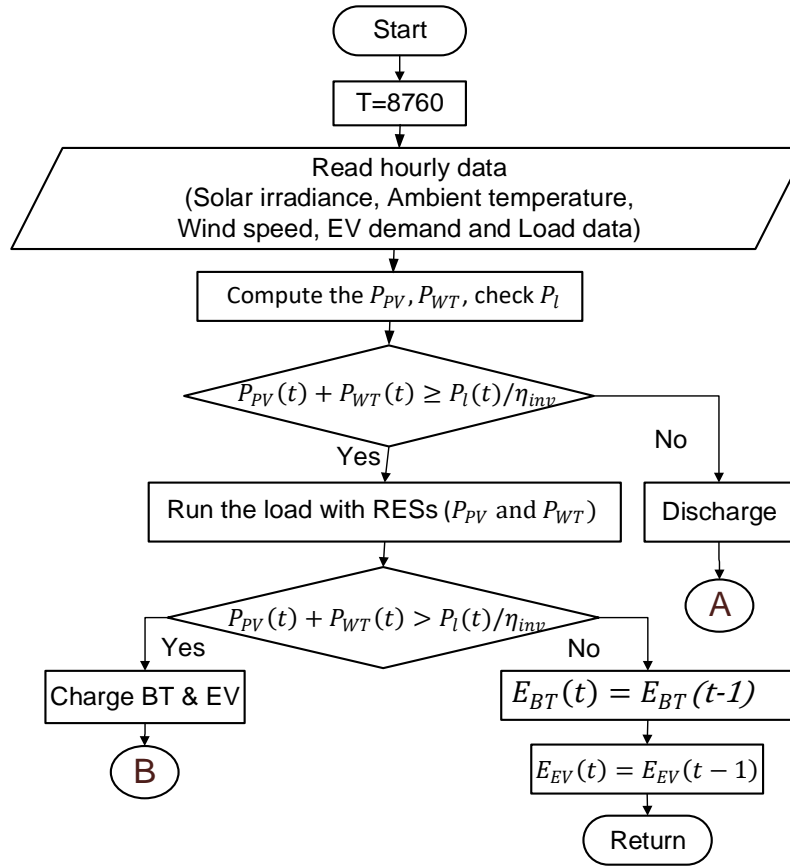
output energy of BT (E_{BTmin}), the EV demand (EV_{dem}), the utility grid demand ($Grid_{dem}$), and the output energy of the EV (E_{EV}). The working principle of the presented diagrams as shown in Figure 3.9 is measuring the climatology conditions for the case study under four seasons. Then, calculating the output power from the RESs (P_{PV} and P_{WT}) and check the average load demand. Based on the *if* and *then* statement, the strategy is begun to implement the proposed strategy modes from Mode 1 – Mode 4. Furthermore, from the result decision of the *if* and *then* statement, the discharging (A) and charging (B) situations are obtained. The simulation confirmed through the initial SOC of BT, PV-rated power (5kW), WT-rated power (5kW), and BT-rated capacity 35.38 kWh is used as RB-EMS input data. The other presented cases in Figure 3.10 (a) are referring to (B) with the consideration of BT and (C) in Figure 3.10 (b) refer to the operation of charging (G2V) and discharging (V2G).

The four proposed operation modes are listed below along with *if-then* operations as tabulated in Table 3.1 that implement in the flowchart in Figure 3.9 and Figure 3.10 with further explanation shown in Figure 3.11 using software implementation only. If the EV charging/discharging is properly managed, the load demand will be decreased during peak hours which means the overloading will not be acquired.

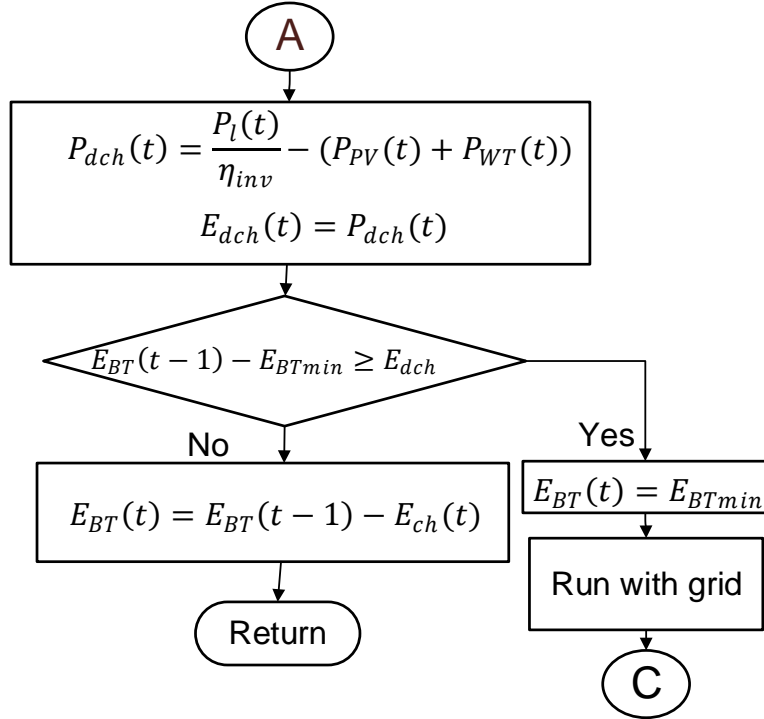
1. Receiving power from RESs (PV and WT) for running the system by charging BT and charging EVs battery.
2. Receiving power from the battery in case of the absents of the grid and low RESs and charging EV.
3. Receiving the power from the main grid (buying-charging-G2V) when EV demand is high and the absence of RESs and BT. This process is known as unidirectional power flow.
4. Receiving the power from the EV (V2G-sell-discharging) when grid demand is high with the absence of RESs and BT. This process is known as bidirectional power flow.

Table 3.1 RB-EMS rules for a grid-connected system with V2G technology.

Rule No.	Modes	IF (condition)	THEN (operation)
1	RESs	$P_{PV}(t) + P_{WT}(t) > P_l(t)$	$P_{PV}(t)$ + $P_{WT}(t)$ to $P_l(t)$ and $EV(t)$
2	Discharge (BT)	$P_b(t) > [P_{WT}(t) + P_{PV}(t) - P_l(t)] * \eta_{inv}$	$P_b(t)$ $> [P_{WT}(t) + P_{PV}(t) - P_l(t)]$ $* \eta_{inv}$ to $P_l(t)$ and $EV(t)$
3	Charge (G2V)	$Grid_{dem} < EV_{dem}$	$Grid_{dem}$ $< EV_{dem}$ to EV (G2V)
4	Discharge (V2G)	$Grid_{dem} > EV_{dem}$	$Grid_{dem}$ $> EV_{dem}$ to grid (V2G)



(a)



(b)

Figure 3.9 The RB-EMS implementation on the microgrid system (a) The RB-EMS flowchart of the system and (b) Discharging operation from BT.

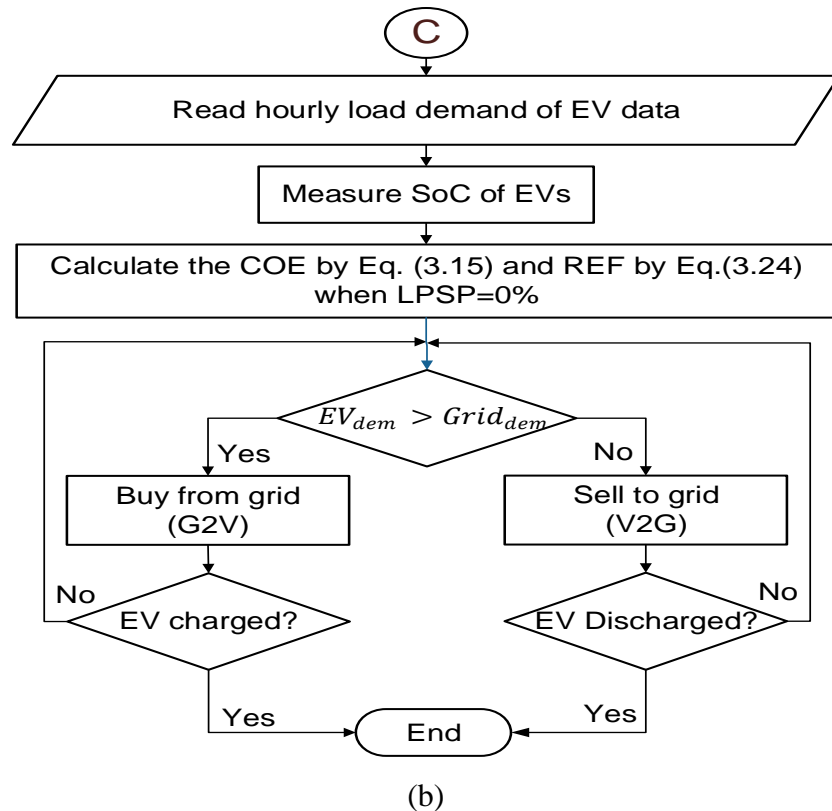
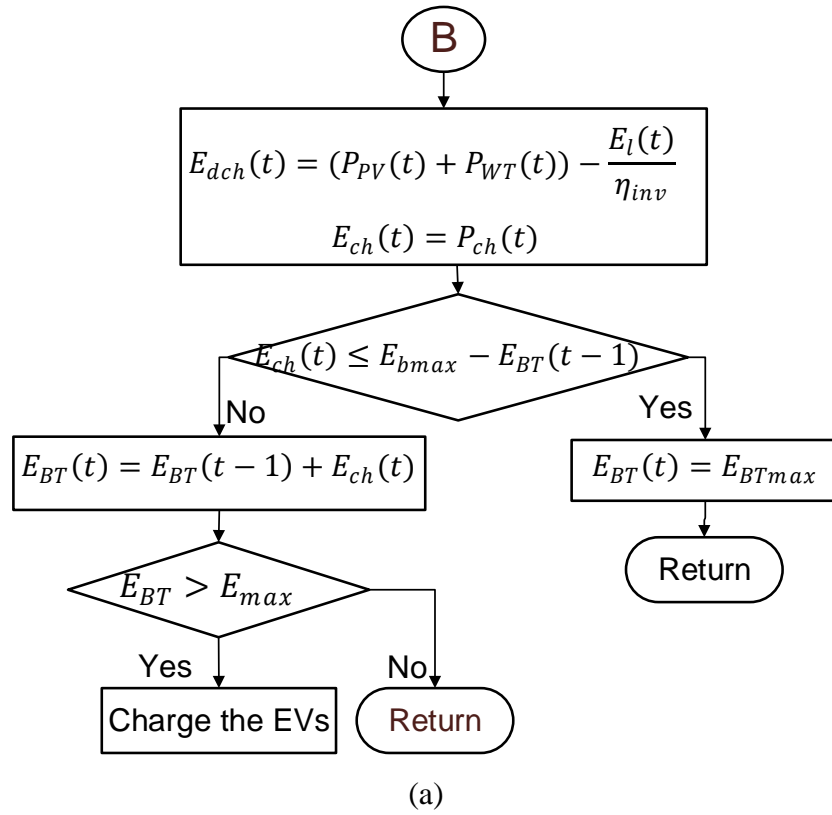


Figure 3.10 The RB-EMS charging and discharging operation (a) Charging from BT and (b) Buying from the grid (G2V operation) and Selling to the grid (V2G operation).

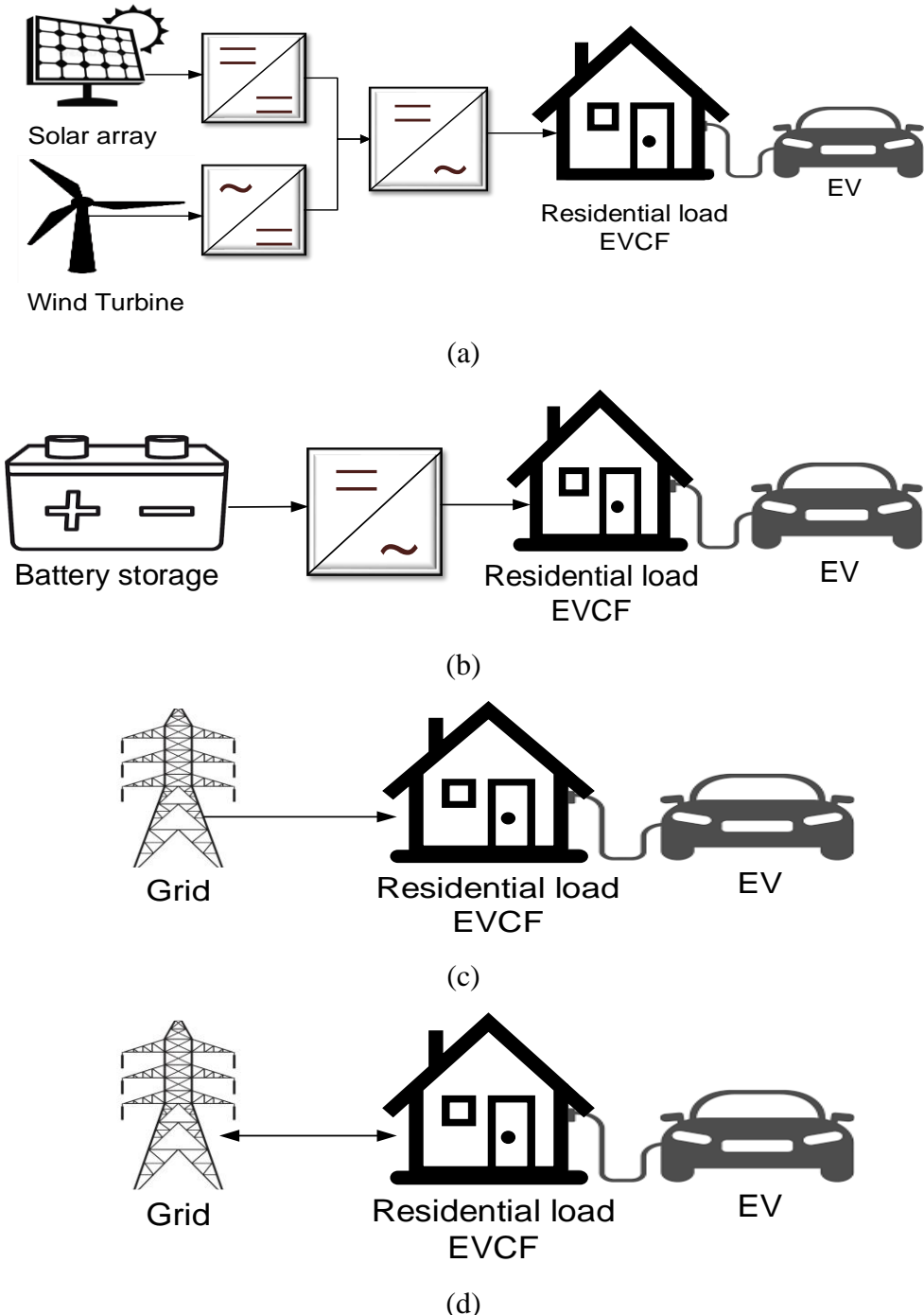


Figure 3.11 Operation modes of the proposed system. (a) Renewable Energy Sources, (b) Deep Cycle Battery units, (c) Grid-to-Vehicle, and (d) Vehicle-to-Grid.

3.5 The Models of the proposed Microgrid Components

Modeling can be defined as the process of identifying objectives, variables, and constraints for a given problem [173]. Many articles have concentrated on

mathematical models for the grid-connected system using V2G technology integration with RESs as an economically-beneficial system [15][46]. Models of the RESs are implemented in this study using MATLAB as a modern software tool to simulate the result of hybrid system components under residential load. The foremost problem with EV drivers is the growing driving range anxiety which means EVCS is required.

Some studies consider PV-EVs integrated with the grid for charging and discharging the EVs [27]. While others hybridize PV and WT at maximum power, and the battery is supporting the system as storage to improve the reliability of the charging station [8], [9]. Designing such a system consists of the presented RESs, sizing is needed and can be presented in [9], [59]. The mathematical model implementation of each component equation will be presented in the next subsections consisting of PV, WT, BT, converter, EVCF, and grid models. The utilized mathematical model equations are widely used among scholars due to their simplicity and cover all the system components [21]. They show the result of reducing the impact of EV demand expansion on the grid [174].

3.5.1 Photovoltaic Model

The most used RESs for producing electricity based on the conversion process from sunlight to produce electricity is PV. The model equation for obtaining the estimated output power generated from the PV system is reported in [158] and presented in Eq.(3.1), while total P_{PV} obtained by multiplying the P_{PV} with N_{PV} at time (t) .

$$P_{PV}(t) = P_{(PV_{rated})} \times \frac{G_{(t)}}{1000} * [1 + \alpha_t(T_c - T_{C_{STC}})] \quad (3.1)$$

where $P_{PV}(t)$ is the output power generated from PV in (Watt), $G_{(t)}$ refers to hourly solar irradiance data in (W/m^2) [158], $1000 \text{ W}/\text{m}^2$ is the rated radiation at the earth's surface, $P_{(PV_{rated})}$ denotes as rated power for PV in (Watt), $T_{C_{STC}}$ is cell temperature at Standard Test Condition (STC), α_t is the temperature coefficient of the panels that

equals to -3.7×10^{-3} ($1/^\circ\text{C}$) [158]. Additionally, the T_C is the cell temperature in ($^\circ\text{C}$) which can be obtained by Eq.(3.2) [59].

$$T_C = T_{amb} + G_{(t)} \times \left(\frac{NOCT - 20}{800} \right) = T_{amb} + G_{(t)} \times (0.03125) \quad (3.2)$$

The T_{amb} is the ambient temperature ($^\circ\text{C}$) that uses time-series data. Besides, the value of 0.03125 $^\circ\text{C}$ was obtained by subtracting the value of Nominal Operation Cell Temperature (NOCT) from air temperature equal to 20 $^\circ\text{C}$. The considered NOCT is 45 $^\circ\text{C}$ in this study depending on the PV module specified by the manufacturer. The acquired result is divided by the irradiance on the cell surface (800 W/m^2) to get 0.03125 $^\circ\text{C}$ [175].

3.5.2 Wind Turbine Model

The second mentioned type of RESs is the most commonly used due to its advantages such as the ability to collect the maximum amount of wind energy for the time of the day. Besides, the ability to adjust the blades' pitch angle to avoid high windstorms. The aforementioned benefits are related to the considered Canadian WT in this study which is Eocycle EO20 with three blades as presented in Table 3.3 [176]. Due to the environmental and economic acquired benefits of using WT as an alternative power generator, WT is exploited. The model equation is presented in Eq. (3.3) for obtaining the generated output power from WT [39].

$$P_{WT}(t) = \begin{cases} 0 & v(t) \leq v_{cut-in} \text{ or } v \geq v_{cut-out} \\ P_r \frac{v(t) - v_{cut-in}}{v_r - v_{cut-out}} & v_{cut-in} < v < v_r \\ P_r & v_r < v(t) < v_{cut-out} \end{cases} \quad (3.3)$$

where v_{cut-in} is the cut-in speed and it is very low, $v_{cut-out}$ is the high cut-out, P_r is rated power in (W). The v_r is rated wind speed (m/s) and P_{WT} refers to the output power generated from WT in (kW) with the help of hourly wind speed data (v), where the total power produced from WT can be acquired by multiplying P_{WT} with N_{WT} at a

time (t). Besides, its hub height (h) is the relationship between height from the surface and wind speed that can be calculated in Eq. (3.4) [59].

$$v = v_{ref} \times \left(\frac{h}{h_{ref}} \right)^{\gamma} \quad (3.4)$$

where v and v_{ref} are the rate turbine speed and wind speed in (m/s) that recorded at h_{ref} which refers to the reference height anemometer 43.6 m, h is the hub height that is equal to 30 m, and γ represents the status of the landscape where the turbine is going to be installed within the range [0.1, 0.25] [177]. Furthermore, the γ varies from location to location depending on the topology surface of the utilized area, where 0.1 refer to the flat area and 0.25 non-flat. The ideal power curve and operation region are illustrated in Figure 3.12.

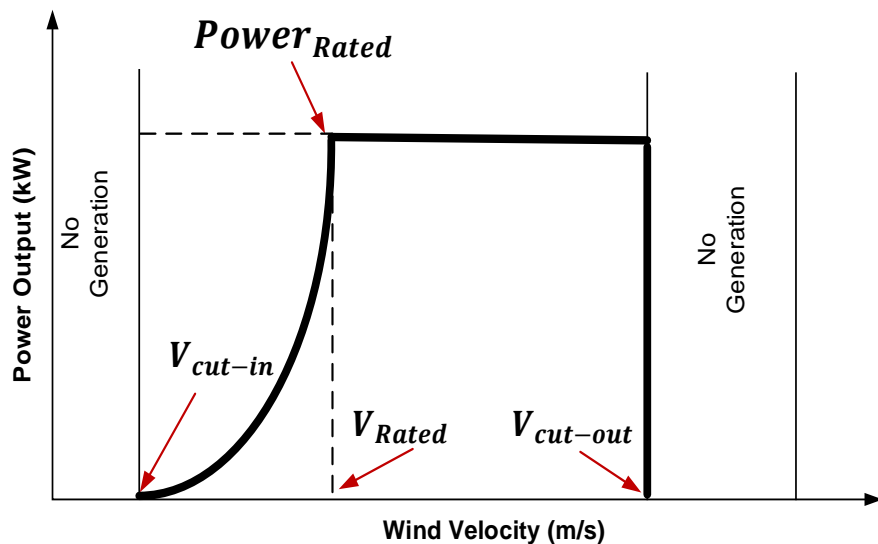


Figure 3.12 The ideal power curve of wind turbines and operation regions [158], [178].

3.5.3 Battery Model

As the backup system of the microgrid in case of sun absences, cloudy days, and issue connection to the main grid or RESs, the battery is used. The mathematical

model of computing the battery capacity can be acquired by using Eq. (3.5). The utilized deep cycle battery is Li-Ion with its datasheet reported in [140], [158].

$$C_B = \frac{P_l \times AD}{DOD \times \eta_{inv} \times \eta_b} \quad (3.5)$$

where C_B is the capacity of the battery in (Ah), P_l is the daily average load demand in (kW), AD is the autonomy days (typically 3-5 days). The DoD is the Depth-of-Discharge (80%), η_b is the battery's efficiencies (85%), and η_{inv} is the inverter's efficiency (95%) [95]. Eq. (3.6) is used to calculate the power delivered from the battery in the case of utilizing RESs only [179].

$$P_{BT}(t) = (P_{PV}(t) + P_{WT}(t)) - \frac{P_l(t)}{\eta_{inv}} \quad (3.6)$$

where $P_{BT}(t)$ is the power delivered from the battery and $P_l(t)$ is the total energy demand. Calculating the SoC (t) of the battery while charging or discharging can be calculated by Eq. (3.7) and Eq. (3.8), respectively [69]. The limitation of the SoC is used to determine the quantity of charge in the battery at a time (t).

$$SoC(t) = SoC(t-1) \cdot (1 - \sigma) + \left((P_{PV}(t) + P_{WT}(t)) - \frac{P_l(t)}{\eta_{inv}} \right) \times \eta_b \quad (3.7)$$

where σ is the self-discharge rate of the battery equals 0.007% hour [59] and the $SoC(t)$ denotes as the state-of-charge of the battery at a time (t) [158]. The discharging of the battery can be presented by Eq. (3.8).

$$SoC(t) = SoC(t-1) \cdot (1 - \sigma) + \left(\frac{P_l(t)}{\eta_{inv}} - (P_{PV}(t) + P_{WT}(t)) \right) \times \eta_b \quad (3.8)$$

The battery is set to operate at an SoC ranging from 20 to 100% which can be expressed as $SoC_{min}^{BT} \leq SoC^{BT} \leq SoC_{max}^{BT}$. The DoD presents the percentage of charge consumed in a battery is dependent on battery life with the temperature. While the SoC presents

the remaining charge in the battery as illustrated in Figure 3.13 the essential concept of battery. This storage can be recharged depending on manufacturer specifications [138], [139]. Table 3.2 presents the specification of LiFePO₄ as the mostly utilized battery.

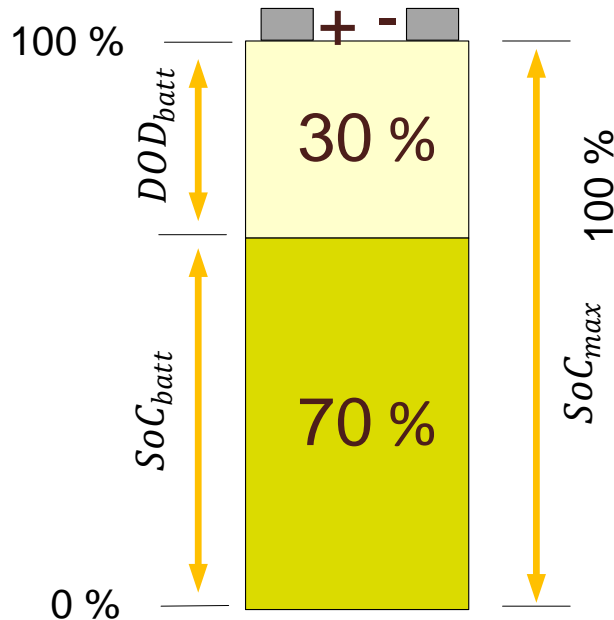


Figure 3.13 The essential concept of battery SoC and DoD.

Table 3.2 Specification of EV (LiFePO₄) battery [140], [141].

Parameters	LiFePO ₄	Units
Nominal voltage	3.2	V
Energy density	120	Wh/Kg
The volumetric energy density	220	Wh/L
Specific power	2000-4500	W/kg
Life cycle	>2000	-
Operating temperature	-45 to +70	1C
Production cost	350	\$/kWh
Efficiency	99	%
Initial Temperature	20	°C
Discharge power	1200	W

3.5.4 Converters Model

To convert the power in the system from DC to AC, a converter is required. They play the role of either rectifier (AC/DC) or inverter (DC/AC) which allows the power transfer between the sources and end-user. The inverter efficiency (η_{inv}) is 95% and the output convergence power ($P_{inv\ output}$) at the time (t) can be calculated using Eq. (3.9) [59].

$$P_{inv\ output}(t) = (P_{PV}(t) + P_{WT}(t)) \times \eta_{inv} \quad (3.9)$$

3.5.5 Electric Vehicle Charging Facility model

The EVCF is a utilized area for charging EVs to continue driving and reduce the anxiety of drivers. The amount of EV power demand can be estimated by Eq. (3.10) [69].

$$P_{EV_{Dem}} = \frac{C_{bat}^{EV} \times (SOC_{max}^{EV} - SOC_{min}^{EV})}{T} \quad (3.10)$$

where the $P_{EV_{Dem}}$ represents the EV power demand in (kW), C_{bat}^{EV} is the EV capacity which is 14 Ah that is considered in this study [8]. The SOC_{EV} is randomly built in the range of 0.2% and 0.95% as ($SOC_{min}^{EV} \leq SOC^{EV} \leq SOC_{max}^{EV}$) using one of the stochastic methods namely normal distribution in range of [0,1] [180], and T indicates the difference between the arrival and departure times ($T = T_{arrive}^{EV} - T_{Dep}^{EV}$) [69].

3.5.6 Utility Grid Model

The main purpose of EVCF is to continuously supply the load with the needed power of EV. During the absence of RESs energy and the battery is not charged, the system can be supplied from the main grid. To count the amount of purchased energy in (kWh) from the grid (P_P^{grid}) to the EV which presents (G2V) can be calculated

using Eq. (3.11) [69], while the amount of sold energy from the EV to the grid (P_S^{grid}) is calculated using Eq. (3.12) [21].

$$P_P^{\text{grid}}(t) = P_{EV_{Dem}}(t) - [P_{PV}(t) + P_{WT}(t) + \left[(\text{SOC}_{BT}(t) - \text{SOC}_{BT}^{min}(t)) \times \eta_{inv} \right]] \quad (3.11)$$

$$P_S^{\text{grid}}(t) = [P_{PV}(t) + P_{WT}(t) + \left[(\text{SOC}_{BT}(t) - \text{SOC}_{BT}^{max}(t)) \times \eta_{inv} \right]] - P_{EV_{Dem}}(t) \quad (3.12)$$

To count the revenue (R_{grid}) from selling energy to the grid can be calculated using Eq. (3.13) [181].

$$R_{grid} = \sum_{t=1}^{8760} rate_{feed-in} \times E_{grid(selling)} \quad (3.13)$$

where the $rate_{feed-in}$ refers to the feed-in tariff rate which is (0.05 \$/kWh) multiplied with $E_{grid(selling)}$ that indicates the selling energy [181]. While 8760 refers to the number of hours for one year per hour. Additionally, the purchasing cost of the bought energy (C_{grid}) from the grid is calculated using Eq. (3.14) [21].

$$C_{grid} = C_p \times \sum_{t=1}^{8760} E_{grid(purchased)} \quad (3.14)$$

The C_p is the cost of buying 1 kW of electricity from the grid which equals (0.04 \$/kWh) in Libya [181], $\sum_{t=1}^{8760} E_{grid(purchased)}$ refers to the summation of buying electricity from the grid for one year [21]. Additionally, the designed variables (control parameters) are listed for the utilized components of the microgrid and are tabulated in Table 3.3 including the PV-WT-BT-EVCF-grid-converter-economic parameters.

Table 3.3 Summary of the hybrid system components.

Components	Parameters	Value	Unit
PV system [127][175]	Lifetime	25	Years
	Rate Power at STC	325	W
	Operation & Maintenance (O&M) cost	20	\$/year
	Initial cost	2.15	\$
	Temperature coefficient (α_t)	-3.7×10^{-3}	1/°C
	Replacement cost	0	\$/year
	Nominal operating cell temperature	45 ± 2	°C
	Regulator Cost	1500	\$
Wind Turbine [176], [179], [181]	Lifetime	25	Years
	Replacement cost	0	\$/year
	Cut-in speed (V_{cut-in})	2.8	m/s
	Cut-out speed ($V_{cut-out}$)	20	m/s
	Rate Power of Wind Turbine	1	kW
	Operation & Maintenance (O&M) cost	50	\$/year
	Rate Speed (V_r)	7.5	m/s
	Blades diameter	15.8	m
	Hub height (h)	30	m
	Overall efficiency	26	%
Battery Storage [182] [158] [8][140]	Lifetime	10	Years
	Initial SoC of battery	100	%
	SoC_{min}	20	%
	SoC_{max}	100	%
	Minimum charge current	17	A
	Maximum charge current	14	A
	The initial cost of the battery	280	\$
	Nominal battery capacity	42	Ah
	Battery capacity	40	Ah
	Replacement cost	280	\$/year
	Hourly self-discharge	0.007	%/hour
	O&M cost	5	\$/year
	Rate capacity	45.2	kWh
	Maximum DoD	80	%
Electric Grid [181]	Power importing price (sell)	0.05	\$/kWh
	Power exporting price (purchase)	0.04	\$/kWh
Electric Vehicle Charge Facility [183] [9][127]	Max/Min capacity of EV battery	24/20	A
	SoC_{max}^{EV}	95	%
	SoC_{min}^{EV}	20	%
	EV capacity	14	kWh
	Energy density of the Li-ion battery	118-250	Wh/kg
Converter [126][127] [158][181]	Lifetime	15	Year
	Efficiency (η_{inv})	92	%
	Rate power	1	kW
	Operation & Maintenance (O & M) cost	1	\$/year
	Initial cost	2500	\$
Economic Parameters	Annual interest rate (i)	3	%
	Project life	25	Years

3.6 Objective Functions Optimization of the proposed microgrids

To be more specific, this study is considering the economic aspects in order to calculate the cost of energy. The study used a grid-connected system in Tripoli city-Libya to achieve and evaluate the proposed objective functions by utilizing the RESs (PV and WT) with BT and EVs forming V2G. The annual investment of the system will be calculated to get a reduction of the Cost of Energy (COE), Losses of Power Supply Probability (LPSP), and maximization of the renewability using the Renewable Energy Fraction (REF) technique, respectively. Additionally, the objective functions of this study are presented in the literature to ensure a reliable power supply at a minimum cost and losses with high renewability [21]. This study proposes a multi-objective function by utilizing the IALO in order to meet the objectives and linearly combined.

3.6.1 Cost of Energy

From an economic point of view, calculating the Cost of Energy (COE) as an objective function is presented in Eq. (3.15) [21] defined as the per capita of electricity [158]. COE is known as an infinite source that provides electricity to a system that applies to run electric appliances [21]. To calculate the COE, the Discounted Cash Flow (DCF) analysis method is applied [184]. Where DCF is utilized to approximate or evaluate the value of capital investment money [21]. The term DCF is a modern economic term and presents the summary that is reflecting the present value of money (cost) of the project lifetime. It is designed to calculate the payback period which means all capital costs (O&M, replacement cost, and installation cost) during the lifetime of the system.

$$COE = \frac{(CRF \times \sum_x NPC_x) + C_{grid-} R_{grid}}{E_{served} + E_{grid-selling}} \quad (3.15)$$

The COE presented in Eq. (3.15) can be obtained with the help of the Capital Recovery Factor (CRF) which is used to calculate the present value of money as presented in Eq. (3.16) [185]. The Net Present Cost (NPC) in (\$) includes the costs (O&M, replacement

cost, and installation cost) for x of years that can be computed by Eq. (3.17). The $E_{grid\text{-}selling}$ indicates the selling energy, E_{served} is the primary load served in (kWh/year) [21].

$$CRF = \frac{i(1+i)^n}{(1+i)^n - 1} \quad (3.16)$$

where i is the real interest rate in (%), n is the amortization period or (system life period) that is equal to the lifetime of the solar panels (25 years) [95]. The ASC refers to the Total Annualized System Cost (\$) [21].

$$NPC(\$) = \frac{ASC}{CRF} \quad (3.17)$$

Calculating the cost of each component in order to obtain the Annualized System Cost (ASC) as presented in the equations from Eq. (3.18)-Eq. (3.22) [179].

$$C_{SOL} = C_{PV}^{INST} + C_{PV}^{REP-C} + C_{PV}^{O&M} \quad (3.18)$$

$$C_{WT} = C_{WT}^{INST} + C_{WT}^{REP-C} + C_{WT}^{O&M} \quad (3.19)$$

$$C_{BATT} = C_{BATT}^{INST} + C_{BT}^{REP-C} + C_{BATT}^{O&M} \quad (3.20)$$

$$C_{INV} = C_{INV}^{INST} + C_{INV}^{REP-C} + C_{INV}^{O&M} \quad (3.21)$$

where C_{INV}^{INST} , C_{PV}^{INST} , C_{BT}^{INST} , and C_{WT}^{INST} are the installation cost of the inverter (per kW), solar panels (per kW), battery (per unit), and wind turbine (per kW), respectively. While the $C_{INV}^{O&M}$, $C_{PV}^{O&M}$, $C_{BT}^{O&M}$, and $C_{WT}^{O&M}$ are the annual operation and maintenance costs of the inverter, solar panels, battery, and wind turbine, respectively. The C_{INV}^{REP-C} , C_{PV}^{REP-C} , C_{BT}^{REP-C} , and C_{WT}^{REP-C} are the replacement cost of the inverter, solar panels, battery, and wind turbine, respectively [127], [179]. The values of the mentioned components are provided in Table 3.3.

$$ASC = F(N_{PV}C_{SOL} + N_{WT}C_{WT} + N_{BT}C_{BT} + P_{INV}C_{INV}) \quad (3.22)$$

where the C_{INV} is the cost of the inverter (per kW), C_{SOL} is the cost of solar panels (per kW), C_{BT} is the cost of the battery (per unit), and the C_{WT} is the cost of a wind turbine (per kW), and the P_{INV} is the rating power of the inverter. F is the obtained value of CRF [127]. Where the values of NPC of the grid as its replacement cost is zero [179].

3.6.2 Losses Power Supply Probability

The second objective function for measuring reliability is using the Losses Power Supply Probability (LPSP) technique that is presented in Eq. (3.23). The LPSP ranges between $(0 \leq LPSP \leq 1)$, where 0 refers to satisfied load and 1 refers to unsatisfied load. It can be defined as the capability of the power system to deliver electricity to consumers in a secure way without power losses [65]. Furthermore, minimizing the LPSP refers to the probability of power supply failure to meet the load demand which can be computed in Eq. (3.23) [9].

$$LPSP(\%) = \frac{\sum_{i=1}^N [P_l(t) - (P_{PV}(t) + P_{WT}(t) + SoC_{BT}(t) + SoC_{EV}(t))] }{\sum_{i=1}^N P_l(t)} \quad (3.23)$$

where the SoC_{BT} denoted as the state-of-charge of a deep cycle battery in a time (t) , while the SoC_{EV} is the state-of-charge of the EV battery at a time (t) .

3.6.3 Renewable Energy Fraction

The last objective function related to this study is to maximize renewability by exploiting the Renewable Energy Fraction (REF) technique [21]. The REF is defined as the quantity of the energy transferred to the load that is generated from RESs that reduces the NPC and CO₂ emission which can be calculated by Eq. (3.24) [111].

$$REF(\%) = \frac{\sum_1^{8760} (P_{PV} + P_{WT}) \times \Delta t}{\sum_1^{8760} (P_{PV} + P_{WT} + P_{grid purchased}) \times \Delta t} \quad (3.24)$$

where the $P_{grid_purchased}$ is referring to the amount of purchased electricity from the grid for one year [21]. The main three presented objective functions have a trade-off. When the LPSP is minimized, the REF is maximized, and the overall system cost rises, increasing the COE. As a result, the designer has to compromise the three objective functions to achieve the optimal result. Additionally, the minimization of the two aforementioned multiple objective functions with the maximization objective has been linearly combined and implemented in IALO as expressed in Eq. (3.25) [59].

$$wF_1 + (1 - w) \times \gamma \times PF \times F_2 + wF_3 \quad (3.25)$$

where the w is the weighting factor that is generated randomly in the range of (0,1) which is set as zero and progressively increases interval of 0.05 up to 1, F_1 , F_2 , and F_3 are the COE, LPSP, and REF, respectively. Additionally, the γ is a scaling factor that is set as 1000 [59], PF is the balancing factor for the different units of the utilized objectives.

3.6.4 Constraints in an optimization framework

The mentioned objective functions (COE, LPSP, and REF) are considered to gain a minimum cost and reliability along with high renewability in a grid-connected system. Out of the aforementioned objective functions, LPSP and REF are the constraints due to the climatology conditions and not meeting power demand. Besides, the SoC_{EV} during arrival (SoC_{arrive}^{EV}) and SoC_{EV} during departure (SoC_{Dep}^{EV}) are considered as a constraint. The number of WT, SoC, PV, and BT in the hybrid system is known as design variables (decision variables) that are evaluated in this study. The boundary (upper and lower) of the components (N_{WT} , N_{PV} , N_{AD} , and N_{BT}) are ranges between $0 \leq 50$, $0 \leq 100$, $0 \leq 5$, and $0 \leq 100$, respectively. While the limits of the design variables (control parameters) is stated in Eq. (3.26). Regarding the number of EVs, this study proposes three cases when integrating 10, 30, and 60 of EVs respectively, which is proposed for each house to have one EV to form V2G technology (charge/discharge). Furthermore, the integration of the three mentioned cases are referring to each EV connected separately in a single house for power exchange.

$$\begin{cases} N_{WT} & N_{WT}^{min} \leq N^{WT} \leq N_{WT}^{max} \\ N_{BT} & N_{BT}^{min} \leq N^{BT} \leq N_{BT}^{max} \\ N_{PV} & N_{PV}^{min} \leq N^{PV} \leq N_{PV}^{max} \\ N_{AD} & N_{AD}^{min} \leq N^{AD} \leq N_{AD}^{max} \end{cases} \quad (3.26)$$

3.7 The Test Function Application of the proposed algorithm

This section presents four popular benchmark test functions in order to validate the results of the proposed IALO method [33]. According to [54], there is no agreed-on test function list as presented in the literature [33], [186], [187]. The exploited test functions for unimodal are namely, Sphere (F_1) and Schwefel2.22 (F_2), while for the multimodal are Ackley (F_{10}) and Penalized 2 (F_{13}) as presented in [187] as presented in Table 3.4. The unimodal is a function with one global solution in the research space, while multimodal is a function with many local solutions and one global solution [186]. Due to the aforementioned function makes the allowability for benchmark performance with other metaheuristic algorithms in terms of exploration and avoids the quick achievement of the local optima.

Table 3.4 illustrated the widely used test functions for testing the optimization algorithms due to their provided benchmark results in microgrid applications. The sphere test function is the most implemented test function due to the accurate provided result that has local minimum dimensional ranges between [-100,100]. The Schwefel2 test function is a complex function with many local minima ranges between [-100,100]. Ackley function is formed in a two-dimensional and categorized by a nearly flat outer region and a large hole at the middle center and ranges between [-20, 20]. Eventually, the Penalized 2 test function is presented in two-dimensional form and ranges between [-5,5] and has several local minima.

Table 3.4 Unimodal and multimodal benchmark function [33], [54].

Function	Mathematical expression	Dimension	Range
Unimodal Benchmark Function			
Sphere Function (F_1)	$F_1(x) = \sum_{i=1}^n x_i^2$	30,200	[-100,100]
Schwefel2.22 Function (F_2)	$F_2(x) = \sum_{i=1}^n x_i + \prod_{i=1}^n x_i $	30,200	[-100,100]
Multimodal Benchmark Functions			
Ackley Function (F_{10})	$F_{10}(x) = -20 \exp\left(-0.2 \sqrt{\frac{1}{n} \sum_{i=1}^n x_i^2}\right)$ $- \exp\left(\frac{1}{n} \sum_{i=1}^n \cos(2\pi x_i)\right) + 20 + e$	30,200	[-20,20]
Penalized 2 Function (F_{13})	$F_{13}(x) = 0.1 \left\{ \sin^2(3\pi x_1) + \sum_{i=1}^n (x_i - 1)^2 [1 + \sin^2(3\pi x_1 + 1)] + (x_n - 1)^2 [1 + \sin^2(2\pi x_n)] \right\} + \sum_i^n u(x_i, 5, 100, 4)$	30,200	[-5,5]

3.8 The Metaheuristic Optimization Algorithms

The proposed algorithm is classified under nature-inspired metaheuristic algorithms, which enable it to overcome microgrid issues [188]. There are numerous methods for solving power flow problems, one of them is Antlion Optimization as presented in the literature with its variations [189]. The main measurement of success or failure of any method is by measuring the time, accuracy, and optimality [6], [20]. The utilized algorithm for sizing the system components has been improved due to the faced limitation in the conventional ALO such as premature convergence and quickly falling in the local optima solution. Whereas the improvements were done to Antlion

Optimization (ALO) namely Improved ALO (IALO) is mathematically presented in Section 3.8.2 and has not been applied to the V2G system in the literature yet.

3.8.1 Antlion Optimization

As the original method has been elaborated with the mathematical equations in the previous chapter. The antlion optimization steps are shown in Table 3.5. Applying RB-EMS-ALO is presented in this section as shown in Figure 3.14 by integrating the data of the parameters, load demand, objective functions (COE, LPSP, and REF) and constraints, and economic and technique data into the original nature-inspired algorithm to form the RE-EMS-ALO.

Table 3.5 Steps of Antlion Optimization.

Steps	Implementing operation
Step 1	<ul style="list-style-type: none"> • Loading weather database (Solar irradiance, Ambient temperature, Wind speed) is shown in Figures 4.2 (a), Figure 4.5 (a), and Figure 4.8 (a), respectively. • The load demand database is figured in Figure 4.18 (c). • The load economic database for the microgrid components is listed in Table 3.3.
Step 2	<ul style="list-style-type: none"> • Set the ALO constants. <ul style="list-style-type: none"> - Population size=5, G=20, Max iteration=100, Search agent=10. • Set constraint. <ul style="list-style-type: none"> - REF and LPSP. • Set the research space: <ul style="list-style-type: none"> - lower and upper bounds for N_{PV} [0,100] - lower and upper bounds for N_{WT} [0,50] - lower and upper bounds for N_{AD} [0,3] - lower and upper bounds for N_{BT} [0,100]. • Update the fitness for each ant and antlion. • Select an antlion using Roulette Wheel Selection.
Step 3	<ul style="list-style-type: none"> • Updating the position between the antlion and elite using Eq. (2.3)
Step 4	<ul style="list-style-type: none"> • Update the position of all ants. • If updated calculate the fitness for each ant and antlion, if not go to step 2
Step 5	<ul style="list-style-type: none"> • Search the optimal solution in the antlion group
Step 6	<ul style="list-style-type: none"> • If the best solution is obtained stop, if not repeat step 2

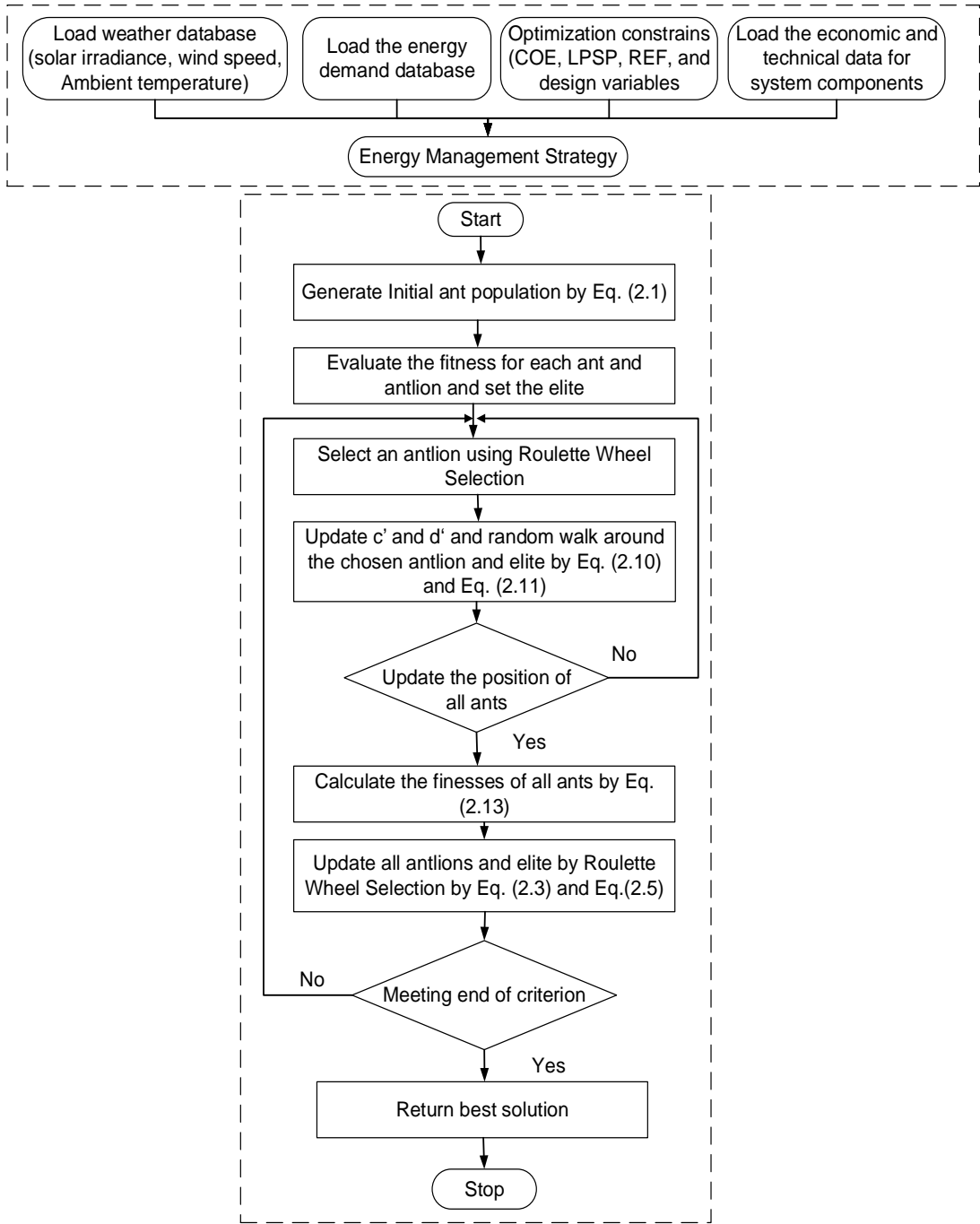


Figure 3.14 Flowchart of Rule-Based Energy Management Strategy of ALO.

3.8.2 The proposed Improved Antlion Optimization

Several metaheuristic algorithms have been improved in the literature through the previous years and applied in various applications. The IALO is one of the developments of the ALO algorithm from the perspective of better accuracy and optimality [190]. Due to the provided merits by ALO, ALO is employed to solve

different optimization problems such as benchmark functions, machine learning, scheduling, and control of power. Besides, smart grid, networking, feature selection, software engineering, and solving the limitation of the ALO method [74]. A challenge that minimizes the size of chosen features and maximizes classification efficiency is known as feature selection [75]. The technique of feature selection involves choosing a meaningful subset of characteristics (selection of individuals in metaheuristic algorithms) from a large set [191]. Where the feature selection classifies into two groups: wrapper-based and filter-based [192]. The former considers machine learning techniques as used in this study. In contrast, the latter considers being computationally inexpensive due to the search for the optimal settings from the vast region of dimensionality [193]. Various feature selections have been projected such as Boltzmann selection, Tournament selection, Roulette Wheel Selection (RWS), Lévy Flight (LF), Linear rank selection, Rough-set, and others [75]. Feature selection can be defined as the process of selecting a significant subset from a huge data.

The differences between ALO and IALO are in the random walk as a selection method as briefly has been elaborated in the previous chapter. Where ALO uses the Roulette Wheel Selection as a feature selection method to choose and update the position of ants and antlions, while IALO uses Lévy Flight [33]. LF is proposed to improve the effectiveness of random walks (local search) in the conventional ALO and is also known as lévy distribution (lévy walk). The LF proposed to address the faced limitations of ALO such as long runtime during the optimization process due to the random movements of the antlion, premature convergence, and quickly falling in the local optima solution. Additionally, RWS is preferable for maximization problems, while LF is utilized with other algorithms for minimization problems as stated in the literature [91]. Both feature selection methods as RWS and LF are used to control the random walk in the proposed algorithm (IALO) and comparison algorithms, however, the latter performs better [33]. Based on the conducted studies, LF has been combined and implemented with other metaheuristic algorithms such as CSA [32], in order to overcome optimization problems in various fields. Additionally, the flowchart of IALO is shown in Figure 3.15, it differs from ALO in updating ant and antlion positions by Eq. (3.27) by applying the LF method as highlighted in action 3. Accordingly, the obtained result from IALO will be benchmarked with the counterparts (ALO, PSO, and CSA) as briefly described in the following subsection.

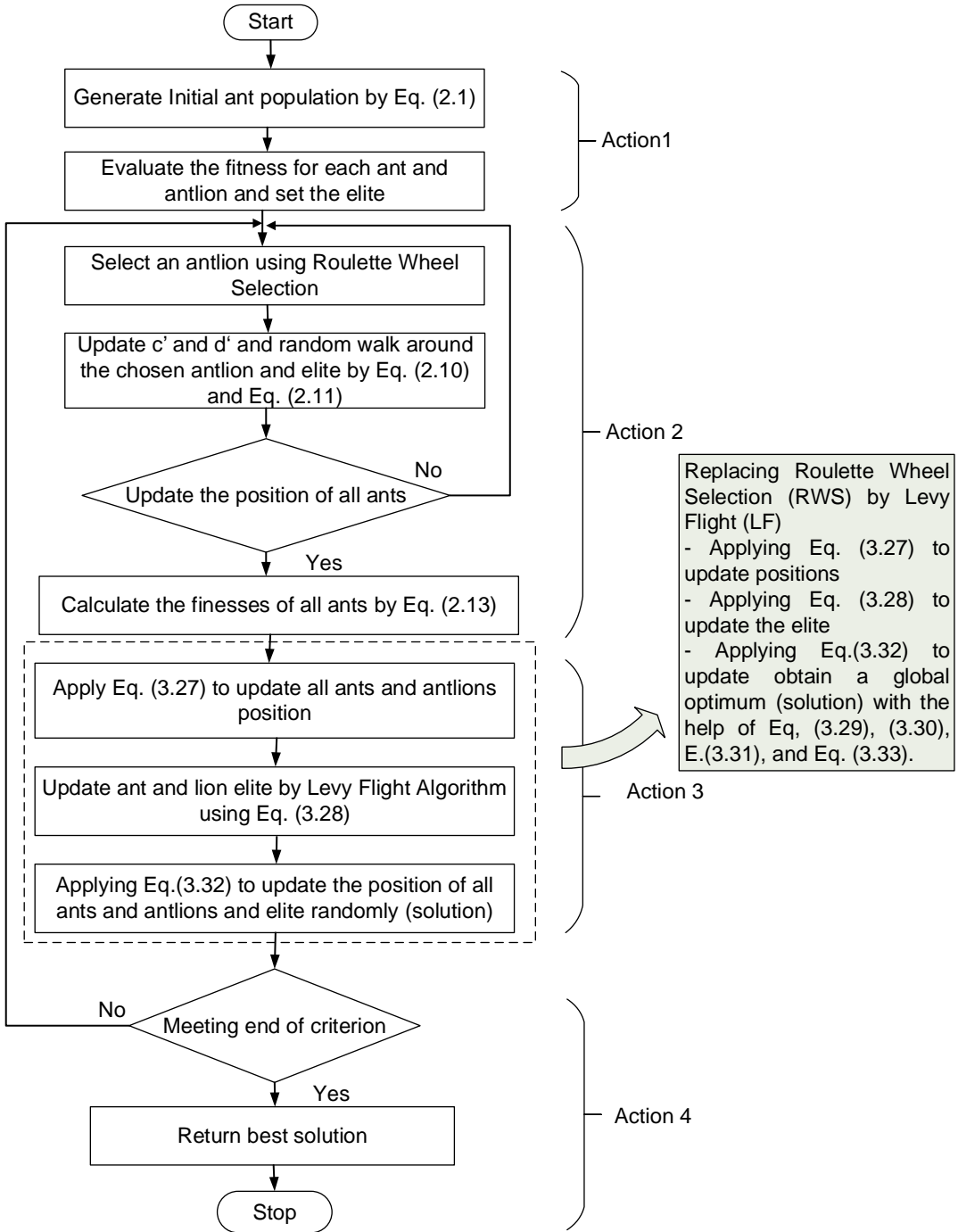


Figure 3.15 Flowchart of the proposed Improved ALO (IALO) Algorithm.

where the improved random walk ($RWX(t)$) can be presented in Eq. (3.27) with the controlled LF that reduces the distance of the random walk.

$$\begin{aligned}
 RWX(t) = & [0, \text{cumsu}(2\text{Lr}(t_1) - 1, \text{cumsu}(2\text{Lr}(t_2) \\
 & - 1.. \text{cumsu}(2\text{Lr}(t_n) - 1,]
 \end{aligned} \tag{3.27}$$

Furthermore, using lévy flight to improve the search of ALO algorithm and solve microgrid optimization problems for the best number of configurations (elite). Eq. (3.26) was utilized to update all ants and antlions' positions by LF algorithm instead of RWS and Eq. (3.28) updates the new position considering LF.

$$x_i^{(t+1)} = x_i^{(t)} + \alpha_{step} \otimes \text{lévy}(s) \quad (3.28)$$

where the $x_i^{(t)}$ is the current position of ant, $x_i^{(t+1)}$ denoted as the new position, α_{step} is considered a constant value and known as step size which is considered as greater than 0. s is the step length that can be mathematically expressed as in Eq. (3.29) and \otimes is the entry-wise multiplication (refers to a matrix with the same dimension). Essentially, LF is providing a random walk, where the steps can be drawn by Eq. (3.30).

$$s = \frac{\varphi \times \mu}{|\alpha|^\gamma} \quad (3.29)$$

$$\text{lévy } (\gamma) \sim u = t^{-\gamma}, 1 < \gamma \leq 3 \quad (3.30)$$

where α and μ are denoted as the normal distribution (standard deviation and mean) in Eq. (3.30), u refers to the uniformly distributed value [1,3], and γ is lowercase gamma that is greater than 1 and less or equal to 3 ($1 < \gamma \leq 3$), it assumed to be 1.5. The φ is called the lowercase of Phi which can be calculated in Eq. (3.31) [75].

$$\varphi = \left[\frac{\Gamma(1 + \gamma) \times \sin(\pi \times \gamma/2)}{\Gamma\left(\left(\frac{1 + \gamma}{2}\right) \times \gamma \times 2^{\left(\frac{\gamma-1}{2}\right)}\right)} \right]^{1/\gamma} \quad (3.31)$$

The Γ refers to the uppercase standard gamma function that equals $\sqrt{\pi}$, where the uniform distribution random walk (*RaWa*) for both ant' and antlion' is performed in Eq. (3.32).

$$RaWa = \text{Ant}_i^t + \omega \times s \times r \times [\text{Antlion}_j^t - \text{Ant}_i^t] \quad (3.32)$$

where ω is a controlling scale for the random walk considering the current iteration (t) and the number of allowable iterations (N) that can be mathematically expressed in Eq. (3.33). The subtracting operation is to update the position of antlion and ant.

$$\omega = 1 - \frac{t}{N} \quad (3.33)$$

Furthermore, the mathematical steps for the proposed algorithm are presented in Eq. (3.27) - Eq. (3.33), and further steps are tabulated in Table 3.6 [78], the implementation process of the RB-EMS-IALO is illustrated in Figure 3.16.

Table 3.6 Steps operation of the proposed IALO and its description.

Steps	Implementing operation
Step 1	Randomly initialize the position of ants and antlions as referred to in action 1 in Figure 3.15.
Step 2	Calculate the fitness of the antlions and ant to choose the antlion whose fitness is best as the elite
Step 3	<ul style="list-style-type: none"> • Select an antlion using the Roulette wheel selection and calculate the random walks around the chosen antlion and the elite. • Update the ants' position with Eq. (2.2) - Eq. (2.9).
Step 4	Repeat step 3 until the positions of all the ants are updated
Step 5	<ul style="list-style-type: none"> • Update the antlions' positions with Eq. (3.30). • Compare the fitness of the new antlions with the fitness of the elite. • If the antlions have better fitness, then the elite will be replaced by the position of the antlion.
Step 6	Update the position of ants and antlion by lévy using Eq. (3.27) - Eq. (3.33) are adopted to search for better antlions and update the elite.
Step 7	Repeat steps 3 to step 7 until the stop criteria are met.

The aforementioned operation steps presented in Table 3.6 for the proposed method (IALO) are placed in steps 5 and 6, while the beginning and the end of the algorithm are similar to the original ALO. The original ALO considered RWS as a feature selection to update the position of ant and antlion, however, it faces premature convergence and acquiring local optima quickly. For addressing the ALO limitations, IALO is enhanced by replacing LF rather than RWS for the same purpose in order to gain a robustness method and improve the randomness.

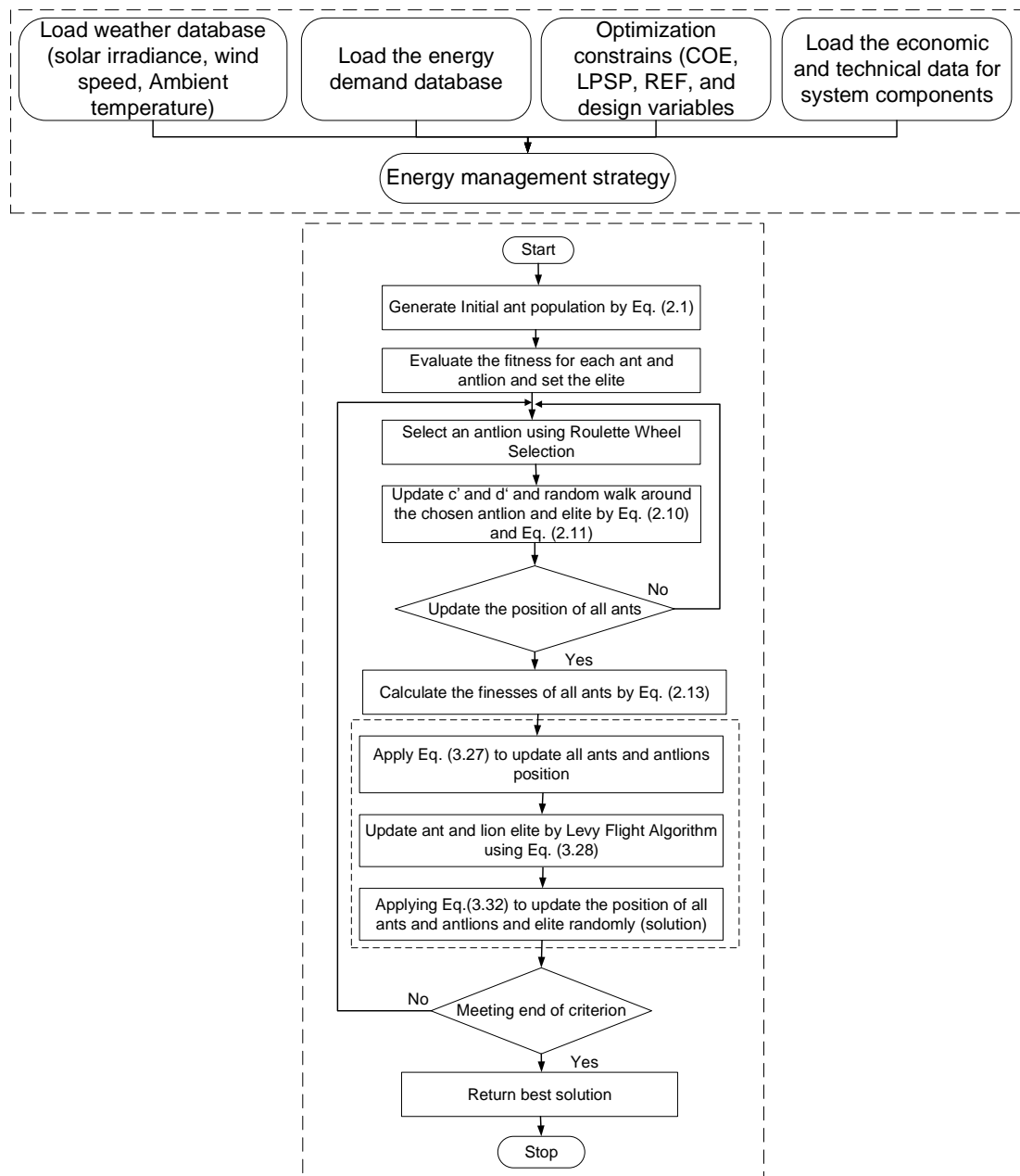


Figure 3.16 Flowchart of the proposed Rule-Based-Energy Management Strategy of IALO (RB-EMS-IALO).

3.9 The benchmark algorithms

The obtained result from the proposed algorithm (IALO) will be validated with other metaheuristic algorithms which are ALO, PSO, and CSA as very well known algorithms. The elaboration for benchmarking utilized algorithms is presented in the subsection below. The benchmarking methods have been chosen as popular methods due to their high efficiency in providing the optimum result. In addition to the complementation of IALO with RB-EMS for the aforesaid methods as RB-EMS-ALO in section (3.8.1), RB-EMS-PSO in section (3.9.1), and RB-EMS-CSA in section (3.9.2) are discussed.

3.9.1 Particle Swarm Optimization

The explanation of PSO has been elaborated in the aforementioned chapter (refer to chapter 2) as a benchmark method for the acquired result from IALO. The flowchart of applying RB-EMS-PSO is presented in Figure 3.17 by inserting load demand, objective functions (COE, LPSP, and REF), and economic and technical data for system components. While the steps of PSO is tabulated in Table 3.7.

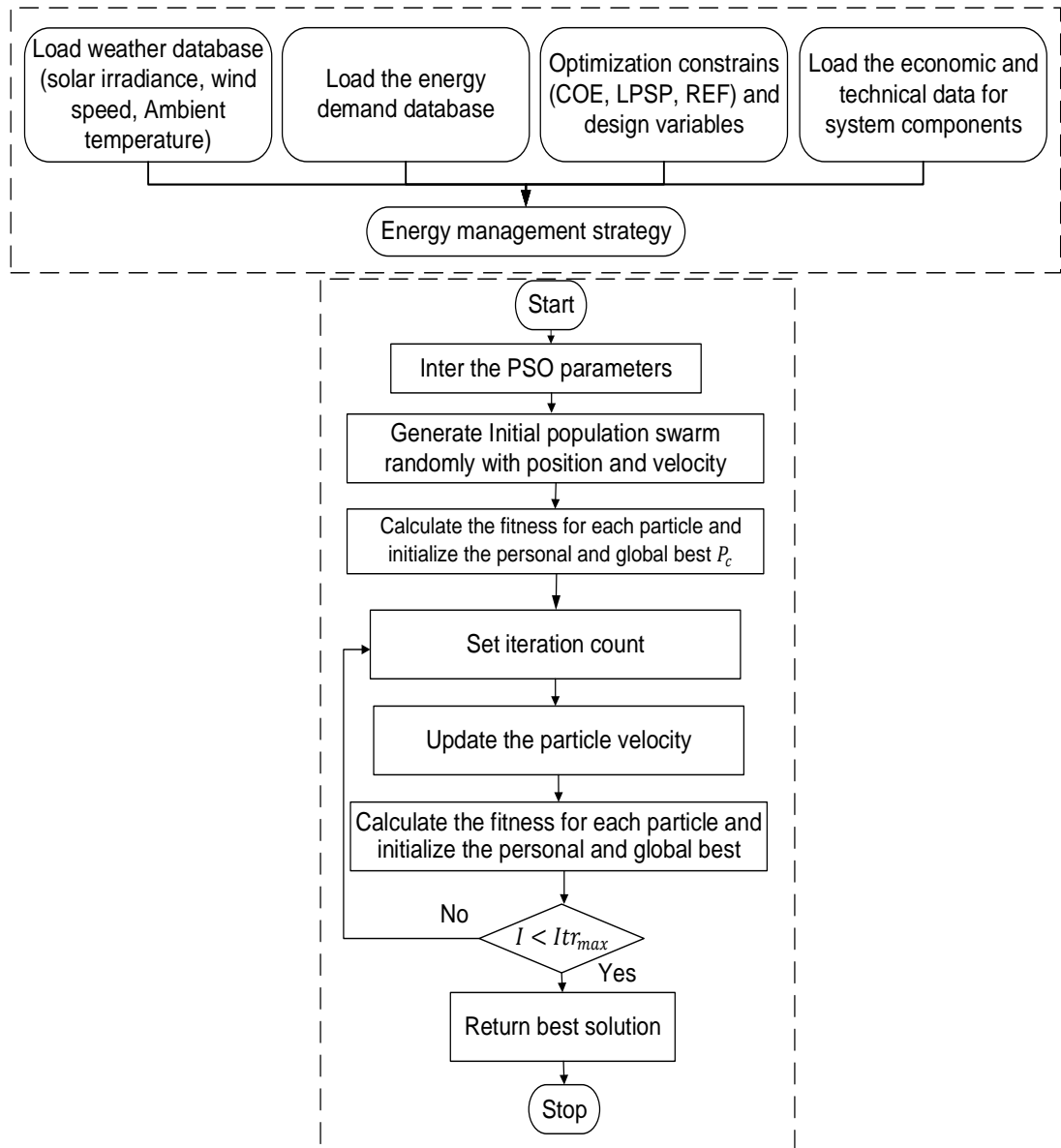


Figure 3.17 Flowchart of the Rule-Based-Energy Management Strategy of Particle Swarm Optimization (RB-EMS-PSO).

Table 3.7 Steps of Particle Swarm Optimization Algorithm.

Steps	Implementing operation
Step 1	<ul style="list-style-type: none"> • Loading weather database (Solar irradiance, Ambient temperature, Wind speed) is shown in Figures 4.2 (a), Figure 4.5 (a), and Figure 4.8 (a), respectively. • The load demand database is figured in Figure 4.18 (c). • The load economic database for the microgrid components is listed in Table 3.3.
Step 2	<ul style="list-style-type: none"> • Set the PSO constants. <ul style="list-style-type: none"> - Max iteration=100, inertia weight damping ratio (W_d) =0.99, Swarm size=20, inertia weight $w=1$, learning coefficient ($c_1 = 2, c_2 = 2$). • Set constraint. <ul style="list-style-type: none"> - REF and LPSP • Set the research space: <ul style="list-style-type: none"> - lower and upper bounds for N_{PV} [0,100]. - lower and upper bounds for N_{WT} [0,50]. - lower and upper bounds for N_{BT} [0,100]. - lower and upper bounds for N_{AD} [0,3].
Step 3	Particles move to a new position based and update the iteration variable, inertia weight, velocity, and position
Step 4	Go back to step 2 and compute the objective functions.
Step 5	If satisfied stop otherwise go to steps 3 and 5
Step 6	If the best solution is obtained stop, if not repeat step 2

3.9.2 Cuckoo Search Algorithm

In the preceding chapter, the explanation of the CSA algorithm has been described. The progress of implementing the RB-EMS using the CSA as a benchmark method is demonstrated in Figure 3.18 by inserting load demand, objective functions (COE, LPSP, and REF), and economic and technical data for system components. Table 3.8 is given the steps of the CSA.

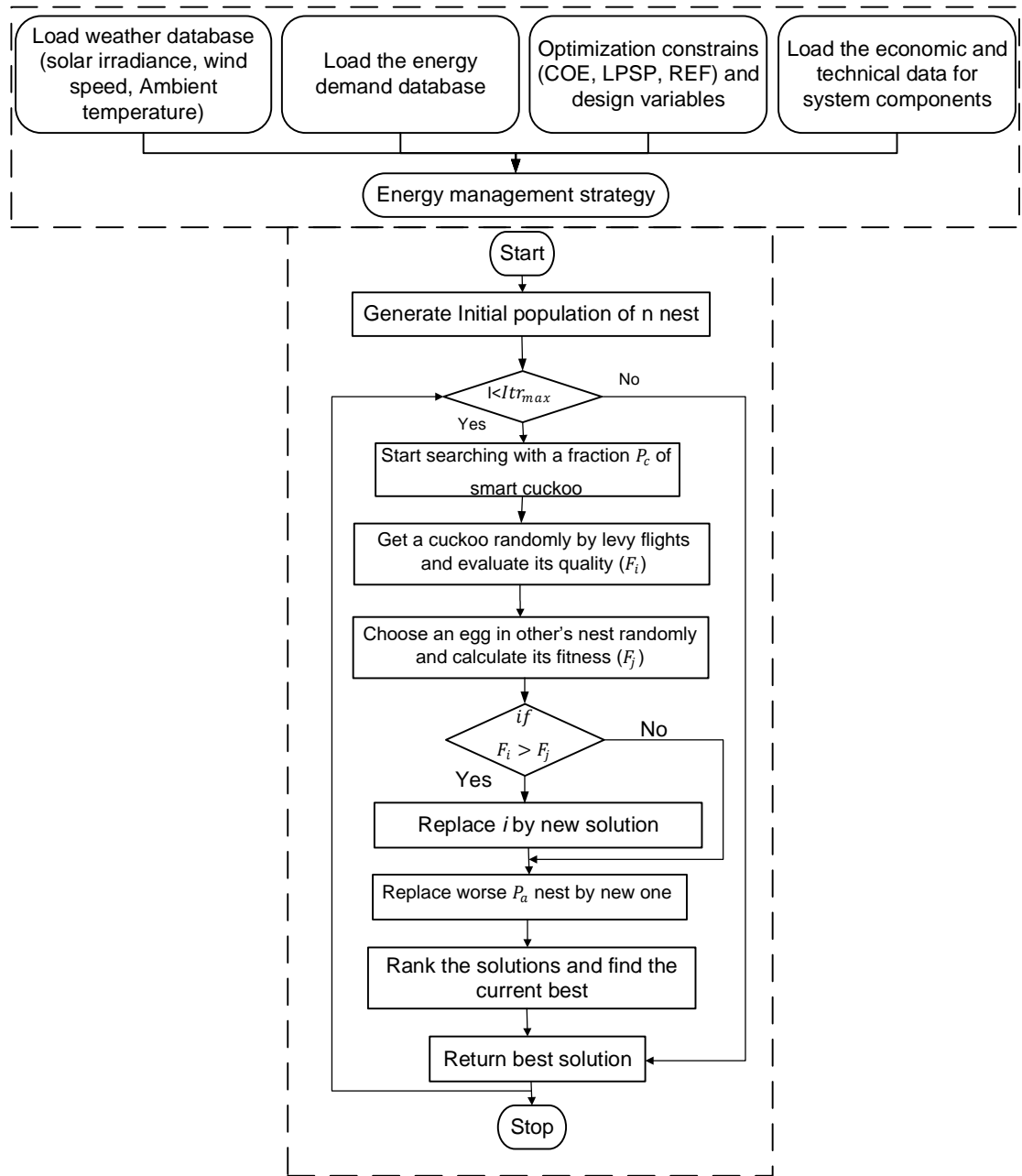


Figure 3.18 Flowchart of the Rule-Based-Energy Management Strategy of Cuckoo Search Algorithm.

Table 3.8 Steps of Cuckoo Search Algorithm.

Steps	Implementing operation
Step 1	<ul style="list-style-type: none"> • Loading weather database (Solar irradiance, Ambient temperature, Wind speed) is shown in Figures 4.2 (a), Figure 4.5 (a), and Figure 4.8 (a), respectively. • Load demand database figured in Figure 4.18 (c) • The load economic database for the microgrid components is listed in Table 3.3.
Step 2	<ul style="list-style-type: none"> • Set the CSA constants. <ul style="list-style-type: none"> - Abandoned nest fraction (P_a) = 0.2, The fraction of the smart nest (P_c) = 0.5, Nest number = 5, Max iteration = 100, • Set constraint. <ul style="list-style-type: none"> - REF and LPSP • Set the research space: <ul style="list-style-type: none"> - lower and upper bounds for N_{PV} [0,100] - lower and upper bounds for N_{WT} [0,50] - lower and upper bounds for N_{BT} [0,100]. - Lower and upper bounds for N_{AD} [0,3]
Step 3	Perform a local search around the population, evaluate the smart cuckoo, and update the best nest.
Step 4	Perform a global search through the lévy flight algorithm, evaluate the new nest, and update the best nest.
Step 5	Substitute fraction of worse nest P_a by new ones selected randomly, evaluate the new nests, and update the best nest.
Step 6	Update the optimum solution and increase the iteration variable
Step 7	If satisfied stop if not return to step 2.

The optimization control parameters for the utilized algorithms (IALO, ALO, PSO, CSA) are tabulated in Table 3.9 and were applied to obtain the presented result.

Table 3.9 The controlling parameters of the utilized optimization algorithms.

IALO & ALO algorithms [33]	CS algorithm [68]	PSO algorithm [94]
Search agents: 5	Number of the nest: 5	Swarm size: 5
Maximum iteration: 100	Maximum iteration: 100	Maximum iteration: 100
Best score: Elite antlion fitness	Fraction of abandoned nests (P_a) = 0.2	Initial weight (w): 1
Best position: Elite antlion position	Fraction of smart nest (P_c) = 0.5	Weighting factors (c_1 and c_2) = 2

3.10 Economic parameter analysis

The Stochastic Monte Carlo Method (SMCM) is a probabilistic numerical technique used to predict the result of a set of data and uncertain (stochastic) data. Furthermore, it is a stochastic tool developed by Neumann and Ulam and implemented in various fields to deal with the randomness of several components [180]. SMCM also known as multiple probability simulation named after a famous gambling city (Monaco-South France) involves large numbers of computer simulations with randomly selected input [43]. Furthermore, it is used when the input data is having complex or random variables such as charging and discharging different EVs for the long term [9]. The random prediction of the arrival and departure number of EVs along with the SMCM working principle is elaborated in the following subsection. This technique can be used to simulate situations that cannot be directly modeled.

Furthermore, the reason for utilizing stochastic methods is due to the goal of gaining information out of randomness. Besides, the popularity of the provided result from stochastic methods in the power system analysis and dealing with uncertain values. The characteristics of SMCM got attention among scholars due to its flexibility, runtime, and accuracy in solving a wide range of optimization problems in various fields [194]. Additionally, SMCM is due to the advantages such as providing multiple possible solutions from large random data [151]. On the contrary, the drawback of SMCM is acquiring different results in each run due to stochastic data [143]. In terms of applications, it is also applied in project management, sciences, engineering, finance, and artificial intelligence [143]. The SMCM utilized an equation for the SoC_{EV} boundary is presented in Eq. (3.34). Furthermore, it is utilized to estimate the process of power flow and EV battery state (SoC) for charging and discharge the EVs for the period of one year [195]. The behavior of EVs is in uncertain number as proposed which ranging from 10 to 60 EVs. Moreover, it assesses the impact of an uncertain number of EVs on the grid.

$$SoC_{EVmin} < SoC_{EV} < SoC_{EVmax} \quad (3.34)$$

3.10.1 The working principle of the Stochastic Monte Carlo Method

SMCM principal work is involving the presented steps in Figure 3.19 after setting the period of time. The steps start with estimating the mathematical equation of system components to insert the output data, determine the needed values for analysis, and create a sample of random data for the SOC_{EVs} . Additionally, analyzing the acquired result followed by checking if the needed result was achieved as the maximum iteration number (17520 times) is reached, if yes, the program is stopped, otherwise go from the beginning to estimate the input data. Generally, in SMCM, the more random generated data, the better the estimated result.

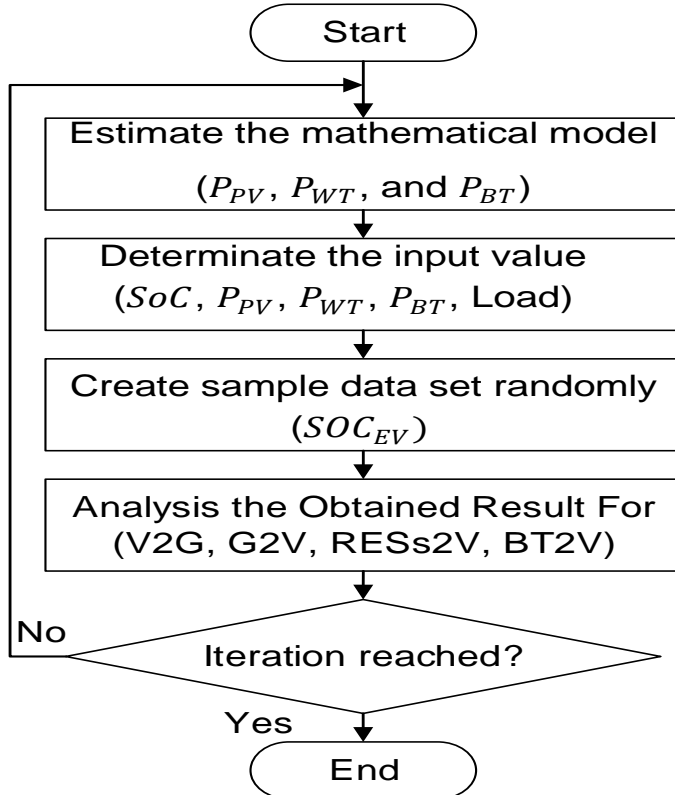


Figure 3.19 Flowchart of Stochastic Monte Carlo Method

3.10.2 Operational analysis of the Stochastic Monte Carlo Method

This section is customized for the implementation process of SMCM by creating uniform random (uniform distribution) data between 0 and 1 using Microsoft Office Excel to simulate the V2G and G2V outcomes. Furthermore, the impacts on

load, charging and discharging, amount of integrated energy from the RESs and grid, amount of exchanged energy from and to the EV (V2G and G2V), and BT2V are analyzed. The randomness of the SMCM is conserved to analyze the uncertain SoC_{EV} integrated with RES under a residential load.

The process starts by setting the types of data that will be processed with hourly data (8760) for a year as the flowchart presented in Figure 3.20. Then read the annual hourly data for (output power from the RESs (PV and WT), SOC_{EV} is randomly created, and Load demand data). Assuming during the simulation the RESs output power and load demand are constant values as obtained from the sizing method. After reading the data, defining the $\text{SOC}_{\text{EVmax}}$ and $\text{SOC}_{\text{EVmin}}$ boundaries, then, implementing uniform distribution operation into the V2G and G2V models to start running the data on the stochastic method. Uniform distribution describes the probability of random numbers for each EV. The size of SOC_{EV} -created data is (8760,1) utilized with yielded power from RESs and grid to meet the objective functions.

The SMCM is exploited due to the provided result and dealing with random variable data to gain results for uncertain situations. Besides, SMCM is utilized to evaluate the various scenarios for the uncertain behavior of EVs. The uncertain behavior refers to the SOC_{EV} battery by considering maximum and minimum SOC as 0.2% and 0.95%, respectively. The main considered scenarios for analysis with the help of SMCM in this study are Vehicle-to-Grid (V2G), Grid-to-Vehicle (G2V), Battery-to-Vehicle (BT2V), RESs2V, and the absence of EV (no EV). Besides, the aforementioned scenarios are analyzed when having a minimum (10) units, medium (30) units, and maximum (60) units of EVs.

In terms of implementation, the proposed scenarios of the case study on the built number of EVs that normally iterate during the year with 8760 hours are considered. While the stopping criteria for SMCM are considered till the highlighted scenarios are achieved. The simulation steps of SMCM were divided into an hourly basis for analyzing the impact of the EV under three scenarios as listed below to obtain a numerical result:

1. Setting the hourly data for the generated output power and load demand.
2. Define the initial SOC with Soc_{EVmin} (0.2%) and Soc_{EVmax} (0.95%) for the arrival and departure number of EVs randomly.
3. Creating hourly random Soc_{EV} data follows uniform distribution considering the scenarios ranges between 0-1 and sized (8760,1).
4. Acquiring the loads when SMCM converged, if yes ending the iteration, if not, return to step one as stopping criteria.

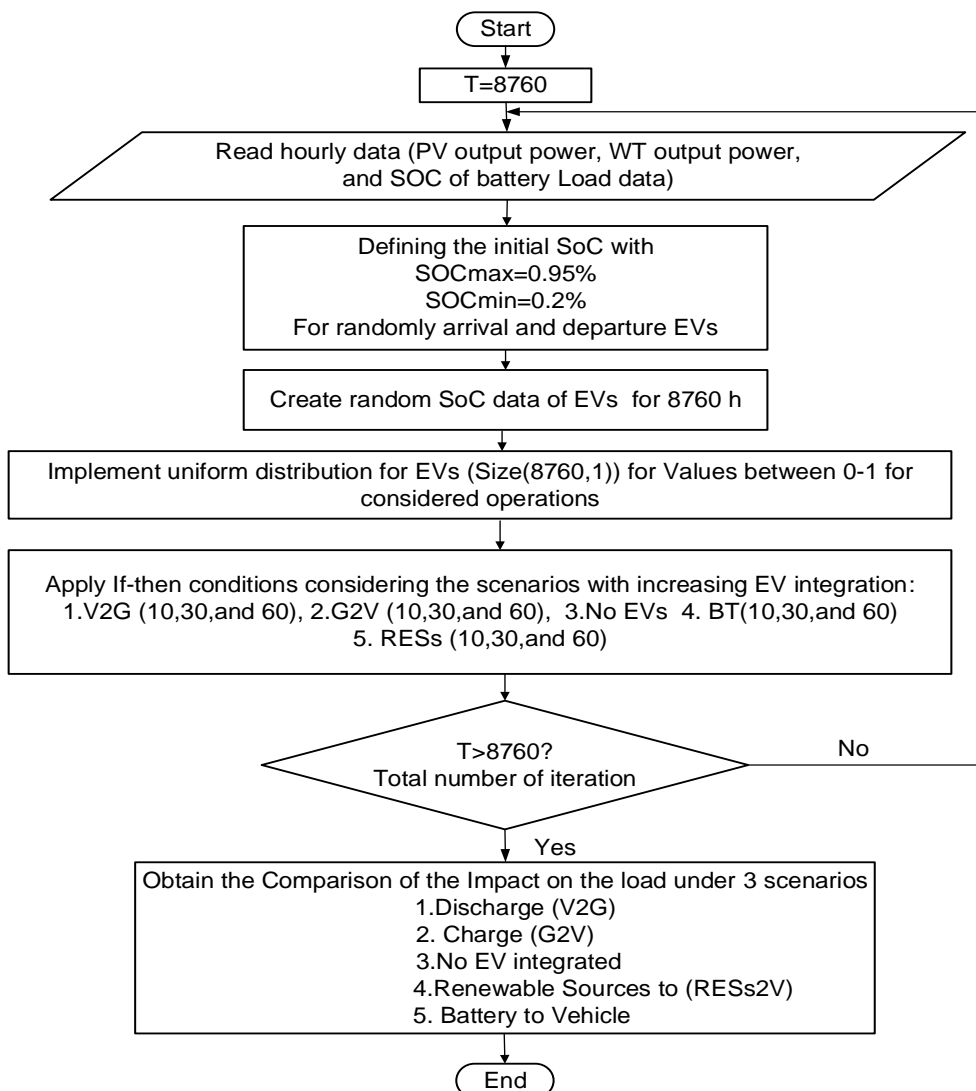


Figure 3.20 Flowchart of Stochastic Monte Carlo Method operation.

The operation of obtaining the result by conserving the case if the SoC_{EV} boundaries are carefully checked to get fully charged mode according to if-then conditions. The if-then condition of the operation of charging and discharging under various scenarios based on Eq. (3.34) is illustrated in Figure 3.21 as presented in Table 3.1. The obtained result from the presented operation is multiplied by the minimum (10), medium (30), and maximum (60) number of EVs to get the estimation of comparison of various scenarios.

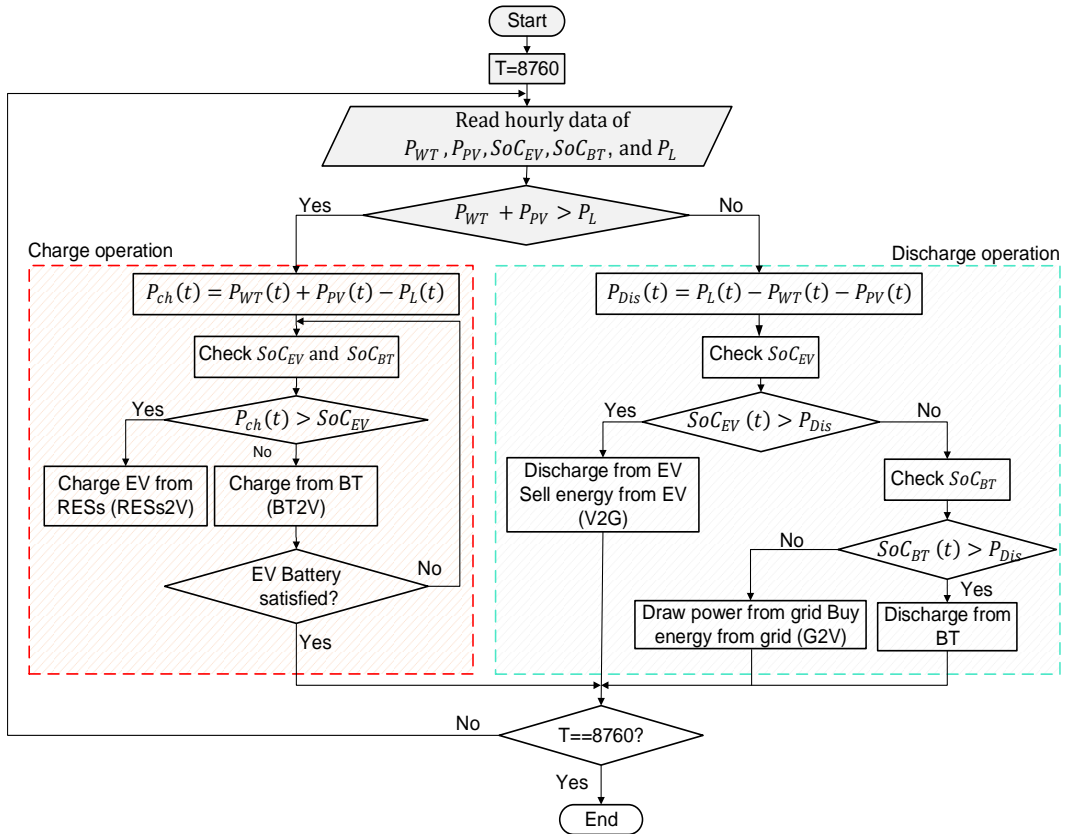


Figure 3.21 Operational strategies flowchart of IF-Then conditions for SMCM.

3.10.3 Arrival and departure time prediction

Based on SMCM as a valuable method for providing an accurate result, the implementation results with the help of mathematical equations will be presented [135][9]. The time prediction of arrival and departure EVs along with the SoC_{EV} are randomly acquired by Eq.(3.35)-Eq.(3.39). The considered charging power level for the charging home area is 11.5 kW which refers to level 2 and its efficiency is 86.5% [155].

$$T_{arrive}^{EV} \sim N(\mu_{EV_a}, \sigma_{EV_a}) \quad (3.35)$$

$$T_{Dep}^{EV} \sim N(\mu_{EV_d}, \sigma_{EV_d}) \quad (3.36)$$

$$SoC_{arrive}^{EV} \sim N(\mu_{EV_a}, \sigma_{EV_a}) \quad (3.37)$$

$$SoC_{Dep}^{EV} \geq 0.2 \times Cap_{EV} \quad (3.38)$$

$$SoC_{arrive}^{EV} < SoC_{Dep}^{EV} \quad (3.39)$$

where N is the normal distribution function depending on the mean (μ) and standard deviation (σ) for arrival (SoC_{arrive}^{EV}), departure time (T_{Dep}^{EV}), and arrival (T_{arrive}^{EV}). Furthermore, departure (SoC_{Dep}^{EV}) is considered a constraint and the EV_d and EV_a are the departure and arrival vehicles. Additionally, between 12 pm - 24, am is the estimated arrival time while the departure estimated time is around 5 am-12 pm [9]. Besides, 0.2 represent the SoC_{EVmin} (0.2 %) of the EV battery and the Cap_{EV} is the EV battery capacity (from the manufacturer depending on the chosen EV) [9]. The listed data in Table 3.10 are utilized in order to estimate the arrival and departure times, and SoC_{EV} .

Table 3.10 The Entry constraints data of EV [8].

EV Constraints	Value	Unit
Maximum state of charge of EV (SoC_{max}^{EV})	0.95	%
Minimum state of charge of EV (SoC_{min}^{EV})	0.2	%
The mean of arrival EVs (μ_{EV_a})	18	-
Standards deviation of departure EV (σ_{EV_a})	2	-
The mean of departure EVs (μ_{EV_d})	7	-
Standards deviation of arrival EV (σ_{EV_d})	2	-
Electric Vehicle Capacity (Cap_{EV})	14	kWh
The arrival time of the EV (T_{arrive}^{EV})	$12 \leq T_{arrive}^{EV} \leq 24$	h
The departure time of the EV ($Time_{Dep}^{EV}$)	$5 \leq Time_{Dep}^{EV} \leq 12$	h

3.10.4 Dynamic payback period analysis

To establish the project's financial profitability, economic research was undertaken based on the NPC and payback duration to show the break-even day [155]. Furthermore, the latter technique process is known as Discounted Payback Period (DPP) which was mathematically expressed in Eq. (3.40) with the help of Eq. (3.41) [196], [197]. The DPP refers to the number of years required to recover the initial investment in a project (free cash flow) [195]. The mathematical equation is used to calculate the NPC in order to gain better cost in comparison with the benchmarks using Discounted Cash Flow (DCF) analyses [184].

$$DPP = \sum_{t=0}^{DPP} S(1 + ir)^{-t} - NPC_T = 0 \quad (3.40)$$

$$S = \text{tariff} \times (PL_{cumulative,sum} + EV_{demand}) \quad (3.41)$$

where S refers to the annual revenue generated by sold electricity to the consumers (EVs) as shown by Eq. (3.41) by assuming the residential tariff rate is \$0.05/kWh. The aforementioned tariff value multiplied by the residential supplied cumulative load ($PL_{cumulative,sum}$) in kW added to EV_{demand} to gain the total revenue which is measured in (\$/kWh). The ir represents the interest rate, $-t$ is the lifetime of the project, NPC_T denoted as Total Net Present Cost (TNPC) can be defined as the sum of the capital cost of components [108].

3.11 Chapter Summary

In this chapter, the methodology framework implemented in the study of the V2G integration system as a grid-connected system has been comprehensively elaborated. The explanation of the location of the case study, climatology conditions details, and energy demand data are described. The considered topology in this study is V2G for the proposed operation modes to charge and discharge EVs under residential load through a bidirectional AC/DC converter. Additionally, the RB-EMS

has been designed for power flow among the system components with the aid of four operation modes. Followed by the mathematical models equations of each component in the system used to obtain the individual yield of each component. The main three objective functions (COE, LPSP, and REF) have been discussed in detail with entry parameters for the utilized components. The aforementioned proposed objective functions of this study have been addressed by the proposed method IALO, while ALO, PSO, and CSA are chosen for benchmarking purposes and elaborated. An economic analysis method is considered to gain the DPP. Although a vast number of optimization algorithms are used to assess the behavior of the arrival and departure number of EVs, the Stochastic Monte Carlo Method is recommended due to its accuracy in providing outcomes. On the contrary, different optimized answers in each run. Chapter 4 details the full implementation of the raised issue related to V2G technology integration and its outcome.

CHAPTER 4

RESULTS AND DISCUSSIONS

4.1 Introduction

In chapter 3, the methodology, the Energy Management Strategies (EMSs), and the sizing algorithm along with the validation algorithms were explained. Besides, sizing is required because it provides the actual size of each parameter in the system that satisfies the load at a minimum cost. The proposed microgrid system illustrated in Figure 3.8 (refer to chapter 3) is considered a grid-connected integrated with RESs, BT, and EV to form Vehicle-to-Grid (V2G) technology.

This chapter presents the obtained result from the proposed method (IALO) and verifies the validity of the contribution for the considered case study. A MATLAB R2016b is running on Intel (R) Core (TM) i5-8250U CPU @1.60 GHz to implement the proposed algorithm and its counterparts. The collected data has been analyzed and comprehensively discussed along with the obtained output power from the utilized RESs as will be presented in the proceeding subsection. The mathematical models of system parameters with their specifications are discussed to meet the objectives.

The proposed objective functions (COE, LPSP, REF) have been met and presented under various scenarios. The impact on the load from the V2G operational integration is estimated using the Stochastic Monte Carlo Method (SMCM) under different scenarios. The economic evaluation using Discounted Cash Flow (DCF) to gain investment knowledge of the hybrid proposed system as the dynamic payback period of the system. Besides, sensitivity analysis is considered to investigate the influence of key affected components on the system that may happen in the future under climatology changes along with the uncertainties of EV integration.

4.2 Input Parameters Data

The geographical site of the case study is characterized by four seasons (winter, spring, summer, and autumn) as illustrated in Figure 3.7 (refers to chapter 3). The hourly annual collected data for the case study in the period (1st January to 31st December 2019) is solar irradiance (G) ranges between 7.1 and 8.1 kWh/m²/day [165]. Besides, wind speed (v) which ranges between 4 to 20 m/s, ambient temperature (T_{am}) vary between 10 to 45 (°C), and load demand (P_l) that vary between 3 to 7 kW (daily). The foregoing climatology data were obtained is taken from the Centre for Solar Energy Research and Studies (CSERS) while load demand from the General Electricity Company of Libya (GECOL). The RESs considered in this study are solar and wind for satisfying the load demand. They also have been selected due to their benefits including low-carbon emissions, economics, and flexibility among others. Data analysis is very vital for a better understanding of consumer load requirements from available RESs to overcome the worse days (unsunny or unwind days) scenarios. The output power generated from the selected RESs is presented and elaborated in the following subsection with the utilization of input parameters.

4.2.1 Photovoltaic

The principle of Photovoltaic (PV) refers to the method of converting energy from sunlight into electrical energy. The type of PV module used in this research is a polycrystalline (KD325GX-LFB). as tabulated in Table 3.3 (refer to chapter 3) with its specifications as presented in [175]. The amount of solar-radiated energy incident on the surface is called irradiance or isolation. The collected solar irradiance data for the case study is plotted as depicted in Figure 4.1. Figure 4.1 (a) shows the annual solar irradiance in W/m², while Figure 4.1 (b) presents the seasonal contour plot of irradiance. From the plot, it can be seen that the study area is highly blessed with abundant solar irradiance over the entire year. The average solar irradiance shows the highest amount of solar radiation in summer which has the high potential of generating electricity from PV, followed by spring, autumn, and winter, respectively.

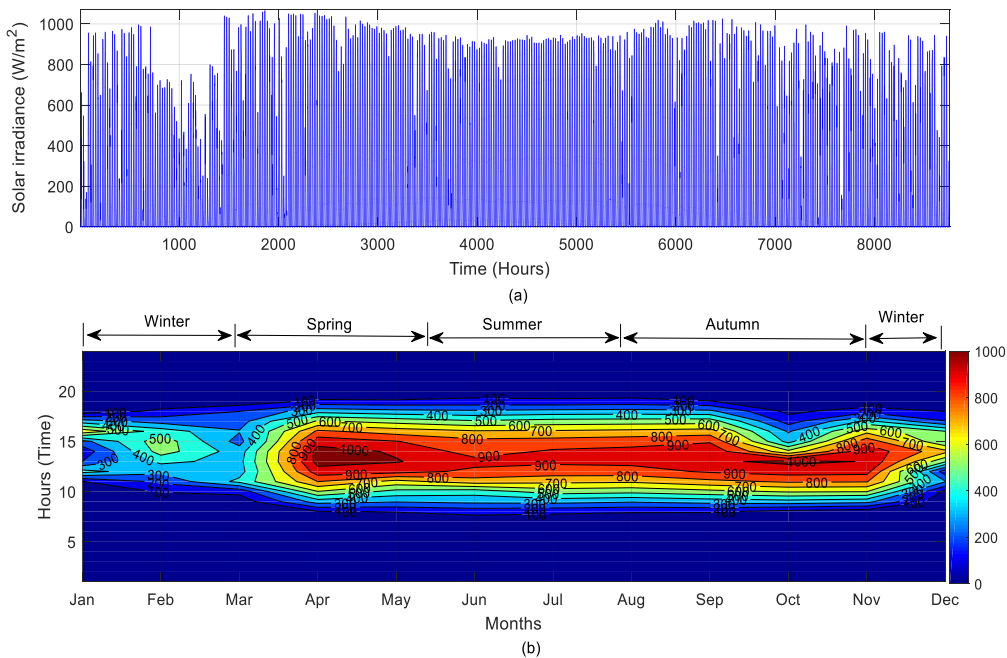


Figure 4.1 Solar irradiance for Tripoli-Libya (a) Annual data and (b) Seasonal Contour plot.

The analyzed annual maximum and mean of solar irradiance are shown in Figure 4.2 and the seasonal solar irradiance analysis for maximum and mean is illustrated in Figure 4.3. Consequently, the annual hourly set of ambient temperature and seasonal contour plot is demonstrated in Figure 4.4 (a) and (b), respectively.

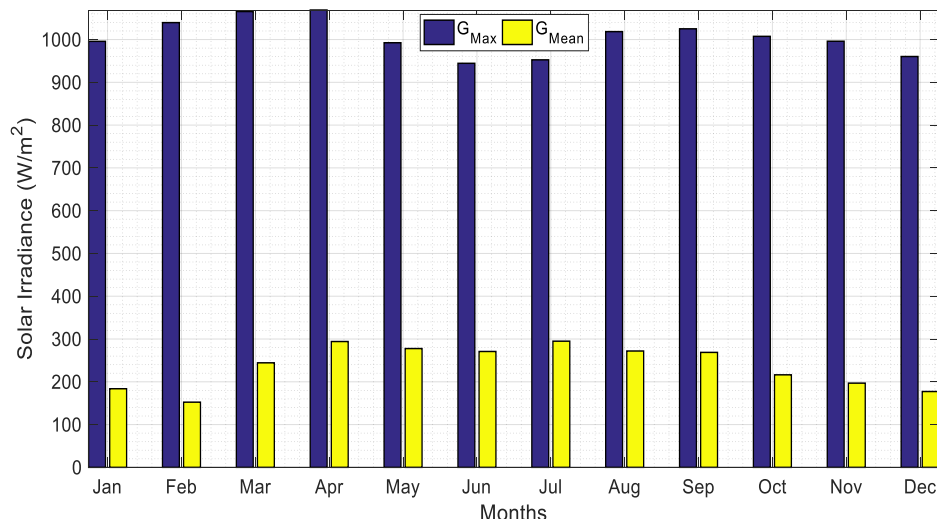


Figure 4.2 Annual maximum and mean of solar irradiance.

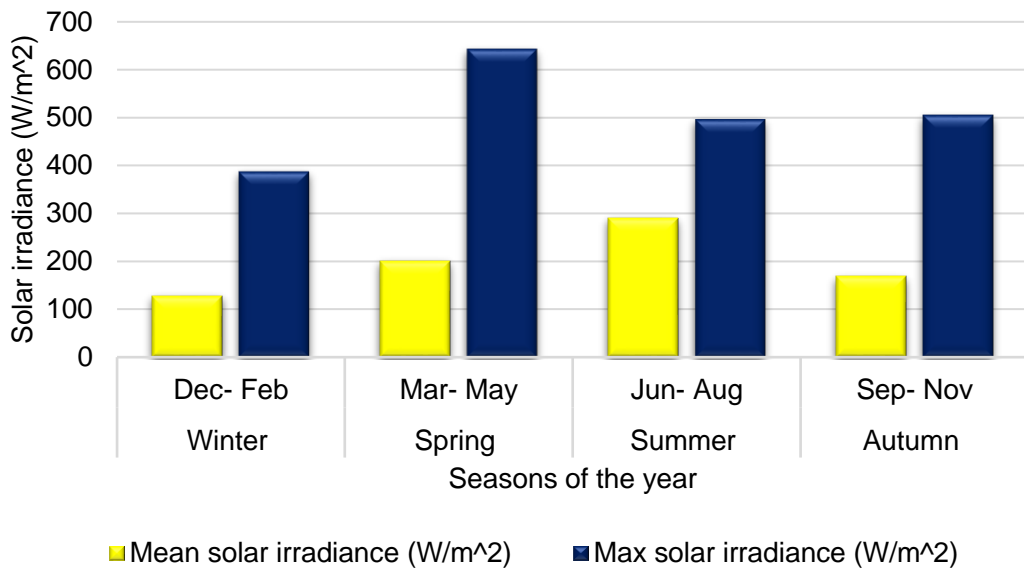


Figure 4.3 Seasonal solar irradiance analysis for maximum and mean.

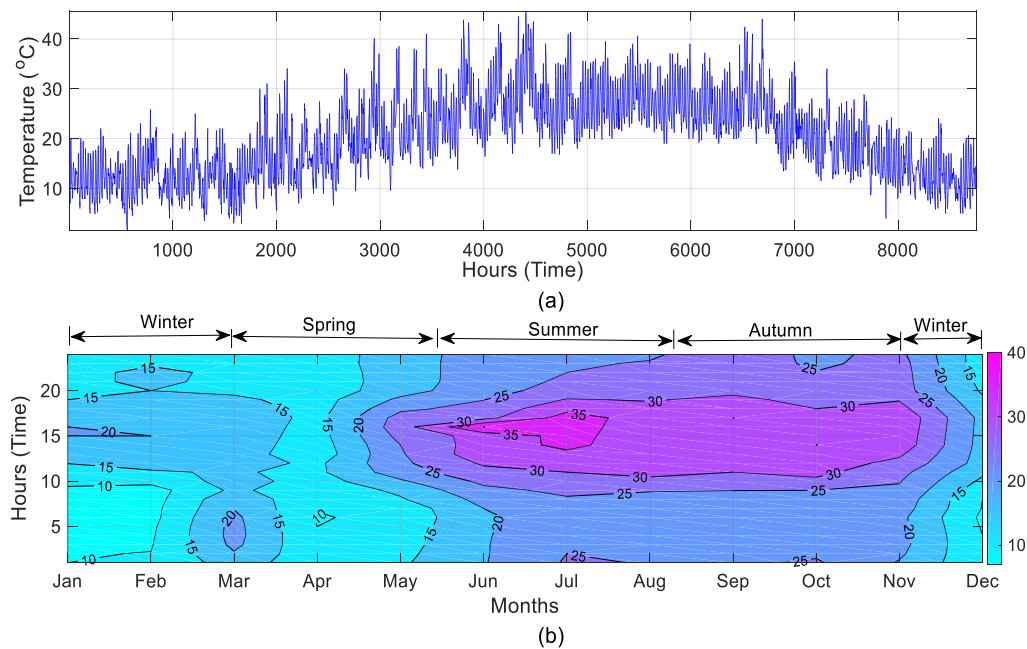


Figure 4.4 Ambient temperature data for Tripoli-Libya (a) Annual data and (b) Seasonal contour plot.

Furthermore, the monthly maximum, minimum, and mean values of the ambient temperature of the study area are demonstrated in Figure 4.5. The highest temperature in the year is in July which is due to the hot season (summer), while the minimum temperature presented is in January as the cold season (winter).

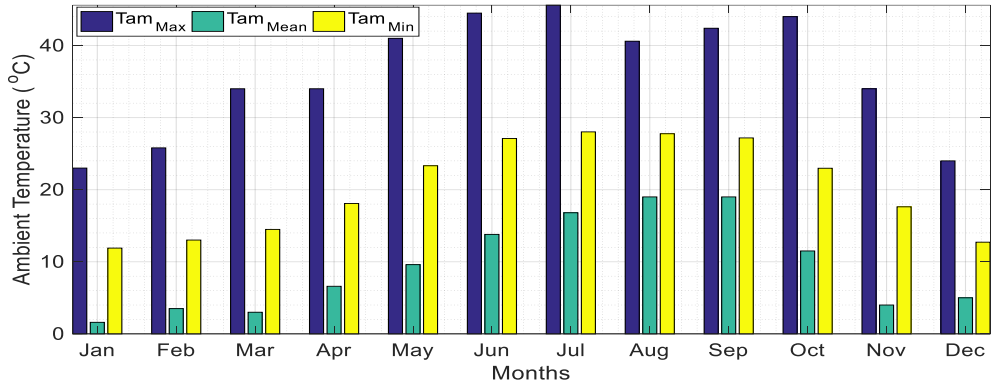


Figure 4.5 Annual maximum, minimum, and mean of ambient temperature (°C).

The obtained output power from the utilized RESs (P_{PV} and P_{WT}) are presenting, respectively. The output power generated from the PV is shown in Figure 4.6 which was determined using Eq. (3.1) with the help of Eq. (3.2). It has been generated with the help of ambient temperature (T_{am}) and solar irradiance (G) as the main consideration climatology conditions.

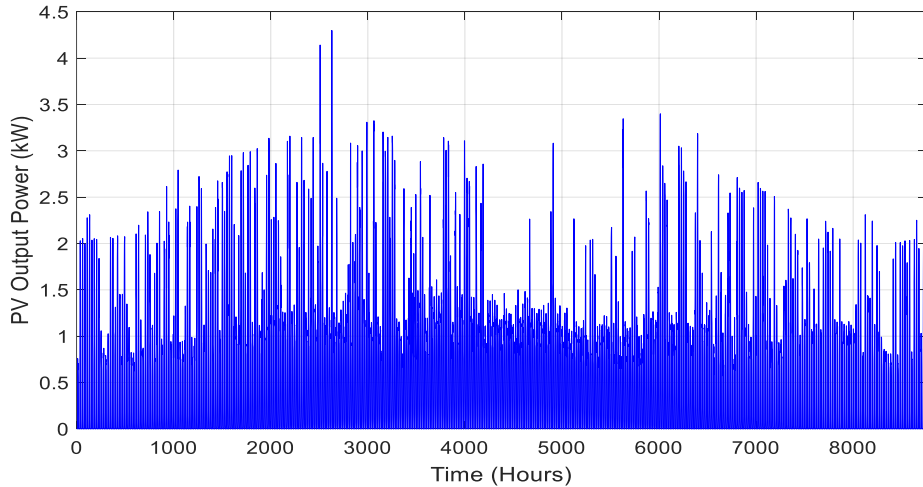


Figure 4.6 Generated Output Power from PV for Tripoli-Libya for one year.

4.2.2 Wind Turbine

The second RESs used in this research is wind energy, where the kinetic energy of the wind is used to obtain the output power of the WT through (Eocycle EO20) [176]. The annual hourly wind speed data collected for the study area is demonstrated

in Figure 4.7 (a) which ranges between 4-20 m/s. While Figure 4.7 (b) illustrated the seasonal contour plot of wind speed that presented annual ranges of wind speed.

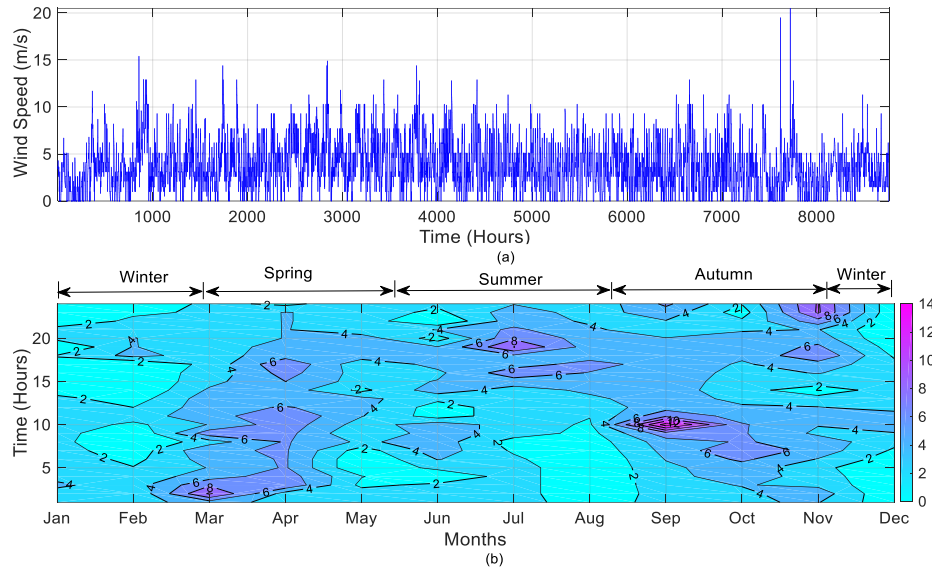


Figure 4.7 Wind speed data for Tripoli-Libya. (a) Annual data (b) Seasonal Contour plot.

Consequently, the seasonal and annual mean and maximum wind speed is shown in Figure 4.8 and Figure 4.9, respectively. The highest average wind speed is recorded in spring then summer, winter, and autumn, respectively with the vast potential of utilizing wind turbines to generate electricity. In winter, most of the consumers operate heaters while in summer the air conditioning is exploited.

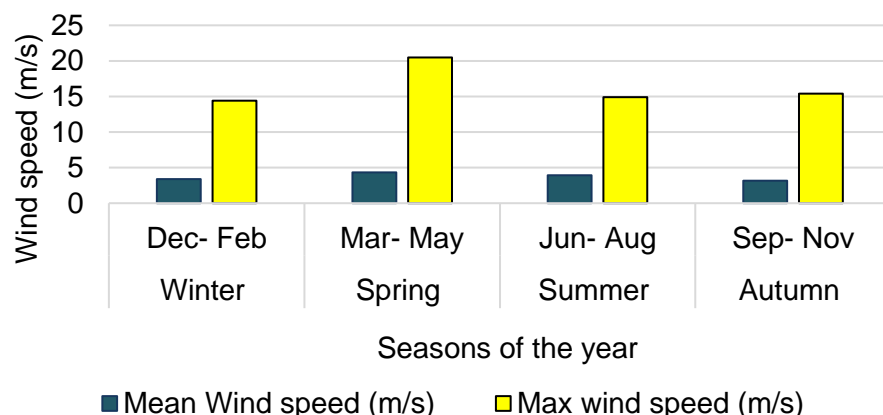


Figure 4.8 Seasonal maximum and mean wind speed (m/s).

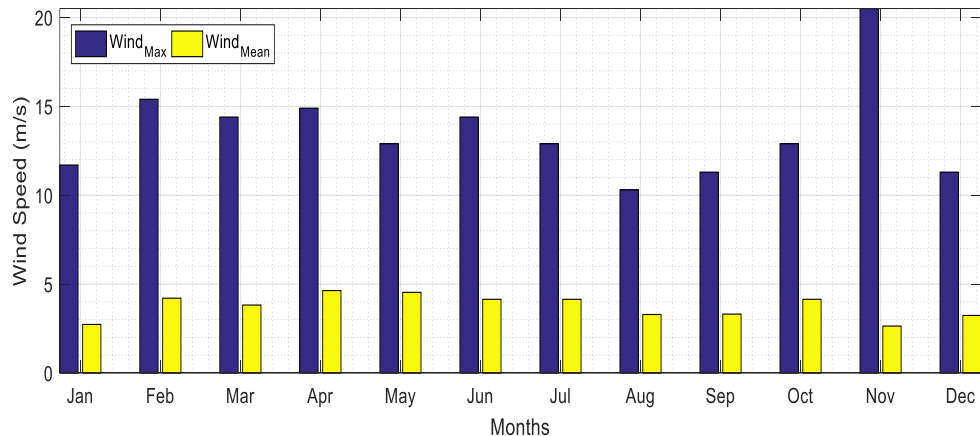


Figure 4.9 Annual means and maximum wind speed (m/s).

The generated output power from WT is obtained with the help of Eq. (3.3) and Eq. (3.4) as shown in Figure 4.10. The WT output power influenced by the cut-in (v_{cut-in}), cut-out ($v_{cut-out}$), and rated speed (v_r) of the WT which is specified by the manufacturer. Thus, the cut-in speed refers to the minimum wind speed that is needed by the turbine to generate power. While the cut-out speed represents the speed point where the turbine should stop rotating to avoid damage due to an increase in speed as demonstrated in Figure 3.12 (refer to Chapter 3).

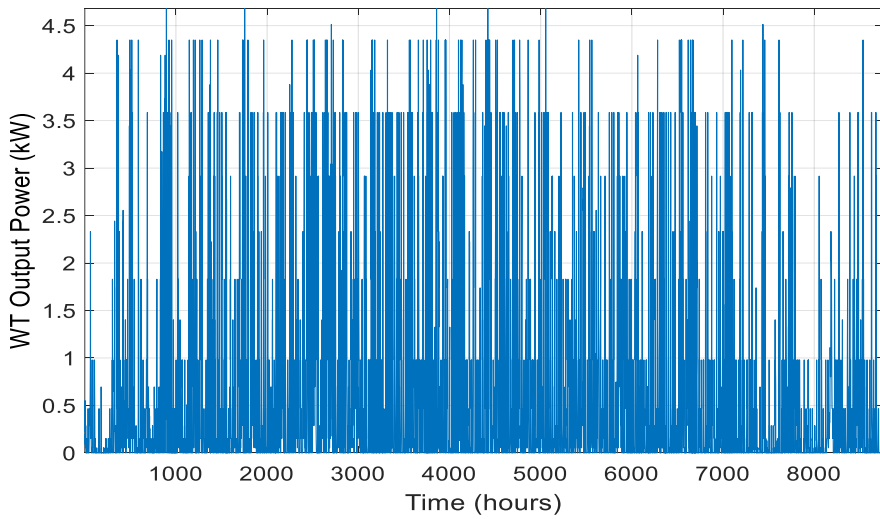


Figure 4.10 Generated Output power from WT for Tripoli-Libya for one year.

The comparison of monthly yielded power from the utilized RESs in (kW) is presented in Figure 4.11. The generated output power from the RESs is differing due to the climatology changes in the study area.

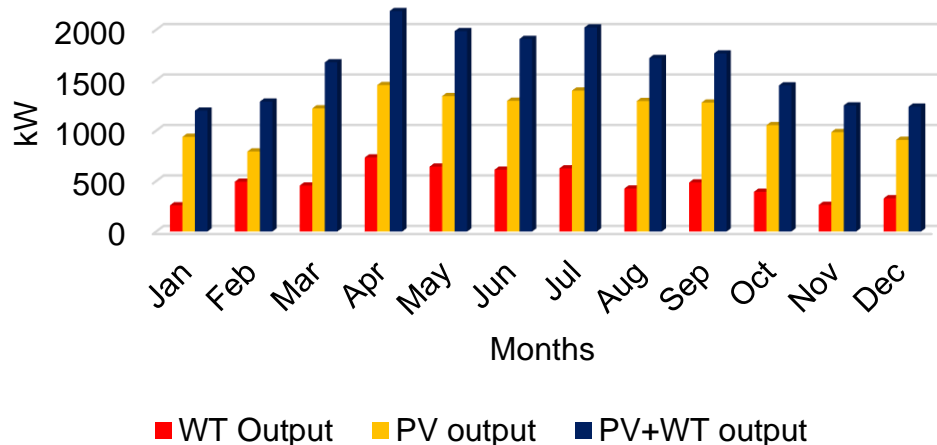


Figure 4.11 Monthly annual output power from RESs.

4.2.3 Energy Storage Battery

Numerous energy storage technologies that store energy in the form of electrochemical are available and implemented in several applications. Lithium-ion (Li-ion), Lead-acid, Nickel-Cadmium (Ni-Ca), and Lithium-iron Phosphate (LiFePO₄) are some of the commonly used storages for charging and discharging purposes. They have been utilized due to their merits such as long lifetime and high-power energy using efficient SoC values. The utilized data for the exploited batteries are tabulated in Table 3.2 (refer to Chapter 3).

4.3 Load profile

The presented load profile in Figure 4.12 of the study area is seasonally considered as listed: Spring (March, April, and May), Summer (June, July, and August), Autumn (September, October, and November), and Winter (December, January, and February), respectively. The contour plot of the annual load profile is shown in Figure 4.12 (a), while the daily residential load profile is figured in Figure

4.12 (b). Additionally, the seasonal load profile for four seasons is depicted in Figure 4.12 (c). As a result of the load profile, summer seems to be a greater season for consuming electricity due to the climatology changes as the hot season and consumers' use of air conditions lead to higher demand than autumn, winter, and spring, respectively. Besides, the seasonal analyses of maximum and minimum of energy demand are demonstrated in Figure 4.13.

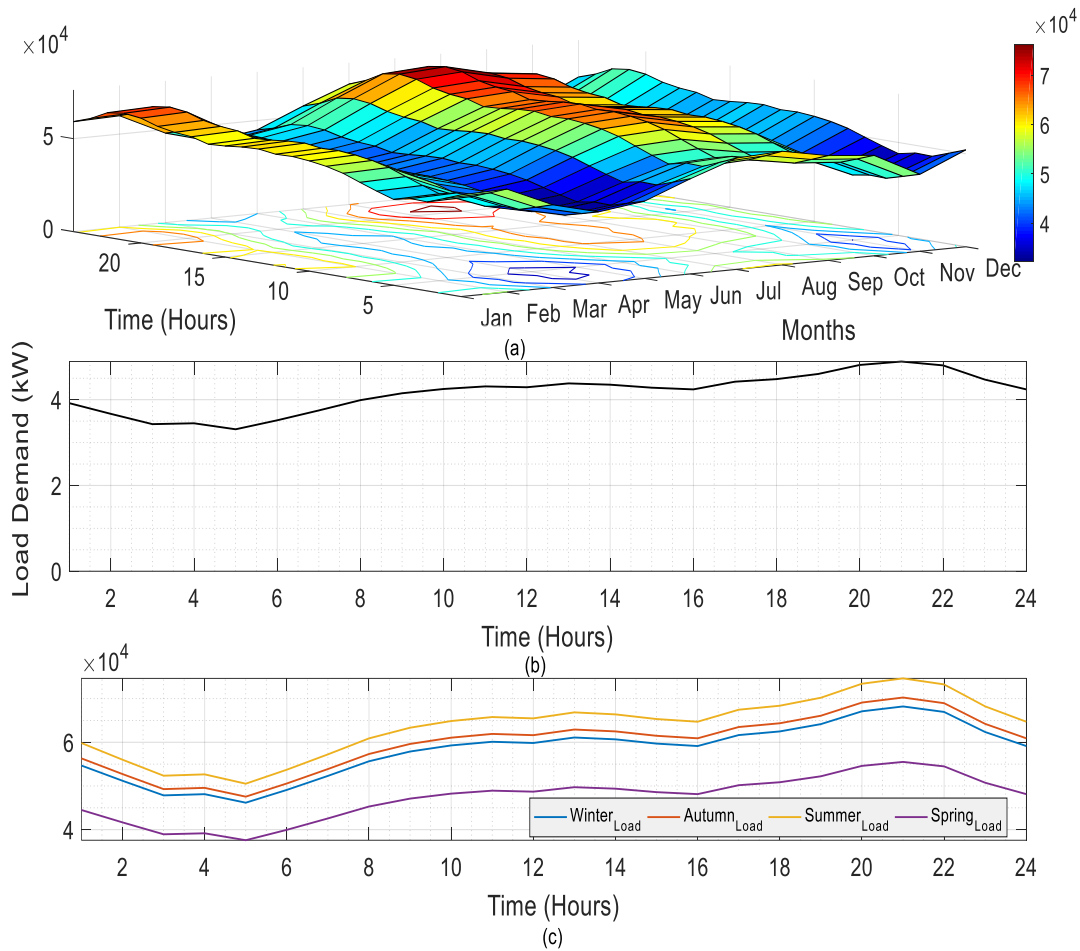


Figure 4.12 Load profile (a) Counter plot (b) Daily, and (c) Seasonal load of the study area.

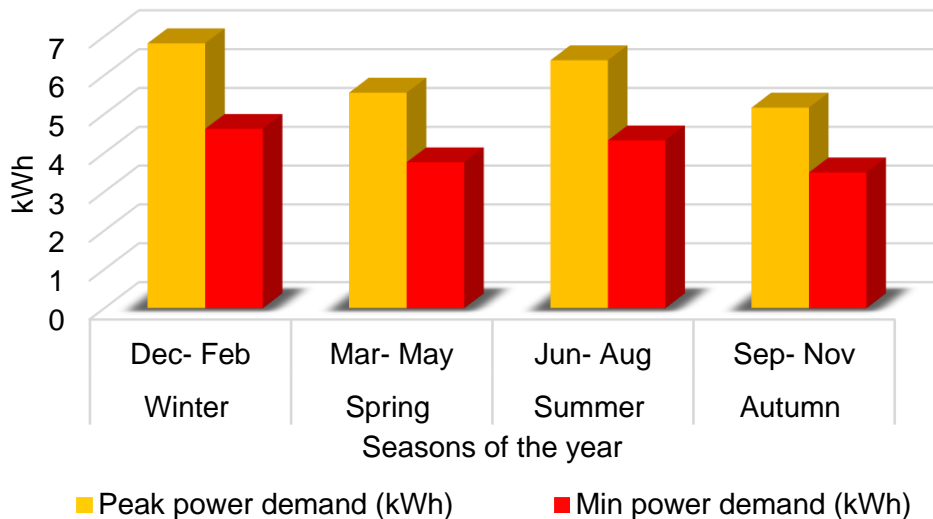


Figure 4.13 Seasonal maximum, and minimum power demand.

Furthermore, the annual analysis data of peak and minimum of load demand is presented in Figure 4.14. The reason for the presented increase of the load demand in summer is because of the air conditions consuming and in winter due to the utilization of heaters as heavy loads.

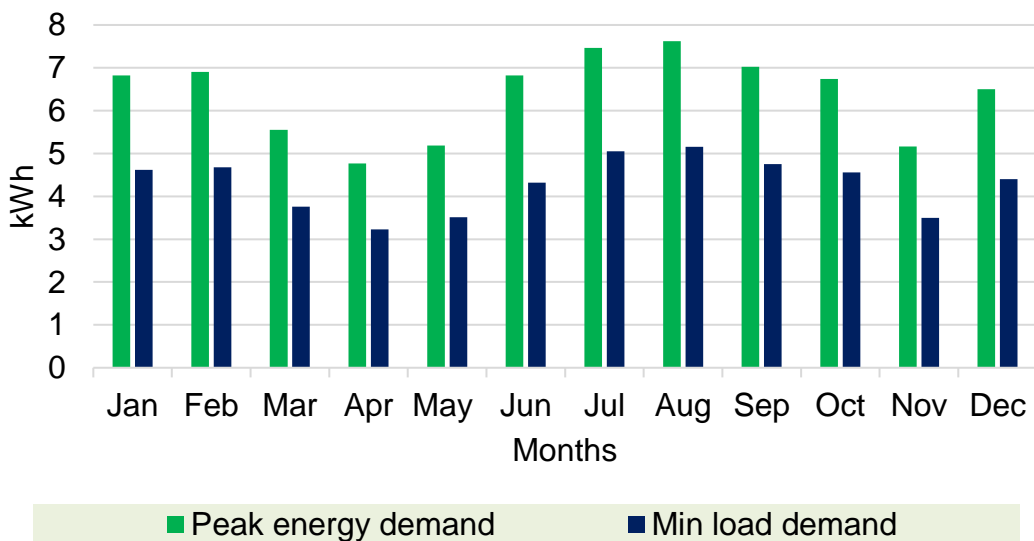


Figure 4.14 Annual peak, and minimum load demand.

The considered residential houses consist of two rooms, two bedrooms, a living room, a kitchen, and two bathrooms using the listed electric appliances as shown in Table 4.1.

Table 4.1 House electric appliances loads with the usage hours per day [198].

Electric appliance type	Load (kW)
Air-con	1.8
Cooling	1.8
Water boiling load	1.9
Bulb lighting loads	0.4
Washing Machine	1.6
hair drier	1.2
Iron	1.2
Electric oven	1.2
Electric Mixer	0.2
Steam Drier	0.2
Refrigerator	0.4
Hoover	0.1
Radio	0.1
TV	0.1
Water pump	1.2
Computer	0.3
EV	2.8

Depending on the considered charging power level 2 (240 V/ 80 A), the presented loads in Table 4.1 show that the total house's appliances loads are 16.5 kW. Additionally, integrating EVs will increase the load. Some EVs can generate almost 2.4-9.6 kW for example (Ford) [121]. Nissan Leaf is another brand and it's the most utilized EV for bidirectional processes in Danville (California) forming V2G operation with other V2G projects as reported in [131].

4.4 The Electric Vehicle Charging Facility

In this thesis, the facility is referred to as a home charger. The number of EVs in the houses ranges from 10 to 60 units with an EV battery capacity of 14 kWh [8]. Furthermore, there is one EV in each house in the three proposed cases, while the number of EVs can be possibly increased or decreased. To estimate the annual SoCEV battery, the Stochastic Monte Carlo Method (SMCM) is used to build uniform distribution data ranges between 0-1 using Microsoft Office Excel. The amount of energy needed to be delivered to an EV is known as EV demand as shown in Figure 4.15 (a) is calculated based on the consumed energy by each EV with the help of Eq. (3.10) (refers to chapter 3). Figure 4.15 (b) presents the zoomed-in of Figure 4.15 (a) for 24 hours (a day). In Figure 4.15 (b), it can be seen that the maximum and minimum demand of EVs are at 05:00 and 13:00 respectively. Since it is a random operation, the presented values with the peak and minimum are the EV demanded power (kW) during the time of connection.

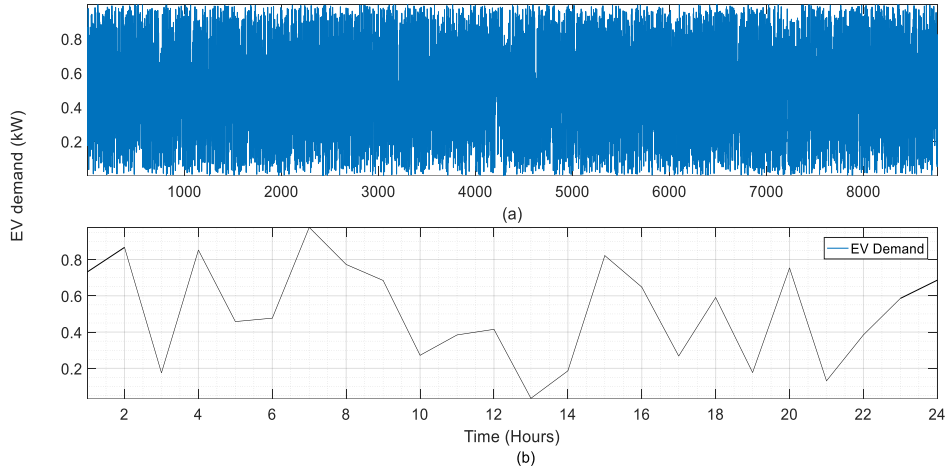
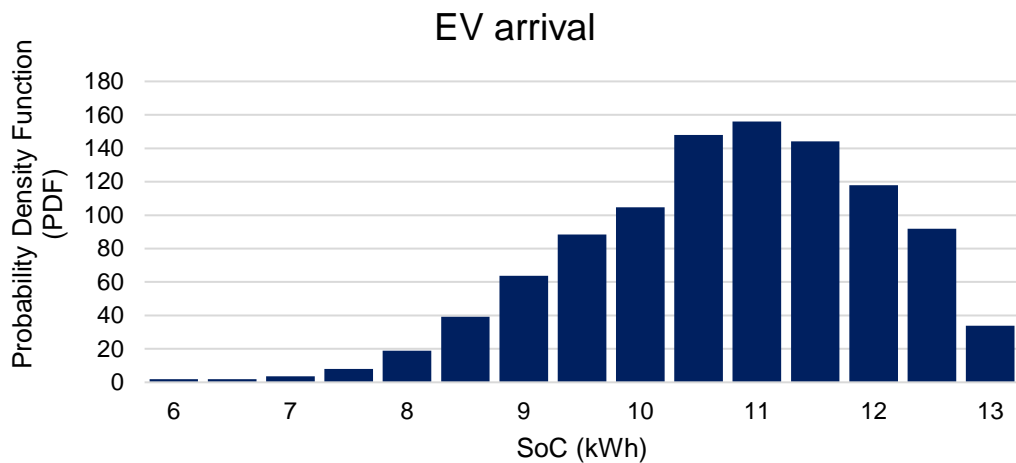


Figure 4.15 Electric Vehicle Demand (a) Annual Vehicle Demand and (b) Daily Demand of EV.

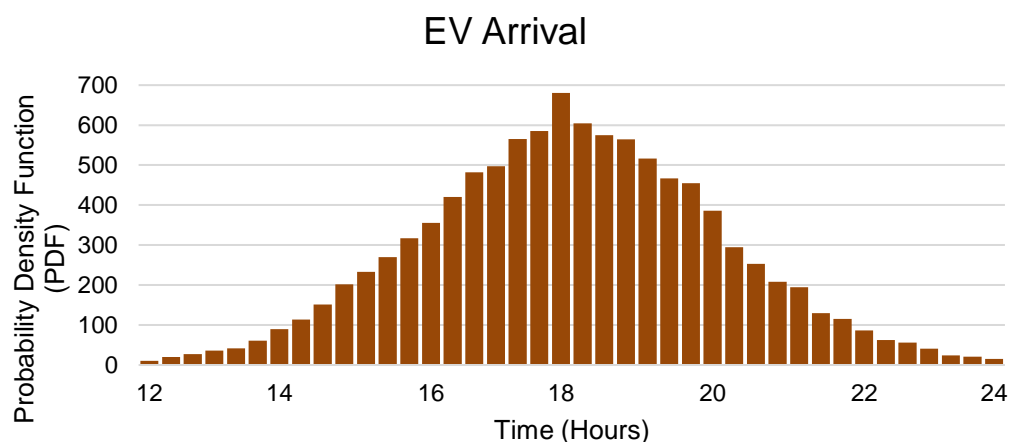
The behavior of exchanging energy between EVs and the grid is the main consideration of this study. Based on the implementation of the mathematical equations, with the help of Eq. (3.35) – Eq. (3.39), the plotted result in Figure 4.16 has been obtained. The amount of arrival/departure of EVs into the EVCF with the

uncertain SoC is random. Additionally, the amount of charging hours depends on the SoC of the EV. The EV operator charger during different hours must charge the EVs battery till the satisfied SoC before the EVs depart the EVCF ($SoC_{Arrive}^{EV} < SoC_{Dep}^{EV}$).

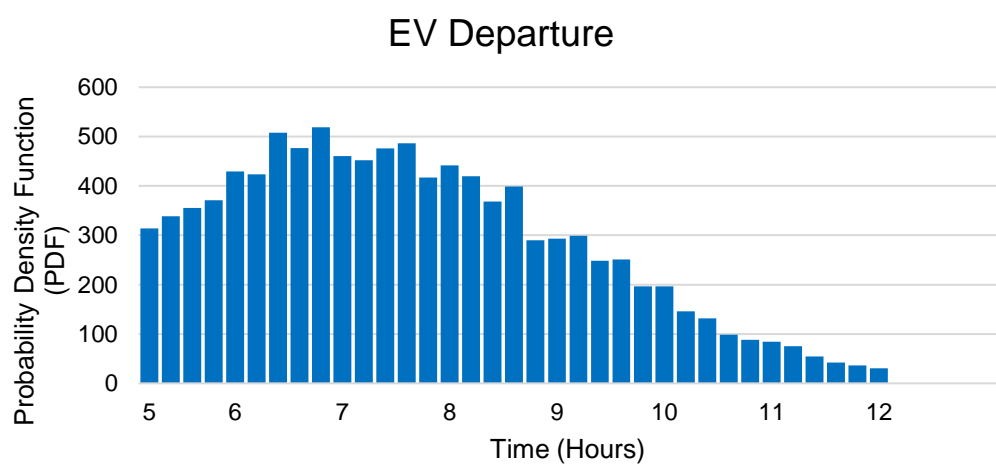
Microsoft Office Excel as a powerful assessment tool is used to deliver the process of SMCM and provide the results in this study. Figure 4.16 (a) shows the SoC_{EV} at arrival which ranges between 6-13 kWh, the estimated arrival time (T_{Arrive}^{EV}) of EV is shown in Figure 4.16 (b), and the departure time (T_{Dep}^{EV}) case should not be lower than 0.2×14 as in Figure 4.16 (d). By following the normal distribution function (gaussian function) as a type of probability distribution function (Probability Density Function (PDF)) with values [0,100], the T_{Arrive}^{EV} and, T_{Dep}^{EV} and SoC were obtained. As seen from the provided PDF, it shows which value likely to appear high and which one with less outcome. For the arrival (EV_a) and departure (EV_d) vehicles's mean (μ) to know how far the data from each other with the help of standard deviation (σ) calculation in order to obtain the bell-shape.



(a)



(b)



(c)

Figure 4.16 Normal distribution of EV (a) SoC of arrival, (b) arrival time, and (c) departure time.

4.5 Comparative analysis of ALO, IALO, PSO, and CSA

Metaheuristic algorithms are usually examined with benchmark test functions in terms of accuracy, time, and optimality to evaluate the performance of the proposed algorithm. The outcome of the analysis such as the mean and standard deviation (StD) of the proposed algorithm (IALO) and its counterparts (ALO, PSO, and CSA) are tabulated in Table 4.2 and refers to the benchmarked result. The aforementioned algorithms are applied due to their wide range of uses for several purposes. As previously mentioned in chapter 3, four popular benchmark test functions are mathematically presented. The comparison convergence of utilized unimodal (Sphere and Schwefel2.22) and multimodal (Ackley and Penalized 2) test functions is illustrated in Figure 4.17. Furthermore, mathematical equations, dimensions, and the range of each of the mentioned test functions were presented in chapter 3 (refer to Table 3.4). The test function was implemented to quantitatively measure the performance of the utilized nature-inspired metaheuristic algorithms. As a result, the performance of the simulation result was carried out in 100 iterations as illustrated in Figure 4.17. The collected result on each algorithm is run 30 times along with the Mean and Standard Deviation (StD) of the best solution to compare the overall performance of utilized algorithms as tabulated in Table 4.2.

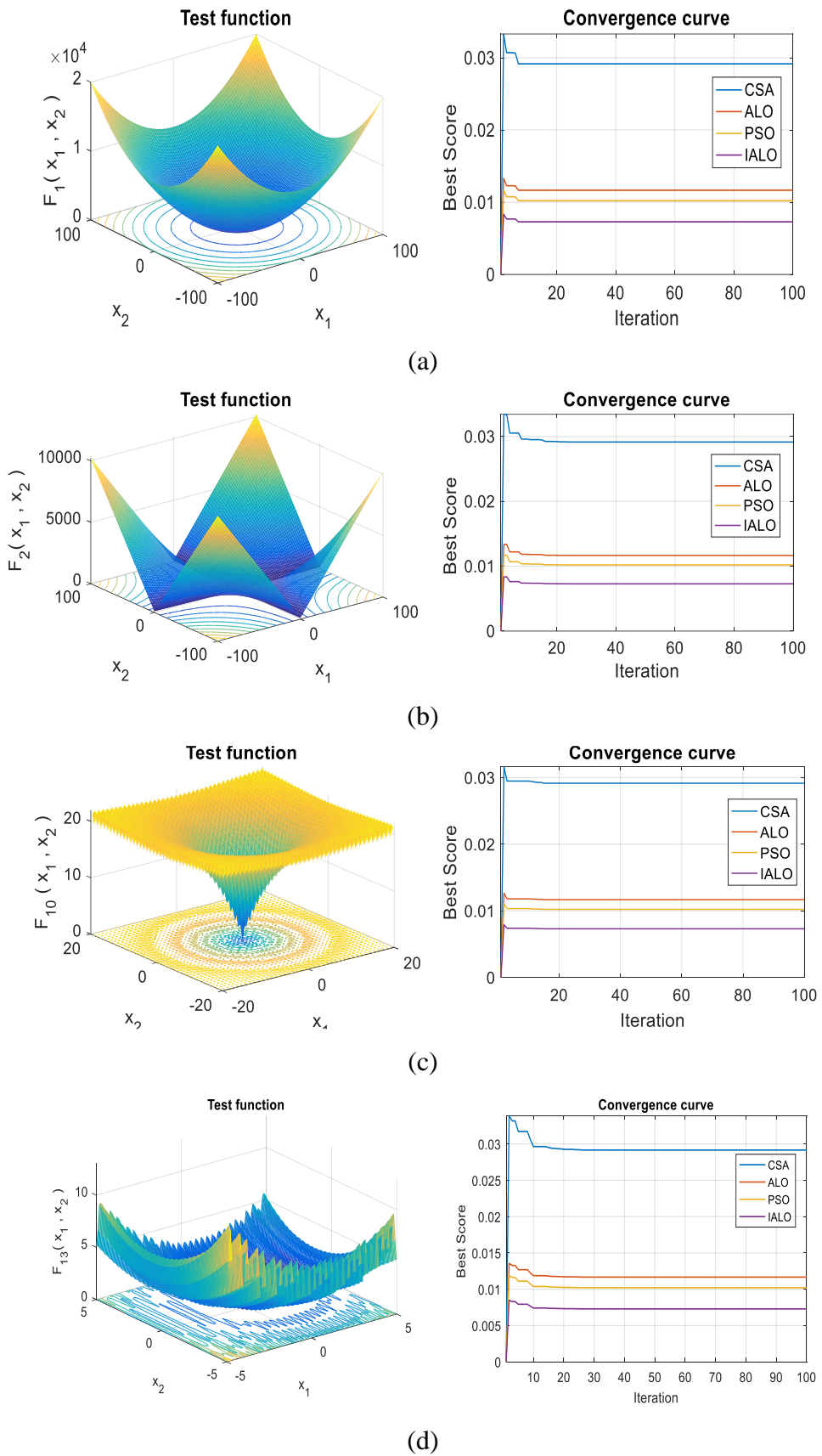


Figure 4.17 The benchmark result test function of the methods. (a) Sphere (F_1) (b) Schwefel2.22 (F_2), (c) Ackley (F_{10}), and (d) Penalized 2 (F_{13}).

Table 4.2 Statistic result of the test functions for the benchmark methods.

	ALO		IALO		PSO		CSA	
	StD	Mean	StD	Mean	StD	Mean	StD	Mean
F ₁	0.067	1.69e ⁻⁶	0.02	1.76 e ⁻⁸	0.095	2.38 e ⁻⁶	0.15	2.45 e ⁻⁶
F ₂	6.73e ⁻⁴	1.57e ⁻¹⁰	2.28e ⁻¹⁰	1.04e ⁻⁴	5.96e ⁻⁵	1.99	2.30e ⁻¹⁰	6.31e ⁻¹²
F ₁₀	1.26e ⁻⁶	2.52	3.45e ⁻⁶	2.60e ⁻⁹	0.011	3.55e ⁻⁷	0.001	1.71
F ₁₃	1.19e ⁻¹⁰	1.78	2.87e ⁻¹⁰	1.63e ¹	0.06	1.69	0.05	1.69

The Sphere function is presented in Figure 4.17 (a), the Schwefel2.22 function is shown in Figure 4.17 (b), the Ackley function is placed in Figure 4.17 (c), and the Penalized2 function is positioned in Figure 4.17 (d). All outcomes of the aforementioned test function for all algorithms should be zero. The presented result shows the Mean and the StD values for the proposed method and the benchmark methods. To avoid the issue of local optima as the challenge of ALO, the unimodal (Sphere and Schwefel2.22) and multimodal (Ackley and Penalized 2) are exploited. Moreover, the best score in each of the utilized algorithms shows IALO provides better results (nearer optimal solution). The acquired result balances the exploration and exploitation of IALO and the slow performance of IALO and ALO is due to the behavior of random walk of antlion in searching space.

4.6 Sizing Optimization result of the proposed microgrid

This section presents the simulation sizing result of the proposed algorithm and counterparts, the RB-EMS result, and the electricity generation result of the utilized sources are presented in the following subsections. The main objective of this study is to minimize the COE and LPSP while maximizing the REF to meet the grid demand using equations Eq. (3.15) to Eq. (3.24). The proposed metaheuristic (IALO) algorithm is applied to acquire the optimal sizing of the utilized components for the hybrid system to gain a cost-effective system.

The comparison sizing result among the examined algorithms is listed in Table 4.3 which presents the performance of RB-EMS-IALO with RB-EMS-ALO, RB-EMS-PSO, and RB-EMS-CSA. The IALO resulted as a better method in terms of

performance and is more economical than its other counterparts as tabulated in Table 4.3. It can be observed that RB-EMS-IALO has the lowest COE (\$0.0936/kWh), while RB-EMS-ALO has the highest value of COE (\$0.5866/kWh). Furthermore, all considered algorithms have the (0%) LPSP due to the various integrated sources, however, the REF is higher in RB-EMS-IALO than in any of its other counterparts.

Table 4.3 Comparison of Results from Different Algorithms.

Parameters	RB-EMS- IALO	RB-EMS- ALO	RB-EMS- PSO	RB-EMS- CSA
Autonomy Days (Days)	3	3	2	3
N_{PV} (Units)	93	96	95	100
N_{WT} (Units)	13	14	14	15
BT bank capacity (kWh)	35.38	38.38	23.59	35.38
LPSP (%)	0	0	0	0
REF (%)	99.40	97.30	95.37	94.35

The best fitness is demonstrated in Figure 4.18 in comparison with the benchmarking algorithms as convergence curves of the listed methods when the lower is the best. It shows the proposed method (IALO) performing better than the other counterparts which ensure the solution is the nearer global optimum point. Furthermore, the first method (ALO) approximately converged at 5 iterations, and the third (PSO) method at 12 iterations, while the second method (CSA) converged at approximately 4 iterations. The different environments of algorithms make the result different along with the complexity of the dealt data. Furthermore, the comparison of the cost of energy of the utilized methods is presented in the last iteration as in Figure 4.19. Based on the obtained result, the IALO shows the lowest cost in comparison with the compared algorithms due to the behavior of the proposed algorithms for comparison purposes (ALO, PSO, CSA) for addressing local optima in the conventional ALO.

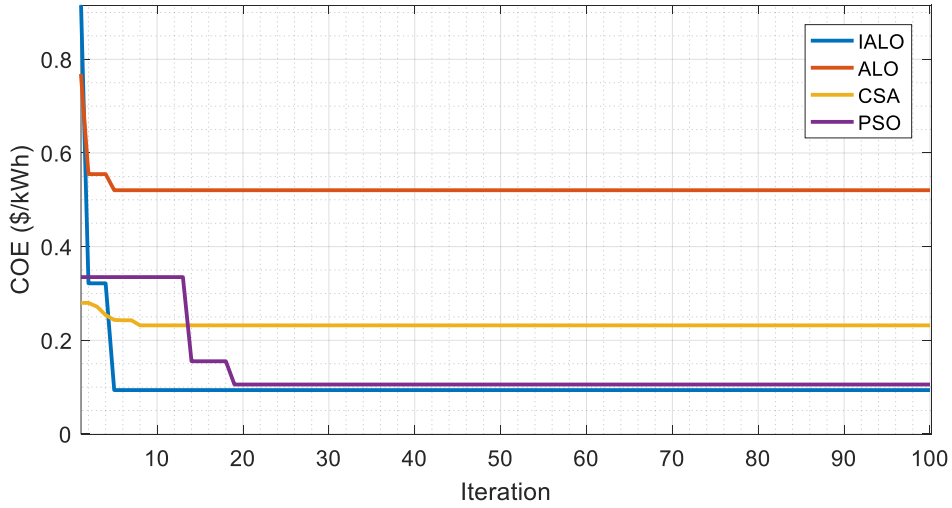


Figure 4.18 Comparison convergence rates for IALO, ALO, PSO, and CSA.

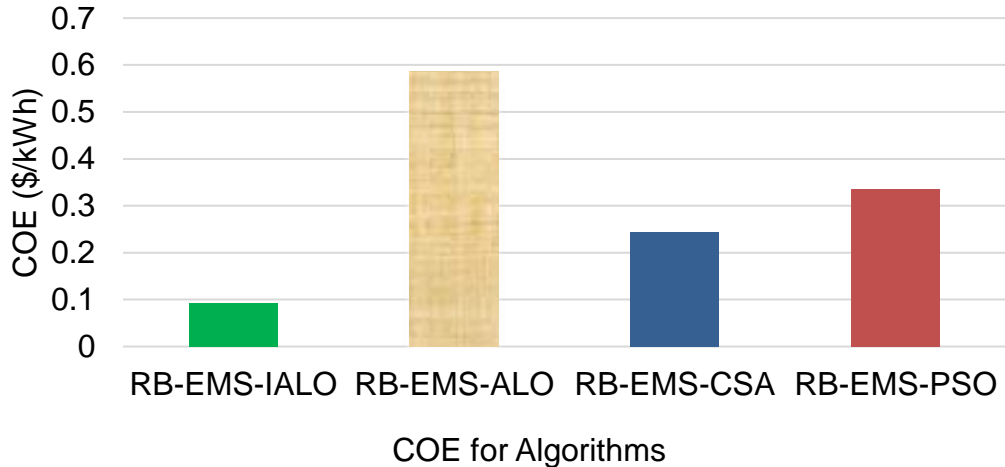


Figure 4.19 Cost of Energy of the proposed system considering EMS.

The obtained amount of total cost was measured in USD (\$) dollars. Where the comparison of the Annualized System Cost (ASC) of the system is demonstrated in

Figure 4.20 where IALO shows the lowest costs annually in comparison with the benchmarked algorithms. Where the annual values of each method are (IALO) \$ 143223.26/year, (ALO) \$ 145300.50/year, (PSO) \$ 149332.26/year, and (CSA) \$ 147223.26/year, respectively. Furthermore, the aforesaid obtained comparison result of ASC calculated with the help of Eq. (3.22) considering the capital cost, O&M, and replacement cost of the system components.

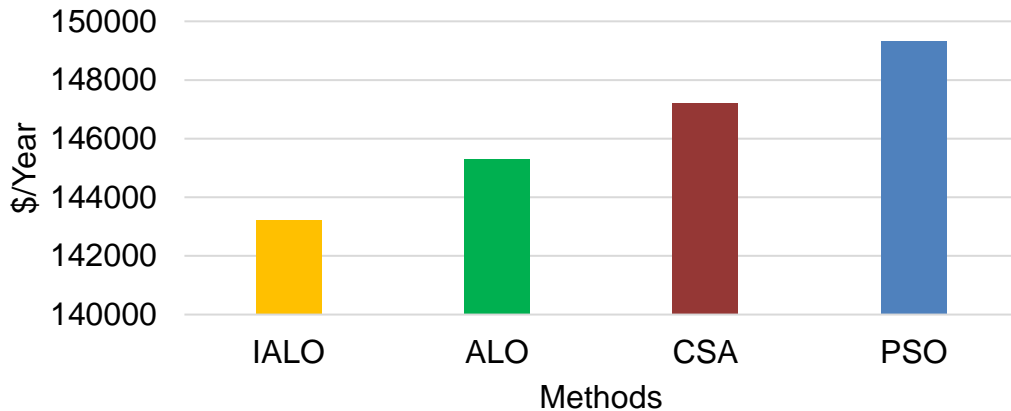


Figure 4.20 The Annualized System Cost with RB-EMS of the utilized methods.

4.7 The Rule-Based Energy Management Strategy scheme for electricity generation

This section presents the hourly seasonal and daily analysis of the electricity generation for the utilized sources using the RB-EMS operation modes as presented in the following subsection. For a better understanding of the EMS system, two days have been selected from each season and presented in the hourly form. The proposed RB-EMS operation modes for the grid-connected system with EV in this study are Mode 1 (RESs2V) considering P_{PV} and P_{WT} to charge EVs and other home appliances. Mode 2 (BT2V) is utilizing the energy storage battery in case RESs, and grid are not sufficient to fulfill the demand. Mode 3 (G2V) is when the EV is charged through the grid in the case of BT and RESs are not available or cannot meet the demand. Eventually, Mode 4 (V2G) refers to the discharging energy from the EV in the case of RESs, BT, and grid are not enough to meet the demand or are not available.

The RB-EMS in conventional power systems is a challenging task due to the dynamic nature of the demand. Similarly, the simulation goal is to examine the robustness of EMS over the period of one year along with fluctuating demand and various climatology conditions. The exploited configurations in the microgrid for this study are RESs (PV and WT) to meet the load demand integrated with BT as backup storage in the case of insufficient RESs to meet the demand. The foregoing components integrated with EV to form V2G technology under residential load. In this

context, BT-rated power is 35.38 kWh, DoD is 80%, and the rated power of PV and WT are 5 kW and 5 kW, respectively.

4.7.1 Seasonally analysis of electricity generation under different conditions

The round generation of electricity during the utilized year for 8760 hours for the period of (1st January to 31st December 2019) is conducted. The various daily analysis under different climatology conditions is presented in this section. The simulation result of the microgrid system is based on RB-EMS under four seasons for the case study presented. The four presented seasons along with categorized hours are (winter (1-1460 and 8032-8760), spring (1461-3650), summer (3651-5840), and autumn (5841-8031) as demonstrated in Figure 3.7 (refer to chapter 3). The time-based analysis is checked for the seasonal generation process of the utilized sources as presented in the next subsections. The ordinates in Figure 4.21 to Figure 4.24 are including the output power (P_{PV} , P_{WT} , P_L , P_{BT} , V2G, and G2V).

4.7.1.1 Winter electricity generation analysis

Winter (cold season) is sited between the end of the year (December) and the two beginning months of the year (January and February) which is around the hours (1-1460 h and 8032-8760 h). The output power of the first 50 hours (2 days) is shown in Figure 4.21 and affects the generated power by P_L and G2V due to the lower generation of RESs at hours between 01:00 h to 50:00 h. For further explanation, Table 4.4 and Figure 4.21 present the hourly analysis of the two first days of the year. As can be seen in Figure 4.21, at 01:00 h to 03:00 h intervals the output power from the PV is not available due to the cloudy hours in winter as such the output power is not sufficient to meet the load demand. Similarly, the WT is generating electricity from 01:00 h to 50:00 h, however, it cannot meet the demand due to the lower wind speed (1.5 m/s). In this case, the P_L is fulfilled by grid which refers to Mode 3. Additionally, from 03:00 h to 06:00 h Mode 4 is activated, at 04:00 h to 09:00 h positioned for Mode 1 using P_{WT} . The presented increase and decrease from the P_{BT} at 11:00 h to 17:00 h is due to the SOC_{EV} at time (t). At 17:00 h to 27:00 h there is no excess generation from PV and WT as sunset time. Moreover, at nighttime, from 27:00 h to 35:00 h, the

output power from the RESs is very low. At 40:00 h to 50:00 h, there is a weak generation from the RESs insufficient to meet the demand as P_{PV} (2.5 kW) and P_{WT} (2.7 kW), respectively. During the above-mentioned two days of operation, Mode 1, Mode 2, Mode 3, and Mode 4 are implemented.

Table 4.4 Hourly Execution of 50 hours of Operation in Winter.

Time (Hours)	Operation conditions	Modes	Consequences
1-4	$P_{PV} + P_{WT} < P_l$	M 3	Grid supply demand (EV) and BT
4-8	$Grid_{dem} > EV_{dem}$	M 4	EV supplies the demand
8-12	$P_{PV} + P_{WT} > P_l$	M 1	P_{WT} supply demand (EV) and BT
12-16	$P_b > [P_{WT} + P_{PV} - P_l]$	M 2	BT supplies the demand
16-20	$Grid_{dem} < EV_{dem}$	M 3	Grid supply demand (EV) and BT
20-24	$Grid_{dem} < EV_{dem}$	M 3	Grid supply demand (EV) and BT
24-28	$Grid_{dem} < EV_{dem}$	M 3	Grid supply demand (EV) and BT
28-32	$Grid_{dem} < EV_{dem}$	M 3	Grid supply demand (EV) and BT
32-36	$Grid_{dem} < EV_{dem}$	M 3	Grid supply demand (EV) and BT
36-40	$P_b > [P_{WT} + P_{PV} - P_l]$	M 2	BT supplies the demand
40-44	$Grid_{dem} < EV_{dem}$	M 3	Grid supply demand (EV) and BT
44-48	$Grid_{dem} < EV_{dem}$	M 3	Grid supply demand (EV) and BT

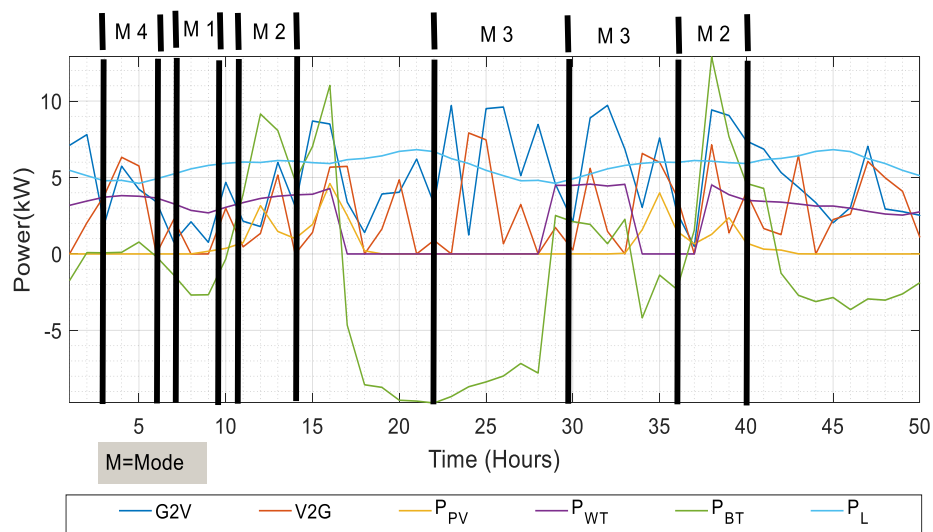


Figure 4.21 Daily output electricity generation in winter.

Based on the SoC_{EV} that was proposed between 0 and 1, the operation of the charging and discharging (V2G and G2V) is presented on the positive side along with the output power from the RESs and the discharging mode of the deep cycle battery. On the contrary, when the deep cycle battery in the charging mode, it refers to the insufficient case of meeting the demand from the battery in the charging mode.

4.7.1.2 Spring electricity generation analysis

Spring (warm season) is the second season of the year and started from March to May which is hourly positioned from 1461 h to 3650 h. The considered hours for examination range between 3651 h to 3699 h. The generated outpower from the RESs in spring is lower than in winter due to the weather condition. Additionally, the hourly analysis of the second season along with the operation modes are tabulated in Table 4.5 and further explained in Figure 4.22. From 1460 h to 1470 h as the sunset period, there is no generation of power from the RESs, as indicated in Mode 3. During sunshine hours from 1470 h to 1485 h Mode 1 is reactivated. At 1485 h to 1492 h, Mode 3 is reactivated due to the continuity of EV integration and grid availability. Through the P_{BT} from 1492 h to 1508 h Mode 2 was activated, at the same time P_{WT} and P_{PV} are generating electricity from 1492 h to 1498 h, however, it is not enough to meet the demand. In the period of the forgoing operating hours, Mode 1, Mode 2, Mode 3, and Mode 4 are operated.

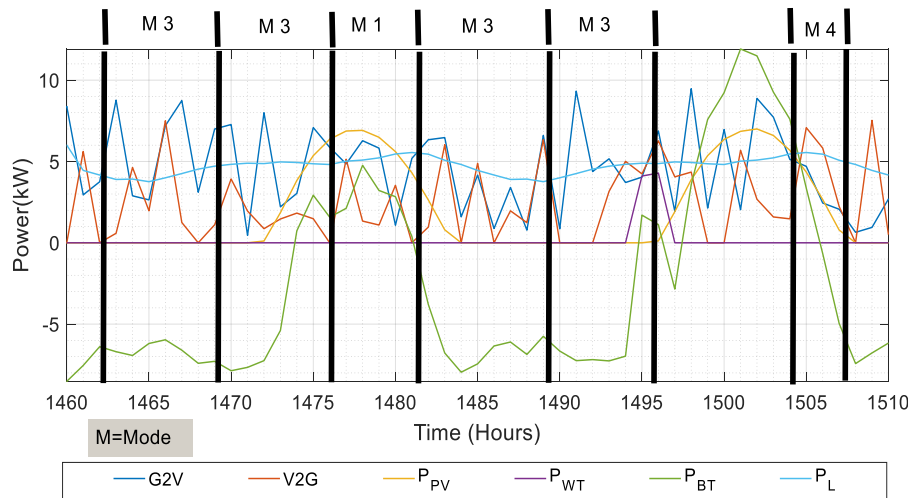


Figure 4.22 Daily output electricity generation in spring.

Table 4.5 Hourly Execution of 50 hours of Operation in Spring.

Time (Hours)	Operation conditions	Modes	Consequences
1460-1464	$Grid_{dem} < EV_{dem}$	M 3	Grid supply demand (EV) and BT
1464-1468	$Grid_{dem} < EV_{dem}$	M3	Grid supply demand (EV) and BT
1468-1472	$Grid_{dem} < EV_{dem}$	M 3	Grid supply demand (EV) and BT
1472-1476	$Grid_{dem} < EV_{dem}$	M 3	Grid supply demand (EV) and BT
1476-1480	$Grid_{dem} > EV_{dem}$	M 4	EV supplies the demand
1480-1484	$Grid_{dem} < EV_{dem}$	M 3	Grid supply demand (EV) and BT
1484-1488	$Grid_{dem} < EV_{dem}$	M 3	Grid supply demand (EV) and BT
1488-1492	$Grid_{dem} < EV_{dem}$	M 3	Grid supply demand (EV) and BT
1492-1496	$Grid_{dem} < EV_{dem}$	M 3	Grid supply demand (EV) and BT
1496-1500	$P_b > [P_{WT} + P_{PV} - P_l]$	M 2	BT supplies the demand
1500-1504	$P_b > [P_{WT} + P_{PV} - P_l]$	M 2	BT supplies the demand
1504-1508	$Grid_{dem} > EV_{dem}$	M 4	EV supplies the demand

4.7.1.3 Summer electricity generation analysis

Summer (hot season) is the third season of the year that affects the loads due to the increasing sunlight. The increase in solar radiation results in the generation of peak power. This season is categorized between June to August and started at 3651 h to 5840 h. Furthermore, the investigated analysis operations start at 3651 h to 3699 h as formulated in Table 4.6 and the electricity generation analysis is presented in Figure 4.23. At 3651 h to 3655 h, the P_L is greater than the P_{PV} and P_{WT} , thus, the load is supplying from the grid which refers to Mode 3. Additionally, from 3655 h to 3670 h Mode 2 was activated. Mode 3 gets going from 3670 h to 3680 h the RESs are switched OFF due to the nighttime which is the reason why it is not generating electricity. Besides, at 3680 h to 3695 h, Mode 2 is reactivated by using a BT bank to supply the load. Eventually, at 3695 h and 3700 h, Mode 3 is replaced as the sunset time. The operation modes limitation of the mentioned 2 days is performing along with all modes except Mode 1 due to the climatology changes in the mentioned season.

Table 4.6 Hour-by-hour execution of 50 hours of operation in summer.

Time (Hours)	Operation conditions	Modes	Consequences
3651-3655	$Grid_{dem} < EV_{dem}$	M 3	Grid supply demand (EV) and BT
3655-3659	$P_b > [P_{WT} + P_{PV} - P_l]$	M 2	BT supplies the demand
3659-3663	$P_b > [P_{WT} + P_{PV} - P_l]$	M 2	BT supplies the demand
3663-3667	$P_b > [P_{WT} + P_{PV} - P_l]$	M 2	BT supplies the demand
3667-3671	$Grid_{dem} > EV_{dem}$	M 4	EV supplies the demand
3671-3675	$Grid_{dem} < EV_{dem}$	M 3	Grid supply demand (EV) and BT
3675-3679	$Grid_{dem} < EV_{dem}$	M 3	Grid supply demand (EV) and BT
3679-3683	$Grid_{dem} < EV_{dem}$	M 3	Grid supply demand (EV) and BT
3683-3687	$P_b > [P_{WT} + P_{PV} - P_l]$	M 2	BT supplies the demand
3687-3691	$P_b > [P_{WT} + P_{PV} - P_l]$	M 2	BT supplies the demand
3691-3695	$Grid_{dem} < EV_{dem}$	M 3	Grid supply demand (EV) and BT
3695-3699	$Grid_{dem} > EV_{dem}$	M 4	EV supply demand

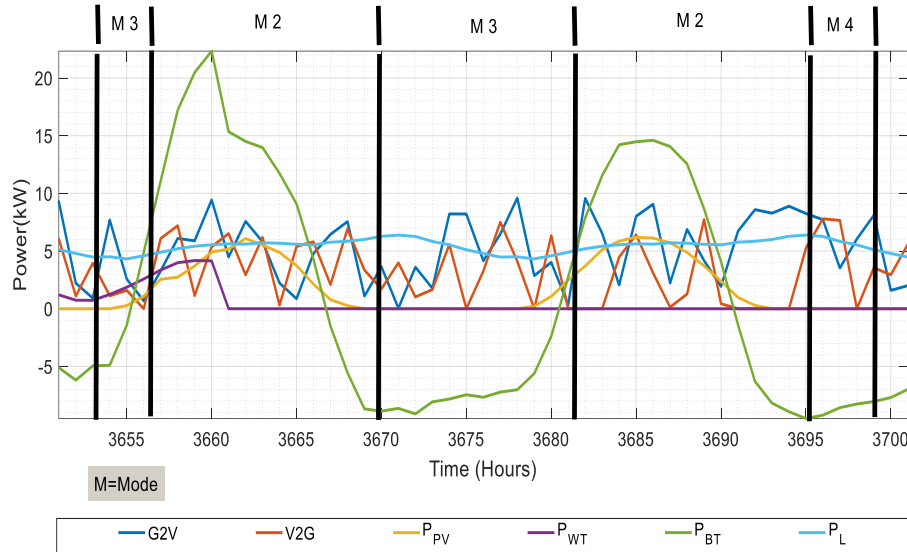


Figure 4.23 Daily output electricity generation in summer.

4.7.1.4 Autumn electricity generation analysis

Autumn (mild season) is the fourth season of the year with warm weather in the case study. It has a lower effect on the power system due to less load being used. It is positioned between September to November, which is within 5841 h to 8031 hours and the examined hours are from 5841 h to 5890 h. Furthermore, Table 4.7 presents the starting hourly electricity generation analysis of the Autumn season and further analysis is shown in Figure 4.22. At 5841 h to 5855 h, the P_{BT} is utilized that meets the demand with that refers to Mode 2, while the P_{WT} is generating electricity with (4 kW) but not sufficient to meet the demand. In the period of 5855 h to 5865 h, Mode 3 and Mode 4 are reactivated with lower generation from the RESs (P_{PV} and P_{WT}). Continuously, at 5865 h to 5875 h Mode 2 is operating. At 5875 h to 5882 is ending the RESs generation and starting with Mode 3. At 5882 h to 5890 h P_{WT} is generating electricity but not meeting the demand, Mode 3 is performing. The employed operation modes in the presented autumn hours are Mode 2, Mode 3, and Mode 4.

Table 4.7 Hour-by-hour execution of 50 hours of operation in autumn

Time (Hours)	Operation conditions	Modes	Consequences
5841-5845	$P_b > [P_{WT} + P_{PV} - P_l]$	M 2	BT supplies the demand
5845-5849	$P_b > [P_{WT} + P_{PV} - P_l]$	M 2	BT supplies the demand
5849-5853	$Grid_{dem} < EV_{dem}$	M 3	Grid supply demand (EV) and BT
5853-5857	$Grid_{dem} < EV_{dem}$	M 3	Grid supply demand (EV) and BT
5857-5861	$Grid_{dem} > EV_{dem}$	M 4	EV supplies the demand
5861-5865	$Grid_{dem} > EV_{dem}$	M 4	EV supplies the demand
5865-5869	$P_b > [P_{WT} + P_{PV} - P_l]$	M 2	BT supplies the demand
5869-5873	$P_b > [P_{WT} + P_{PV} - P_l]$	M 2	BT supplies the demand
5873-5877	$Grid_{dem} < EV_{dem}$	M 3	Grid supply demand (EV) and BT
5877-5881	$Grid_{dem} < EV_{dem}$	M 3	Grid supply demand (EV) and BT
5881-5885	$Grid_{dem} < EV_{dem}$	M 3	Grid supply demand (EV) and BT
5885-5889	$Grid_{dem} < EV_{dem}$	M 3	Grid supply demand (EV) and BT

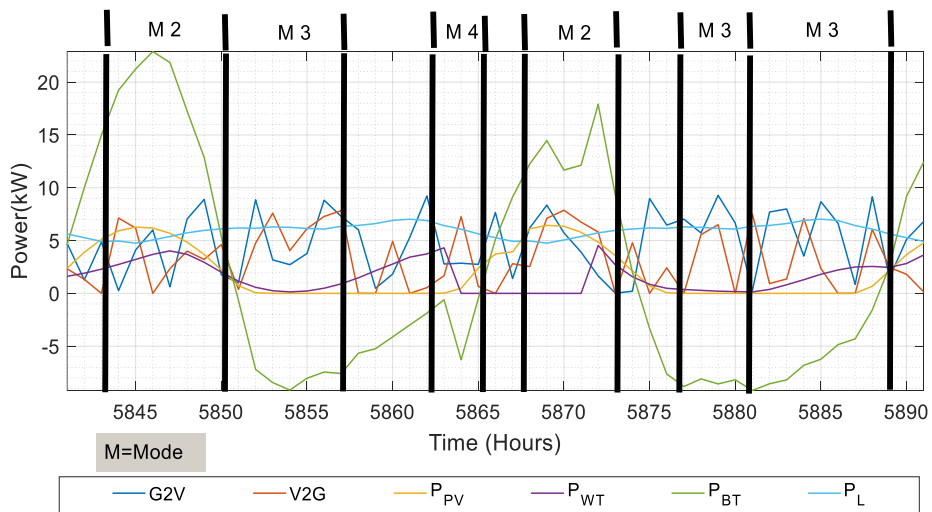


Figure 4.24 Daily output electricity generation in autumn.

4.7.2 Annual output power result

The annual round generated electricity from PV, WT, BT, V2G, G2V, and load demand (P_L) are shown in Figure 4.25 (a). The zoomed-in version of Figure 4.25 (a) is demonstrated in Figure 4.25 (b). As presented in Figure 4.25, the light brown straight line is the (P_{PV}), purple straight line refers to the (P_{WT}), and load demand (P_L) is aqua color. Continuously, RB-EMS can manage and control the microgrid subsystems' operation efficiently. The annual considered load is equal to 47 MWh without EVs integration and with the EVs $P_{L(EV)}$ integration that forms V2G operational is 51 MWh.

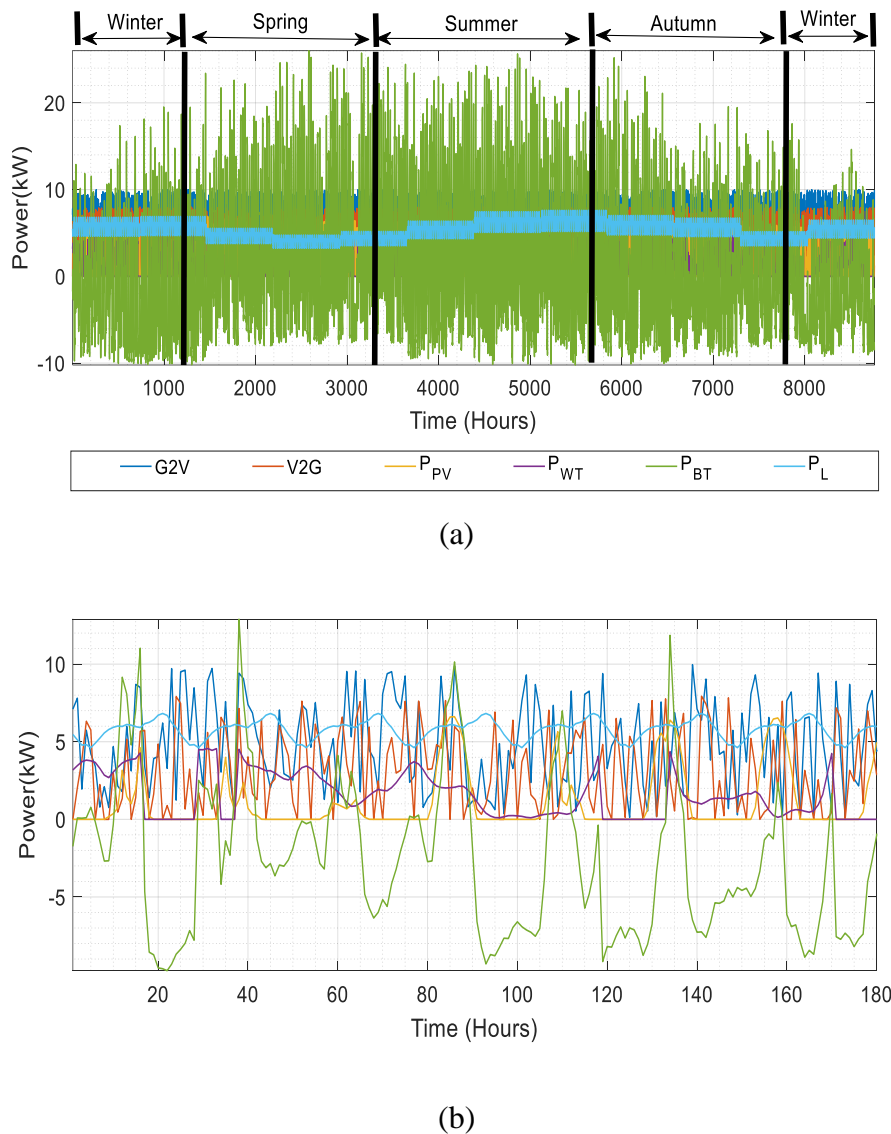


Figure 4.25 Electricity generated (a) Annually charge/discharge, and load for one year, (b) A week Zoomed-in of (a).

Moreover, the aforementioned increase in the load during V2G integration refers to the shifted load (with EV) due to the integration of EV as a charging load. The SoC refers to the ratio of remaining capacity (Ah) in a range of minimum (SOC_{BTmin}) and maximum (SOC_{BTmax}) of the SoC of the battery as 20% and 100%, respectively. The expected annual SoC of the battery is shown in Figure 4.26 (a), whereas the seasonal with the SOC_{BTmin} and SOC_{BTmax} of the first week of the year have been illustrated in Figure 4.26 (b). It can be observed from the plot that, the high exploitation of the BT is in winter as compared to spring. This is due to the high demand for energy during this season for heating applications. Moreover, the least usage of BT is in summer and autumn due to significant solar radiation exploited to produce electricity.

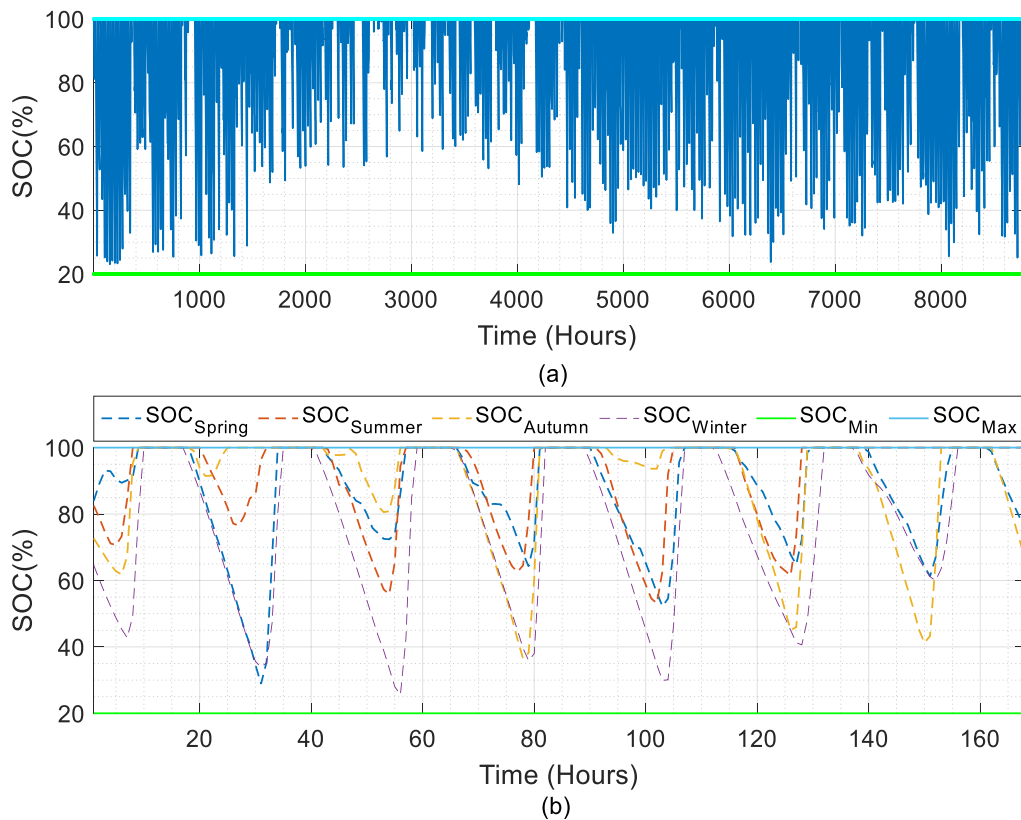


Figure 4.26 The State of Charge of the battery (a) Annually and (b) Weekly for four seasons.

The operation of charging and discharging considering the exploited energy sources in the study is based on the situation of SOC_{EV} and SOC_{BT} . Figure 4.27 presented the output power of the battery (BT_{Dis}), renewables ($RESs_{Ch}$), EV (EV_{Dis}),

grid (Grid_{Ch}), and load demand (P_L) considering three samples. Sample (a) presents the situation of three cases when discharging from the EV, but it is not sufficient to meet the demand (4.8 kWh), while the grid generates electricity to charge the EV, but the EV demand at 06:00 met by the RESs with (7.8 kWh). Besides, sample (b) presents the case of charging of the deep cycle battery at 17:00 with the energy of (-4.2 kWh), at the aforesaid hour, the BT is not sufficient to meet the demand. Eventually, sample (c) represents the case when the grid is supplying the load. All the cases have been met throughout the year.

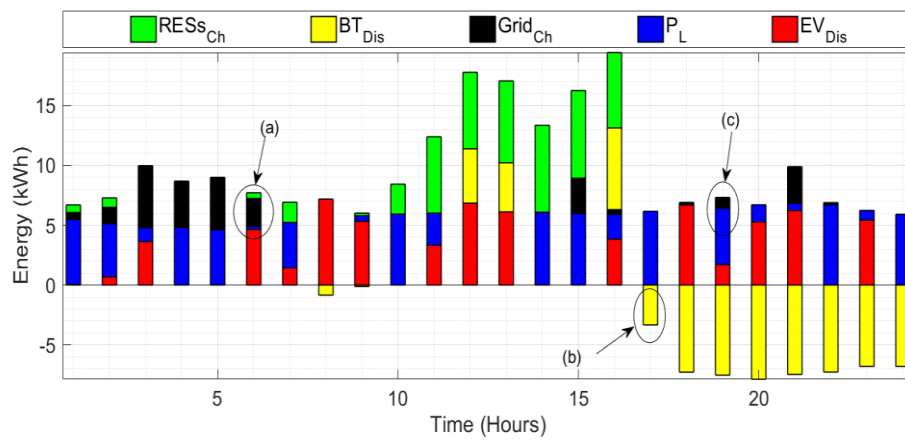


Figure 4.27 The V2G operation based on the State of Charge.

4.8 Economic analysis of the system

By calculating the cost of the whole project lifetime (capital cost), the DCF has been considered due to its adoption of RES design and planning systems with the help of Eq. (3.39) and Eq. (3.40). Additionally, DCF is carried over the same period of the project's lifetime, the DPP is 9 years which refers to the breakeven point (the project becomes profitable) as presented in Figure 4.28. In order to determine the point at which an investment plan turns a profit while accounting for the discount rate, the DPP criterion combines the DPP technique with DCF analysis. The increasing revenue presents in linear form due to the constant load demand during the whole project lifetime. On the contrary, the nonlinearity of the annualized cost is caused by the cost of the components (O&M, capital cost, and replacement cos) as shown in Figure 4.29.

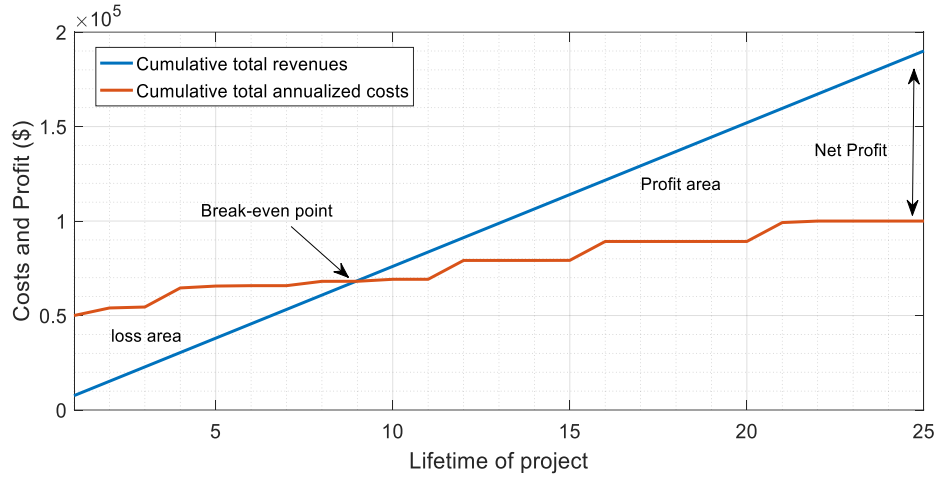


Figure 4.28 The break-even of the project over 25 years.

4.8.1 Economic breakdown of the components

The breakdown of the energy system and costs is listed in Table 4.8. In terms of components cost installed in the system, the PV annual cost is around \$ 76466.76 while WT is \$ 54156.54. From the tabulated result, we realized that a wind turbine system cost is more economical than a PV system in terms of installation cost. The integration of V2G is a cost-effective system due to the provided advantages such as reducing the dependency on the grid, being environmentally friendly, emergency cases, and having profit acquired.

Table 4.8 The energy and cost breakdown of the system.

Parameters	Value	Units
Renewable Energy Sources surplus	284.34	\$
Total Photovoltaic output	50977.84	MW
Total Wind Turbine output	27078.24	MW
Annual Total Electric Vehicle demand	4379.96	kWh
Annual Residential load demand	47288.91	kWh
Annual Purchased energy from the grid (G2V)	1891.5567	\$/kWh/y
Annual Sold energy to the grid (V2G)	2364.1725	\$/kWh/y

4.8.2 Capital Costs and Net Present Cost

By exploiting MATLAB packaging software, the Life Cycle Cost (LCC) analysis of the system can be achieved. The LCC is including the replacement cost, capital cost, and operation and maintenance costs. The capital cost of the proposed system components considering EMS in terms of breakdown details of NPC is illustrated in Figure 4.29. Since the cost of the system is considered in this system, the LCC is calculated due to the utilization of different RESs integrated into the grid and EV. The lifetime of the project is 25 years.

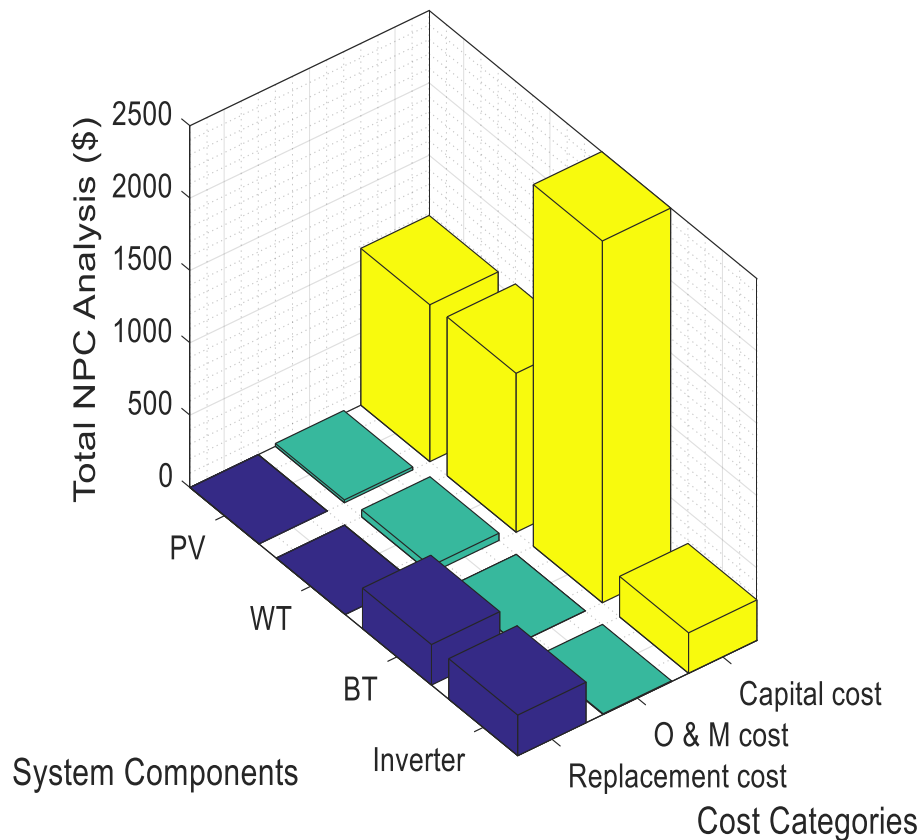


Figure 4.29 Breakdown of cash flow of the system components and cost categories.

4.8.3 Objective function analysis

The primary three objective functions are trade-offs. To produce the best outcome, the designer must compromise on the three objective functions. The REF is

maximized when the LPSP is decreased, which raises the cost of the entire system. For calculating the revenue of the electricity as presented in Eq. (3.13) and the purchase cost of the power in Eq. (3.14). The load demand is seasonally changeable due to the fluctuating loads during the four seasons and increasing energy demand. A comparison of buying and selling energy for the first 24 hours is demonstrated in Figure 4.30. Furthermore, the consumed energy from EVs (sell) is presented in Figure 4.30 (blue), while the sold energy from the utility grid to charge EVs is shown in (brown). The presented figure is an action for the first 24 hours, the changes depend on the demand for the EVs. For instance, at 4 am there is a higher buying time for charging due to the EV demand, while the higher selling time is shown at 06:00 am show a higher seller time. All the previous actions depend on the EV status.

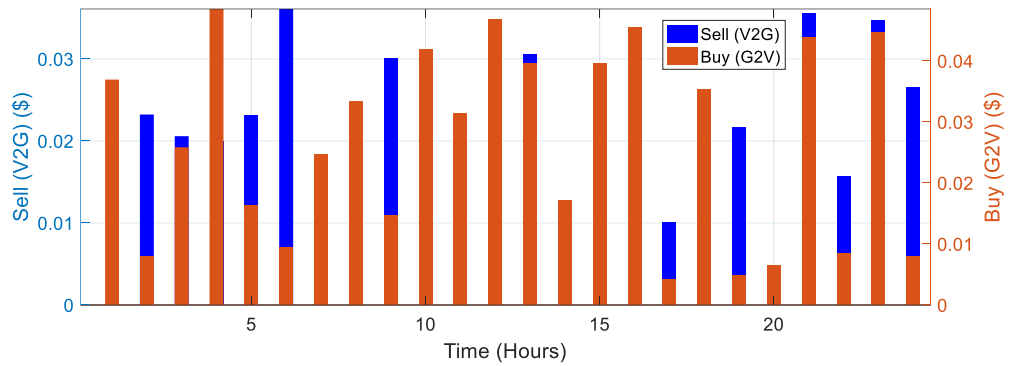


Figure 4.30 Comparison of buying and selling energy.

The other objective functions LPSP and REF are also considered for analysis which represent the amount of change increasing by (10%). The impacts of EVs on the grid considering the stochastic method are resulting in the reduction of the LPSP which affects the EVs system. The LPSP ranges between 0-1 as mentioned in the literature depending on load satisfaction. Due to the unstable power from the suppliers (RESs and grid), the LPSP is changing during the year. Numerically speaking, the case of 10% has a maximum increase of 0.02%, 30% has a maximum increase of 0.06%, and 60% has an increase of 0.12%.

4.9 Impact of EVs integrating

The increasing number of EVs will also affect the incremental in the domestic load when utilizing G2V technology. This will be presented in the following subsection under various scenarios. In order to address the presented issue by integrating RESs as charging infrastructures with the local grid in order to charge EVs (RESs2V) to gain an environmentally friendly system and reduce the dependency on the grid. Besides, in the case of RESs or the grid are not sufficient to meet the demand, the BT2V can be utilized. The benefit of V2G technology is to exchange the power between the grid and the vehicle in a bidirectional way. In addition, EVs can be used in vast cases such as electricity interruption (load cannot be met) based on the SOC_{EV} , environmental benefits, used as load and source, and reducing the cost of energy obtaining financial profit as a driver in the case of the on-peak load period.

4.9.1 Impacts of G2V integration

In the case of G2V, the amount of consumed energy in Winter is higher than in other seasons due to the heavy loads (heaters and water boilers). Where the energy consumed by chargers shows an increase due to the high demand considering EVs and other appliances, followed by the RESs, Energy from the grid, then the exported energy from the EVs. The changes for all cases for 24 hours when integrating 10 EVs (black), 30 EVs (red), 60 EVs (blue), and No EVs (green) are shown in Figure 4.31. The amount of transferred energy in the absence of EV integration shows low changes not exceeding 5 kWh due to the consideration of only residential load. Additionally, the case of integrating 10 EVs shows rapid changes due to the randomness of EV data.

Due to the uncertain situation of the SOC_{EV} during the year, some increases and decreases are affecting the load. In the aforementioned case of G2V, the three proposed integration scenarios (10, 30, and 60) of EVs are dissected. For instance, the consumption energy for $G2V_{10}$, $G2V_{30}$, $G2V_{60}$, and no EV for sample (a) at 07:00 pm are (1.49, 22.53, 37.35, and 5.23 kWh). Additionally, sample (b) for $G2V_{10}$, $G2V_{30}$, $G2V_{60}$, and no EV at 18: 00 pm are (0.23, 22.8, 41.16, and 6.24 kWh). Eventually, in

sample (c) for the G2V₁₀, G2V₃₀, G2V₆₀, and no EV at 24:00 am the consumed energy are (8.39, 0.29, 34.15, and 5.91 kWh), respectively.

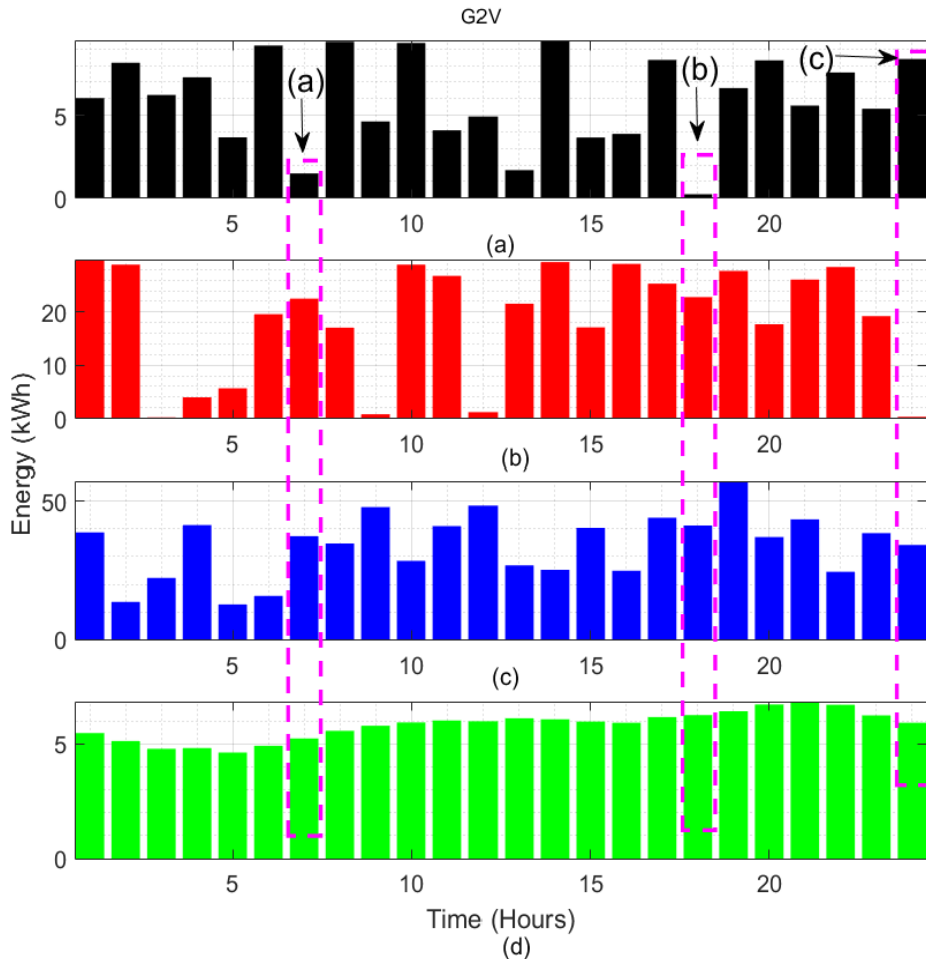


Figure 4.31 The load impact of Grid-to-Vehicle for the scenarios for the first 24 hours (a) 10 EVs, (b) 30 EVs, (c) 60 EVs, and (d) no EVs.

4.9.2 Impact of V2G integration

The acquired analysis result for the scenarios of V2G under proposed integrations 10 (blue), 30 (black), 60 (red), and No EV (green) is figured out in Figure 4.32. The situation of V2G as mentioned earlier is a bidirectional exchange operation. The amount of transferred energy varies between the proposed integrated EVs. Almost all the cases show quick change due to the uncertainties of SOC_{EV} value as the main considered factor when integrated loads (EV) with the grid to form V2G.

The main consideration of the thesis is the implementation of V2G technology, and the impacts on the load when integrating 10, 30, 60, and no EV in the proposed system. Figure 4.32 shows the three cases of integration $V2G_{10}$, $V2G_{30}$, and $V2G_{60}$ along with no EV integration, respectively. Sample (a) at 07:00 shows the consumed energy with the mentioned integration cases as (2.75, 10.59, and 22.49 kWh) while without integrating EV consumed energy is 5.23 kWh (utilizing the load demand with the absence of EV). Besides, in sample (b) at 17:00 the energy consumed for the various EV integration is (0, 0, and 4.05 kWh) while without EV is 6.16 kWh. Finally, in sample (c) at 23:00 the consumption energy is (kWh) without the integration of EV is (4.15, 1.36, and 15.02 kWh) while the case of not integrating EV is 6.23 kWh. Since it is randomly integrated for one year, some energy consumptions are not showing due to the SOC_{EV} at the time of multiplication.

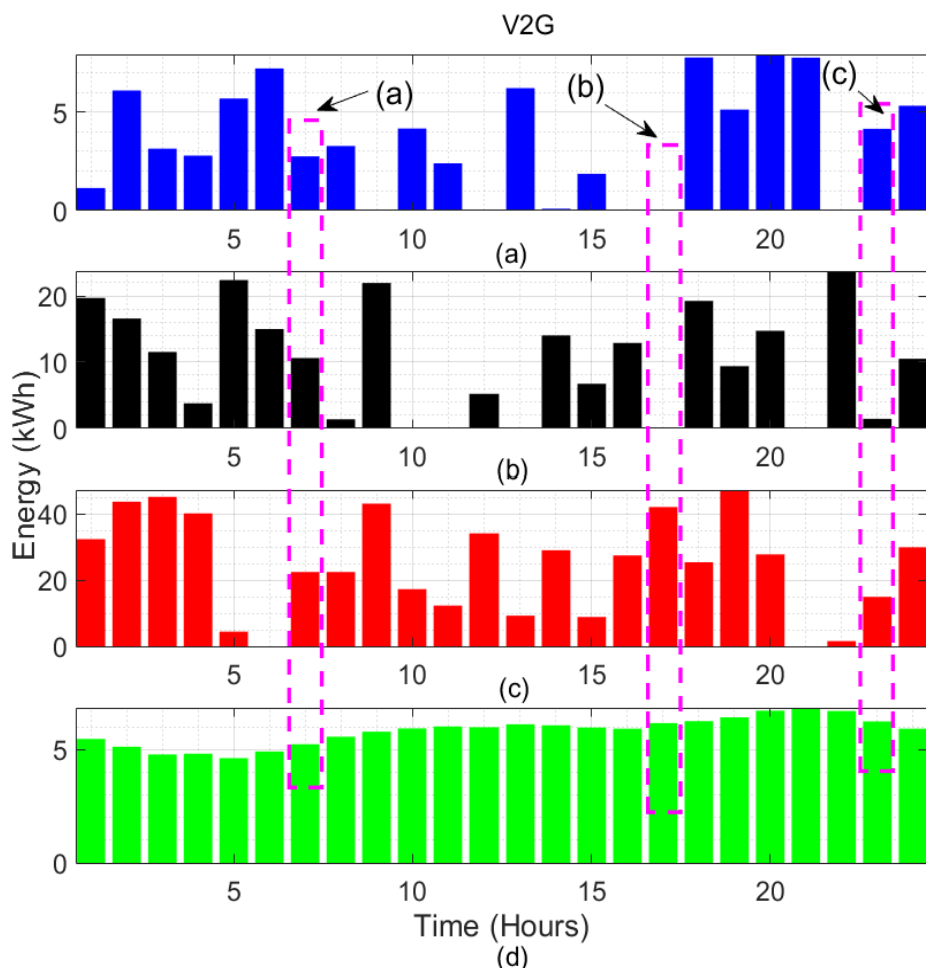


Figure 4.32 The load impact of Vehicle-to-Grid for the first 24 hours (a) 10 EVs, (b) 30 EVs, (c) 60 EVs, and (d) no EVs hours.

4.9.3 Impact of RESs2V integration

The RESs are accepted among consumers due to proving green energy and overcoming power challenges. The EV batteries can discharge to provide electricity when the output from RESs is low. However, this will shorten the battery's cycle during the operation of charges and discharges. The mentioned limitation can be overcome by scheduling the charging time of the EV. The load impacts in Figure 4.33 is presented for the EV in charging mode from the utilized RESs when integration 10 (blue), 30 (black), 60 (red), and no EV (green). Although the changes in delivering the energy (kWh) from the RESs to the EVs that are presented in Figure 4.33 is due to the intermittency and fluctuation of weather in the case study, the load has been met. Some samples were taken as an example of the flow energy for the RESs2V, the considered cases when having RESs2V_{10} , RESs2V_{30} , RESs2V_{60} , and no EV for instance, at 07:00, 15:00, and 23:00, respectively. In sample (a) at 07:00 am the cases of RESs2V_{10} , RESs2V_{30} , RESs2V_{60} , and no EV that consumes (3.69, 23.88, 8.27, and 5.23 kWh). Sample (b) presents the impacts at 15:00 with RESs2V_{10} , RESs2V_{30} , RESs2V_{60} , and no EV produced (3.87, 2.44, 57.46, and 5.97 kWh). Eventually, the consumed energy for sample (c) at 23:00 is (6.54, 11.24, 56.6, and 6.23 kWh).

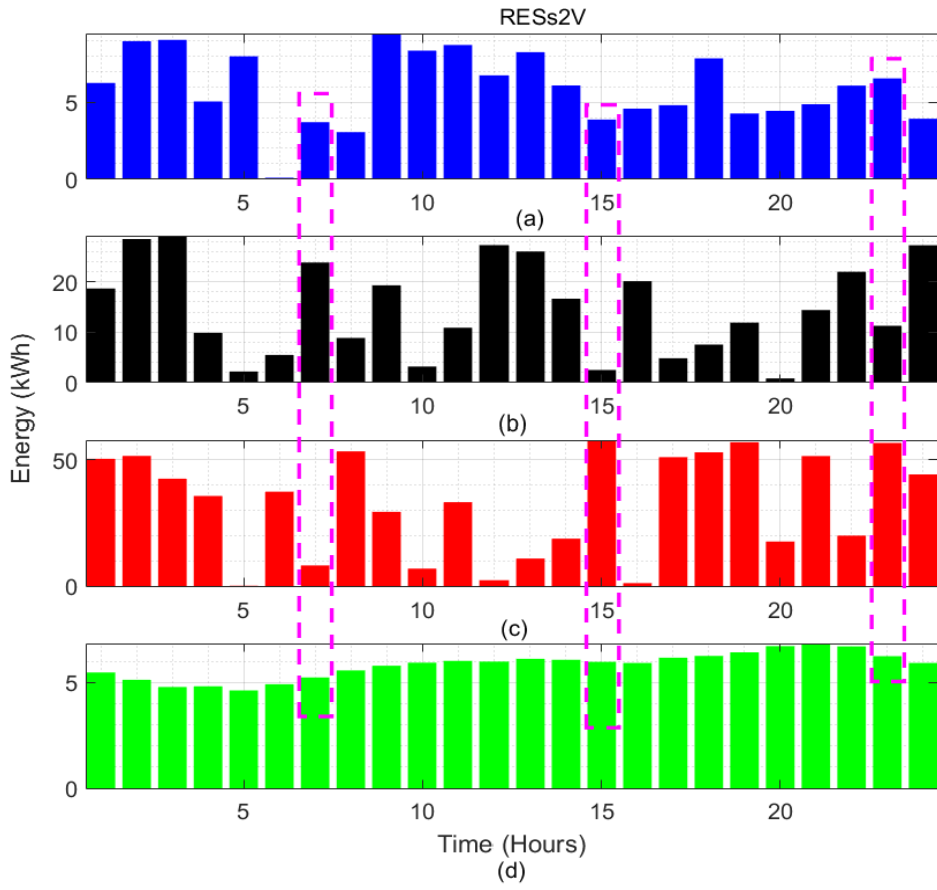


Figure 4.33 Renewable Energy Sources impact for the first 24 hours (a) 10 EVs, (b) 30 EVs, (c) 60 EVs, and (d) no EVs.

4.9.4 Impact of BT2V integration

The output power from the storage battery is measured in kWh based on the energy consumed as demonstrated in Figure 4.34 for the first 24 hours of the year. The amount of obtained power from the battery in the case of charging and discharging has been estimated using a stochastic random method to charge the EVs. As mentioned earlier, the priority of charging the EVs is from the RESs. If RESs are not sufficient to fulfill the EVs, energy will be taken from BT.

In the case of not integrating EV with the integration of 10, 30, and 60 EVs show the output power acquired from BT to charge and discharge cases is demonstrated in Figure 4.34. In some of the presented samples of exporting the energy from the BT, for example, at 02:00 am as sample (a) under $BT2V_{10}$, $BT2V_{30}$, and

BT2V₆₀, the received energy from the BT in previous cases is (14.46, 26.99, 68.13, 5.11 kWh). Furthermore, the consumed energy for sample (b) at 08:00 are (-5.88, -18.5, -22.67, and 5.56 kWh). Eventually, sample (c) energy consumption at 17:00 is (-39.21, -104.8, -226.7, and 6.16 kWh).

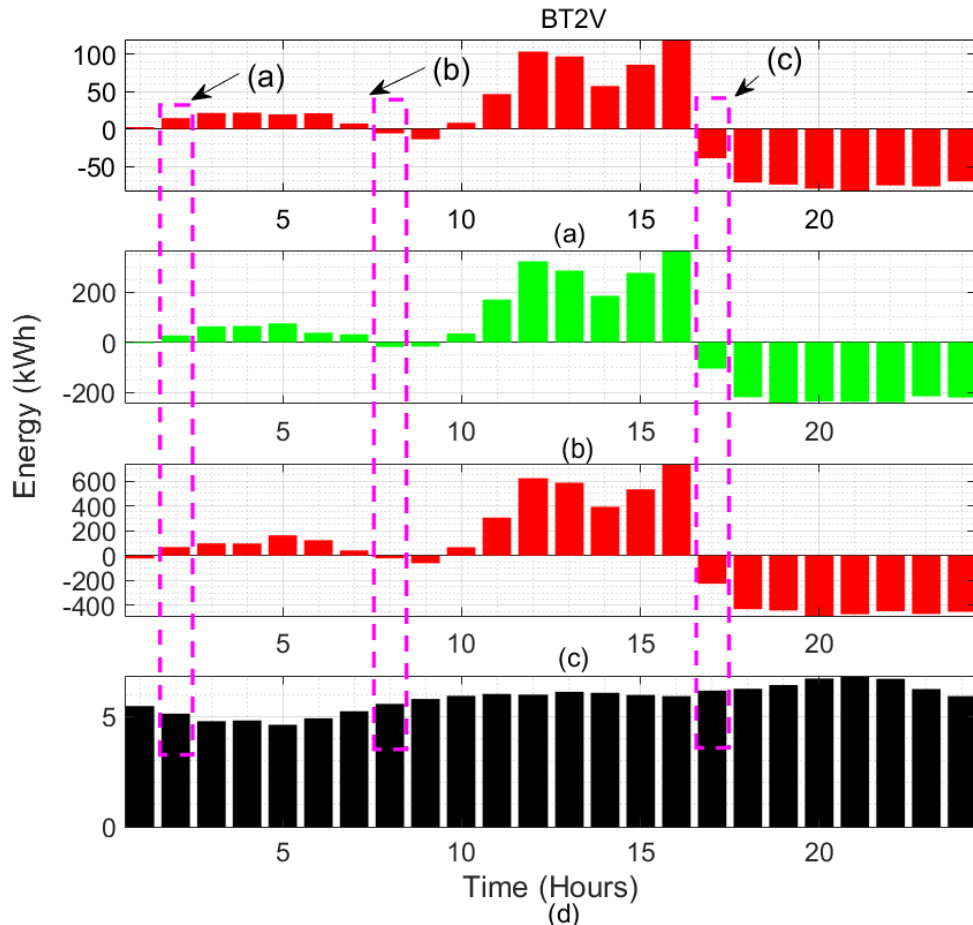


Figure 4.34 Generated output power from the battery to EV for the first 24 hours
 (a) 10 EVs, (b) 30 EVs, (c) 60 EVs, and (d) no EVs.

4.10 The Sensitivity Analysis

The sensitivity analysis is presented in this section and utilized for a grid-connected system. It is employed to provide a better understanding of impacts on the load and examine the performance of the integration system under various scenarios. Furthermore, it is utilized in order to evaluate the influence of various configurations on system operation. The sensitivity analysis for this study is conducted in two parts

for the key affected components of the system result. The first one is the impact of uncertainty on the output power from the RESs (P_{PV} and P_{WT}) due to climatology changes (wind speed, solar irradiance, and temperature). The second one is related to the comparison of COE with REF and LPSP in the case of insufficient power provided by the RESs along with the EV integration.

4.10.1 Impact of Changes in Climatology Condition

The impact of changes in climatology conditions on energy production has been investigated and analyzed in this section. The selected configurations have been chosen due to the listed reasons.

- The climatology changes are considered to overcome the worse days (unsunny or unwind days) scenario.
- The energy storage battery is the less lifespan component carried out for sensitivity analysis due to the backup in the case of insufficient RESs power.
- The integration of EVs potentially affects the output power result (when charging and discharging).

Based on the acquired result from RB-EMS-IALO for the microgrid (refers to Table 4.3 and Figure 4.18) is opted to be presented in Figure 4.35.. Due to the uncertain changes from RESs (PV and WT) from the proposed algorithm, the components have been investigated. It can be seen that the presented drops refer to the generation drop from the RESs, the cost is increasing. Moreover, 1 refers to the original case (point of no increase or decrease occurred). The most affected microgrid sources in the system are PV and WT due to the climatology changes, and the relationship between the PV output power and wind turbine. The curve of sensitivity is considering the P_{PV} and P_{WT} in contradiction with the COE as demonstrated in Figure 4.35.

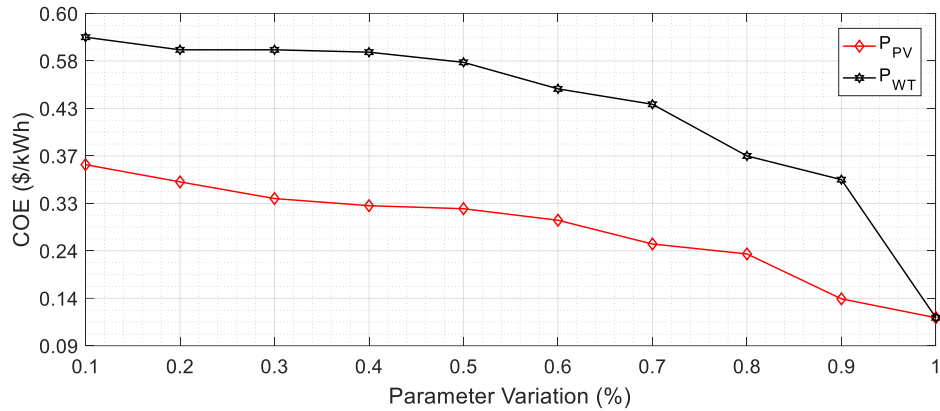


Figure 4.35 Sensitivity Analysis: Comparison between P_{PV} and P_{WT} against COE.

4.10.2 Impact of deep cycle battery and EVs integration on the grid

It can be seen that from Figure 4.36 (a), the increase in REF potentially affects the COE result. As the high renewability is provided in the case study, the increase in the REF reduces the cost. Based on the COE calculated by RB-EMS-IALO (refers to Table 4.3), increasing the number of EVs increases the COE as shown in Figure 4.36 (b). Integrating the various number of EVs influence the load. Ultimately, due to the fact that the COE and LPSP are trade-offs, the COE against the LPSP is demonstrated in Figure 4.36 (c). Besides, in this study the considered increase of LPSP is taken as 10 %, whenever the LPSP is increasing the COE is increasing and vice versa. Additionally, when the SoC of BT (parameter variation) increased by 10 % as proposed, the COE is increasing as presented in Figure 4.36 (d).

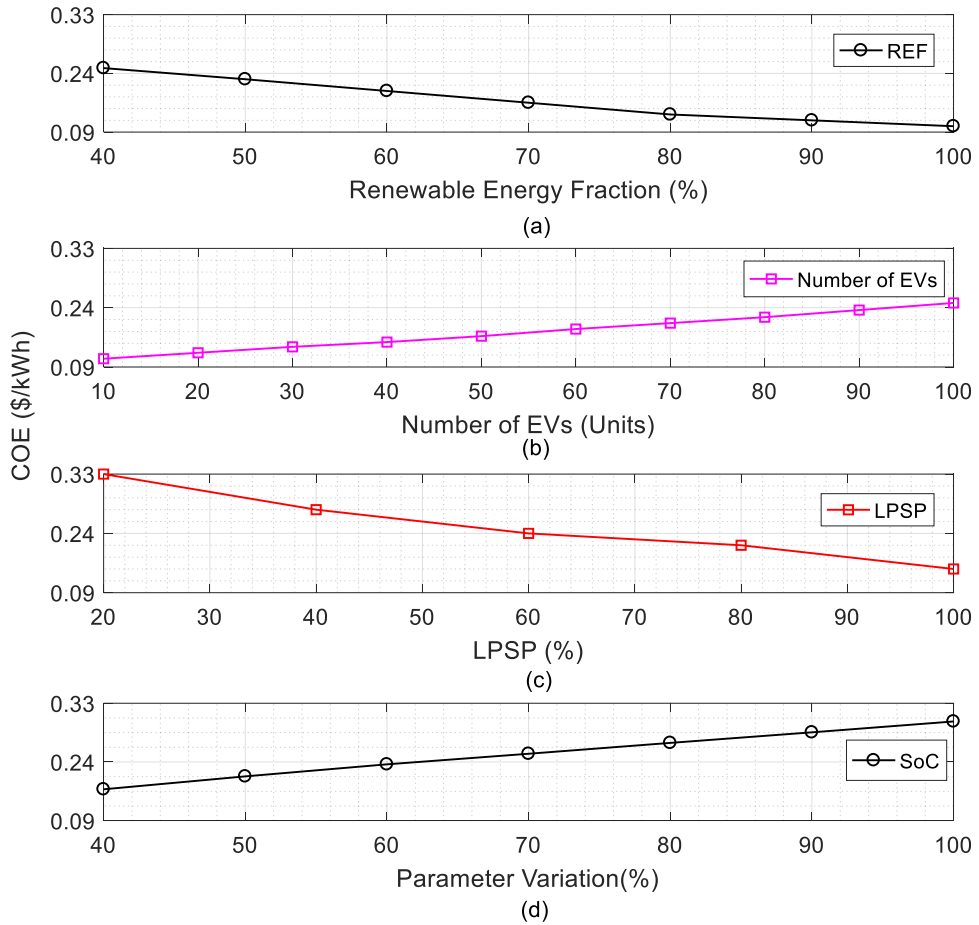


Figure 4.36 Sensitivity Analysis: (a) Comparison of COE and REF of the microgrid system, (b) COE against EV increase, (c) COE against LPSP, and (d) SoC against the COE.

4.11 Chapter Summary

In this chapter, the details background of the input data of the utilized components and the load profile of the study region are discussed. The results of the components of the microgrid such as the output power of RESs (PV and WT), SoC_{max} and SoC_{min} of the battery have been demonstrated. In addition, the sizing methods used are based on a nature-inspired metaheuristic algorithm using IALO. The obtained results of IALO were benchmarked with ALO, PSO, and CSA. The acquired result from the proposed method shows better performance in terms of low COE and LPSP and maximizing the REF than the benchmarked methods under various climate

conditions. In conclusion, by implementing the supervisory control for the proposed methods (RB-EMS-IALO) and its counterparts (RB-EMS-ALO), (RB-EMS-PSO), and (RB-EMS-CSA), RB-EMS-IALO is performing better. It is believed that utilizing V2G technology could achieve clean and affordable energy, higher renewable fraction, and lower NPC which meets the SDG7. The SMCM acquired result from a probability perspective under various scenarios is discussed for the number of EVs ranging from 10 to 60 EVs. The load impact for the process of charging (G2V), and discharging (V2G), along with other scenarios such as RESs2V (Charging), and BT2V (Charging) examined under 3 cases (10, 30, and 60 EVs) along with no EV integrated is considered. Lastly, DPP is conducted followed by sensitivity analysis is carried out to emphasize the effects of any future uncertainties from components on the system input.

CHAPTER 5

CONCLUSION AND RECOMMENDATIONS

5.1 Conclusion

This chapter presents a summary of the done work in this thesis considering residential grid-connected systems using the V2G technology integrated with RESs. The climatology data and load demand data of Tripoli-Libya are exploited for the aforementioned system considered for planning and addressing power issues in the country. The considered microgrid components in this research are, PV, WT, BT, and EV integration into the utility grid to form V2G in order to achieve the proposed system objectives. The proposed method for monitoring and controlling the flow of power in the system is the RB-EMS algorithm, while the sizing method is the IALO. The optimization algorithms described how a hybrid system is optimized in terms of size to improve economic benefits. Therefore, IALO is used to find the best configuration of the integrated system in a residential area. The IALO simulation results show better performance in terms of low COE and maximum REF than other benchmark algorithms (ALO, PSO, and CSA). From the standpoint of system-level design, these two factors are typically so closely related that it is unreasonable to examine them individually.

The system components are sized by IALO coupled with RB-EMS to control the flow of power in the system with some constraints. A microgrid system integrated with solar and wind-powered EVCF using V2G technology for the residential load was implemented. The modeling of RESs integrated into power generation based on V2G technology has attracted very high interest in the electricity market. The proposed system is not only for residential loads, but it can also be for commercial or industrial loads. The RESs (PV and WT) are considered due to their abundant nature which can be considered a good alternative source to promote electrification, improve energy access for the study area, and meet SDG7.

The used simulation tool (MATLAB) was able to yield efficient results for RB-EMS-IALO and sizing that achieves the proposed objectives (COE, LPSP, and REF). Therefore, the aforementioned objective functions are the main basic need for each community to gain an improved standard of living in several fields such as education, healthcare, and the economy. It concluded that the results have solved the problem statement of the study. The obtained result from RB-EMS-IALO has validated the effectiveness with RB-EMS-ALO, RB-EMS-PSO, and RB-EMS-CSA that demonstrating the improvement of ALO provides an optimal result in a shorter time than ALO. Additionally, the number of integrated EV impacts was assessed by a stochastic method namely Monte Carlo Method. The aforementioned random method provides the results for the impact of EV integration on the load under three scenarios when having 10, 30, and 60 EVs. Eventually, the economic assessments along with the sensitivity analysis results to present the cost-profit percentage and estimate the impact on the grid within the uncertain number of EVs and changeable weather were discussed.

Various concerns have been handled during the study process, and these issues have been converted into the research's contribution, which is listed out below.

- i. This study has successfully established and implemented an enhanced metaheuristic technique called Improved Antlion Optimization (IALO). The IALO was utilized for sizing optimization of grid-connected microgrid components taking into account economic and technical factors. Due to the limitation of ALO such as premature convergence, and meeting local optima by using RWS. ALO has been improved by replacing RWS with LF in order to overcome ALO challenges. The main superiority of LF is to update the position of ant and antlion with the help of Eq. (3.26) and Eq. (3.32) which refers to improving the effectiveness, robustness, and convergence of random walks (local search). The proposed system consists of PV-WT-BT integrated with an EV charger in residential load to form the V2G technology as a new generation of smart-houses. Moreover, the aforementioned configurations have been sized by the proposed algorithm (IALO) and compared with their counterparts to obtain the best minimum components. The IALO has a higher

chance than its counterparts (ALO, PSO, and CAS) of finding the global optimum solution and efficient output in terms of sizing and objective functions. The proposed algorithm (IALO) has been implemented and complemented with the RB-EMS to be RB-EMS-IALO. In terms of optimality of the provided solution from the proposed metaheuristic algorithm (IALO) has been confirmed through the counterparts when tested using standard benchmarking test functions. As a result, from the utilized test function, IALO obtain a better performance in unimodal and multimodal searching space in comparison with benchmarks.

- ii. Design a suitable system using the RB-EMS scheme specifically for the V2G system for smoothing power flow among the proposed system. The RB-EMS is considered under four operation modes, and it is proven for delivering power in sequence for the various energy sources utilized in the proposed hybrid system. The acquired result from the RB-EMS-IALO has been validated with RB-EMS-ALO, RB-EMS-PSO, and RB-EMS-CSA for the confirmation of effective power delivery from different sources. The RB-EMS-IALO yields better results in terms of objective functions (COE, LPSP, and REF) as compared with its counterparts. The RB-EMS-IALO has been investigated under the four climatology condition seasons along with the fluctuating demand. As a result, the proposed operation modes were met throughout the year. The RB-EMS-IALO presented in this thesis was specially created for the case study at hand under four operation modes (V2G, G2V, RESs2V, and BT2V). Furthermore, the methodology is applicable to all situations, therefore it can serve as a user manual for system designers when creating a system with a comparable function. This is crucial since the successful operation of the microgrid depends on the best capacity planning.
- iii. Analysis of the acquired result from the COE point of view using the DCF analysis method to gain the DPP or break-even point. The short payback period leads to a profit of 513600.68 \$ for the whole period lifetime of the project. The DCF utilized to calculate the LCC for gaining revenue has been presented along with the LPSP and REF. The annual randomness (uncertain) of the

arrival and departure behavior of EVs is fully modeled based on the SMCM combined with a grid-connected model to form V2G technology under three scenarios. SMCM results are presenting the impact amount of charged and discharged power to the grid, from the EVs, SoC, and exporting power from the RESs when integrating 10, 30, and 60 EVs. Four strategies have been taken into consideration namely (V2G, G2V, RESs2V, and BT2V) to examine the EV integration impact on the load. Followed by details of the sensitivity analysis to present the performance of the microgrid by examining the impact of the uncertainties that are expected to be occurred in the future due to the climatology conditions, REF, LPSP, and BT capacity.

5.2 Suggestions for Future Works

Some avenues for future research efforts have been identified as a result of this study. Consequently, it is suggested that future development concentrates on the important areas named as follows.

- a) A residential load has been considered in this study to charge and discharge EVs, however, the commercial load can be exploited for future researchers' work under the same case study as conductive charging, Wireless Power Transfer (WPT) Technology, or Inductive Power Transfer (IPT) Technology charging techniques can be considered along with the time of charge and discharge [122]. In addition to charging sources, the Energy Internet (EI) technology is a future grid to unify power, transportation, communication, transfer power through boilers and chillers for heating and cooling purposes, feed the electric appliances, and charge EVs may be conducted in the future [10].
- b) This study proposed IALO as a nature-inspired metaheuristic algorithm, future work should consider other different algorithms or hybridization with more than one method such as Lion-Optimization Algorithm (LOA) [199], Sea Lion Optimization (SLnO) [200], and Bat Algorithm (BA) [201]. Feature selection can be classified into filter-based and wrapper-based. This study considers the

wrapper-based using Lévy Flight (LF) while the expected future work to implement a filter-based considers other feature selections such as Tournament Selection, Truncation, and Boltzmann Selection [75].

- c) The power has been controlled based on RB-EMS in this study under DC/AC bus bar, attention can be paid to Optimization-Based EMS (OB-EMS) or Learning-Based EMS (LB-EMS) in future research work [28]. Additionally, the limitation performance of RB-EMS in this study is simulation-based. Furthermore, it is believed that the topologies under Vehicle-to-Everything (V2X) such as V2G, and V2H can be physically implemented as hardware and validated with the software simulation result.
- d) This research considers deep cycle batteries (Li-ion) as a single energy storage, future work should consider the implementation of an Ultracapacitor (UC), or Fuel Cell (FC) using Hydrogen (H_2) as backup energy for hybrid systems [18]. Additionally, the PHEV battery has been considered in this study, future work direction may use other types of EV such as BEV or HEV.
- e) Discounted Cash Flow analysis method has been considered to analyze the economic cost of the microgrid system during the lifetime of the project [184]. The SMCM is utilized to investigate the impact of the changes on the load when integrating an uncertain number of EVs, another stochastic method can be employed such as the Taguchi method [8], Markov Decision Process (MDP) can be used in the future research as the main function is to solve sequential decision-making problems under uncertainties [202]. Time of use (ToU) can be utilized in future studies to evaluate the influence on power flow and cost from the effects of parameters on the system performance for sensitivity analysis [185].

REFERENCES

- [1] R. P. Narasipuram and S. Mopidevi, “A technological overview & design considerations for developing electric vehicle charging stations,” *J. Energy Storage*, vol. 43, no. June, p. 103225, 2021, doi: 10.1016/j.est.2021.103225.
- [2] Y. E. García Vera, R. Dufo-López, and J. L. Bernal-Agustín, “Energy Management in Microgrids with Renewable Energy Sources: A Literature Review,” *Appl. Sci.*, vol. 9, no. 18, p. 3854, Sep. 2019, doi: 10.3390/app9183854.
- [3] M. F. Zia, E. Elbouchikhi, and M. Benbouzid, “Microgrids energy management systems: A critical review on methods, solutions, and prospects,” *Appl. Energy*, vol. 222, no. April, pp. 1033–1055, 2018, doi: 10.1016/j.apenergy.2018.04.103.
- [4] V. Muthiah-Nakarajan, S. H. C. Cherukuri, B. Saravanan, and K. Palanisamy, “Residential energy management strategy considering the usage of storage facilities and electric vehicles,” *Sustain. Energy Technol. Assessments*, vol. 45, no. March, p. 101167, Jun. 2021, doi: 10.1016/j.seta.2021.101167.
- [5] A. S. Aziz, M. F. N. Tajuddin, M. R. Adzman, M. F. Mohammed, and M. A. M. Ramli, “Feasibility analysis of grid-connected and islanded operation of a solar PV microgrid system: A case study of Iraq,” *Energy*, vol. 191, p. 116591, Jan. 2020, doi: 10.1016/j.energy.2019.116591.
- [6] C.-T. Ma, “System Planning of Grid-Connected Electric Vehicle Charging Stations and Key Technologies: A Review,” *Energies*, vol. 12, no. 21, p. 4201, Nov. 2019, doi: 10.3390/en12214201.
- [7] B. Belgasm, Y. Aldali, M. J. R. Abdunnabi, G. Hashem, and K. Hossin, “The potential of concentrating solar power (CSP) for electricity generation in Libya,” *Renew. Sustain. Energy Rev.*, vol. 90, no. March, pp. 1–15, Jul. 2018, doi: 10.1016/j.rser.2018.03.045.
- [8] D. Sadeghi *et al.*, “Designing, optimizing and comparing distributed generation technologies as a substitute system for reducing life cycle costs, CO₂ emissions, and power losses in residential buildings,” *Energy*, vol. 253, p. 123947, 2022, doi: 10.1016/j.energy.2022.123947.
- [9] D. Sadeghi, A. Hesami Naghshbandy, and S. Bahramara, “Optimal sizing of

- hybrid renewable energy systems in presence of electric vehicles using multi-objective particle swarm optimization,” *Energy*, vol. 209, p. 118471, Oct. 2020, doi: 10.1016/j.energy.2020.118471.
- [10] H. S. Das, M. M. Rahman, S. Li, and C. W. Tan, “Electric vehicles standards, charging infrastructure, and impact on grid integration: A technological review,” *Renew. Sustain. Energy Rev.*, vol. 120, no. December, p. 109618, Mar. 2020, doi: 10.1016/j.rser.2019.109618.
 - [11] N. Shaukat *et al.*, “A survey on electric vehicle transportation within smart grid system,” *Renew. Sustain. Energy Rev.*, vol. 81, no. May 2017, pp. 1329–1349, Jan. 2018, doi: 10.1016/j.rser.2017.05.092.
 - [12] Y. Ma *et al.*, “An overview on V2G strategies to impacts from EV integration into power system,” in *2016 Chinese Control and Decision Conference (CCDC)*, May 2016, pp. 2895–2900, doi: 10.1109/CCDC.2016.7531477.
 - [13] K. Kasturi, C. K. Nayak, and M. R. Nayak, “Electric vehicles management enabling G2V and V2G in smart distribution system for maximizing profits using MOMVO,” *Int. Trans. Electr. Energy Syst.*, vol. 29, no. 6, Jun. 2019, doi: 10.1002/2050-7038.12013.
 - [14] M. S. Adnan Khan, K. M. Kadir, K. S. Mahmood, M. I. Ibne Alam, A. Kamal, and M. M. Al Bashir, “Technical investigation on V2G, S2V, and V2I for next generation smart city planning,” *J. Electron. Sci. Technol.*, vol. 17, no. 4, p. 100010, Dec. 2019, doi: 10.1016/j.jnlest.2020.100010.
 - [15] T. U. Solanke, V. K. Ramachandaramurthy, J. Y. Yong, J. Pasupuleti, P. Kasinathan, and A. Rajagopalan, “A review of strategic charging–discharging control of grid-connected electric vehicles,” *J. Energy Storage*, vol. 28, p. 101193, Apr. 2020, doi: 10.1016/j.est.2020.101193.
 - [16] A. Singh and S. S. Letha, “Emerging energy sources for electric vehicle charging station,” *Environ. Dev. Sustain.*, vol. 21, no. 5, pp. 2043–2082, Oct. 2019, doi: 10.1007/s10668-018-0151-x.
 - [17] A. Banerji, K. Sharma, and R. R. Singh, “Integrating Renewable Energy and Electric Vehicle Systems into Power Grid: Benefits and Challenges,” in *2021 Innovations in Power and Advanced Computing Technologies (i-PACT)*, Nov. 2021, pp. 1–6, doi: 10.1109/i-PACT52855.2021.9696887.
 - [18] T. U. Solanke, P. K. Khatua, V. K. Ramachandaramurthy, J. Y. Yong, and K. M. Tan, “Control and management of a multilevel electric vehicles

- infrastructure integrated with distributed resources: A comprehensive review,” *Renew. Sustain. Energy Rev.*, vol. 144, no. March, p. 111020, Jul. 2021, doi: 10.1016/j.rser.2021.111020.
- [19] M. A. Quddus, M. Kabli, and M. Marufuzzaman, “Modeling electric vehicle charging station expansion with an integration of renewable energy and Vehicle-to-Grid sources,” *Transp. Res. Part E Logist. Transp. Rev.*, vol. 128, no. June, pp. 251–279, 2019, doi: 10.1016/j.tre.2019.06.006.
 - [20] O. Ouramdane, E. Elbouchikhi, Y. Amirat, and E. Sedgh Gooya, “Optimal Sizing and Energy Management of Microgrids with Vehicle-to-Grid Technology: A Critical Review and Future Trends,” *Energies*, vol. 14, no. 14, p. 4166, Jul. 2021, doi: 10.3390/en14144166.
 - [21] S. Barakat, H. Ibrahim, and A. A. Elbaset, “Multi-objective optimization of grid-connected PV-wind hybrid system considering reliability, cost, and environmental aspects,” *Sustain. Cities Soc.*, vol. 60, no. March, p. 102178, Sep. 2020, doi: 10.1016/j.scs.2020.102178.
 - [22] S. Twaha and M. A. M. Ramli, “A review of optimization approaches for hybrid distributed energy generation systems: Off-grid and grid-connected systems,” *Sustain. Cities Soc.*, vol. 41, pp. 320–331, Aug. 2018, doi: 10.1016/j.scs.2018.05.027.
 - [23] H. Yu, S. Niu, Y. Shang, Z. Shao, Y. Jia, and L. Jian, “Electric vehicles integration and vehicle-to-grid operation in active distribution grids: A comprehensive review on power architectures, grid connection standards and typical applications,” *Renew. Sustain. Energy Rev.*, vol. 168, no. April, p. 112812, 2022, doi: 10.1016/j.rser.2022.112812.
 - [24] M. Dubarry, A. Devie, and K. McKenzie, “Durability and reliability of electric vehicle batteries under electric utility grid operations: Bidirectional charging impact analysis,” *J. Power Sources*, vol. 358, no. August, pp. 39–49, Aug. 2017, doi: 10.1016/j.jpowsour.2017.05.015.
 - [25] E. I. Come Zebra, H. J. van der Windt, G. Nhumaiio, and A. P. C. Faaij, “A review of hybrid renewable energy systems in mini-grids for off-grid electrification in developing countries,” *Renew. Sustain. Energy Rev.*, vol. 144, no. April, p. 111036, Jul. 2021, doi: 10.1016/j.rser.2021.111036.
 - [26] E. Costa, P. Wells, L. Wang, and G. Costa, “The electric vehicle and renewable energy: Changes in boundary conditions that enhance business model

- innovations,” *J. Clean. Prod.*, vol. 333, no. December 2021, p. 130034, 2022, doi: 10.1016/j.jclepro.2021.130034.
- [27] A. R. Bhatti and Z. Salam, “A rule-based energy management scheme for uninterrupted electric vehicles charging at constant price using photovoltaic-grid system,” *Renew. Energy*, vol. 125, no. January, pp. 384–400, Sep. 2018, doi: 10.1016/j.renene.2018.02.126.
- [28] D. D. Tran, M. Vafaeipour, M. El Baghdadi, R. Barrero, J. Van Mierlo, and O. Hegazy, “Thorough state-of-the-art analysis of electric and hybrid vehicle powertrains: Topologies and integrated energy management strategies,” *Renew. Sustain. Energy Rev.*, vol. 119, p. 109596, 2020, doi: 10.1016/j.rser.2019.109596.
- [29] C. Wang, R. Liu, and A. Tang, “Energy management strategy of hybrid energy storage system for electric vehicles based on genetic algorithm optimization and temperature effect,” *J. Energy Storage*, vol. 51, no. December 2021, p. 104314, Jul. 2022, doi: 10.1016/j.est.2022.104314.
- [30] S. Mirjalili, J. Song Dong, and A. Lewis, *Ant colony optimizer: Theory, literature review, and application in AUV path planning*, vol. 811. Springer International Publishing, 2020.
- [31] A. R. Bhatti *et al.*, “Optimized sizing of photovoltaic grid-connected electric vehicle charging system using particle swarm optimization,” *Int. J. Energy Res.*, vol. 43, no. 1, pp. 500–522, Jan. 2019, doi: 10.1002/er.4287.
- [32] X.-S. Yang and S. Deb, “Cuckoo Search via Levy Flights,” *2009 World Congr. Nat. Biol. Inspired Comput. NABIC 2009 - Proc.*, pp. 210–214, Mar. 2010, doi: 10.1109/NABIC.2009.5393690.
- [33] S. Mirjalili, “The Ant Lion Optimizer,” *Adv. Eng. Softw.*, vol. 83, pp. 80–98, May 2015, doi: 10.1016/j.advengsoft.2015.01.010.
- [34] S. P. Adam, S.-A. N. Alexandopoulos, P. M. Pardalos, and M. N. Vrahatis, “No Free Lunch Theorem: A Review,” in *Springer Optimization and Its Applications*, vol. 145, no. May, 2019, pp. 57–82.
- [35] L. Olatomiwa, S. Mekhilef, M. S. Ismail, and M. Moghavvemi, “Energy management strategies in hybrid renewable energy systems: A review,” *Renew. Sustain. Energy Rev.*, vol. 62, pp. 821–835, Sep. 2016, doi: 10.1016/j.rser.2016.05.040.
- [36] “Climatology Data,” *The Center for Solar Energy Research and Studies, Libya*.

<http://csers.ly/en/> (accessed Nov. 24, 2020).

- [37] “General Electricity Company of Libya (GECOL),” 2021. https://www.gecol.ly/gecol_en/ (accessed Mar. 24, 2021).
- [38] F. Mwasilu, J. J. Justo, E. K. Kim, T. D. Do, and J. W. Jung, “Electric vehicles and smart grid interaction: A review on vehicle to grid and renewable energy sources integration,” *Renew. Sustain. Energy Rev.*, vol. 34, pp. 501–516, 2014, doi: 10.1016/j.rser.2014.03.031.
- [39] R. Shi, S. Li, P. Zhang, and K. Y. Lee, “Integration of renewable energy sources and electric vehicles in V2G network with adjustable robust optimization,” *Renew. Energy*, vol. 153, pp. 1067–1080, Jun. 2020, doi: 10.1016/j.renene.2020.02.027.
- [40] T. M. Tawfik, M. A. Badr, E. Y. El-Kady, and O. E. Abdellatif, “Optimization and energy management of hybrid standalone energy system: a case study,” *Renew. Energy Focus*, vol. 25, no. 00, pp. 48–56, 2018, doi: 10.1016/j.ref.2018.03.004.
- [41] M. F. El-Naggar and A. A. A. Elgammal, “Multi-Objective Optimal Predictive Energy Management Control of Grid-Connected Residential Wind-PV-FC-Battery Powered Charging Station for Plug-in Electric Vehicle,” *J. Electr. Eng. Technol.*, vol. 13, no. 2, pp. 742–751, 2018, doi: 10.5370/JEET.2018.13.2.742.
- [42] J. F. Manwell, “Hybrid Energy Systems,” in *Encyclopedia of Energy*, vol. 3, First edition. | Boca Raton, FL : CRC Press, 2021. |: Elsevier, 2004, pp. 215–229.
- [43] S. M. Moghaddas-Tafreshi, S. Mohseni, M. E. Karami, and S. Kelly, “Optimal energy management of a grid-connected multiple energy carrier micro-grid,” *Appl. Therm. Eng.*, vol. 152, no. January, pp. 796–806, 2019, doi: 10.1016/j.applthermaleng.2019.02.113.
- [44] N. M. Isa, C. W. Tan, and A. H. M. Yatim, “A comprehensive review of cogeneration system in a microgrid: A perspective from architecture and operating system,” *Renew. Sustain. Energy Rev.*, vol. 81, no. February 2016, pp. 2236–2263, Jan. 2018, doi: 10.1016/j.rser.2017.06.034.
- [45] M. Gharibi and A. Askarzadeh, “Size and power exchange optimization of a grid-connected diesel generator-photovoltaic-fuel cell hybrid energy system considering reliability, cost and renewability,” *Int. J. Hydrogen Energy*, vol. 44, no. 47, pp. 25428–25441, Oct. 2019, doi: 10.1016/j.ijhydene.2019.08.007.

- [46] M. J. A. J. Hossain, H. R. Pota, M. J. A. J. Hossain, and F. Blaabjerg, “Evolution of microgrids with converter-interfaced generations: Challenges and opportunities,” *Int. J. Electr. Power Energy Syst.*, vol. 109, no. February, pp. 160–186, Jul. 2019, doi: 10.1016/j.ijepes.2019.01.038.
- [47] C. Ammari, D. Belatrache, B. Touhami, and S. Makhloifi, “Sizing, optimization, control and energy management of hybrid renewable energy system—A review,” *Energy Built Environ.*, no. December 2020, May 2021, doi: 10.1016/j.enbenv.2021.04.002.
- [48] S. Hussain, R. Alammari, A. Iqbal, and A. Shikfa, “Optimal sizing of a stand-alone hybrid PV-WT-BT system using artificial intelligence based technique,” in *2020 IEEE International Conference on Informatics, IoT, and Enabling Technologies (ICIoT)*, Feb. 2020, pp. 55–60, doi: 10.1109/ICIoT48696.2020.9089549.
- [49] W. L. Theo, J. S. Lim, W. S. Ho, H. Hashim, and C. T. Lee, “Review of distributed generation (DG) system planning and optimisation techniques: Comparison of numerical and mathematical modelling methods,” *Renew. Sustain. Energy Rev.*, vol. 67, pp. 531–573, Jan. 2017, doi: 10.1016/j.rser.2016.09.063.
- [50] K. Anoune, M. Bouya, A. Astito, and A. Ben Abdellah, “Sizing methods and optimization techniques for PV-wind based hybrid renewable energy system: A review,” *Renew. Sustain. Energy Rev.*, vol. 93, no. April, pp. 652–673, 2018, doi: 10.1016/j.rser.2018.05.032.
- [51] G. R. R. Chandra Mouli, P. Bauer, and M. Zeman, “System design for a solar powered electric vehicle charging station for workplaces,” *Appl. Energy*, vol. 168, no. 2016, pp. 434–443, Apr. 2016, doi: 10.1016/j.apenergy.2016.01.110.
- [52] H. S. V. S. K. Nunna, S. Battula, S. Doolla, and D. Srinivasan, “Energy Management in Smart Distribution Systems With Vehicle-to-Grid Integrated Microgrids,” *IEEE Trans. Smart Grid*, vol. 9, no. 5, pp. 4004–4016, Sep. 2018, doi: 10.1109/TSG.2016.2646779.
- [53] C. Mokhtara, B. Negrou, A. Bouferrouk, Y. Yao, N. Settou, and M. Ramadan, “Integrated supply–demand energy management for optimal design of off-grid hybrid renewable energy systems for residential electrification in arid climates,” *Energy Convers. Manag.*, vol. 221, no. April, p. 113192, Oct. 2020, doi: 10.1016/j.enconman.2020.113192.

- [54] Xin-She Yang, *Nature-Inspired Optimization Algorithms*, vol. 118. 2014.
- [55] S. Habib, M. M. Khan, J. Huawei, K. Hashmi, M. T. Faiz, and H. Tang, “A study of implemented international standards and infrastructural system for electric vehicles,” in *2018 IEEE International Conference on Industrial Technology (ICIT)*, Feb. 2018, vol. 120, pp. 1783–1788, doi: 10.1109/ICIT.2018.8352454.
- [56] Y. Huang *et al.*, “A review of power management strategies and component sizing methods for hybrid vehicles,” *Renew. Sustain. Energy Rev.*, vol. 96, no. August, pp. 132–144, 2018, doi: 10.1016/j.rser.2018.07.020.
- [57] V. S. B. Kurukuru, A. Haque, S. Padmanaban, and M. A. Khan, “Rule-Based Inferential System for Microgrid Energy Management System,” *IEEE Syst. J.*, pp. 1–10, 2021, doi: 10.1109/JSYST.2021.3094403.
- [58] I.-S. Sorlei *et al.*, “Fuel Cell Electric Vehicles—A Brief Review of Current Topologies and Energy Management Strategies,” *Energies*, vol. 14, no. 1, p. 252, Jan. 2021, doi: 10.3390/en14010252.
- [59] A. L. Bukar, C. W. Tan, L. K. Yiew, R. Ayop, and W.-S. Tan, “A rule-based energy management scheme for long-term optimal capacity planning of grid-independent microgrid optimized by multi-objective grasshopper optimization algorithm,” *Energy Convers. Manag.*, vol. 221, no. April, p. 113161, Oct. 2020, doi: 10.1016/j.enconman.2020.113161.
- [60] F. Zhang, L. Wang, S. Coskun, H. Pang, Y. Cui, and J. Xi, “Energy management strategies for hybrid electric vehicles: Review, classification, comparison, and outlook,” *Energies*, vol. 13, no. 13, 2020, doi: 10.3390/en13133352.
- [61] P. Zhang, F. Yan, and C. Du, “A comprehensive analysis of energy management strategies for hybrid electric vehicles based on bibliometrics,” *Renew. Sustain. Energy Rev.*, vol. 48, no. 205, pp. 88–104, Aug. 2015, doi: 10.1016/j.rser.2015.03.093.
- [62] H. Liu and T. Li, “Energy Management Strategy Development for Fuel Cell Hybrid Loaders,” *IOP Conf. Ser. Earth Environ. Sci.*, vol. 189, no. 5, p. 052015, Nov. 2018, doi: 10.1088/1755-1315/189/5/052015.
- [63] S. Ferahtia *et al.*, “Optimal Adaptive Gain LQR-Based Energy Management Strategy for Battery–Supercapacitor Hybrid Power System,” *Energies*, vol. 14, no. 6, p. 1660, Mar. 2021, doi: 10.3390/en14061660.
- [64] S. K. Dinkar and K. Deep, “Opposition based Laplacian Ant Lion Optimizer,”

- J. Comput. Sci.*, vol. 23, pp. 71–90, 2017, doi: 10.1016/j.jocs.2017.10.007.
- [65] A. L. Bukar and C. W. Tan, “A review on stand-alone photovoltaic-wind energy system with fuel cell: System optimization and energy management strategy,” *J. Clean. Prod.*, vol. 221, pp. 73–88, Jun. 2019, doi: 10.1016/j.jclepro.2019.02.228.
- [66] B. Yang *et al.*, “Comprehensive overview of meta-heuristic algorithm applications on PV cell parameter identification,” *Energy Convers. Manag.*, vol. 208, no. January, p. 112595, Mar. 2020, doi: 10.1016/j.enconman.2020.112595.
- [67] M. D. A. Al-falahi, S. D. G. Jayasinghe, and H. Enshaei, “A review on recent size optimization methodologies for standalone solar and wind hybrid renewable energy system,” *Energy Convers. Manag.*, vol. 143, pp. 252–274, 2017, doi: 10.1016/j.enconman.2017.04.019.
- [68] M. Shehab, A. T. Khader, and M. A. Al-Betar, “A survey on applications and variants of the cuckoo search algorithm,” *Appl. Soft Comput.*, vol. 61, no. March, pp. 1041–1059, Dec. 2017, doi: 10.1016/j.asoc.2017.02.034.
- [69] M. Bilal, I. Alsaidan, M. Alaraj, F. M. Almasoudi, and M. Rizwan, “Techno-Economic and Environmental Analysis of Grid-Connected Electric Vehicle Charging Station Using AI-Based Algorithm,” *Mathematics*, vol. 10, no. 6, p. 924, Mar. 2022, doi: 10.3390/math10060924.
- [70] P. Tozzi and J. H. Jo, “A comparative analysis of renewable energy simulation tools: Performance simulation model vs. system optimization,” *Renew. Sustain. Energy Rev.*, vol. 80, no. February, pp. 390–398, 2017, doi: 10.1016/j.rser.2017.05.153.
- [71] F. S. Mahmoud *et al.*, “Optimal sizing of smart hybrid renewable energy system using different optimization algorithms,” *Energy Reports*, vol. 8, pp. 4935–4956, 2022, doi: 10.1016/j.egyr.2022.03.197.
- [72] E. S. Ali, S. M. Abd Elazim, and A. Y. Abdelaziz, “Ant Lion Optimization Algorithm for Renewable Distributed Generations,” *Energy*, vol. 116, pp. 445–458, Dec. 2016, doi: 10.1016/j.energy.2016.09.104.
- [73] S. Kumar and A. Kumar, “A brief review on antlion optimization algorithm,” in *2018 International Conference on Advances in Computing, Communication Control and Networking (ICACCCN)*, Oct. 2018, pp. 236–240, doi: 10.1109/ICACCCN.2018.8748862.

- [74] L. Abualigah, M. Shehab, M. Alshinwan, S. Mirjalili, and M. A. Elaziz, “Ant Lion Optimizer: A Comprehensive Survey of Its Variants and Applications,” *Arch. Comput. Methods Eng.*, vol. 28, no. 3, pp. 1397–1416, May 2021, doi: 10.1007/s11831-020-09420-6.
- [75] E. Emary, H. M. Zawbaa, · Hossam, and M. Zawbaa, “Feature selection via Lèvy Antlion optimization,” *Pattern Anal. Appl.*, vol. 22, no. 3, pp. 857–876, 2019, doi: 10.1007/s10044-018-0695-2.
- [76] M. W. Guo, J. S. Wang, L. F. Zhu, S. S. Guo, and W. Xie, “Improved Ant Lion Optimizer Based on Spiral Complex Path Searching Patterns,” *IEEE Access*, vol. 8, pp. 22094–22126, 2020, doi: 10.1109/ACCESS.2020.2968943.
- [77] Z. Li, Y. Cao, L. Van Dai, X. Yang, and T. T. Nguyen, “Finding Solutions for Optimal Reactive Power Dispatch Problem by a Novel Improved Antlion Optimization Algorithm,” *Energies*, vol. 12, no. 15, p. 2968, Aug. 2019, doi: 10.3390/en12152968.
- [78] T. Tian, C. Liu, Q. Guo, Y. Yuan, W. Li, and Q. Yan, “An Improved Ant Lion Optimization Algorithm and Its Application in Hydraulic Turbine Governing System Parameter Identification,” *Energies*, vol. 11, no. 1, p. 95, Jan. 2018, doi: 10.3390/en11010095.
- [79] C. Chen and L. Yu, “A hybrid ant lion optimizer with improved Nelder–Mead algorithm for structural damage detection by improving weighted trace lasso regularization,” *Adv. Struct. Eng.*, vol. 23, no. 3, pp. 468–484, Feb. 2020, doi: 10.1177/1369433219872434.
- [80] K. Zhang, J. Ma, X. Zhao, X. Liu, and Y. Zhang, “Parameter Identification and State of Charge Estimation of NMC Cells Based on Improved Ant Lion Optimizer,” *Math. Probl. Eng.*, vol. 2019, no. 12, pp. 1–18, Jul. 2019, doi: 10.1155/2019/4961045.
- [81] R. Manuel and G. Emayavaramban, “PALONN: Parallel Ant Lion Optimizer and Artificial Neural Network for Power Flow Control of the Micro Grid-Connected System,” *IETE J. Res.*, vol. 0, no. 0, pp. 1–18, 2019, doi: 10.1080/03772063.2019.1644208.
- [82] S. Mouassa, T. Bouktir, and A. Salhi, “Ant lion optimizer for solving optimal reactive power dispatch problem in power systems,” *Eng. Sci. Technol. an Int. J.*, vol. 20, no. 3, pp. 885–895, 2017, doi: 10.1016/j.jestch.2017.03.006.
- [83] H. Hu, Y. Li, Y. Bai, J. Zhang, and M. Liu, “The Improved Antlion Optimizer

- and Artificial Neural Network for Chinese Influenza Prediction," *Complexity*, vol. 2019, pp. 1–12, Aug. 2019, doi: 10.1155/2019/1480392.
- [84] H. Kılıç and U. Yüzgeç, "Tournament selection based antlion optimization algorithm for solving quadratic assignment problem," *Eng. Sci. Technol. an Int. J.*, vol. 22, no. 2, pp. 673–691, Apr. 2019, doi: 10.1016/j.jestch.2018.11.013.
- [85] M. TOZ, "An improved form of the ant lion optimization algorithm for image clustering problems," *TURKISH J. Electr. Eng. Comput. Sci.*, vol. 27, no. 2, pp. 1445–1460, Mar. 2019, doi: 10.3906/elk-1703-240.
- [86] S. K. Dinkar and K. Deep, "Accelerated Opposition-Based Antlion Optimizer with Application to Order Reduction of Linear Time-Invariant Systems," *Arab. J. Sci. Eng.*, vol. 44, no. 3, pp. 2213–2241, 2019, doi: 10.1007/s13369-018-3370-4.
- [87] S. K. Dinkar and K. Deep, "Opposition-based antlion optimizer using Cauchy distribution and its application to data clustering problem," *Neural Comput. Appl.*, vol. 32, no. 11, pp. 6967–6995, 2020, doi: 10.1007/s00521-019-04174-0.
- [88] S. K. Dinkar and K. Deep, "An efficient opposition based Lévy flight antlion optimizer for optimization problems," *J Comput Sci*, vol. 29, pp. 119–141, Nov. 2018, doi: 10.1016/j.jocs.2018.10.002.
- [89] K. R. Subhashini and J. K. Satapathy, "Development of an Enhanced Ant Lion Optimization Algorithm and its Application in Antenna Array Synthesis," *Appl. Soft Comput. J.*, vol. 59, pp. 153–173, 2017, doi: 10.1016/j.asoc.2017.05.007.
- [90] A. Rajan, K. Jeevan, and T. Malakar, "Weighted elitism based Ant Lion Optimizer to solve optimum VAr planning problem," *Appl. Soft Comput. J.*, vol. 55, pp. 352–370, 2017, doi: 10.1016/j.asoc.2017.02.010.
- [91] H. Kılıç and U. Yüzgeç, "Improved antlion optimization algorithm via tournament selection and its application to parallel machine scheduling," *Comput. Ind. Eng.*, vol. 132, no. June 2018, pp. 166–186, Jun. 2019, doi: 10.1016/j.cie.2019.04.029.
- [92] P. Hu *et al.*, *ALO-DM: A smart approach based on ant lion optimizer with differential mutation operator in big data analytics*, vol. 10829 LNCS. Springer International Publishing, 2018.
- [93] R. Eberhart and James Kennedy, "A New Optimizer Using Particle Swarm Theory," *Sixth Int. Symp. Micro Mach. Hum. Sci.*, vol. 0-7803–267, pp. 39–43,

- 1995, doi: 10.1.1.470.3577.
- [94] D. Wang, D. Tan, and L. Liu, “Particle swarm optimization algorithm: an overview,” *Soft Comput.*, vol. 22, no. 2, pp. 387–408, Jan. 2018, doi: 10.1007/s00500-016-2474-6.
 - [95] J. Lian, Y. Zhang, C. Ma, Y. Yang, and E. Chaima, “A review on recent sizing methodologies of hybrid renewable energy systems,” *Energy Conversion and Management*, vol. 199. Elsevier Ltd, p. 112027, Nov. 01, 2019, doi: 10.1016/j.enconman.2019.112027.
 - [96] Eberhart and Yuhui Shi, “Particle swarm optimization: developments, applications and resources,” in *Proceedings of the 2001 Congress on Evolutionary Computation (IEEE Cat. No.01TH8546)*, 2001, vol. 1, pp. 81–86, doi: 10.1109/CEC.2001.934374.
 - [97] X. S. Yang and S. Deb, “Engineering optimisation by cuckoo search,” *Int. J. Math. Model. Numer. Optim.*, vol. 1, no. 4, p. 330, 2010, doi: 10.1504/IJMMNO.2010.035430.
 - [98] A. S. Joshi, O. Kulkarni, G. M. Kakandikar, and V. M. Nandedkar, “Cuckoo Search Optimization- A Review,” *Mater. Today Proc.*, vol. 4, no. 8, pp. 7262–7269, 2017, doi: 10.1016/j.matpr.2017.07.055.
 - [99] M. Mareli and B. Twala, “An adaptive Cuckoo search algorithm for optimisation,” *Appl. Comput. Informatics*, vol. 14, no. 2, pp. 107–115, 2018, doi: 10.1016/j.aci.2017.09.001.
 - [100] S. Sanajaoba and E. Fernandez, “Maiden application of Cuckoo Search algorithm for optimal sizing of a remote hybrid renewable energy System,” *Renew. Energy*, vol. 96, pp. 1–10, 2016, doi: 10.1016/j.renene.2016.04.069.
 - [101] A. H. Gandomi, X.-S. Yang, and A. H. Alavi, “Cuckoo search algorithm: a metaheuristic approach to solve structural optimization problems,” *Eng. Comput.*, vol. 29, no. 1, pp. 17–35, Jan. 2013, doi: 10.1007/s00366-011-0241-y.
 - [102] I. Fister, X. S. Yang, D. Fister, and I. Fister, “Cuckoo Search: A Brief Literature Review,” *Stud. Comput. Intell.*, vol. 516, pp. 49–62, Aug. 2014, doi: 10.1007/978-3-319-02141-6_3.
 - [103] G. Wang, “A Comparative Study of Cuckoo Algorithm and Ant Colony Algorithm in Optimal Path Problems,” *MATEC Web Conf.*, vol. 232, p. 03003, Nov. 2018, doi: 10.1051/matecconf/201823203003.

- [104] X.-S. Yang and S. Deb, “Cuckoo search: recent advances and applications,” *Neural Comput. Appl.*, vol. 24, no. 1, pp. 169–174, Jan. 2014, doi: 10.1007/s00521-013-1367-1.
- [105] T. Lehtola and A. Zahedi, “Solar energy and wind power supply supported by storage technology: A review,” *Sustain. Energy Technol. Assessments*, vol. 35, no. February, pp. 25–31, Oct. 2019, doi: 10.1016/j.seta.2019.05.013.
- [106] M. Aslani, A. Imanloozadeh, H. Hashemi-Dezaki, M. A. Hejazi, M. Nazififard, and A. Ketabi, “Optimal probabilistic reliability-oriented planning of islanded microgrids considering hydrogen-based storage systems, hydrogen vehicles, and electric vehicles under various climatic conditions,” *J. Power Sources*, vol. 525, no. December 2021, p. 231100, 2022, doi: 10.1016/j.jpowsour.2022.231100.
- [107] M. Nizam and F. X. R. Wicaksono, “Design and Optimization of Solar, Wind, and Distributed Energy Resource (DER) Hybrid Power Plant for Electric Vehicle (EV) Charging Station in Rural Area,” in *2018 5th International Conference on Electric Vehicular Technology (ICEVT)*, Oct. 2018, no. 1, pp. 41–45, doi: 10.1109/ICEVT.2018.8628341.
- [108] F. A. Khan, N. Pal, and S. H. Saeed, “Review of solar photovoltaic and wind hybrid energy systems for sizing strategies optimization techniques and cost analysis methodologies,” *Renew. Sustain. Energy Rev.*, vol. 92, pp. 937–947, Sep. 2018, doi: 10.1016/j.rser.2018.04.107.
- [109] M. Heidari, “Design the optimal number of components in a grid-connected hybrid power generation system,” *Int. J. Renew. Energy Res.*, vol. 8, no. 1, pp. 357–364, 2018.
- [110] R. Ayop, N. M. Isa, and C. W. Tan, “Components sizing of photovoltaic stand-alone system based on loss of power supply probability,” *Renew. Sustain. Energy Rev.*, vol. 81, no. May 2016, pp. 2731–2743, Jan. 2018, doi: 10.1016/j.rser.2017.06.079.
- [111] A. Hiendro, I. Yusuf, F. Trias Pontia Wigyarianto, K. H. Khwee, and Junaidi, “Optimum renewable fraction for grid-connected photovoltaic in office building energy systems in Indonesia,” *Int. J. Power Electron. Drive Syst.*, vol. 9, no. 4, pp. 1866–1874, 2018, doi: 10.11591/ijpeds.v9n4.pp1866-1874.
- [112] A. Bouaouda and Y. Sayouti, “Hybrid Meta-Heuristic Algorithms for Optimal Sizing of Hybrid Renewable Energy System: A Review of the State-of-the-Art,”

- Arch. Comput. Methods Eng.*, vol. 29, no. 6, pp. 4049–4083, Oct. 2022, doi: 10.1007/s11831-022-09730-x.
- [113] M. A. M. Ramli, H. R. E. H. Bouchekara, and A. S. Alghamdi, “Optimal sizing of PV/wind/diesel hybrid microgrid system using multi-objective self-adaptive differential evolution algorithm,” *Renew. Energy*, vol. 121, pp. 400–411, Jun. 2018, doi: 10.1016/j.renene.2018.01.058.
 - [114] S. Mahdi, H. Baygi, and J. Farzaneh, “Application of Artificial intelligence techniques for optimum design of hybrid grid-independent PV / WT / battery power system,” *Int. J. Ind. Electron. Control Optim.*, vol. 3, no. 3, pp. 275–289, 2020.
 - [115] A. Eid, M. Ibrahim, and S. Kamel, “Optimal Planning of Microgrids Including Charging Stations and Renewable Energy Sources,” in *2021 22nd International Middle East Power Systems Conference (MEPCON)*, Dec. 2021, pp. 503–508, doi: 10.1109/MEPCON50283.2021.9686196.
 - [116] B. Bibak and H. Tekiner-Moğulkoc, “A comprehensive analysis of Vehicle to Grid (V2G) systems and scholarly literature on the application of such systems,” *Renew. Energy Focus*, vol. 36, no. March, pp. 1–20, Mar. 2021, doi: 10.1016/j.ref.2020.10.001.
 - [117] W. Kempton and S. E. Letendre, “Electric vehicles as a new power source for electric utilities,” *Transp. Res. Part D Transp. Environ.*, vol. 2, no. 3, pp. 157–175, Sep. 1997, doi: 10.1016/S1361-9209(97)00001-1.
 - [118] S. Goel, R. Sharma, and A. K. Rathore, “A review on barrier and challenges of electric vehicle in India and vehicle to grid optimisation,” *Transp. Eng.*, vol. 4, no. August 2020, p. 100057, Jun. 2021, doi: 10.1016/j.treng.2021.100057.
 - [119] M. R. Khalid, I. A. Khan, S. Hameed, M. S. J. Asghar, and J.-S. Ro, “A Comprehensive Review on Structural Topologies, Power Levels, Energy Storage Systems, and Standards for Electric Vehicle Charging Stations and Their Impacts on Grid,” *IEEE Access*, vol. 9, pp. 128069–128094, 2021, doi: 10.1109/ACCESS.2021.3112189.
 - [120] K. M. Tan, V. K. Ramachandaramurthy, and J. Y. Yong, “Integration of electric vehicles in smart grid: A review on vehicle to grid technologies and optimization techniques,” *Renew. Sustain. Energy Rev.*, vol. 53, pp. 720–732, Jan. 2016, doi: 10.1016/j.rser.2015.09.012.
 - [121] M. İnci, M. M. Savrun, and Ö. Çelik, “Integrating electric vehicles as virtual

- power plants: A comprehensive review on vehicle-to-grid (V2G) concepts, interface topologies, marketing and future prospects,” *J. Energy Storage*, vol. 55, no. September, p. 105579, Nov. 2022, doi: 10.1016/j.est.2022.105579.
- [122] X. Sun, Z. Li, X. Wang, and C. Li, “Technology Development of Electric Vehicles: A Review,” *Energies*, vol. 13, no. 1, p. 90, Dec. 2019, doi: 10.3390/en13010090.
- [123] Vadi, Bayindir, Colak, and Hossain, “A Review on Communication Standards and Charging Topologies of V2G and V2H Operation Strategies,” *Energies*, vol. 12, no. 19, p. 3748, Sep. 2019, doi: 10.3390/en12193748.
- [124] J. A. Sanguesa, V. Torres-Sanz, P. Garrido, F. J. Martinez, and J. M. Marquez-Barja, “A Review on Electric Vehicles: Technologies and Challenges,” *Smart Cities*, vol. 4, no. 1, pp. 372–404, Mar. 2021, doi: 10.3390/smartcities4010022.
- [125] L. G. González, E. Siavichay, and J. L. Espinoza, “Impact of EV fast charging stations on the power distribution network of a Latin American intermediate city,” *Renew. Sustain. Energy Rev.*, vol. 107, no. March, pp. 309–318, 2019, doi: 10.1016/j.rser.2019.03.017.
- [126] S. Khan *et al.*, “Energy Management Scheme for an EV Smart Charger V2G/G2V Application with an EV Power Allocation Technique and Voltage Regulation,” *Appl. Sci.*, vol. 8, no. 4, p. 648, Apr. 2018, doi: 10.3390/app8040648.
- [127] S. Singh, P. Chauhan, and N. Jap Singh, “Feasibility of Grid-connected Solar-wind Hybrid System with Electric Vehicle Charging Station,” *J. Mod. Power Syst. Clean Energy*, vol. 9, no. 2, pp. 295–306, 2021, doi: 10.35833/MPCE.2019.000081.
- [128] A. Tavakoli, S. Saha, M. T. Arif, M. E. Haque, N. Mendis, and A. M. T. Oo, “Impacts of grid integration of solar PV and electric vehicle on grid stability, power quality and energy economics: a review,” *IET Energy Syst. Integr.*, vol. 2, no. 3, pp. 243–260, Sep. 2020, doi: 10.1049/iet-esi.2019.0047.
- [129] N. M. Kumar, S. S. Chopra, A. A. Chand, R. M. Elavarasan, and G. M. Shafiullah, “Hybrid Renewable Energy Microgrid for a Residential Community: A Techno-Economic and Environmental Perspective in the Context of the SDG7,” *Sustainability*, vol. 12, no. 10, p. 3944, May 2020, doi: 10.3390/su12103944.
- [130] C. Liu, K. T. Chau, D. Wu, and S. Gao, “Opportunities and Challenges of

Vehicle-to-Home, Vehicle-to-Vehicle, and Vehicle-to-Grid Technologies,” *Proc. IEEE*, vol. 101, no. 11, pp. 2409–2427, Nov. 2013, doi: 10.1109/JPROC.2013.2271951.

- [131] A. W. Thompson and Y. Perez, “Vehicle-to-Everything (V2X) energy services, value streams, and regulatory policy implications,” *Energy Policy*, vol. 137, no. December 2019, p. 111136, Feb. 2020, doi: 10.1016/j.enpol.2019.111136.
- [132] U. Datta, N. Saiprasad, A. Kalam, J. Shi, and A. Zayegh, “A price-regulated electric vehicle charge-discharge strategy for G2V, V2H, and V2G,” *Int. J. Energy Res.*, vol. 43, no. 2, pp. 1032–1042, Feb. 2019, doi: 10.1002/er.4330.
- [133] C. S. Ioakimidis, D. Thomas, P. Rycerski, and K. N. Genikomsakis, “Peak shaving and valley filling of power consumption profile in non-residential buildings using an electric vehicle parking lot,” *Energy*, vol. 148, pp. 148–158, Apr. 2018, doi: 10.1016/j.energy.2018.01.128.
- [134] H. Fathabadi, “Novel grid-connected solar/wind powered electric vehicle charging station with vehicle-to-grid technology,” *Energy*, vol. 132, pp. 1–11, Aug. 2017, doi: 10.1016/j.energy.2017.04.161.
- [135] B. Naghibi, M. A. S. Masoum, and S. Deilami, “Effects of V2H Integration on Optimal Sizing of Renewable Resources in Smart Home Based on Monte Carlo Simulations,” *IEEE Power Energy Technol. Syst. J.*, vol. 5, no. 3, pp. 73–84, Sep. 2018, doi: 10.1109/JPETS.2018.2854709.
- [136] M. S. Whittingham, “Electrical Energy Storage and Intercalation Chemistry,” *Science (80-.).*, vol. 192, no. 4244, pp. 1126–1127, Jun. 1976, doi: 10.1126/science.192.4244.1126.
- [137] M. A. Hannan, M. S. H. Lipu, A. Hussain, and A. Mohamed, “A review of lithium-ion battery state of charge estimation and management system in electric vehicle applications: Challenges and recommendations,” *Renew. Sustain. Energy Rev.*, vol. 78, no. May, pp. 834–854, Oct. 2017, doi: 10.1016/j.rser.2017.05.001.
- [138] P. R. C. Mendes, L. V. Isorna, C. Bordons, and J. E. Normey-Rico, “Energy management of an experimental microgrid coupled to a V2G system,” *J. Power Sources*, vol. 327, pp. 702–713, Sep. 2016, doi: 10.1016/j.jpowsour.2016.07.076.
- [139] C. Li, L. Zhang, Z. Ou, Q. Wang, D. Zhou, and J. Ma, “Robust model of electric vehicle charging station location considering renewable energy and storage

- equipment,” *Energy*, vol. 238, p. 121713, Jan. 2022, doi: 10.1016/j.energy.2021.121713.
- [140] RELiON Batteries, “Rechargeable Deep Cycle Lithium Batteries Rb75 12.8,” 2020. <https://reliionbattery.com/products/lithium/application/electric-vehicles>, 2020.
- [141] Y. Miao, P. Hynan, A. von Jouanne, and A. Yokochi, “Current Li-Ion Battery Technologies in Electric Vehicles and Opportunities for Advancements,” *Energies*, vol. 12, no. 6, p. 1074, Mar. 2019, doi: 10.3390/en12061074.
- [142] A. Mohammad, R. Zamora, and T. T. Lie, “Integration of Electric Vehicles in the Distribution Network: A Review of PV Based Electric Vehicle Modelling,” *Energies*, vol. 13, no. 17, p. 4541, Sep. 2020, doi: 10.3390/en13174541.
- [143] B. Bibak and H. Tekiner-Mogulkoc, “Influences of vehicle to grid (V2G) on power grid: An analysis by considering associated stochastic parameters explicitly,” *Sustain. Energy, Grids Networks*, vol. 26, p. 100429, 2021, doi: 10.1016/j.segan.2020.100429.
- [144] J. Y. Yong, V. K. Ramachandaramurthy, K. M. Tan, and N. Mithulananthan, “A review on the state-of-the-art technologies of electric vehicle, its impacts and prospects,” *Renew. Sustain. Energy Rev.*, vol. 49, pp. 365–385, Sep. 2015, doi: 10.1016/j.rser.2015.04.130.
- [145] M. Nour, J. P. Chaves-Ávila, G. Magdy, and Á. Sánchez-Miralles, “Review of Positive and Negative Impacts of Electric Vehicles Charging on Electric Power Systems,” *Energies*, vol. 13, no. 18, p. 4675, Sep. 2020, doi: 10.3390/en13184675.
- [146] H. Shareef, M. M. Islam, and A. Mohamed, “A review of the stage-of-the-art charging technologies, placement methodologies, and impacts of electric vehicles,” *Renew. Sustain. Energy Rev.*, vol. 64, no. October, pp. 403–420, Oct. 2016, doi: 10.1016/j.rser.2016.06.033.
- [147] S. M. Shariff *et al.*, “A state-of-the-art review on the impact of fast EV charging on the utility sector,” *Energy Storage*, vol. 4, no. 4, pp. 1–21, 2022, doi: 10.1002/est.2.300.
- [148] M. T. Hussain, D. N. Bin Sulaiman, M. S. Hussain, and M. Jabir, “Optimal Management strategies to solve issues of grid having Electric Vehicles (EV): A review,” *J. Energy Storage*, vol. 33, no. November 2020, p. 102114, Jan. 2021, doi: 10.1016/j.est.2020.102114.

- [149] D. B. Richardson, “Electric vehicles and the electric grid: A review of modeling approaches, Impacts, and renewable energy integration,” *Renewable and Sustainable Energy Reviews*, vol. 19, pp. 247–254, Mar. 2013, doi: 10.1016/j.rser.2012.11.042.
- [150] M. A. Masrur *et al.*, “Military-Based Vehicle-to-Grid and Vehicle-to-Vehicle Microgrid—System Architecture and Implementation,” *IEEE Trans. Transp. Electrif.*, vol. 4, no. 1, pp. 157–171, Mar. 2018, doi: 10.1109/TTE.2017.2779268.
- [151] Z. A. Arfeen, M. P. Abdullah, U. U. Sheikh, A. Hamza Sule, H. T. Alqaraghuli, and R. Kolawole Soremekun, “Rule-Based Enhanced Energy Management Scheme for Electric Vehicles Fast-Charging Workplace Using Battery Stacks and Solar Power,” in *2020 IEEE International Conference on Power and Energy (PECon)*, Dec. 2020, no. December, pp. 113–118, doi: 10.1109/PECon48942.2020.9314614.
- [152] J. Van Roy, N. Leemput, F. Geth, R. Salenbien, J. Buscher, and J. Driesen, “Apartment Building Electricity System Impact of Operational Electric Vehicle Charging Strategies,” *IEEE Trans. Sustain. Energy*, vol. 5, no. 1, pp. 264–272, Jan. 2014, doi: 10.1109/TSTE.2013.2281463.
- [153] R. Atia and N. Yamada, “Sizing and Analysis of Renewable Energy and Battery Systems in Residential Microgrids,” *IEEE Trans. Smart Grid*, vol. 7, no. 3, pp. 1204–1213, May 2016, doi: 10.1109/TSG.2016.2519541.
- [154] H. Turker, “Optimal Charging of Plug-in Electric Vehicle (PEV) in Residential Area,” in *2018 IEEE Transportation Electrification Conference and Expo (ITEC)*, Jun. 2018, no. 5, pp. 243–247, doi: 10.1109/ITEC.2018.8450125.
- [155] B. Santoso and W. Wahyu Purwanto, “Analysis on Business Development and Pricing for Electric Vehicle Charging in Indonesia,” in *2021 3rd International Conference on E-Business and E-commerce Engineering*, Dec. 2021, no. 55, pp. 102–107, doi: 10.1145/3510249.3510269.
- [156] G. Chiandussi, M. Codegone, S. Ferrero, and F. E. Varesio, *Comparison of multi-objective optimization methodologies for engineering applications*, vol. 63, no. 5. Elsevier Ltd, 2012.
- [157] A. Yahiaoui, K. Benmansour, and M. Tadjine, “Control, analysis and optimization of hybrid PV-Diesel-Battery systems for isolated rural city in Algeria,” *Sol. Energy*, vol. 137, pp. 1–10, 2016, doi:

- 10.1016/j.solener.2016.07.050.
- [158] A. L. Bukar, C. W. Tan, and K. Y. Lau, “Optimal sizing of an autonomous photovoltaic/wind/battery/diesel generator microgrid using grasshopper optimization algorithm,” *Sol. Energy*, vol. 188, no. May, pp. 685–696, Aug. 2019, doi: 10.1016/j.solener.2019.06.050.
 - [159] A. Mahesh and K. S. Sandhu, “Optimal Sizing of a Grid-Connected PV/Wind/Battery System Using Particle Swarm Optimization,” *Iran. J. Sci. Technol. - Trans. Electr. Eng.*, vol. 43, no. 1, pp. 107–121, Mar. 2019, doi: 10.1007/s40998-018-0083-3.
 - [160] A. Chakir *et al.*, “Optimal energy management for a grid connected PV-battery system,” *Energy Reports*, vol. 6, no. September 2019, pp. 218–231, Feb. 2020, doi: 10.1016/j.egyr.2019.10.040.
 - [161] O. Ekren, C. Hakan Canbaz, and Ç. B. Güvel, “Sizing of a solar-wind hybrid electric vehicle charging station by using HOMER software,” *J. Clean. Prod.*, vol. 279, p. 123615, 2021, doi: 10.1016/j.jclepro.2020.123615.
 - [162] H. Al-Najjar, H. J. El-Khozondar, C. Pfeifer, and R. Al Afif, “Hybrid grid-tie electrification analysis of bio-shared renewable energy systems for domestic application,” *Sustain. Cities Soc.*, vol. 77, p. 103538, Feb. 2022, doi: 10.1016/j.scs.2021.103538.
 - [163] C. Li, Y. Shan, L. Zhang, L. Zhang, and R. Fu, “Techno-economic evaluation of electric vehicle charging stations based on hybrid renewable energy in China,” *Energy Strateg. Rev.*, vol. 41, no. November 2021, p. 100850, 2022, doi: 10.1016/j.esr.2022.100850.
 - [164] X. Wu, X. Hu, X. Yin, and S. J. Moura, “Stochastic Optimal Energy Management of Smart Home With PEV Energy Storage,” *IEEE Trans. Smart Grid*, vol. 9, no. 3, pp. 2065–2075, May 2018, doi: 10.1109/TSG.2016.2606442.
 - [165] A. O. M. Maka, S. Salem, and M. Mehmood, “Solar photovoltaic (PV) applications in Libya: Challenges, potential, opportunities and future perspectives,” *Clean. Eng. Technol.*, vol. 5, p. 100267, 2021, doi: 10.1016/j.clet.2021.100267.
 - [166] S. A. S. & A. S. KHALIL I. AL-SAMARRAI, “Policies of Conventional and Non-Conventional Energy for Sustainability in Libya,” *Int. J. Gen. Eng. Technol.*, vol. 6, no. 6, pp. 1–12, 2017, [Online]. Available:

http://iaset.us/view_archives.php?year=2017&id=74&jtype=2&page=2.

- [167] O. A. Mohamed and S. H. Masood, “A brief overview of solar and wind energy in Libya: Current trends and the future development,” *IOP Conf. Ser. Mater. Sci. Eng.*, vol. 377, no. 1, p. 012136, Jun. 2018, doi: 10.1088/1757-899X/377/1/012136.
- [168] Walid Alsuessi, “General Electric Company of Libya (GECOL),” *Eur. Int. J. Sci. Technol.*, vol. 4, no. 1, pp. 61–69, 2015, [Online]. Available: www.eijst.org.uk.
- [169] WDI, “World Bank indicator,” 2019. <https://data.worldbank.org/products/wdi> (accessed Sep. 05, 2019).
- [170] M. M. Islam and M. Hasanuzzaman, “Introduction to energy and sustainable development,” in *Energy for Sustainable Development*, Elsevier, 2020, pp. 1–18.
- [171] SolarGis, “Solar resource maps of Libya,” © 2019 Solargis. All rights reserved, 2019. <https://solargis.com/maps-and-gis-data/download/libya>.
- [172] Y. Kassem, H. Çamur, and R. A. F. Aateg, “Exploring Solar and Wind Energy as a Power Generation Source for Solving the Electricity Crisis in Libya,” *Energies*, vol. 13, no. 14, p. 3708, Jul. 2020, doi: 10.3390/en13143708.
- [173] C. Gamarra and J. M. Guerrero, “Computational optimization techniques applied to microgrids planning: A review,” *Renew. Sustain. Energy Rev.*, vol. 48, pp. 413–424, 2015, doi: 10.1016/j.rser.2015.04.025.
- [174] A. Al Wahedi and Y. Bicer, “Development of an off-grid electrical vehicle charging station hybridized with renewables including battery cooling system and multiple energy storage units,” *Energy Reports*, vol. 6, no. 2020, pp. 2006–2021, 2020, doi: 10.1016/j.egyr.2020.07.022.
- [175] Multicrystal, “Kyocera KD325GX-LFB (325W) Solar Panel,” *SolarDesignTool*, 2020. <http://www.solardesigntool.com/components/module-panel-solar/Kyocera/2788/KD325GX-LFB/specification-data-sheet.html> (accessed Sep. 19, 2020).
- [176] W. Turbine and L. B. & S. Matysik, “Eocycle EO20,” *wind-turbine-models.com*, 2021. <https://en.wind-turbine-models.com/turbines/1640-eocycle-eo20> (accessed Jan. 26, 2021).
- [177] S. Mohseni and A. C. Brent, “Economic viability assessment of sustainable hydrogen production, storage, and utilisation technologies integrated into on-

- and off-grid micro-grids: A performance comparison of different metaheuristics," *Int. J. Hydrogen Energy*, vol. 45, no. 59, pp. 34412–34436, Dec. 2020, doi: 10.1016/j.ijhydene.2019.11.079.
- [178] G. T. Udeh, S. Michailos, D. Ingham, K. J. Hughes, L. Ma, and M. Pourkashanian, "A modified rule-based energy management scheme for optimal operation of a hybrid PV-wind-Stirling engine integrated multi-carrier energy system," *Appl. Energy*, vol. 312, no. September 2021, p. 118763, 2022, doi: 10.1016/j.apenergy.2022.118763.
- [179] S. Singh, M. Singh, and S. C. Kaushik, "Feasibility study of an islanded microgrid in rural area consisting of PV, wind, biomass and battery energy storage system," *Energy Convers. Manag.*, vol. 128, pp. 178–190, 2016, doi: 10.1016/j.enconman.2016.09.046.
- [180] X. Zheng and Y. Yao, "Multi-objective capacity allocation optimization method of photovoltaic EV charging station considering V2G," *J. Cent. South Univ.*, vol. 28, no. 2, pp. 481–493, Feb. 2021, doi: 10.1007/s11771-021-4616-y.
- [181] A. Elbaz and M. T. Guneser, "Multi-Objective Optimization Method for Proper Configuration of Grid-Connected PV-Wind Hybrid System in Terms of Ecological Effects, Outlay, and Reliability," *J. Electr. Eng. Technol.*, vol. 16, no. 2, pp. 771–782, Mar. 2021, doi: 10.1007/s42835-020-00635-y.
- [182] J. Bandopadhyay and P. K. Roy, "Application of hybrid multi-objective moth flame optimization technique for optimal performance of hybrid micro-grid system," *Appl. Soft Comput.*, vol. 95, p. 106487, Oct. 2020, doi: 10.1016/j.asoc.2020.106487.
- [183] C. Iclodean, B. Varga, N. Burnete, D. Cimerdean, and B. Jurchiș, "Comparison of Different Battery Types for Electric Vehicles," *IOP Conf. Ser. Mater. Sci. Eng.*, vol. 252, no. 1, p. 012058, Oct. 2017, doi: 10.1088/1757-899X/252/1/012058.
- [184] S. Mohseni, A. C. Brent, and D. Burmester, "A comparison of metaheuristics for the optimal capacity planning of an isolated, battery-less, hydrogen-based micro-grid," *Appl. Energy*, vol. 259, p. 114224, Feb. 2020, doi: 10.1016/j.apenergy.2019.114224.
- [185] M. M. Rahman, E. A. Al-Ammar, H. S. Das, and W. Ko, "Optimal Design of Grid Connected PV Battery System for Probabilistic EVCS Load," in *2020 Advances in Science and Engineering Technology International Conferences*

- (ASET), Feb. 2020, no. June, pp. 1–6, doi: 10.1109/ASET48392.2020.9118225.
- [186] M. Jamil and X. S. Yang, “A literature survey of benchmark functions for global optimisation problems,” *Int. J. Math. Model. Numer. Optim.*, vol. 4, no. 2, p. 150, 2013, doi: 10.1504/IJMMNO.2013.055204.
- [187] D. Bingham, “Virtual Library of Simulation Experiments: Test Functions and Datasets.” <https://www.sfu.ca/~ssurjano/optimization.html>.
- [188] L. Mariam, M. Basu, and M. F. Conlon, “Microgrid: Architecture, policy and future trends,” *Renew. Sustain. Energy Rev.*, vol. 64, pp. 477–489, Oct. 2016, doi: 10.1016/j.rser.2016.06.037.
- [189] A. S. Assiri, A. G. Hussien, and M. Amin, “Ant Lion Optimization: Variants, Hybrids, and Applications,” *IEEE Access*, vol. 8, pp. 77746–77764, 2020, doi: 10.1109/ACCESS.2020.2990338.
- [190] Y. Chen *et al.*, “An Optimizing and Differentially Private Clustering Algorithm for Mixed Data in SDN-Based Smart Grid,” *IEEE Access*, vol. 6, 2018.
- [191] M. Wang, C. Wu, L. Wang, D. Xiang, and X. Huang, “A feature selection approach for hyperspectral image based on modified ant lion optimizer,” *Knowledge-Based Syst.*, vol. 168, pp. 39–48, 2019, doi: 10.1016/j.knosys.2018.12.031.
- [192] M. M. Mafarja and S. Mirjalili, “Hybrid binary ant lion optimizer with rough set and approximate entropy reducts for feature selection,” *Soft Comput.*, vol. 23, no. 15, pp. 6249–6265, 2019, doi: 10.1007/s00500-018-3282-y.
- [193] U. M. Khaire and R. Dhanalakshmi, “Stability of feature selection algorithm: A review,” *J. King Saud Univ. - Comput. Inf. Sci.*, vol. 34, no. 4, pp. 1060–1073, 2022, doi: 10.1016/j.jksuci.2019.06.012.
- [194] Y. Jin, B. Yu, M. Seo, and S. Han, “Optimal Aggregation Design for Massive V2G Participation in Energy Market,” *IEEE Access*, vol. 8, pp. 211794–211808, 2020, doi: 10.1109/ACCESS.2020.3039507.
- [195] E. Mortaz and J. Valenzuela, “Optimizing the size of a V2G parking deck in a microgrid,” *Int. J. Electr. Power Energy Syst.*, vol. 97, no. October 2017, pp. 28–39, Apr. 2018, doi: 10.1016/j.ijepes.2017.10.012.
- [196] S. Mohseni, A. C. Brent, and D. Burmester, “A demand response-centred approach to the long-term equipment capacity planning of grid-independent micro-grids optimized by the moth-flame optimization algorithm,” *Energy Convers. Manag.*, vol. 200, p. 112105, Nov. 2019, doi:

10.1016/j.enconman.2019.112105.

- [197] S. Mohseni and A. C. Brent, “Economic viability assessment of sustainable hydrogen production, storage, and utilisation technologies integrated into on- and off-grid micro-grids: A performance comparison of different metaheuristics,” *Int. J. Hydrogen Energy*, vol. 45, no. 59, pp. 34412–34436, Dec. 2020, doi: 10.1016/j.ijhydene.2019.11.079.
- [198] A. Elbaz and M. T. Güneşer, “Optimal Sizing of a Renewable Energy Hybrid System in Libya Using Integrated Crow and Particle Swarm Algorithms,” *Adv. Sci. Technol. Eng. Syst. J.*, vol. 6, no. 1, pp. 264–268, Jan. 2020, doi: 10.25046/aj060130.
- [199] M. Yazdani and F. Jolai, “Lion Optimization Algorithm (LOA): A nature-inspired metaheuristic algorithm,” *J. Comput. Des. Eng.*, vol. 3, no. 1, pp. 24–36, Jan. 2016, doi: 10.1016/j.jcde.2015.06.003.
- [200] R. Masadeh, B. A., and A. Sharieh, “Sea Lion Optimization Algorithm,” *Int. J. Adv. Comput. Sci. Appl.*, vol. 10, no. 5, pp. 388–395, 2019, doi: 10.14569/IJACSA.2019.0100548.
- [201] X. S. Yang and X. He, “Bat algorithm: literature review and applications,” *Int. J. Bio-Inspired Comput.*, vol. 5, no. 3, p. 141, 2013, doi: 10.1504/IJBIC.2013.055093.
- [202] Y. Wu, J. Zhang, A. Ravey, D. Chrenko, and A. Miraoui, “Real-time energy management of photovoltaic-assisted electric vehicle charging station by markov decision process,” *J. Power Sources*, vol. 476, no. May, p. 228504, Nov. 2020, doi: 10.1016/j.jpowsour.2020.228504.

Appendix A MATLAB CODE

Battery modeling section:

```
%% battery
#####inputs#####
Nbat=x(3); % no. of batteries that are selected by PSO
uinv=0.95;
dod=0.8;% battery depth of discharge. it indicates how much % the
charge can be drawn from the battery.
AD=3;
EL=convert;
Vs=48;
Bcap=AD*EL/uinv*n_bat*dod*Vs;
SOCmin=xlsread('SOCmin.xlsx',1,'A1:A180');
SOCmax=xlsread('SOCmax.xlsx',1,'B1:B180');
```

PV modeling section:

```
%% solar
solar=xlsread('g.xlsx',1,'E19:E8778');
% solar irradiance data W/m^2
temp=xlsread('g.xlsx',1,'F19:F8778'); %% temperature data
0C
Tam=temp; %% ambient
temperature 0C
%%%%% -----Plotting of PV_out-----%%%%%
Gref=1000; %% reference solar radiation (W/m^2)
NOCT=45; %% Nominal cell operating temperature
kt=-3.7e-3; %% Temperature coefficient
Tref=25; %% Temperature at reference condition
Tc=Tam+((NOCT-20)/800).*solar; % cell temperature
pv_eff=7.3; %% solar panels efficiency (rated power
under reference condition)
G=solar;
PV_out=(pv_eff.* (G/Gref)).*(1+kt.* (Tc-Tref));
%PV output power
pp=PV_out;

figure ;plot(pp);axis tight;box on;grid on
xlabel('Time (hours)');ylabel('PV output power (kW)');title(' Output
power generated from PV')
```

Wind turbine modeling section:

```
%% WIND
%% Modelling of Wind turbine
%Calculation of wind speed at HUB height
%conversion of wind speed from reference to hub height
wind=xlsread('g.xlsx',1,'G19:G8778'); %% wind speed data m/s
load('WindTurbines.mat'); %% LOAD WIND DATA
V1=wind; %% wind speed
h2=70; %% Wind turbine at hub height
h1=43.6; %% Wind turbine at hub height
alfa=0.25; %% for heavily forested landscape (power law
exponential)
V2=V1*(h2/h1)^ (alfa); %% (V2)= Wind speed at hub height
%% wind turbine model
WTM=4; %%Choosen wind turbine
model
bd=cell2mat(WindTurbines(WTM,2)); %%Blades diameter(m) (6.4)
```

```

as=cell2mat(WindTurbines(WTM, 3)); %Area swept by the
blade(m) (as=pi*(rw)^2
eff=cell2mat(WindTurbines(WTM, 4)); %%Efficiency 95%
vcut=cell2mat(WindTurbines(WTM, 5)); %%cut out speed 40m/s
vin=cell2mat(WindTurbines(WTM, 6)); %%cut out speed 2.5m/s
vr=cell2mat(WindTurbines(WTM, 7)); %%cut out speed 9.5m/s
pr=cell2mat(WindTurbines(WTM, 8)); %%rated power pr=5kw
pcut=cell2mat(WindTurbines(WTM, 9)); %%output power at cut-out
speed pcut=4kw
pmax=cell2mat(WindTurbines(WTM, 10)); %%maximum output power

for t=1:1:8760
    if V2(t)<vin
        pwt(t)=0;
    elseif vin<=V2(t) && V2(t)<=vr
        pwt(t)=((V2(t))^3*(pr/((vr)^3-(vin)^3))-
pr*((vin)^3/((vr)^3-(vin)^3));
    elseif vr<V2(t) && V2(t)<vcut
        pwt(t)=0;
    end
    pwg(t)=pwt(t)*eff; %Electric power from wind turbine
end
Nwt=wind/pwg;
figure; yyaxis right;hold on;plot(pp); hold on; ylabel('PV output
power (kW)'); yyaxis left;hold on;plot(pwg);ylabel('Wind turbine
output (kW)');hold off; axis tight; box on;title('P_pv &
P_wt'); xlabel('Time (hours)')

figure ; plot (pwg);grid on;axis tight;box on;xlabel('Time
(hours)');
ylabel('Wind Turbine output (kW)');title('Output power generated
from wind')

```

Section: plotting the population and load demand

```

Population_Number=xlsread('book1.xlsx',1,'I237:I258');
POWER_DEMAND=xlsread('book1.xlsx',1,'J237:J258');

figure; yyaxis right;hold on;plot(Population_Number); hold
on;ylabel('Population Number (Million)');

yyaxis left;hold on;plot(POWER_DEMAND);ylabel('Power demand
(MW)');grid on; hold off; axis tight; box on;xlabel('Years')

```

charge and discharge section

```

%%%%%CHARGE %%%%%%%%
function [Eb,Ech,Edch,Egrid_s,Ev] =
charge(Eb,Ebmax,P1,t,Ech,Edch,Pw,Ps,n_bat,Egrid_s,Ev,car_av)
%^^^^^CHARGE^^^^^
uconv=0.95; % CONVERTER efficiency
uinv=0.95; % inverter efficiency
C_Rate=7.2; %=7.4;%battery charge rate kw/h
Evmax=24; %=75; capacity of EV BATTERY
temp2=0; % temporary variable 2 STARTING CHARGING CASE
Edch(t)=0;
Egrid_s(t)=0;

Pch(t)=((Pw(t)+Ps(t))*uinv)-(P1(t)/uinv);
%n_bat is battery round trip efficiency.

```

```

        Ech(t)=Pch(t).*n_bat.*uconv;%The energy available to
battery after extracted converter and battery efficiency adn
    if Ech(t)<=Ebmax-Eb(t-1)
        Eb(t)=Eb(t-1)+Ech(t);
        Ev(t)=Ev(t-1);
    else
        Eb(t)=Ebmax; % max SOC constraint is implemented here, in
the else condition, the available charging is more than capacity,
instead, SOC is limited to 100%(Ebmax)
        Egrid_s(t)=(Ech(t)-(Ebmax-Eb(t-1)))/(n_bat); % the
ammount of energy supplied to grid.
        Ech(t)=Ebmax-Eb(t-1);

        if Egrid_s(t)>C_Rate %deciding whether the available
Ech is greater than the charging rate of Ev
            temp1=C_Rate;
        else
            temp1=Egrid_s(t);
        end
        Ev(t)=Ev(t-1);
        if ((Ev(t-1)<=Evmax) && (car_av(t)==1)) %deciding whether
the car is at home and available Ev is less than critical SOC of Ev
            if (temp1+Ev(t-1))>Evmax
                Ev(t)=Evmax;
                temp2=(Evmax-Ev(t-1));
                Ech(t)=Ech(t)+temp2;
                Egrid_s(t)=Egrid_s(t)-temp2;
            else
                Ev(t)=Ev(t-1)+temp1;
                temp2=temp1;
                Ech(t)=Ech(t)+temp1;
                Egrid_s(t)=Egrid_s(t)-temp1;
            end
        end
    end
end

%%%%%DISCHARGE %%%%%%
function [Eb,Edch,Ech,Egrid_p,Ev] =
discharge(Pw,Ps,Eb,Ebmax,P1,t,Ebmin,Edch,Ech,Egrid_p,Ev,car_av)
%^^^^^^DISCHARGE^^^^^
uconv=0.95;
uinvs=0.95;
Pdch(t)=(P1(t)/uinvs)-((Pw(t)+Ps(t))*uconv);
Edch(t)=Pdch(t)*1; %one hour iteration time
Ech(t)=0;
Egrid_p(t)=0;
D_Rate=7.2;%7.4; %battery discharge rate
Evmax=24;%=75;
temp1=0;

if (Ev(t-1)<(Evmax*.2) && (car_av(t)==1))
    [Ev,Egrid_p]=charge_Ev(Ev,Egrid_p,t);
end

if (Eb(t-1)-Ebmin)>=(Edch(t)/uconv)
    Eb(t)=Eb(t-1)-(Edch(t)/uconv);
    Egrid_p(t)=0; % no energy taken from grid
    Ev(t)=Ev(t-1);
else

```

```

        if (((Ev(t-1)-(Edch(t)-Eb(t-
1)+Ebmin))>Evmax*.2)&&(car_av(t)==1)&&((D_Rate)+Eb(t-1)-
Ebmin>=Edch(t)))
            Eb(t)=Ebmin;
            Ev(t)=Ev(t-1)-(Edch(t)-Eb(t-1)+Ebmin);
            Edch(t)=Eb(t-1)-Ebmin;
        else
            temp=Eb(t-1)-Ebmin;
            Eb(t)=Eb(t-1);
            Ev(t)=Ev(t-1);
            Egrid_p(t)=Edch(t);
            Edch(t)=0;
        end
    end
end

plotting section

%% Plotting section
figure; yyaxis right;hold on;plot(Ps); hold on;ylabel('PV output
power (kW)'); yyaxis left;hold on;plot(Pw);ylabel('wind turbine
output (kW)');hold off; axis tight; box on;title('P_p_v &
P_w_t'); xlabel('Time (hours)')

%%%% ***** %%%%%%
m1=1;m2=m1+167; % m1 referses to the week whos graphs to be dispayed.

t1=1:1:168;
figure;
% area(t1,load1(m1:m2),'DisplayName','Load','FaceColor',[1 0 1])
plot(t1,convert(m1:m2),'DisplayName','Load','LineStyle','--');hold
on
plot(t1,Edch(m1:m2),'DisplayName','Bat_o_u_t');hold on
% area(t1,Edch(m1:m2),'DisplayName','Bat_o_u_t','FaceColor',[1 0 0])
temp=Pw(m1:m2);
plot(t1,temp(1:168),'DisplayName','P_W_T');hold on
% area(t1,temp,'DisplayName','P_W_T','FaceColor',[1 1 0])
plot(t1,Egrid_p(m1:m2),'DisplayName','Grid_P_u_r_c_h_a_s_e');hold
off
%
area(t1,Egrid_p(m1:m2),'DisplayName','Grid_P_u_r_c_h_a_s_e','FaceCol
or',[0 0 1])
ylabel('Energy(KW)'); xlabel('Time (Hours)');grid on;grid minor;axis
tight ;legend show

figure;area(t1,convert(m1:m2),'DisplayName','Load','FaceColor',[1 0
1])
% plot(t1,load1(m1:m2),'DisplayName','Load','LineStyle','--');
hold on
plot(Ech(m1:m2),'DisplayName','Bat_i_n','Color',[1 0 0]); hold on
temp=Egrid_p(m1:m2)+Pw(m1:m2)+Ps(m1:m2)+Edch(m1:m2).*uinv;
% plot(t1,temp(m1:m2),'DisplayName','Total Power +
Bat_o_u_t+Grid_P')
area(t1,temp(m1:m2),'DisplayName','P_L+
Bat_o_u_t+Grid_P','FaceColor',[0 0 1])
hold off; ylabel('Energy(KW)'); xlabel('Time (Hours)');axis tight
;legend show; grid on;grid minor

figure;plot(t1,-Egrid_s(m1:m2),'DisplayName','Grid_s_a_l_e_s');hold
on

```

```

plot(t1,Egrid_p(m1:m2),'DisplayName','Grid_p_u_r_c_h_a_s_e');hold
off
ylabel('Energy(kW)');xlabel('Time (Hours)');axis tight;legend show;
grid on;grid minor

figure;yyaxis left;hold on
% area(t1,load1(m1:m2),'DisplayName','Load','FaceColor',[1 1
0],'LineStyle',':')
plot(convert(m1:m2),'DisplayName','Load','LineWidth',1,'LineStyle',
--, 'Color',[0 1 1])
plot(Pw(m1:m2),'DisplayName','P_W_T','LineWidth',1,'LineStyle',
--, 'Color',[0 0 1])
plot(Edch(m1:m2),'DisplayName','B_o_u_t');ylabel('Energy(kW)');xla
bel('Time (Hours)');grid on;grid minor
yyaxis right
plot(t1,Eb(m1:m2)*100/Ebmax,'DisplayName','SOC')
% area(t1,Eb(m1:m2)*100/Ebmax,'DisplayName','SOC','FaceColor',[1 0
1])
ylabel('SOC(%)');axis tight;legend show;grid on;grid minor

figure;plot(t1,-Ech(m1:m2),'DisplayName','Bat_i_n');hold
on;plot(t1,Edch(m1:m2),'DisplayName','Bat_o_u_t');hold off
ylabel('Energy(kW)');xlabel('Time (Hours)');legend show;grid on;grid
minor

figure;plot(-Ech,'DisplayName','Bat_i_n');hold
on;plot(Edch,'DisplayName','Bat_o_u_t'); hold off
ylabel('Energy(KW)');xlabel('Time (Hours)');legend show ;grid
on;grid minor

figure;plot(Eb*100/Ebmax,'DisplayName','SOC');ylabel('SOC(%)');xla
bel('Time (Hours)');legend show;grid on;grid minor

figure; plot(convert,'DisplayName','load');ylabel('Load Demand
(KW)');xlabel('Time (Hours)');axis tight;legend show;grid on;grid
minor

figure;plot(Pw,'DisplayName','P_W_T');ylabel('Wind Power
(KW)');xlabel('Time (Hours)');axis tight;legend show;grid on;grid
minor

figure;plot(Ps,'DisplayName','P_P_V');ylabel('Solar Power (KW)');
xlabel('Time (Hours)');axis tight;legend show;grid on;grid minor
%% -----
%% Four seasons SOC
%% 1th season starting from (Mar-Apr-May).
m1=1418;m2=m1+167; % m1 refers to starting hour of the season to be
displayed.
figure;plot(t1,Eb(m1:m2)*100/Ebmax,'--','DisplayName','SOC');hold on
plot(SOCmin,'c.-','Linewidth',3);hold on
plot(SOCmax,'g.-','Linewidth',3);hold off
axis tight;grid on;grid minor
ylabel('SOC(%)');xlabel('Time (Hours)');title ('Spring (Mar-Apr-
May)')
legend ('SOC_S_p_r_i_n_g','SOC_m_i_n','SOC_m_a_x')
%% 2nd season starting from Jun-Jul-Aug.
m1=3626;m2=m1+167; % m1 refers to starting hour of the season to be
displayed.
figure;plot(t1,Eb(m1:m2)*100/Ebmax,'--','DisplayName','SOC');hold on
plot(SOCmin,'c.-','Linewidth',3);hold on
plot(SOCmax,'g.-','Linewidth',3);hold off

```

```

axis tight; ylabel('SOC (%)'); xlabel('Time (Hours)');
title ('Summer (Jun-Jul-Aug)'); grid on; grid minor
legend ('SOC_S_u_m_m_e_r','SOC_m_i_n','SOC_m_a_x')
%% 3rd season starting from Sep-Oct-Nov.
m1=5834;m2=m1+167; % m1 refers to starting hour of the season to be
displayed.
figure;plot(t1,Eb(m1:m2)*100/Ebmax,'--','DisplayName','SOC');hold on
plot(SOCmin,'c.-.);hold on
plot(SOCmax,'g.-.);hold off;axis tight
ylabel('SOC (%)'); xlabel('Time (Hours)');
title ('Autumn (Sep-Oct-Nov)'); grid on; grid minor
legend ('SOC_A_u_t_u_m_n','SOC_m_i_n','SOC_m_a_x')
%% 4th season starting from Dec-Jan-Feb.
m1=8018;m2=m1+167; % m1 refers to starting hour of the season to be
displayed.
figure
plot(t1,Eb(m1:m2)*100/Ebmax,'--','DisplayName','SOC');hold on
plot(SOCmin,'c.-.);hold on
plot(SOCmax,'g.-.);hold off
axis tight; ylabel('SOC (%)'); xlabel('Time (Hours)'); grid on; grid
minor
title ('Winter (Dec-Jan-Feb)'); legend
('SOC_W_i_n_t_e_r','SOC_m_i_n','SOC_m_a_x')
%%%%%% all in one
figure;
yyaxis left
plot(pp,'DisplayName','P_P_V');hold on
plot(pwg,'DisplayName','P_W_T');hold on
plot(convert,'DisplayName','load');hold on
plot(grids,'DisplayName','Grid_s_u_p_p_l_y');hold off
% plot(t1,-Egrid_s,'DisplayName','Grid_s_a_l_e_s');hold on
% plot(t1,Egrid_p,'DisplayName','Grid_p_u_r_c_h_a_s_e');hold off
ylabel('Power (KW)'); xlabel('Time (Hours)'); axis tight ; grid on; grid
minor; legend
('P_P_V','P_W_T','P_L','Grid_s_u_p_p_l_y','Bat_i_n','Bat_o_u_t')

yyaxis right
plot(-Ech,'DisplayName','Bat_i_n');hold on
plot(Edch,'DisplayName','Bat_o_u_t');hold off
ylabel('Bat_i_n&Bat_o_u_t'); axis tight ; grid minor; grid on; legend
show
-----
objective functions
%% objective function
figure
REAL_INTREST=3;
ir=REAL_INTREST/100;
CRF=ir.* (1+ir)^20/(1+ir)^20-1; %% capital recovery factor
NPC=ASC/CRF;
plot(NPC); axis tight; grid on; xlabel ('Renewable electricity
fraction'); ylabel ('NPC ($)')
title ('Total NPC')
display(['The value of NPC is : ', num2str(NPC)])
-----
%% Objective function (1)
Grid_sale=0.015;
Grid_p=0.023;
grid_cost=sum(Grid_p).*0.023-sum(Grid_sale).*0.015
Grid_purchased=sum(Grid_p)
Grid_sale=sum(Grid_sale)

```

```

Cgrid=0.0425.*Grid_p; %% 0.023 is the buying price Cgrid is the
cost of buying electricity
display(['The value of Cgrid is : ', num2str(Cgrid)])
-----
REF=sum(Pw+Ps)./sum(Pw+Ps+Grid_purchased); %% 0.980932456190068
ref=REF*100
GCF=1-REF;
display(['The value of REF is : ', num2str(REF)])
display(['The value of GCF is : ', num2str(GCF)])
ob=min (GCF);
%% objective function (2)
Egrid_s=zeros(1,8760);
R_grid=sum(0.02).*Egrid_s; %%=0.0003
display(['The value of R_grid is : ', num2str(R_grid)])
-----
COE=((CRF.*sum(NPC))+grid_cost-R_grid./convert+Grid_sale); %% COE IN
$KWH
% display(['The value of COE is : ', num2str(COE)])
figure
ef=[0.8 .85 .9 .95 1 ];
lcoe_value=[0.2351 0.2212 0.2089 0.1980 0.1881];
plot(ef,lcoe_value,'DisplayName','SOC','Marker','*', 'Color',[1 0 1])
ylabel('LCOE($/KWh)'); xlabel('Round trip efficiency'); grid on; grid
minor; axis tight; legend show
-----
%% LPSP OBJECTIVE (3)
R_grid=sum(0.02).*Egrid_s; %%=0.0003
% LPSP=sum(Ps+Pw)/sum(load1); %% LPSP (%)
% LPSP=sum(pp+pwg)/sum(convert); %%%=0.4975
LPS=(convert-(pp+pwg)+R_grid);
LPSP=sum(LPS)/sum(convert);
display(['The value of LPSP is : ', num2str(LPSP)]) %%=0.49854
lpsp=LPSP*100;

```

Work stage and Research schedule (Gant chart)

The presented work is partially divided through the period of study as three years, the period of the work as expected has been tabulated in Table I as a Gantt chart.

Table Gantt chart

Research activities	2019/2 020-2	2020/2 021-1	2020/2 021-2	2021/2 022-1	2021/2 022-2	2022/2 023-1
	Sem-1	Sem-2	Sem-3	Sem-4	Sem-5	Sem-6
Literature review and review paper writing						
Resource data collection						
Modeling of microgrid component						
Sizing component systems						
Development of RB-EMS algorithm						
Implementation of the proposed algorithm (IALO)						
Analysis of the proposed system result						
Benchmarking obtained results from IALO with ALO, PSO, and CSA.						
Technical paper writing						
Thesis writing						

Appendix B PSEUDOCODE OF THE ALGORITHMS

Pseudocode of ALO

Begin

1. Initialize the first population of ants and antlions randomly
2. Calculate the fitness of ants and antlions
3. Find the best antlions and assume it as the elite (determined optimum)
4. **while** the end criterion is not satisfied
5. **for** every ant
6. Select an antlion using Roulette Wheel
7. Update c and d using Eqs. (2.10) and (2.11).
8. Create a random walk and normalize it using Eqs. (2.1) and (2.7)
9. Update the position of the ant using Eq. (2.13).
10. **end for**
11. Calculate the fitness of all ants
12. Replace an antlion with its corresponding ant if becomes fitter (Eq. (2.12))
13. Update elite if an antlion becomes fitter than the elite
14. **end while**
15. **Return** elite

Pseudocode of PSO.

1. **Begin**
2. for each particle in the swarm initialize its position & velocity randomly
3. **end for**
4. do for each particle in the swarm
5. Evaluate the fitness function
6. If the objective fitness value set is better than the personal best objective fitness value
7. (P_{best}) in history, current fitness values are set as the new personal best ((P_{best}))
8. **end if**
9. **end for**
10. From all the particles or neighbourhoods, choose the particle with the best Fitness value as the (G_{best})
11. for each particle in the swarm
12. Update the particle position according to Eq. (2.14).
13. Update the particle velocity according to Eq. (2.15).
14. **end for**
15. Until stopping criteria are satisfied
16. **end begin**

Pseudocode of CSA.

- 1. Begin**
2. Objective function $f(x)$
3. Generate initial population of n host nest
4. Evaluate fitness and rank eggs
5. **While** ($t > \text{MaxGeneration}$) or stop criterion
6. $t = t + 1$
7. get a cuckoo randomly/generate a new solution by lévy flights
8. evaluate quality/fitness F_i
9. Choose a random nest j
10. If ($F_i > F_j$)
11. Replace j with the new solution
- 12. end if**
13. The worst nest is abandoned with a probability P_a and a new nest is built
14. Evaluate fitness Rank the solutions and find the current best
- 15. end while**
- 16. Post-process results and visualization**
- 17. end**

Pseudocode of IALO.

1. Initialize the first population of ants and antlions randomly
2. Calculate the fitness of ants and antlions
3. Find the best antlions and assume it as the elite (determined optimum)
4. **while** the end criterion is not satisfied
5. **for** every ant
6. Select an antlion using lévy flight using Eq. (3.28)
7. Update c and d using Eqs. (2.10) and (2.11).
8. Create a random walk and normalize it using Eqs. (2.1) and (2.7)
9. Update the position of the ant using Eq. (2.13).
- 10. end for**
11. Calculate the fitness of all ants
12. Replace an antlion with its corresponding ant if becomes fitter (Eq. (3.32))
13. Update elite if an antlion becomes fitter than the elite
- 14. end while**
- 15. Return** elite

Pseudocode of SMCM

1. **Begin**
2. T=1:8760
3. Read data for P_{PV} , P_{WT} , Load, SoC_{EV} , SoC_{BT}
4. If $(P_{PV} + P_{WT})$ meet the load $(P_L + EV_{Dem})$ then
5. Charge the EV battery from the RESs
6. If $SoC_{EV}(t) \geq SoC_{EVmax}$
7. Charge BT
8. If $SoC_{BT}(t) \geq SoC_{BTmax}$
9. Export to grid (V2G)
10. End
11. End
12. End
13. If RESs $< P_L$
14. Discharge from the EV to Grid
15. When $SoC_{EVmin}(t)=0.2$
16. Charge from BT
17. When $SoC_{BTmin}(t)=20$
18. Charge from the grid (G2V)
19. End
- 20.** T=8760
- 21.** End

Some of the utilized mathematical equations for calculating the costs, μ , and σ as listed below.

$$Z = \frac{X - \mu}{\sigma} \quad (1)$$

$$Z\sigma = X - \mu \quad (2)$$

$$\mu = Z\sigma + X \quad (3)$$

$$\sigma (StD) = \sqrt{\frac{\sum(X - \mu)^2}{n - 1}} \quad (4)$$

$$Deviation = |X - \mu| \quad (5)$$

Appendix C List of Classification of Terminologies

Some of the listed problems while integrating EVs into the grid as tabulated in Table V. If the charging has been unwell scheduled the system will face overcurrent and under-voltage problems in the EVs. The effect of the aforementioned issue is the high power at a specific peak load.

Table Grid Faced challenges with electric vehicles.

Problem Type	Effects	Expected solution
Overloading	<ul style="list-style-type: none"> • Reducing the lifespan of a transformer • Transformer failure 	Time Scheduling charging
Voltage instability	<ul style="list-style-type: none"> • Low voltage in the power system • Power outage • Damaging home appliances 	Using power conversion
Excessive harmonic injection	<ul style="list-style-type: none"> • Effects on EVs chargers by generating harmonics • Poor Power Quality • Current flow in the neural cable 	Using power conversions
Power losses	<ul style="list-style-type: none"> • Massive power losses • Voltage deviation 	Coordinating EV charging with a fewer number of EVs
Voltage dip/sag	<ul style="list-style-type: none"> • Decreasing charging controls • Voltage dip limitation 	Using Charging control
Voltage unbalance/imbalance	Poor power quality affects the power phasing system (three-phase only).	<ul style="list-style-type: none"> • Nature-inspired algorithms • Intelligent charging strategies
Frequency variation and consequently	<ul style="list-style-type: none"> • Frequency variation caused by penetration of EVs and unwell-coordinated charging • Damaging the electrical system 	Coordinate EV charging

Table Comparison between V2H and V2G [130].

	V2H	V2G
Feature	<ul style="list-style-type: none"> • Single EV to a single home • Most simple and least flexible • Simple infrastructure • Easy installation • Operation in home-grid 	<ul style="list-style-type: none"> • A large number of EVs • Offering power services • Least simple and most flexible • Operation on a large scale • High infrastructure complexity
Functions	<ul style="list-style-type: none"> • Acts as a home backup generator and controllable load • Cooperate with domestic electric devices for load shifting • Sell (discharge) energy back to the grid at a high peak period • Charge (buy) energy at the less expensive time (off-peak) • Microgrid contribute 	<ul style="list-style-type: none"> • Act as energy sources to provide grid ancillary services • Act as controllable load • Act as distributed storage • Stabilize the grid for a short period

List of ancillary services for the technology of V2G [20].

Table Ancillary services terminologies

Terms	Definitions
Peak shaving	Sending power back to the grid when demand is high
Load leveling	Decreasing the peak electricity demand supplied by traditional power plants (peak shaving) and increasing the peak-off demand (valley filling) at the same time.
Frequency and voltage regulation	Used by the system operator to hold frequency and voltage within a given range
Spinning reserve	Standbys provided by online generators, which contain unused power capacity that is ready to synchronize and provide energy quickly to the grid

List of commonly used definitions in the study.

Table Definitions of some commonly used terminologies

	Terms	Definition
Objective Functions	EMS	<ul style="list-style-type: none"> • It is referring to an Energy Management Strategy. • Also, can be defined as collecting all systematic procedures to control and minimize the quantity and the cost of energy used to provide certain applications with their requirements.
	LPSP	<ul style="list-style-type: none"> • The reliability is known as the ratio of the deficit in energy generation to the demand using Losses Power Supply Probability (LPSP) technology. • The ability of the electric power system to continuously supply the load) or refers to the probability of power supply failure to meet the load demand.
	REF	<ul style="list-style-type: none"> • It is referring to the Renewable Energy Fraction (REF) and can be defined as the portion of the energy transferred to the load generated from RESs. • The quantity of energy produced from RESs.
	COE	<ul style="list-style-type: none"> • It refers to the Cost of Electricity (COE) and means the per capita of electricity. • It is the ratio of TNPC, and energy consumed by the system.
	ASC	<ul style="list-style-type: none"> • Refers to the Annualized System Cost (ASC) known as the annual amount of investment cost.
	TNPC	<ul style="list-style-type: none"> • Refers to the Total Net Present Cost (TNPC) that includes (O&M, replacement cost, and present cost), the sum of the capital cost of components.
Constructions	Microgrid	<ul style="list-style-type: none"> • It is a system for one island area as an off-grid or for the community as an on-grid system that is locally generated and locally distributed of clean energy. • Can be called Distributed Generation (DG). • Can be defined as producing energy close to the customer regions.

Listed different supervisory control algorithms as Integrated-Energy Management Strategies (I-EMSs) with their classifications and references. The EMS is divided into offline and online categories [61]. Offline optimization techniques like ALO, PSO CSA, ABC, and GA cannot be used in real-time applications since they require prior knowledge of all available information and a significant amount of computing work. Stochastic methods are regarded as one of the offline algorithms as well. On the other hand, power flow is managed using online algorithms like RB. Offline algorithms differ from those used online by requiring prior knowledge and requiring lengthy operations.

Table Integrated - Energy Management Strategies [28][61][58][56][29].

Algorithms	Strategies	Classification	
Rule-based (High-level control)	Deterministic	Optimal working condition-based	The Thermostat on/off Power Flower State Machine Control
		Frequency-decoupling	Low Pass Filter Gliding average (Phlegmatising strategy) Wavelet-transform
		Optimized membership	
		Conventional fuzzy strategy	
		Adaptive FL	
		Predictive FL	
	Real-time optimization (Online)	Equivalent Consumption Minimisation Strategy (ECMS)	Traditional ECMS (Global EF optimization) Adaptive ECMS (A-ECMS) Predictive ECMS (P-ECMS)
		Model Predictive Control (MPC)	Deterministic MPC (D-MPC) Adaptive MPC (A-MPC) Prescient Artificial Intelligent Frozen-time Exponential-varying Telematics MPC (T-MPC) Stochastic MPC (S-MPC)
			Robustness Control
			Extremum Seeking
			Decoupling Control
			Pseudospectral Optimal Control
			Sliding Mode Control
		Gradient	Linear Programming

Global optimization (Offline)	Derivative-Free	Quadratic Programming
		Sequential Quadratic Programming
		Convex Programming
		Genetic Algorithm (GA)
		Particle Swarm Optimization (PSO)
		Simulating Annealing
		Cuckoo Search Algorithm (CSA)
	Direct	Antlion Optimization (ALO)
		Divided Rectangular (DIRECT)
		Dynamic Programming (DDP, SP-SDP)
	Indirect	Pontryagin's Minimisation Principle (PMP)
	Others	Game Theory (GT)
Learning-based	Reinforcement	Deep Reinforcement Learning (DRL)
	Supervised/Unsupervised	Clustering
	Neural Network	Artificial Neural Network (ANN)
		Elman Neural Network (ENN)

Based on the if-then operation, the charge and discharge of EVs are conducted in this study as presented in the Table below.

Table the IF-Then implementation on the microgrid system.

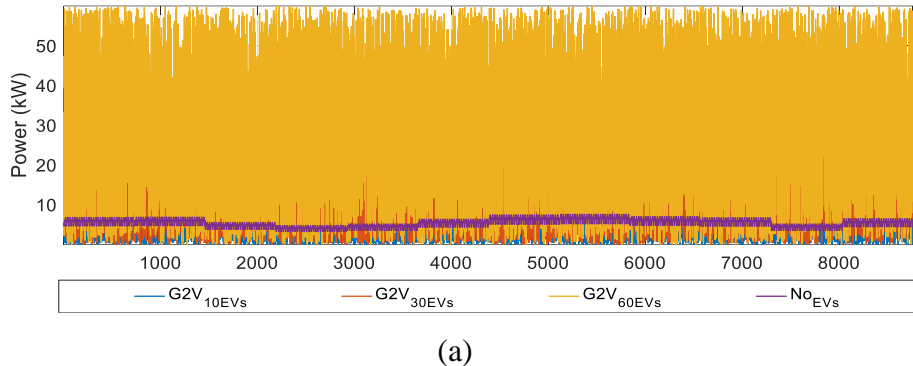
Operation modes	If	Then
RES2V	$SOC_{EV} < 0.95$	$0.95 - SOC_{EV}$
BT2V	$SOC_{EV} < 0.95$	$0.95 - SOC_{EV}$
G2V	$SOC_{EV} < 0.95$	$0.95 - SOC_{EV}$
V2G	$SOC_{EV} > 0.2$	$SOC_{EV} - 0.2$

Feature Selection (FS) is the process of selecting a significant subset of properties from a huge set. Furthermore, it is a strategy that uses to minimize the size of selected features and maximizes the classification performance.

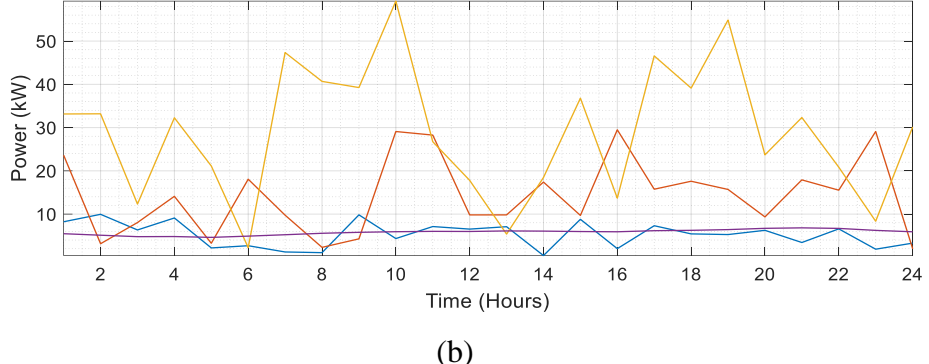
Table Selection techniques and their features [75] [191][192].

Selection techniques	Features
Roulette Wheel Selection	The most common fitness-proportionate selection technique. The roulette wheel is one of the causes of the undesired results as well as ineffectively premature convergence
Lévy Flight	Is a random walk space used to enhance the challenge in metaheuristic methods to avoid local optima
Fitness-Proportionate Selection	To give every individual a chance of being selected to breed but to make fitter candidates more likely to be chosen than weaker individuals.
Linear Rank Selection	It uses due to its addressing more efficient time complexity. is similar to fitness-proportionate selection except that selection probability is proportional to relative fitness rather than absolute fitness
Elitism Selection	It is used to re-discover lost good candidates and improvements in a subsequent generation but there is no guarantee involves copying a small proportion of the fittest candidates, unchanged, into the next generation.
Tournament Selection	It is chosen by two random individuals and chooses the most appropriate individual among them, even in the worst-case scenario.
Steady-State Selection	It uses to replace a few individuals at a time in GA.
Sigma Scaling	It is used to moderate selection pressure over time so that it is not too strong in early generations and not too weak once the population has stabilized and fitness differences are smaller.
Stochastic Universal Sampling	It is used to ensure that the observed selection frequencies of each individual are in line with the expected frequencies.
Truncation Selection	Also known as truncation point defined as the selected as parents for the next generation.
Rough-Set	To find the optimally selected feature

The annual and seasonal output power from the proposed scenarios are demonstrated below:

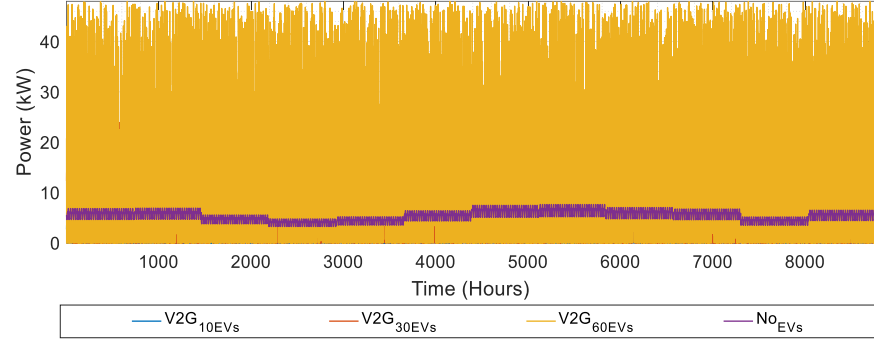


(a)

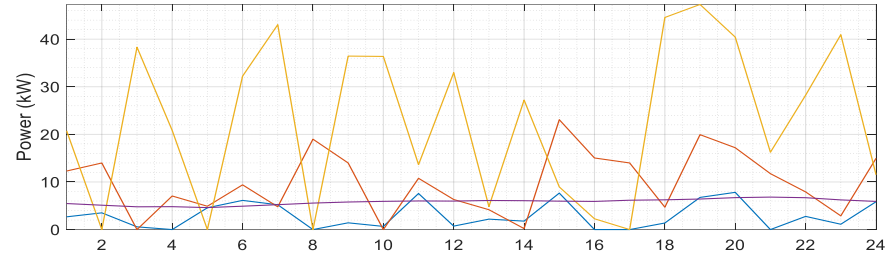


(b)

Figure Impacts of Vehicle to grid integration under (a) 10, 30, 60 EVs and (b) zoom-in of (a).

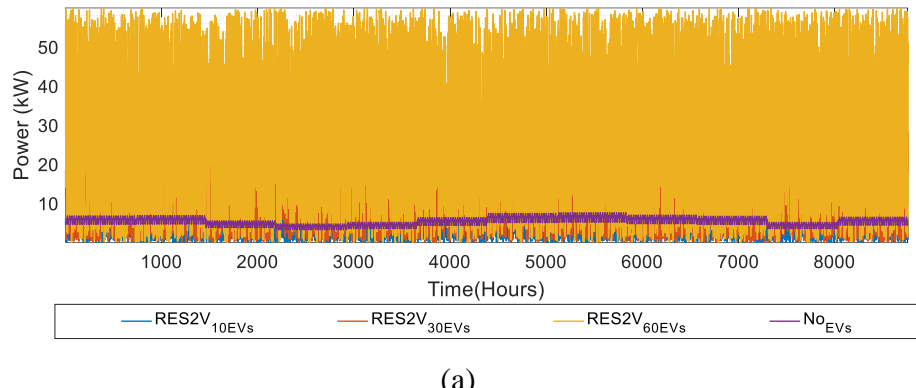


(a)

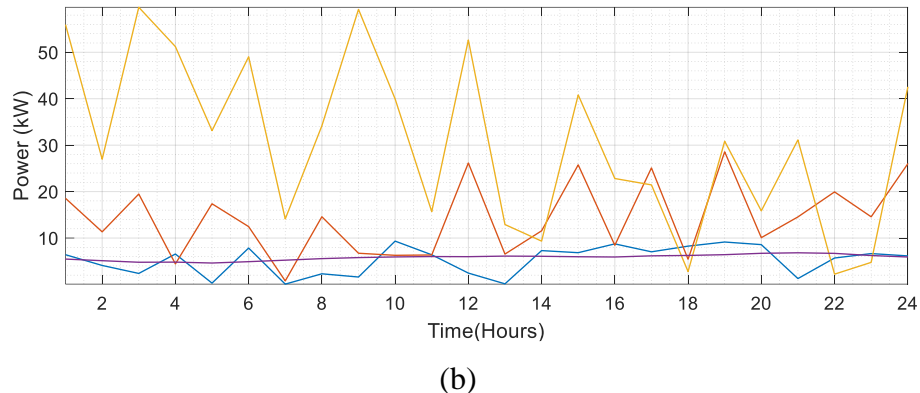


(b)

Figure Impacts of Vehicle to grid integration under (a) 10, 30, 60 EVs and (b) zoom-in of (a).

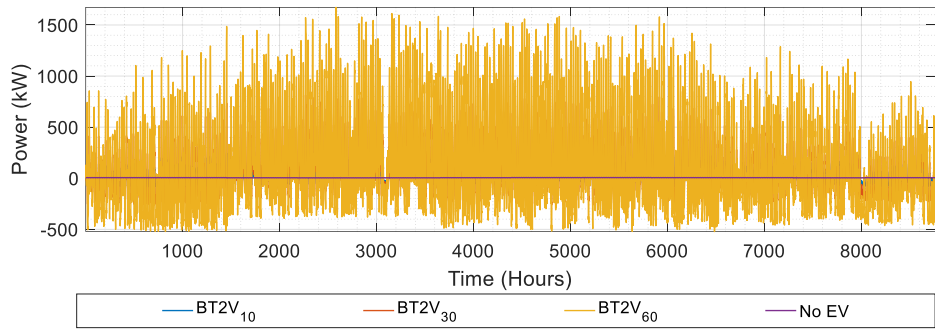


(a)

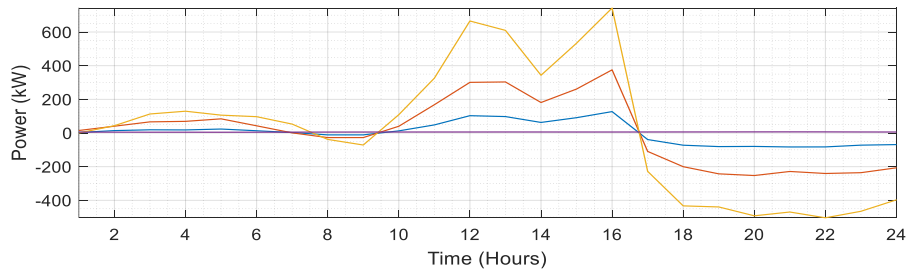


(b)

Figure Impacts of Renewable energy sources integration with EV (a) 10, 30, 60 EVs and (b) zoom-in of (a).



(a)



(b)

Figure Impacts of Battery to Vehicle integration under (a) 10, 30, 60 EVs and (b) zoom-in of (a).

The annual and seasonal State-of-Charge of Electric vehicles (SOC_{EV}) is presented in Figure.

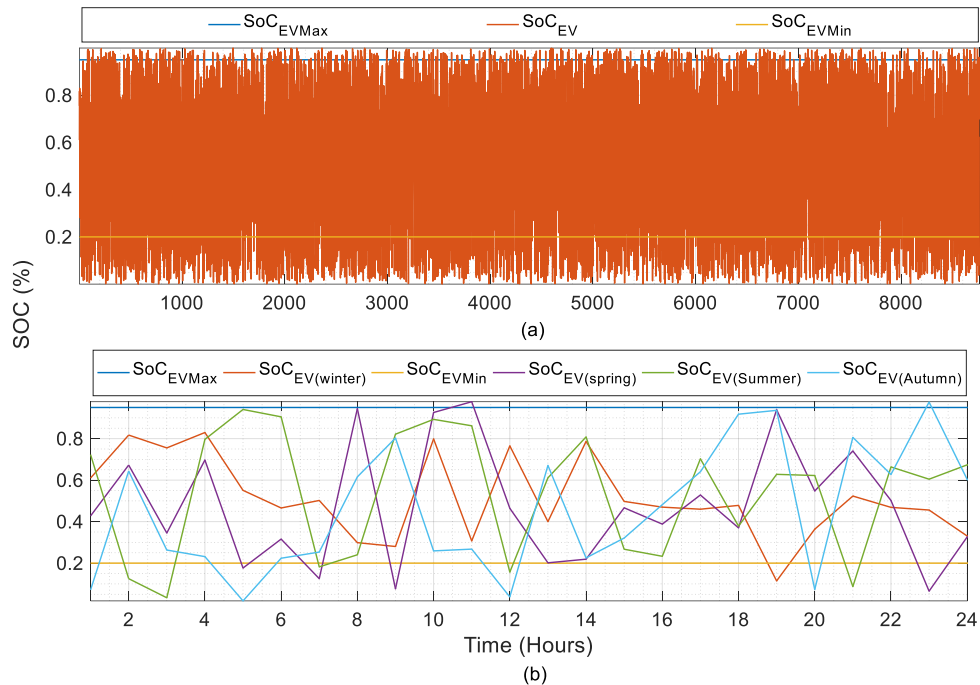


Figure State-of-Charge of Electric Vehicle (a) Annual SOC_{EV} and (b) Seasonal SOC_{EV}.

Appendix D MATLAB Software Environment

MATLAB is a computer program that is known as multi-intelligent software that is utilized to solve problems, plot, and analyze data for different fields [20]. Besides, it is a high-performance language for technical computing and has been written by Cleve Moler in the 1970s. MATLAB is used to provide a graphical interface for dynamic systems, design a model, build mathematical models and verify them. The Simulink environment is fixed boxes used to create different electric, electronic circuits, mathematical, and mechanical circuits. MATLAB can be integrated for computation, visualization, and programming which can be implemented in several applications such as:

- Application development.
- Scientific and engineering graphics.
- Mathematical and computational.
- Data analysis and exploration.
- Algorithm developments.
- Modeling and simulation.

LIST OF PUBLICATIONS

1. **A. Alsharif**, C. W. Tan, R. Ayop, K. Y. Lau, and A. M. Dobi, "A rule-based power management strategy for Vehicle-to-Grid system using antlion sizing optimization," *J. Energy Storage*, vol. 41, no. July, p. 102913, Sep. 2021, doi: 10.1016/j.est.2021.102913. (**ISI: Q1-IF:8.907 (Published)**).
2. **A. Alsharif**, C. W. Tan, R. Ayop, A. Dobi, and K. Y. Lau, "A comprehensive review of energy management strategy in Vehicle-to-Grid technology integrated with renewable energy sources," *Sustain. Energy Technol. Assessments*, vol. 47, no. January, p. 101439, Oct. 2021, doi: 10.1016/j.seta.2021.101439. (**ISI: Q2-IF: 7.632 (Published)**).
3. **A. Alsharif**, C. W. Tan, R. Ayop, A. Ali Ahmed, F. H. Kuwil, M. Mohamed Khaleel. Impact of Electric Vehicle on Residential Power Distribution Considering Energy Management Strategy and Stochastic Monte Carlo Algorithm. *Energies*, pp. 1–24, 2023, doi: 10.3390/en16031358. (**Q1, IF: 3.252 (Published)**)
4. **A. Alsharif**, C. W. Tan, R. Ayop, K. Y. Lau and C. L. Toh, "Sizing of Photovoltaic Wind Battery system integrated with Vehicle-to-Grid using Cuckoo Search Algorithm," *2021 IEEE Conference on Energy Conversion (CENCON)*, 2021, pp. 22-27, doi: 10.1109/CENCON51869.2021.9627291. (**Indexed by SCOPUS-Published**).
5. **A. Alsharif**, C. W. Tan, R. Ayop, A. Ali Ahmed, M. Mohamed Khaleel and A. K. Abobaker, "Power Management and Sizing Optimization for Hybrid Grid-Dependent System Considering Photovoltaic Wind Battery Electric Vehicle," *2022 IEEE 2nd International Maghreb Meeting of the Conference on Sciences and Techniques of Automatic Control and Computer Engineering (MI-STA)*, 2022, pp. 645-649, doi: 10.1109/MI-STA54861.2022.9837749. (**Indexed by SCOPUS-Published**).
6. **Alsharif, A.**, Tan, C. W., Ayop, R., Hussin, M. N., & Bukar, A. L. (2022). Sizing Optimization Algorithm for Vehicle-to-Grid System Considering Cost and Reliability Based on Rule-Based Scheme. *ELEKTRIKA- Journal of Electrical Engineering*, 21(3), 6–12. <https://doi.org/10.11113/elektrika.v21n3.353> (**Indexed by SCOPUS Published**)